EPA-600/4-76-016a
May 1976

Environmental Monitoring Series

CONTINUED RESEARCH IN MESOSCALE AIR POLLUTION SIMULATION MODELING: Volume I - Assessment of Prior Model Evaluation Studies and Analysis of Model Validity and Sensitivity

Environmental Sciences Research Laboratory
Office of Research and Development
U.S. Environmental Protection Agency
Research Triangle Park, North Carolina 27711

RESEARCH REPORTING SERIES

Research reports of the Office of Research and Development, U.S. Environmental Protection Agency, have been grouped into five series. These five broad categories were established to facilitate further development and application of environmental technology. Elimination of traditional grouping was consciously planned to foster technology transfer and a maximum interface in related fields. The five series are:

1. Environmental Health Effects Research
2. Environmental Protection Technology
3. Ecological Research
4. Environmental Monitoring
5. Socioeconomic Environmental Studies

This report has been assigned to the ENVIRONMENTAL MONITORING series. This series describes research conducted to develop new or improved methods and instrumentation for the identification and quantification of environmental pollutants at the lowest conceivably significant concentrations. It also includes studies to determine the ambient concentrations of pollutants in the environment and/or the variance of pollutants as a function of time or meteorological factors.

This document is available to the public through the National Technical Information Service. Springfield, Virginia 22161.

EPA 600/4-76-016 A
May 1976

CONTINUED RESEARCH IN MESOSCALE AIR POLLUTION SIMULATION MODELING: VOLUME I - ASSESSMENT OF PRIOR MODEL EVALUATION STUDIES AND ANALYSIS OF MODEL VALIDITY AND SENSITIVITY

by

M. K. Liu
D. C. Whitney
J. H. Seinfeld
P. M. Roth

Systems Applications, Incorporated
950 Northgate Drive
San Rafael, California 94903

68-02-1237

Project Officer

Kenneth L. Demerjian
Meteorology and Assessment Divison
Environmental Sciences and Research Laboratory
Research Triangle Park, North Carolina 27711

U.S. ENVIRONMENTAL PROTECTION AGENCY
OFFICE OF RESEARCH AND DEVELOPMENT
ENVIRONMENTAL SCIENCES RESEARCH LABORATORY
RESEARCH TRIANGLE PARK, NORTH CAROLINA 27711

DISCLAIMER

This report has been reviewed by the Office of Research and Development, U.S. Environmental Protection Agency, and approved for publication. Mention of trade names or commercial products does not constitute endorsement or recommendation for use.

CONTENTS

ILLUSTRATIONS

TABLES

ACKNOWLEDGMENT

We wish to thank Dr. Richard I. Pollack for his comments on Chapter II and his modifications of some of the computations.

I OVERVIEW

This report presents a series of studies carried out for the Environmental Protection Agency (EPA) to evaluate three "first generation" photochemical air pollution models to determine what modifications or extensions should be made in developing a "second generation" model.

The three models studied were developed during the period 1969 to 1973 under the sponsorship of the EPA:

Type of Model	Developer	EPA Contract
Trajectory	General Research Corporation	68-02-0336
	Pacific Environmental Services, Inc.	68-02-0345
Grid	Systems Applications, Inc.	68-02-0339

None of these models as constituted in mid-1973 appeared to be capable of adequately simulating the physical and chemical processes that occur in a polluted urban atmosphere, hence the motivation for further model development. However, before a second generation model could be developed, certain issues required resolution:

- In view of their different structures, what is the quality of performance of each first generation model when compared with observational data?
- From a theoretical point of view, what is the degree of validity of each modeling approach?
- From a practical point of view, what are the processes that most significantly affect urban photochemical air pollution levels?

Chapters II, III, and IV of this volume describe our efforts to answer these questions. An assessment of past model performance provides some insight into the sources of inaccuracy of the first generation models and, ultimately, an indication of their relative merits. The validity studies we carried out point out some of the fundamental shortcomings of these models. And the sensitivity analyses indicate which physical and chemical processes must be included in the second generation model and to what level of accuracy they must be represented.

Chapter II presents a comparative analysis of the predicted and observed pollutant concentrations in the Los Angeles basin reported by the three developers of first generation models. Owing to the different modes of data usage and model operation, we could not directly compare the results of the three studies; consequently, our analysis was limited to an investigation of some of the statistical properties of predicted and measured values for each study.

The results of the analysis indicate that none of the models can consistently reproduce measured pollutant concentrations such that the residual differences between the predicted and measured values can be ascribed with reasonable assurance to random errors alone. Our investigation of the causes of these discrepancies revealed both inadequacies in the models and inappropriateness of the data base. Specifically, overly simplistic kinetic mechanisms, emissions distributions, and diffusion algorithms all contributed to discrepancies between the predicted and spatially averaged observed values. Even more significant were the results of our comparison of site-specific station measurements with pollutant concentrations calculated using emissions that were averaged over a four square mile area and winds that were interpolated among meteorological stations ten to twenty miles apart. The disparity in scales involved in these comparisons, together with the nonrepresentative locations of the measuring stations, presented major barriers to our evaluation of the relative performance of the models. A true test of model capabilities will require a more suitable data base.

Chapter III discusses the validity of airshed models based on the trajectory and grid approaches. Predictions of both models for realistic but simplified situations were compared with the exact solutions to the full atmospheric diffusion equation. The sources of errors in each of the two approaches were first identified as follows:

Type of Model	Source of Error
Trajectory	Neglect of horizontal diffusion
	Neglect of the vertical component of the wind
	Neglect of wind shear in the vertical direction
Grid	Introduction of numerical errors due to finite differencing

Further calculations showed that for trajectory models errors involved in the neglect of horizontal diffusion were always less than 10 percent, but neglect of the vertical wind component can lead to errors in prediction as great as a factor of 2, and neglect of vertical wind shear, to errors in excess of 50 percent. Numerical errors in the grid model can result in prediction errors as high as 50 percent after more than nine hours of simulation if a conventional second-order finite difference scheme is used.

Chapter IV describes the use of the SAI model as a vehicle to assess the sensitivity of photochemical air pollution levels to relative changes in wind speed, horizontal and vertical diffusivities, mixing depth, radiation intensity, and emissions rate. The results indicate that, in general, the effect of changes in variables on predictions is:

- Highly time dependent, indicating that proper inclusion of the initial pollutant distributions and other time-dependent features is essential in urban airshed modeling.
- Strongly spatially dependent, revealing the importance of adequate spatial resolution in a model. (It should be at least comparable to that of the emissions distribution.)

> Different for different chemical species. The relative sensitivity of predictions to changes in variables or parameters is given in the following ranking (A = most important and D = least important):

Parameter or Variable	CO	NO	O_3	NO_2
Wind speed	A	A	A	A
Horizontal diffusivity	D	D	D	D
Vertical diffusivity	C	C	C	C
Mixing depth	B	B	B	B
Radiation intensity	D	A	A	B
Emissions rate	B	A	B	B

II ANALYSIS OF THE RESULTS OF PAST MODEL VERIFICATION STUDIES

A. INTRODUCTION

Each of the three firms that developed the first generation photochemical air pollution models discussed in this chapter carried out extensive validation studies of its model. The description of each study, the measured and calculated concentration values used, and the statistical analysis of the results appear in the following final reports:

> "Further Development and Evaluation of a Simulation Model for Estimating Ground Level Concentrations of Photochemical Pollutants," R73-19, Systems Applications, Incorporated, Beverly Hills (now in San Rafael), California (February 1973).

> "Evaluation of a Diffusion Model of Photochemical Smog Simulation," EPA-R4-73-012, Volume A (CR-1-273), General Research Corporation, Santa Barbara, California (October 1972).

> "Controlled Evaluation of the Reactive Environmental Simulation Model (REM)," EPA-R4-73-013a, Volume I, Pacific Environmental Services, Incorporated, Santa Monica, California (February 1973).

These reports also contain discussions of the possible origins of the deviations between measured and calculated concentrations.

The objective of the study reported here* was to reevaluate the results of these analyses in light of the additional experience gained over the past two years. Toward this end, we used a self-consistent data base that ties together the three sets of results of these statistical analyses as a basis

*To avoid confusion between SAI's role as one of the three model developers discussed and its role as the evaluator of all three studies, we use the third person reference "SAI" to denote the former and the first person "we" and "our" for the latter.

for discussing the physical, mathematical, and modeling sources of the discrepancies between the measured and predicted concentration values obtained by the three firms. Our discussion draws heavily upon the three final reports cited above for both data and analyses. For convenience, we refer to these reports using the initials of the company (SAI, GRC, and PES) and the corresponding page number.

B. THE DATA BASE

The use of trajectory models by GRC and PES and a grid model by SAI created a disparity in the set of available data points. Based on hourly calculations of pollutant concentrations within 2 x 2 mile squares of a 50 x 50 mile grid, the SAI model produces more data points than do the GRC and PES models. Moreover, the SAI model can essentially reproduce any trajectory reported by PES and GRC simply by giving the concentration values for each square through which the trajectory passes. Given this disparity, we decided to let the size of the data base depend on the nature of the trajectories reported by PES and GRC; the SAI contribution was thus simply a one-for-one match of each of the PES and GRC points.

Unfortunately (or perhaps fortunately, as shown later), PES chose not to present the results of its hour-by-hour predictions along each trajectory, but instead set up its model trajectories so that they would pass near certain measuring stations at preselected times; thus, PES could directly compare the measured and predicted values (PES, p. IV.3). PES tabulated only the values calculated at or near one of these stations (PES, pp. A.2-A.13), though consistent, detailed maps of each trajectory for all hours were presented (PES, pp. A.14-A.19). In contrast, GRC reported predicted concentrations only along its model trajectories. GRC data, presented only in graphics, (GRC, pp. 101-147) may contain small errors from interpolation due to digitization. More significantly, the GRC trajectories were depicted on somewhat free-form maps of various sizes (GRC, pp. 100-146), thus introducing substantial uncertainty in selecting the appropriate SAI grid square to match a given point on a GRC trajectory.

Another type of data used in our evaluation was a set of results produced by the SAI automated input program for the airshed model (SAI, Volume III). These results compare the measured pollutant concentration at a station with the calculated concentration at that station obtained by interpolation from measured values at a set of neighboring stations. Although these results were originally intended to validate the SAI interpolation scheme, the disparities between the interpolated and measured values reveal a general problem in the use of station measurements in such a study, as explained in detail below. In the discussion that follows, we refer to these values as "interpolated station points."

As part of its validation effort, each of the three firms was required to use the available measurement data on pollutant concentrations in the Los Angeles basin for six smoggy days in late summer and early fall of 1969 as the basis of comparison between observed and predicted pollutant concentrations. These data were reported as hourly averages by 10 monitoring stations of the Los Angeles Air Pollution Control District (LAAPCD) scattered throughout the Los Angeles basin. In addition, measurements taken by Scott Research Laboratories were used by GRC (p. 86) and SAI (p. 67) in carrying out interpolation calculations for measured values at nonstation locations; SAI (p. 67) also used data from three stations of the Orange County Air Pollution Control District (OCAPCD) for such calculations. The locations of all of these measuring stations are shown in Figure II-1.

On the basis of these available data, we selected the following types of values for inclusion in the "data base":

- All measured (PESM) and predicted (PESC) concentration values reported by Pacific Environmental Services (PES, pp. A.2-A.13) at each of six stations--Burbank (BURK), downtown Los Angeles (CAP), Pasadena (PASA), Whittier (WHTR), Azusa (AZU), and Pomona (POMA).
- All measured (SAIM) and predicted (SAIC) concentration values reported by Systems Applications (SAI, pp. 102-143) at the six

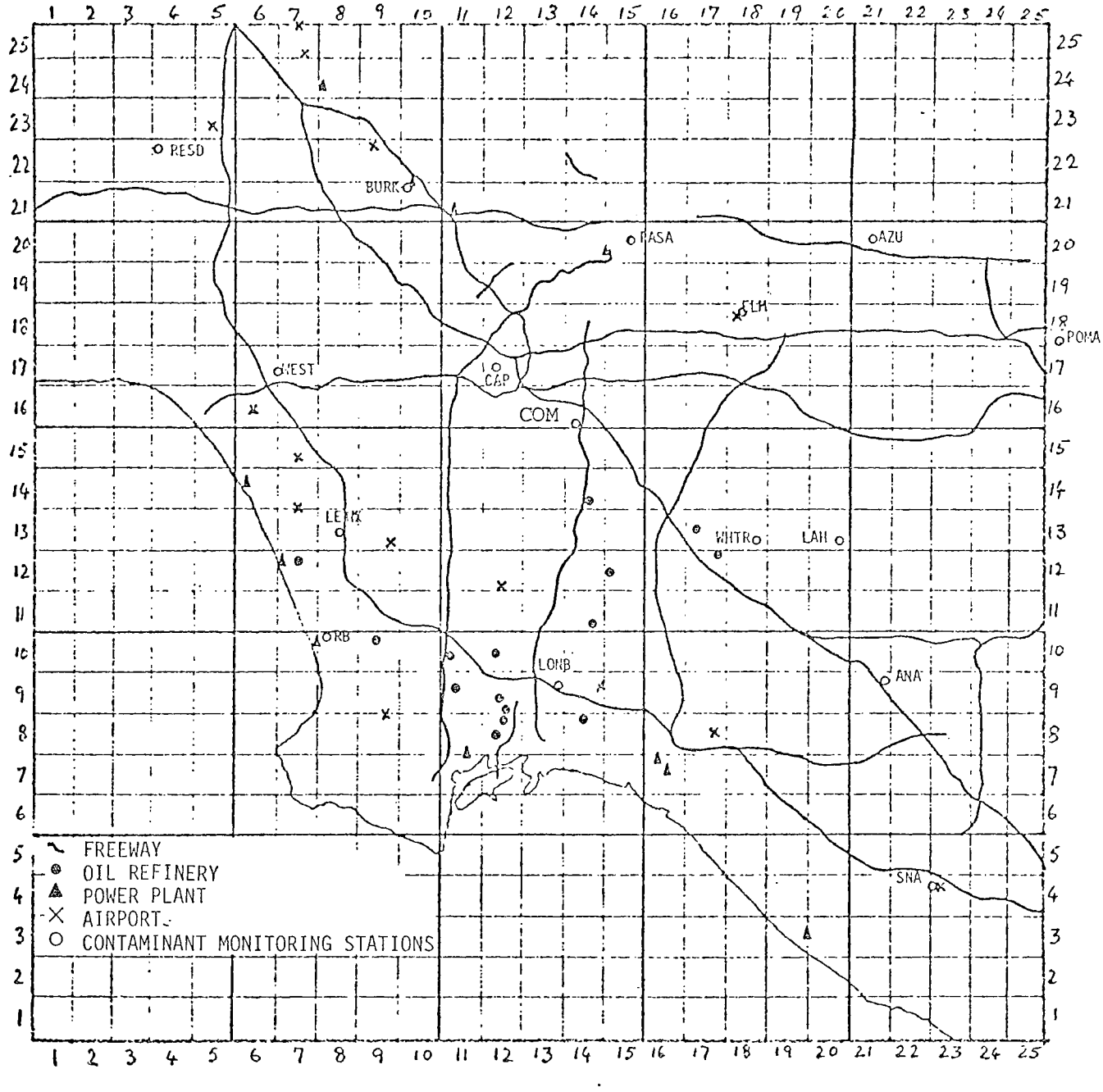

FIGURE II-1. LOCATIONS OF MONITORING STATIONS RELATIVE TO MAJOR CONTAMINANT SOURCES IN THE LOS ANGELES BASIN

stations listed above. SAI reported values for other stations as well, but these six were selected to provide representative coverage for comparison.

- All measured (CORM) and interpolated (CORC) concentration values computed by SAI (unpublished data using programs described in SAI, Volume III) at the six stations listed above (COR is shorthand for correlated station.)
- All interpolated (GRCI) and predicted (GRCT) concentration values reported by General Research Corporation (GRC, pp. 101-147) for each of four trajectories on each day. These trajectory points did not, in general, correspond to station locations.
- All interpolated (SAII) and predicted (SAIT) concentration values computed by Systems Applications (SAI, unpublished data generated using programs described in Volume II) in grid squares corresponding to the four GRC trajectories mentioned above.

In every case, data were collected for all six validation days and for four species--CO, NO, NO_2, and O_3. Hydrocarbon data were not compiled, since neither PES nor GRC reported them; moreover, SAI (p. 40) had serious doubts about the reliability of certain of the measurement data reported by the APCDs.

Direct comparison of these data (i.e., predicted and measured or interpolated values) among the five sets of results listed above was difficult because of discrepancies in the measurement data, differences in the methods used to interpolate for missing data, and wide variations in the reporting of calculated pollutant concentrations among the three investigating firms. Since these factors and the assumptions used strongly affect the significance of the data analysis, they are discussed in detail below.

In addition to the basic set of LAAPCD measurement data used by all three firms, SAI and GRC used data reported for the same days at Commerce and El Monte by Scott Research Laboratories. SAI also used data for La Habra, Anaheim,

and Santa Ana as reported by the OCAPCD. In its evaluation of these data, SAI determined that the measurements carried out by both APCDs were subject to a consistent bias; thus, for NO and O_3, these data were modified by SAI (pp. 39-40) as follows:

$$\text{Actual NO} = \text{Observed NO} \times 1.25$$
$$\text{Actual } O_3 = \text{Observed } O_3 + \text{Observed } SO_2 - 0.2 \times \text{Observed } NO_2$$

The Scott data were obtained using different methods and did not need correction. In addition, the "correction" for ozone at some stations (notably Long Beach, due to the high SO_2 concentrations in that area) was unrealistically large--sometimes resulting in negative concentrations--and thus could not be applied. SAI (p. 39) also pointed out that PAN interferes to some extent with NO_2 measurement and that the pollutant concentration data in general are of no better than ±10 percent precision. Numerous data items are missing, and some of the reported values may be incorrect. An even more serious problem in using the APCD data is the disparity in scales involved in the assumption that the readings at a single point can be compared with predictions having a spatial resolution of four square miles, especially when many of the measuring stations are located near strong emissions sources. This topic is discussed extensively later.

Since the trajectories in the PES and GRC models do not, in general, pass through the measuring stations, it was necessary for each firm to develop an interpolation scheme to project station readings to nearby squares. The ones used by GRC (p. 91) and SAI (Volume III) are similar in concept, but the different algorithms for station acceptance or rejection and the variations in the measured values data base mentioned above introduced some discrepancies. PES chose to accept any point within a five mile radius of a measuring station as being "at" that station (PES, p. A.2); some of the PES outlying data points were adjusted using the SAI interpolation scheme. Even when extrapolations of 30 miles or more were allowed, occasionally no observed data were available to calculate values for some squares or stations; all three firms interpolated these values temporally when needed.

Selection and verification of the calculated data were troublesome. The time of sampling of data varied among all three firms: PES (p. IV.3) used an instantaneous reading (even though the resolution of emissions and meteorological data was no finer than two miles), GRC (p. 82) used an hourly average for the trajectory (which could have passed through as many as four grid squares during the hour), and SAI (p. 59) used an hourly average for each grid square. All PES readings began at 0830 and terminated at 1330, SAI's ran from 0500 to 1400, and GRC used variable run times--with most runs beginning between 0500 and 0800 and terminating in the early afternoon. With the exception of 29 October, PES reported only one or two points for NO_2, NO, and O_3; moreover, these were in the early afternoon, when the NO values had decreased essentially to background levels. Assignment of the trajectories to the rectangular grid was hampered by the lack of a scale on the GRC maps and by the lack of times on the PES maps. Owing to the experimental data adjustments mentioned above, SAI had different initial conditions from those of PES and GRC. GRC reduced the NO emissions encountered along the trajectory path by 75 percent (GRC, p. 96) and adjusted diffusion coefficients and rate constants (GRC, p. 84).

Given all of these incongruences, it is amazing that any sort of consistent data base could be constructed at all. In fact, we did not attempt to create a single set of measured station points or interpolated observations; instead, each firm's sets of measured and predicted values were retained intact for comparison.

This lack of uniformity should in no way be associated with incorrect interpretation of EPA's contract requirements or laxness on the part of any of the contractors in performing their validations studies. Each firm was free to interpret the available data base in any appropriate fashion, and each did indeed create a self-consistent validation study from these data and the model used.

Nevertheless, it is unfortunate that these disparities in the selection of validation methods exist, since any efforts to match the results using the different models immediately generates an "apples versus oranges" criticism. Consequently, we did not attempt to compare across sets, and the ramifications of this inability to make direct comparisons among the models are discussed in the following section.

C. SELECTION OF ANALYSES OF THE DATA

Given the above defined sets of data points, one question summarizes the initial focus of all three studies: How well do the pollutant concentration values predicted by each model represent the actual pollutant concentrations? Unfortunately, the term "actual pollutant concentrations" admits to a variety of definitions, depending on the type of analysis and modeling being done. In particular, the selection of definition is subject to the problem of disparity in scales. This topic has been treated in depth elsewhere (SAI, p. 43); the following is a brief summary of the SAI analysis.

Measurement of meteorological variables and pollutant concentrations is, of necessity, instantaneous in both space and time, as are the chemical reactions that may occur among the various pollutant species. Readings taken at some arbitrary time will not necessarily reproduce those taken five minutes earlier. Similarly, readings taken at some arbitrary location will not necessarily agree with those taken a block away. In an urban area such as Los Angeles, these observations are especially appropriate. Nevertheless, from a purely practical standpoint, it is necessary to make compromises; the ideal of continuous measurements at contiguous locations must give way to the reality of fiscal responsibility in both modeling accuracy and station location and operation. The question then becomes: Given the existence of known or estimated variations in the spatial and temporal distributions of and statistical fluctuations in ambient concentrations, what types of analyses of the data are meaningful, and what sorts of explanations will account for the expected discrepancies?

It is necessary from the start to define the term "representative." The measured value of pollutant concentration from a station is representative of the concentration at that site. The models, however, work from an emissions base that is defined in terms of a 2 x 2 mile square and from meteorological and initial conditions data that represent, on the average, one station for every 25 to 40 square miles. If the smallest area for which a meaningful average pollutant concentration can be calculated is the 2 x 2 mile square, then a station "representative" of the square in which it was located would have to record consistently pollutant concentrations equal to the average values in that square. Thus, we examine next the locations of the stations and the likelihood of their being representative of the grid squares in which they are located.

As previously mentioned, Figure II-1 shows the locations of the monitoring stations relative to the major pollutant sources and the 50 x 50 mile grid of the Los Angeles basin. Table II-1 describes the physical site of each station and the expected effect of that location on the representativeness of the station readings. It can readily be seen that the majority of the stations are exposed to relatively high emissions, with respect not only to the basin as a whole, but also to the 2 x 2 mile grid square containing the station. Since vehicular emissions are the major single source of pollutants in the areas of most monitoring stations, one might expect that locally high readings of the directly emitted pollutants, CO, NO, and hydrocarbons, would be observed near major roadways and that the chemically formed pollutants, NO_2 and O_3, would be underrepresented.

Some stations are located so as to be representative of the grid squares in which they are situated; in fact, some of them may even underrepresent their areas (in terms of primary pollutant concentrations) under certain meteorological conditions. Viewed basin-wide, the readings from these stations tend to "temper" the readings from those stations that are more heavily influenced by vehicular traffic. This leads to the occurrence of an interesting phenomenon whenever measurement data are prepared for grid squares that do

Table II-1

LOCATION OF CONTAMINANT MONITORING STATIONS OF THE LOS ANGELES AIR POLLUTION CONTROL DISTRICT

Station Number	Code Name	Approximate Location	Expectation of Local Effects
1	CAP	Surrounded by four freeways 1500 meters from each. Sampling probe is suspended outside a sixth-floor window.	Strong.
60	AZU	600 meters north of the Foothill Freeway.	Mild.
69	BURK	150 meters southwest of the Burbank power plant and 300 meters southwest of the Golden State Freeway.	Strong.
71	WEST	400 meters northeast of the San Diego Freeway and 400 meters north of the Santa Monica Freeway.	Strong--predominant southwesterly winds during the day.
72	LONB	200 meters north of the San Diego Freeway.	Strong--predominant south winds during the day.
74	RESD	3000 meters north of the Ventura Freeway.	None.
75	POMA	500 meters south of the San Bernardino Freeway.	Mild.
76	LENX	Immediately west of the San Diego Freeway and immediately southeast of Los Angeles International Airport.	Strong.

Table II-1 (Concluded)

Station Number	Code Name	Approximate Location	Expectation of Local Effects
78	RB	300 meters northeast of the Redondo Beach power plant. The station measures only SO_2.	Moderate.
79	PASA	2000 meters east/northeast of the Pasadena power plant.	Mild for SO_2 measurements during the day.
80	WHTR	On a main street--no other major sources nearby.	Mild.
91	LAH	Near Beach Boulevard and the Imperial Highway, both of which carry very light traffic in this area.	None.
92	ANA	Immediately northwest of the Santa Ana Freeway.	Strong--predominant south-westerly winds during the day.
93	SNA	Orange County Airport, 400 meters south of the San Diego Freeway.	Moderate--from aircraft and vehicular emissions.
98	COM	Immediately west of the Long Beach Freeway and 1500 meters south of the Santa Ana Freeway.	Strong.
99	ELM	El Monte Airport, 1500 meters north of the San Bernardino Freeway.	Mild.

not contain a monitoring station: The pollutant concentration values obtained by interstation interpolation for a grid square may be more representative of that square than are the direct readings from a station within the same square. In other words, a distribution of the (weighted) readings from several stations of various degrees of representativeness over a large area is more likely to approximate the results obtained from the determination of an "average" value for the pollutant concentration within a 2 x 2 grid square than would the reading from a single, and probably nonrepresentative, monitoring station in the absence of complex topographical features.

Pollutant concentrations reported by the monitoring stations were used as inputs to the models under discussion. All three models used station readings (or, more often, interpolations among stations) to determine initial conditions; in general, the significance of these values was attenuated by the contribution from the emissions over the first few hours of the morning. SAI also used station readings in the calculation of boundary conditions, but the reported values were reduced (SAI, Volume III) to represent the presumably lower pollutant concentrations at the border squares. The models relied mainly on the emissions inventory (averaged over each grid square) and the meteorology (smoothed into integral isotachs and streamlines), coupled with chemical reactions, to calculate pollutant concentrations. No pretension was made of presenting anything other than average values over the grid square area. If a model is expected to reproduce accurately a reading from an admittedly nonrepresentative monitoring station, it must carry out the calculations at the subgrid-scale level; none of the models under consideration have this capability.

The concept of subgrid-scale modeling is dealt with more fully in Volume III of this report, but it is important here to recognize the implications of dealing with nonrepresentative monitoring stations in attempting to analyze the validation results presented in each final report. The question is not how well the calculated values agree with the measured ones, but rather, how well the calculated values reflect the trends of the measurement data, and whether it is possible to explain discrepancies between measured and calculated values in terms of the general characteristics of those measurements. The

chances are that calculations that agree too closely with measurements should be looked upon with a certain amount of suspicion, lest the modeling process might be degenerating into an exercise in glorified curve-fitting!

Despite the above warnings about the nonrepresentativeness of the measurement data, several statistical analyses were worth performing on these validation results, if only to demonstrate that the conjectures about station sites were correct and that significant data trends exist. They are described below.

> The correlation coefficient

$$\beta = \frac{\sum_{i=1}^{I} (x_i - \bar{x})(y_i - \bar{y})}{\left(\sum_{i=1}^{I} (x_i - \bar{x})^2 \sum_{i=1}^{I} (y_i - \bar{y})^2 \right)^{1/2}}$$

is a measure of how well the values of x and y tend to follow one another in their peregrinations about their means; i.e., do the calculated and measured values show the same trends?

> The deviation

$$\sigma_d = \left[\frac{\sum_{i=1}^{I} (x_i - y_i)^2}{I-1} \right]^{1/2}$$

is a measure of the variation between the calculated and observed concentrations; this measure provides an absolute value for the discrepancy between the two sets of data.

> The goodness-of-fit statistic can be expressed as

$$\chi^2 = \sum_{i=1}^{I} \frac{\left[f(x_i - y_i) - fr_i\right]^2}{fr_i}$$

where

$f(x_i - y_i)$ = number of occurrences of the observed residuals $x_i - y_i$ within a given interval,

fr_i = number of occurrences of a similar residual r_i from a normal distribution with the same mean and standard deviation as the observed set of residuals,

I = number of intervals.

When compared with the expected chi-squared value for a given probability level, the goodness-of-fit statistic indicates whether the predicted values can be considered to have been randomly drawn from the distribution defined by the measured values.

> Scatter plots of predicted versus measured values graphically illustrate the tendency of the model to under- or over-predict the concentration values.

> Residual plots show trends in the deviations between predicted and measured values; four are of particular interest:

- Histogram--the number of occurrences of each residual value.
- Time series--variation of the residual values with time of day.
- Prediction--variation of the residual values with the size of the predicted value.
- Observation--variation of the residual values with the size of the measured values.

Each of the above types of statistics is useful in describing a particular facet of the behavior of the models. By measuring trends, the correlation coefficient allows an assessment of the capability of the model to respond to changes in pollutant concentrations, even if the calculated and measured concentrations are not identical because of some other defect in the model. The deviation shows how well, in an absolute sense, the model is matching its predicted values with the measured ones. The chi-squared statistic permits determination of whether the differences between predicted and measured values can be considered to be attributable to chance or are statistically significant and thus indicative of a flaw in the model. The plots are particularly useful in assessing the accuracy of the models and the nature of the errors. The results of statistical tests are relatively insensitive indicators of model performance because of the limited quantity of data, the varying conditions and assumptions, the nondistributional character of the data, and the complexity of the potential sources of error. One should not substitute statistical analysis results for an examination of the plots.

Theoretically, the analyses described above could be applied to a comparison of any two sets of data from this study. Realistically, for reasons delineated earlier, we felt that comparison of results from the three different models, though feasible, would not be justified; the temptation to declare one model "better" than another could become irresistible despite warnings about incongruent data sets or incomparable assumptions used to obtain such results. Therefore, the only comparisons we made involved, in every case, sets of predicted and measured (or interpolated) values as reported by a single firm using a particular set of assumptions.

However, one set of comparisons, although indirect, is highly pertinent to the disparity in scale arguments presented above. Because PES, even though it used a trajectory model, chose to present its results as station-based (i.e., grid-point) data, it was necessary to create two sets of results for

the SAI model--one set for PES station locations, and another for GRC trajectories. Since the same SAI model, operating under the same set of assumptions, was used to calculate these values, we could do a legitimate comparison of the results of the statistical analyses of these two types of data. To the extent that they differed, we could hypothesize relationships between these differences and the disparity in scales between the station (point) measurements and the trajectory (square-average) measurements. Again, we stress that, because of the differing assumptions of the three contractors, no direct comparison of model could be made; only the availability of both "station" and "trajectory" values for the SAI model enabled the secondary effect of disparity in scales to be addressed.

The availability of the interpolated station points offered additional aid in the evaluation of the contributions of disparity-in-scales and nonrepresentativeness to discrepancies between predicted and measured values for all three models. In the ideal case, there would be a smooth continuum of pollutant concentrations throughout a region. Given this assumption, it should be possible, through distance-weighted interpolation, to calculate the concentration at any point from the observations at a representative set of well-spaced measurement stations within that region. Similarly, it should be possible to calculate the expected concentration at the site of a particular measuring station by eliminating that station from the interpolation process. The extent to which a value obtained by this interpolation process differs from that actually measured at the station reflects the questionability of the assumptions of representativeness of the station measurements and the validity of the assumptions that underlie the interpolation scheme. More particularly, it should not be expected that the statistical results for those models that depend on interpolation of station measurements for either input or comparative data would be any better than that demonstrated by the station interpolation statistics themselves.

D. RESULTS

1. Data Set Selection

Using the five types of data listed earlier, we calculated the statistics and plotted the deviations at three levels of detail. The finest level represents the comparison of predicted and measured (or interpolated, in the trajectory model case) concentration values for each of the four pollutants at each of the six stations (or along each of the four trajectories) on each of the six days represented by each of the five sets of results--a total of 720 runs. Although we obtained significant findings at this level, we do not present them in this report. The small number of data points per run, the repetitiveness of the plots and statistics, and the sheer bulk of information (3600 pages) do not justify their reproduction. Instead, a single copy of the entire computer printout will be forwarded to the EPA for researchers who may be interested in the fine details of the analysis.

By combining the individual data sets described above, we reduced the number of sets for analysis. Two such combinations were made: all stations or trajectories for each day and all days for each station (since the trajectories themselves were nonreproducible from day to day, they could not be combined). These combinations gave rise to a total of 192 runs--again, too many to include in this report (a single copy of the computer printout will be sent to the EPA).

By combining the composite data sets described above, we reached the third and most inclusive level. At this level, there was a single data set for each pollutant from each of the five sets of results; each of these 20 data sets contained from 50 to 350 points. From a statistical point of view, these were the most significant sets for interpretive work. However, the large number of points tended to obscure some of the graphical results, especially when multiple points with the same value overprinted one another. These results are dealt with in detail below. The bulk of the discussion centers on the statistical and graphical picture they portray.

2. Statistical Analysis

Table II-2 presents the statistical analysis of the validation results for all dates at all stations. In this table, the "standard chi-squared value" represents the level at which there is a 90 percent probability that the residuals could have been drawn from a normal distribution. The discussion begins with the emitted primary pollutants CO and NO, followed by the secondary reaction products NO_2 and O_3.

Carbon monoxide is an "inert" species in the sense that any chemical reactions it undergoes are slow relative to its dispersion by winds and diffusion. Thus, the CO results present a clearer picture than do those of the other species of the effects of disparity in scales and nonrepresentativeness of the measuring station locations on the comparison of predicted and measured values. As shown in Table II-2, the correlation coefficients for all sets of CO data are quite high, indicating that the models were able to predict trends in the concentration values fairly well. It is especially significant that the highest correlation coefficient was associated with the SAI station results. As shown later, the SAI model did very well in relating emissions and meteorology to CO concentrations, except during the morning rush hours, when the model consistently underpredicted the high CO concentrations. If one assumes that most of the monitoring stations, owing to their roadside locations, were measuring anomalously high CO concentrations from engine emissions that had not yet dispersed evenly over the grid area, this underprediction would be expected.

The results from the models were better, in all respects, than those obtained using the input station correlation calculation for interpolation. Since CO emissions arise almost solely from automobile traffic, measuring stations generally tend to over- or under-represent their grid squares, depending on whether they are downwind or upwind of the most heavily travelled streets in their vicinity. If the location of a station with respect to the CO dispersion were not similar to that of neighboring stations, we would expect

Table II-2

STATISTICAL ANALYSIS FOR ALL LOCATIONS

Species	Data Analyzed	Correlation Coefficient	Deviation σ_d	Degrees of Freedom	Measured Chi-Squared	Standard Chi-Squared
CO	PESC	0.68	4.27	7	10.33	12.02
	SAIC	0.84	3.52	7	81.38	12.02
	CORC	0.64	4.61	9	67.96	14.68
	GRCT	0.82	3.39	6	29.37	10.64
	SAIT	0.79	3.18	6	30.39	10.64
NO	PESC	0.77	3.18	--	--	--
	SAIC	0.87	9.13	10	170.67	15.99
	CORC	0.63	13.90	13	110.30	19.81
	GRCT	0.87	8.70	7	54.48	12.02
	SAIT	0.86	8.13	7	56.81	12.02
NO_2	PESC	0.68	8.36	1	0.96	2.71
	SAIC	0.65	6.82	11	72.47	17.27
	CORC	0.33	8.14	17	27.22	24.77
	GRCT	0.43	10.05	8	39.57	13.36
	SAIT	0.52	12.62	7	108.66	12.02
O_3	PESC	0.50	8.26	1	0.96	2.71
	SAIC	0.60	8.56	13	38.66	19.81
	CORC	0.80	5.32	11	167.36	17.27
	GRCT	0.91	3.82	3	45.32	6.25
	SAIT	0.69	8.75	5	39.84	9.24

large discrepancies in predictions of CO concentrations at that station on the basis of those measured at neighboring stations. However, the models were able to use the variations in emissions and meteorology in the vicinity of, though not necessarily adjacent to, the station. To the extent that the winds and emissions are known within a 2 x 2 mile square, they are better determinants of a point measurement within that square than are the point measurements from stations 5 to 10 miles distant.

A similar effect appeared in the comparison of the PES and GRC results for CO. One major difference between the PES and GRC models is the partitioning by GRC of the moving column of air: The former used a single cell containing the entire column, whereas the latter divided the column into several superimposed layers. By keeping fresh emissions near the ground, the GRC model was better able to follow significant rapid changes in CO concentrations (e.g., during and after the morning rush hour) and thus to simulate more closely the environment sensed by the network of CO monitoring stations. The dispersion artifact intrinsic to the PES model, coupled with the acceptance, for comparison purposes, of any trajectory that passed within five miles of a station, considerably increased the effective volume over which the CO concentration was being averaged and thus the disparity in scales between this calculation and the point measurement.

The results of the chi-squared calculations clearly demonstrate the effects of the nonrepresentativeness of the station measurements and the problem of disparity in scales. As shown in Table II-2, the only set of values that met the 90 percent chi-squared criterion is that of PES. Relatively, the PES results met the chi-squared criterion better than either the correlation coefficient or the deviation. In the PES model, uniform mixing over a five mile radius and the entire column height was assumed, and the model is usually executed from 0830 onward, thus missing the major CO peak. The greater averaging and the elimination of some of the high values apparently enabled the differences between measured and calculated values to be normally distributed while not greatly improving the ability of the model to match trends in the data or to reduce the deviations significantly. Moreover,

since the simulation began near the peak in CO concentrations, the model had to reproduce only the slow descent from the morning peak to the midday plateau in concentrations. In other words, no particular stress was placed on the model's capability to follow rapidly changing emissions patterns and the corresponding CO peak.

The contrast between the chi-squared values for the trajectory-type (GRCT and SAIT) and the station-type (SAIC and CORC) calculations is striking. Although neither was able to satisfy the 90 percent criterion, the former values were significantly lower than the latter. The difference can most readily be ascribed to the contrast between the attempt to match values calculated for 2 x 2 mile grid square averages with (1) the point measurements from the stations, which are likely to yield large and--since the station measurements tend to be high rather than low with respect to the predictions--nonrandomly distributed residuals, and (2) the interpolated, and, therefore less disparate in scale, "measured" values used in the trajectory comparisions. This conclusion is supported by the residual plots and the high SAIC correlation coefficient, indicating that trends can be reproduced well by both types of models and that the discrepancy lies in the estimation of the overall magnitudes.

Turning next to the results for NO, the reader can see that the distribution of correlation coefficients is quite similar to that for CO. Like CO, NO is a primary emissions species; and for those monitoring sites that are not representative of the grid squares, much of the discussion above for CO pertains also to NO. However, major differences in behavior between NO and CO affect this analysis. First, NO is emitted in significant amounts from power plants, refineries, and other large point sources. Since most of these sources are distant from any of the measuring stations, these emissions tend to become reasonably well dispersed throughout the grid squares in which stations are located. Thus, the problem of disparity in scales pertains only to that portion of NO emitted by automobiles, and the point readings can be expected, by and large, to better reflect the average NO concentrations within the corresponding grid square. The generally high correlation coefficients for NO, compared with those for CO, may be partially ascribable to this "smoothing" effect.

The second, and more significant, difference between NO and CO is the greater chemical reactivity of NO. Because NO is more reactive and because its reaction times are short relative to the hourly averaging process used in data reporting and modeling, the chemical kinetic mechanism and rate constants chosen for use in each model strongly affect the calculated NO (and, correspondingly, NO_2 and O_3) concentrations. As demonstrated elsewhere in this report, the mechanisms used in all the models are inadequate to represent the formation process of photochemical smog in both temporal (time to reach peak concentrations) and quantitative (concentrations of key species) senses. Thus, errors in the calculated concentrations of NO (and the reaction products NO_2 and O_3) can be anticipated, as borne out by the standard deviation and chi-squared calculations for both the SAI and GRC models.

The low PES and high COR deviations (σ_d) deserve special comment. Almost all the PES calculations were reported only for midday conditions, when NO concentrations had decreased to their background level of 1 pphm; thus, the relatively low deviations represent essentially background concentration calculations. In contrast, the SAI and GRC calculations were spread throughout the day, including the morning hours when NO concentrations were on the order of 40 pphm; thus, they generated significantly higher, but statistically more valid, concentrations and much more meaningful predictions for evaluation.

The high value for station interpolation reflects to some extent the high chemical reactivity of NO. NO, once released by an emissions source, does not persist in an ozone-containing atmosphere but rather is rapidly oxidized to NO_2. Thus, during a major portion of the day, only insignificant amounts of NO generated near a given station are carried downwind and can be detected at another station. As a result, if one station is in an area of high emissions and some of its neighbors are in areas of low emissions, any attempt to project the neighboring values into the area of high

emissions is bound to produce a low result; similar problems arise when a low-emissions area is adjacent to several areas with high emissions. The models all include methods of taking the reactivity of NO into account and of thereby "damping out" the downwind transport. The interpolation scheme, which is much simpler than the models, projects the inappropriately high or low numbers to nearby stations. Of the four pollutants studied, NO and its reaction product NO_2 show this anomalous behavior most strongly; the inert CO and the regenerative reaction product O_3 are dispersed throughout the basin, and less steep concentration gradients between stations are encountered for these two species.

Owing to the poor statistics for the distribution of NO residuals from the PES model (almost all of the measured and calculated values were at the background level of 1 pphm), the chi-squared value could not be calculated. The station and trajectory values from the SAI and GRC models show behavior similar to that demonstrated for the CO values, in that the chi-squared statistic for the station values is higher. The reasoning given for CO holds here: The smaller disparity in scales between calculated and interpolated values provides a more random distribution of residuals. The proportionately higher numbers compared with those measured for CO are probably due to biases introduced by the inadequacies in the chemical mechanism.

Since NO_2 is a secondary product of combustion, formed almost entirely from emitted NO, a fair amount of mixing and dispersion of the NO will have occurred by the time it is converted to NO_2. Thus, station readings of NO_2 concentration are likely to be more representative than the corresponding readings for NO. Assuming that their chemical mechanism submodels are reasonable approximations of the smog formation process, the models should provide better estimates of the values that are both read by the stations and obtained by interstation interpolation. The high chi-squared value for the GRC model may indicate a systematic bias in the kinetics mechanism; see the comments below on ozone. The PES values again are clustered around midday, and the chi-squared statistic is probably unrepresentative.

The correlation coefficients for NO_2 are uniformly lower than those for NO. This result can be readily accounted for since the NO curves for concentration as a function of time at most stations start high and fall to background levels in a reasonably smooth manner, whereas the corresponding NO_2 curves tend to pass through a maximum and then oscillate around a fairly high afternoon concentration value. Since the correlation coefficient measures the extent to which the measured and predicted values follow the same trends, the models all encounter extreme difficulty in attempting to reproduce the contours of these curves.

Turning finally to the ozone results in Table II-2, we note several significant points. The exceptionally good GRC values are a direct result of GRC's intent (p. 91) to achieve a good ozone fit, even at the expense of fits involving other species. To reach this goal, GRC (p. 84) used three of the six validation days for "calibration" of the model, altering certain parameters to improve the agreement between the measured and predicted concentration values. Such a "hands-on" process is useful and easily achieved with a trajectory model, and the EPA specified in its statement of work that up to three of the six days could be used for this purpose. As demonstrated elsewhere in this report, the simple chemical kinetics mechanisms used in these validation runs do not properly account for the behavior of concentration as a function of time of both ozone and oxides of nitrogen. Since oxidant concentration standards are the ones most often exceeded during pollution episodes, GRC's choice to concentrate its "tuning" on ozone production is reasonable. However, even GRC's efforts to better represent the ozone concentration did not bring the chi-squared value within the 90 percent confidence level. This failure again indicates the inadequacy of the chemical mechanisms used to deal with the formation and distribution of a highly reactive secondary pollutant such as ozone.

Equally striking are the results of the station interpolation (CORC). For species other than ozone, the interstation correlation results ranked near the bottom in terms of their correlation coefficients and deviations σ_d.

For ozone, the results were better than all but the finely tuned GRC results. The reason for such exceptionally good results for ozone lies in the nature of the "chemical stew" that produces this pollutant. The initial ingredients of this "stew"--hydrocarbons and nitric oxide--are prepared during the morning rush hour. The morning winds tend to disperse these ingredients throughout the basin, but the winds are too weak to blow them out of the basin; moreover, the previous day's pollutant load, which drifts out to sea overnight, is returned to the basin by light onshore winds. Under the influence of the catalyzing effect of sunlight, ozone begins to form; but its relatively slow reaction rate, combined with the continued presence of NO, keeps the concentrations low. Only several hours after the emissions peak occurs do appreciable amounts of ozone appear. Since, during this time, the ingredients have become reasonably well dispersed, the ozone is also dispersed. Moreover, in areas of abnormally high hydrocarbon emissions, such as those near several monitoring stations, where one can presume that ozone would be formed at a faster rate, the higher concentration of NO acts as a scavenging agent. Thus, station readings in high emissions areas are likely to slightly underrepresent ozone concentrations.

In light of this dispersed and relatively constant ozone concentration, it is not surprising that station correlation is so successful. Most of the stations in a given area provide readings representative of the average grid square concentrations, and the concentration gradients between areas are small. Also, the nature of the ozone reaction kinetics tends to smooth out any irregularities in pollutant concentrations. The three models, however, must rely on the inadequately known kinetic mechanisms in their attempts to calculate ozone concentrations, since ozone is a secondary product only tenuously related to the emissions pattern that enables the models to do so well for CO.

The high chi-squared statistic for COR is a consequence of the distribution of the measured values. Most of these values are low and fairly uniform throughout the basin, but occasionally in the afternoon one or two stations show high values. When these values are used to calculate concentrations at other stations, the residuals (measured minus calculated values) are always negative. It is this negative "hump," coupled with the few large positive values when those anomalous station concentrations are calculated, that produces the large chi-squared value.

3. Scatter Plots

Plots of measured versus calculated concentrations (i.e., "scatter plots") for each of the five sets of CO results are presented in Figures II-2(a) through II-2(e). Similar results for NO appear in Figures II-3(a) through II-3(e); for NO_2, in Figures II-4(a) through II-4(e); and for O_3, in Figures II-5(a) through II-5(e).

At first glance, the PES, GRC, and SAI trajectory results shown in Figure II-2 for CO generally appear to be randomly distributed about the 45° line. However, the SAI and correlated station results definitely indicate a trend toward measured concentrations larger than the predicted values. A more detailed examination of the PES, GRC, and SAI trajectory results shows, moreover, that a similar tendency is also present at high measured concentrations (say, greater than 12 ppm). Similar but more highly skewed behavior is shown in the NO scatter plots (Figure II-3).

Both CO and NO are primary emissions products that arise principally from automobile exhaust. Possible reasons for the underprediction of their concentrations, especially near the measurement stations, include measurement inaccuracies, overestimation of vertical transport, and underestimation of emissions rates. More likely, the consistent prediction of concentrations lower than the measured values at high observed concentrations results from the disparity in spatial scales between measurements (on the order of tens of meters) and predictions (on the order of 3000 meters). These results provide additional evidence that microscale models must be further developed to provide an adequate means of comparing airshed model predictions with point measurements.

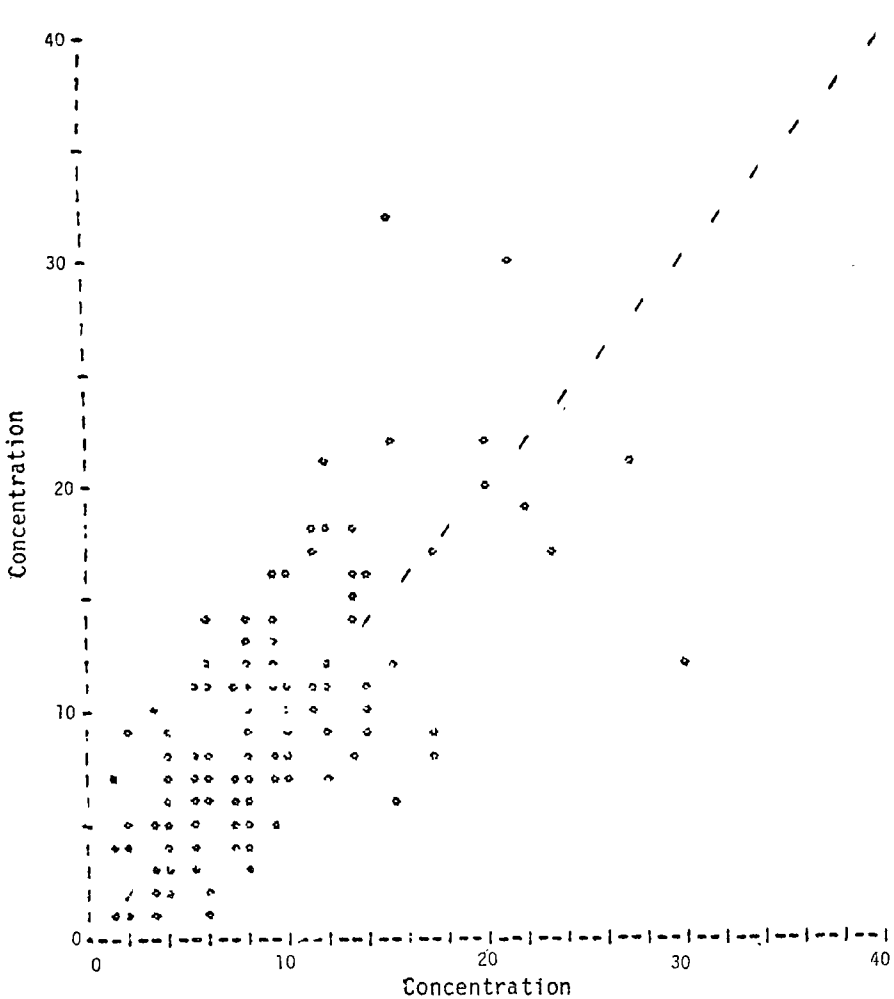

(a) PES--Horizontal Axis = PESC,
Vertical Axis = PESM

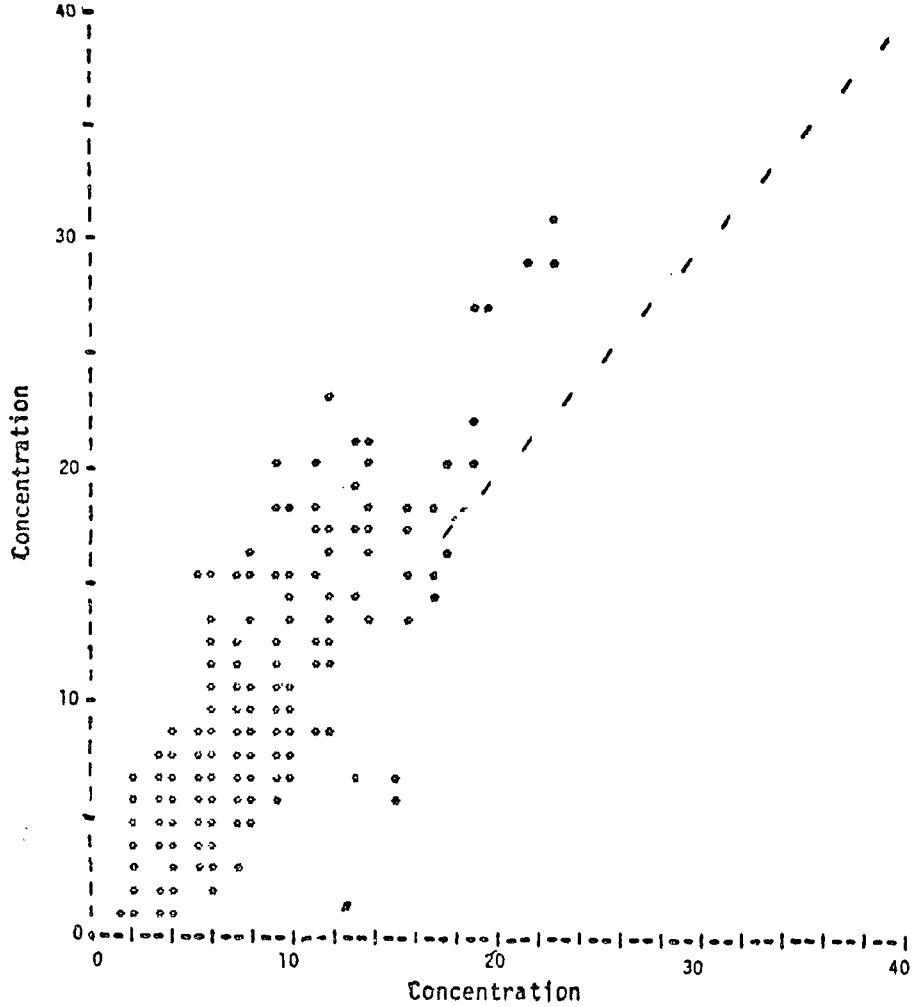

(b) SAI--Horizontal Axis = SAIC,
Vertical Axis = SAIM

FIGURE II-2. SCATTER PLOTS FOR THE CO RESULTS

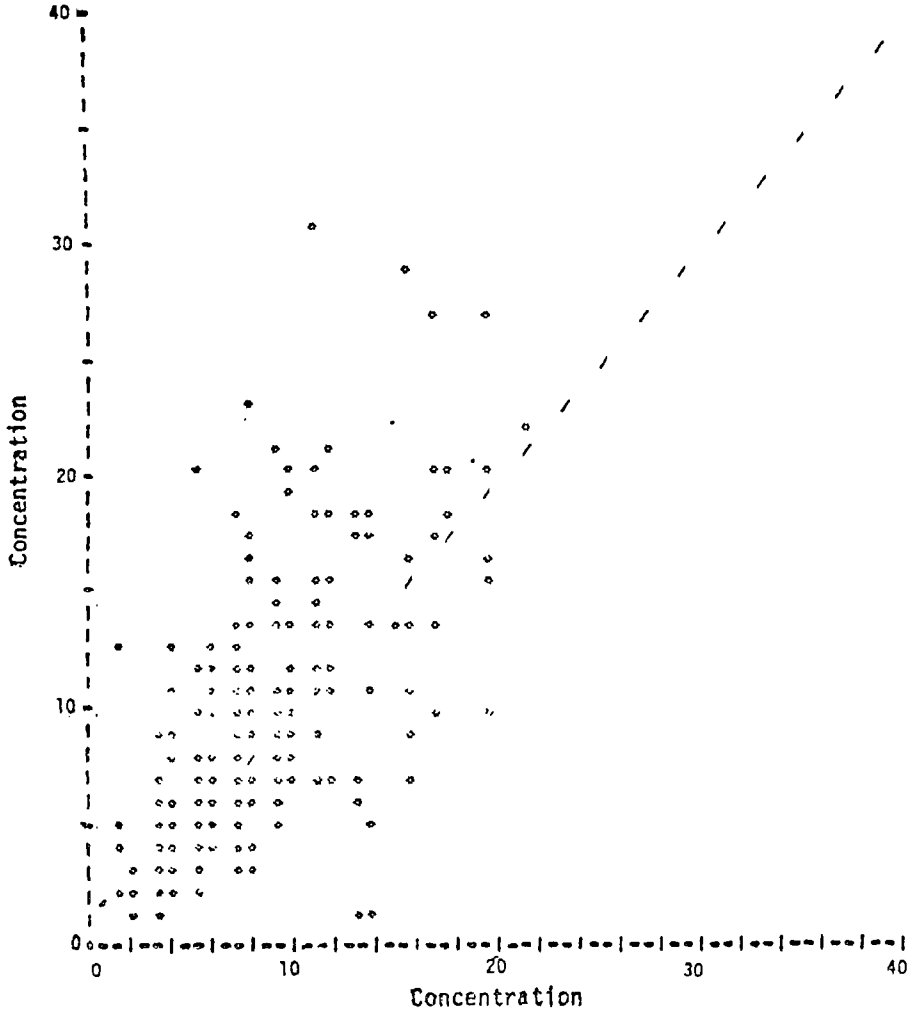

(c) Correlated Station--Horizontal Axis = CORC, Vertical Axis = CORM

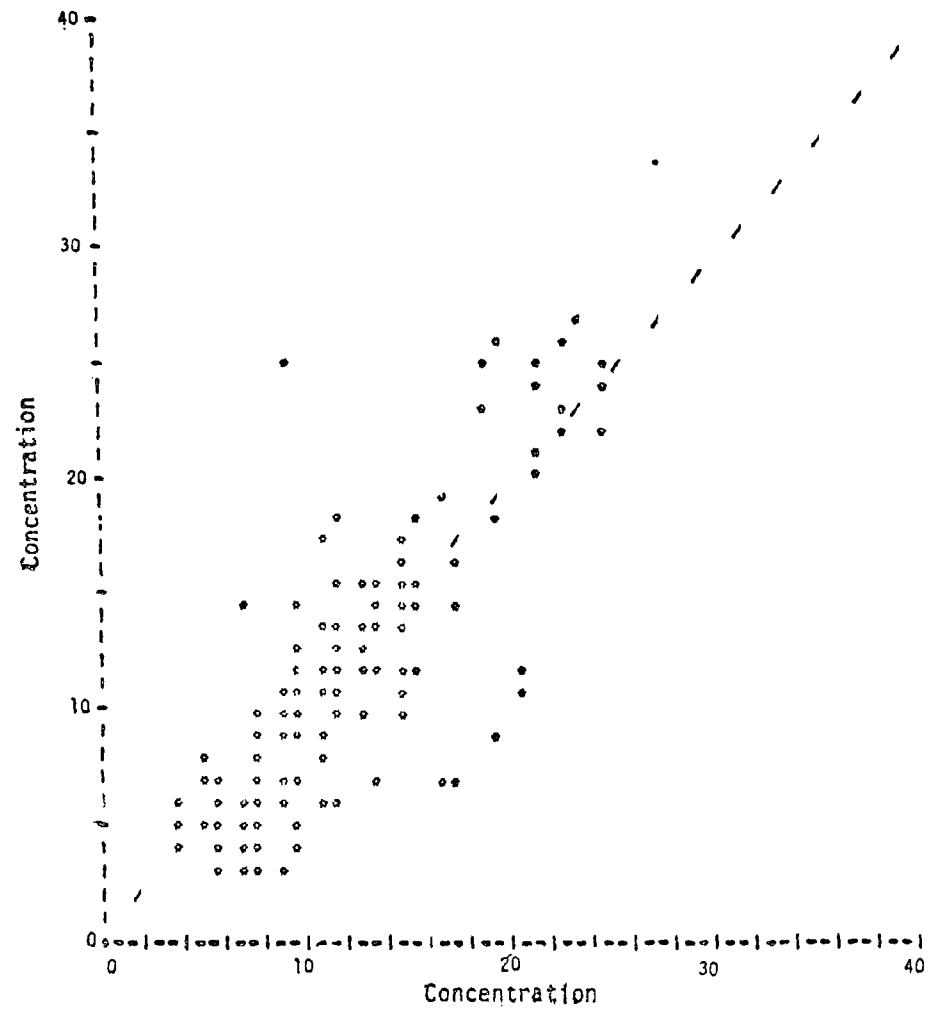

(d) GRC--Horizontal Axis = GRCT, Vertical Axis = GRCI

FIGURE II-2. SCATTER PLOTS FOR THE CO RESULTS (Continued)

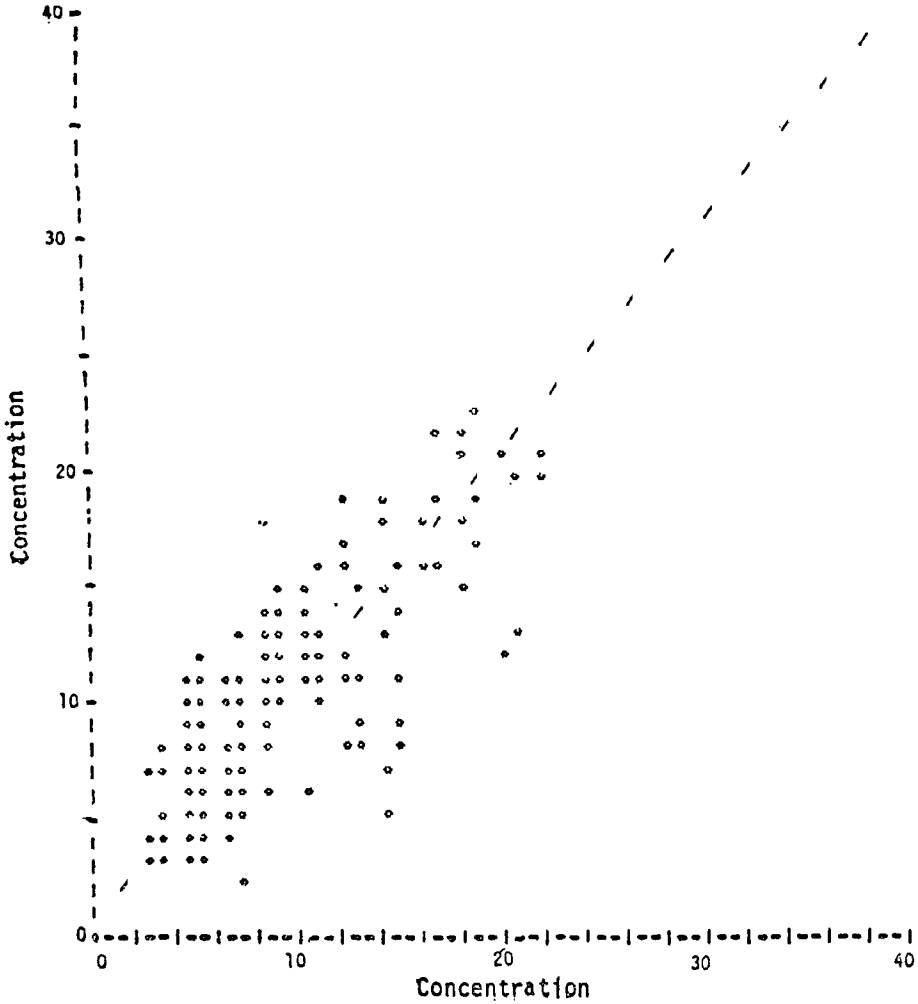

(e) SAI--Horizontal Axis = SAIT,
Vertical Axis = SAII

FIGURE II-2. SCATTER PLOTS FOR THE CO RESULTS (Concluded)

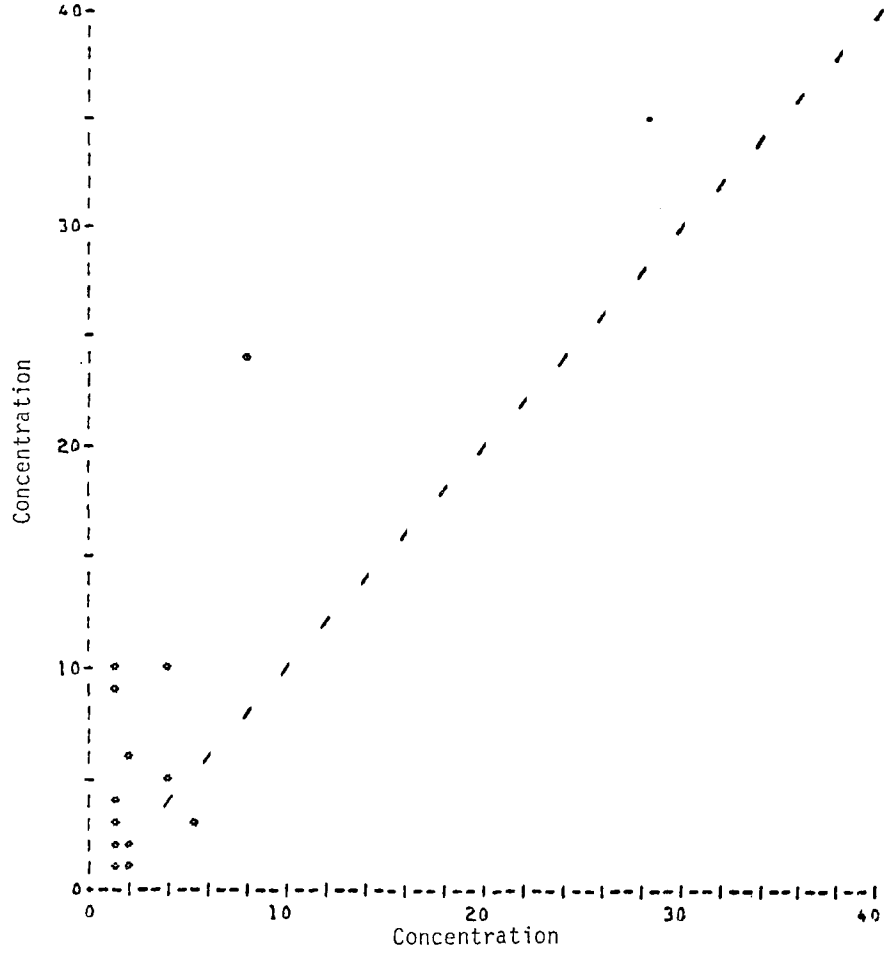

(a) PES--Horizontal Axis = PESC,
Vertical Axis = PESM

FIGURE II-3. SCATTER PLOTS FOR THE NO RESULTS

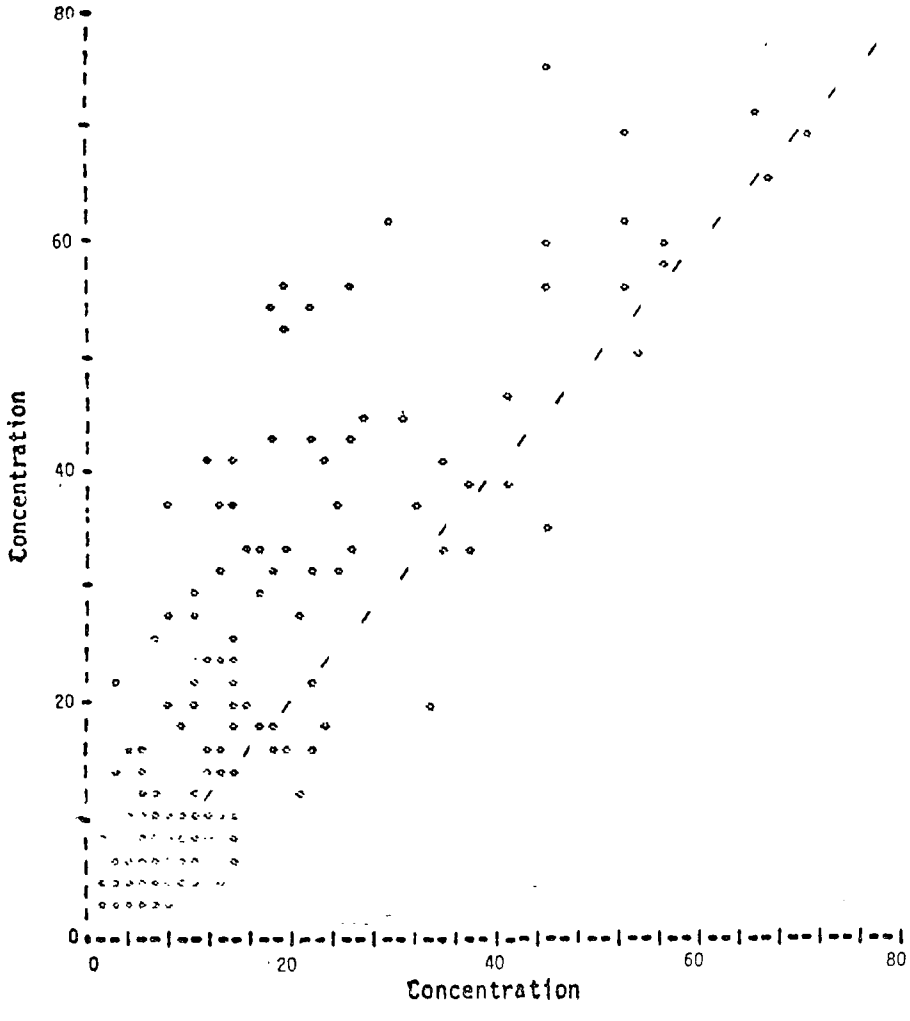

(b) SAI--Horizontal Axis = SAIC, Vertical Axis = SAIM

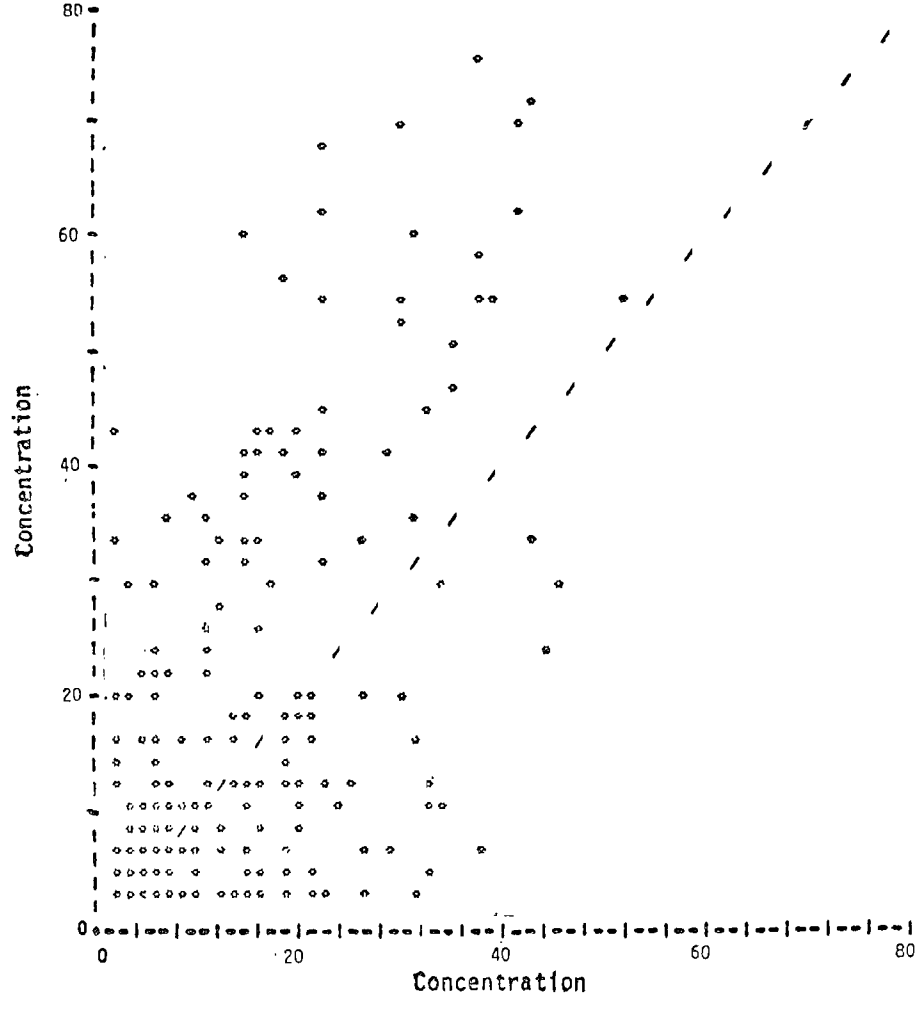

(c) Correlated Station--Horizontal Axis = CORC, Vertical Axis = CORM

FIGURE II-3. SCATTER PLOTS FOR THE NO RESULTS (Continued)

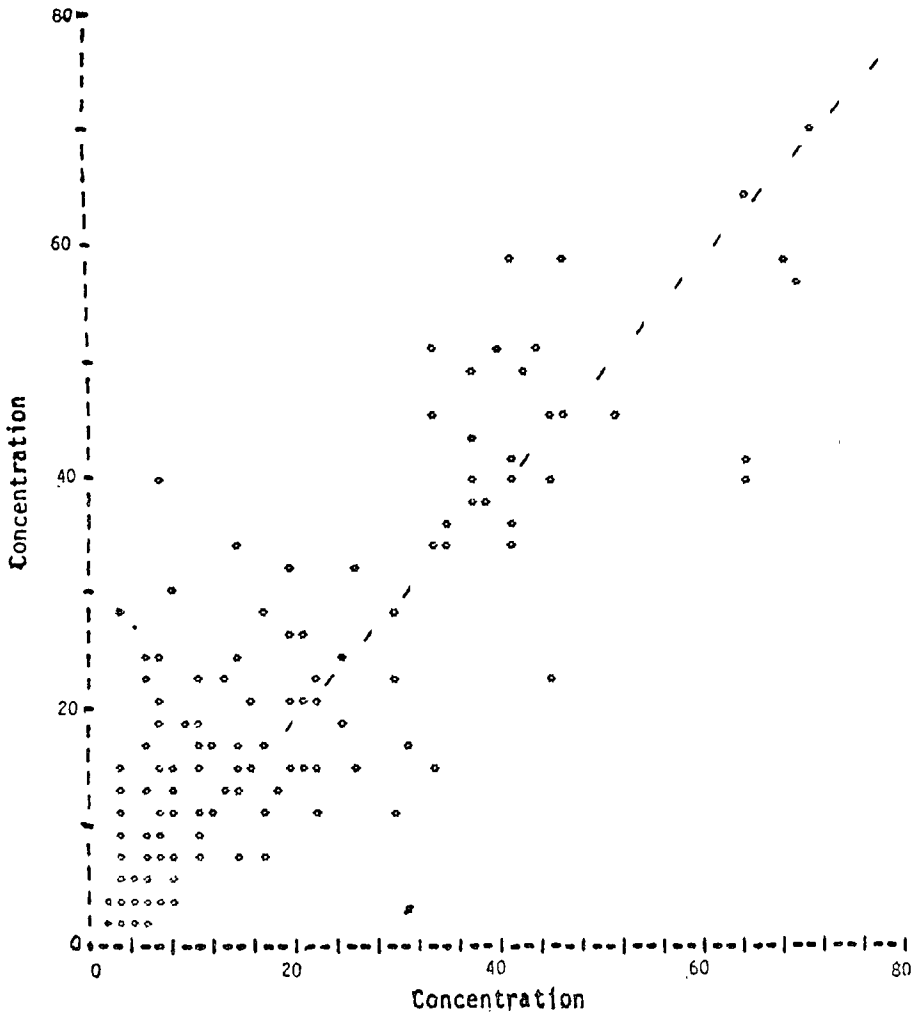

(d) GRC--Horizontal Axis = GRCT, Vertical Axis = GRCI

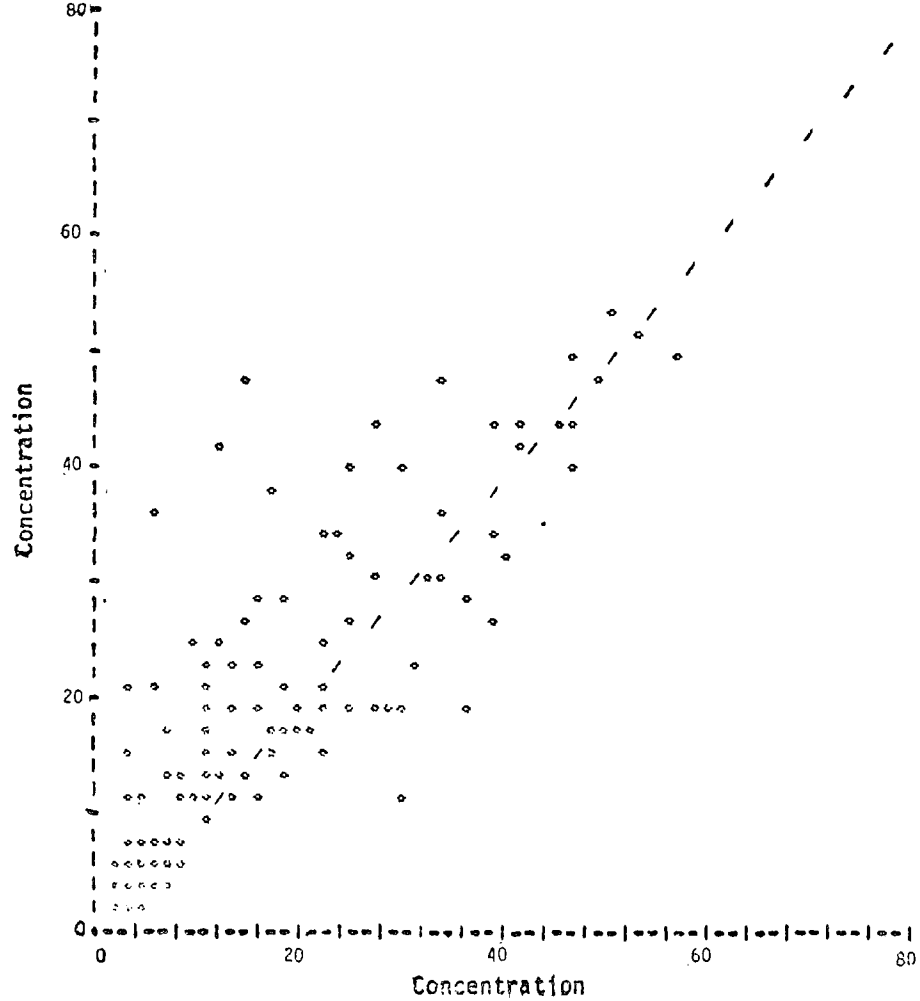

(e) SAI--Horizontal Axis = SAIT, Vertical Axis = SAII

FIGURE II-3. SCATTER PLOTS FOR THE NO RESULTS (Concluded)

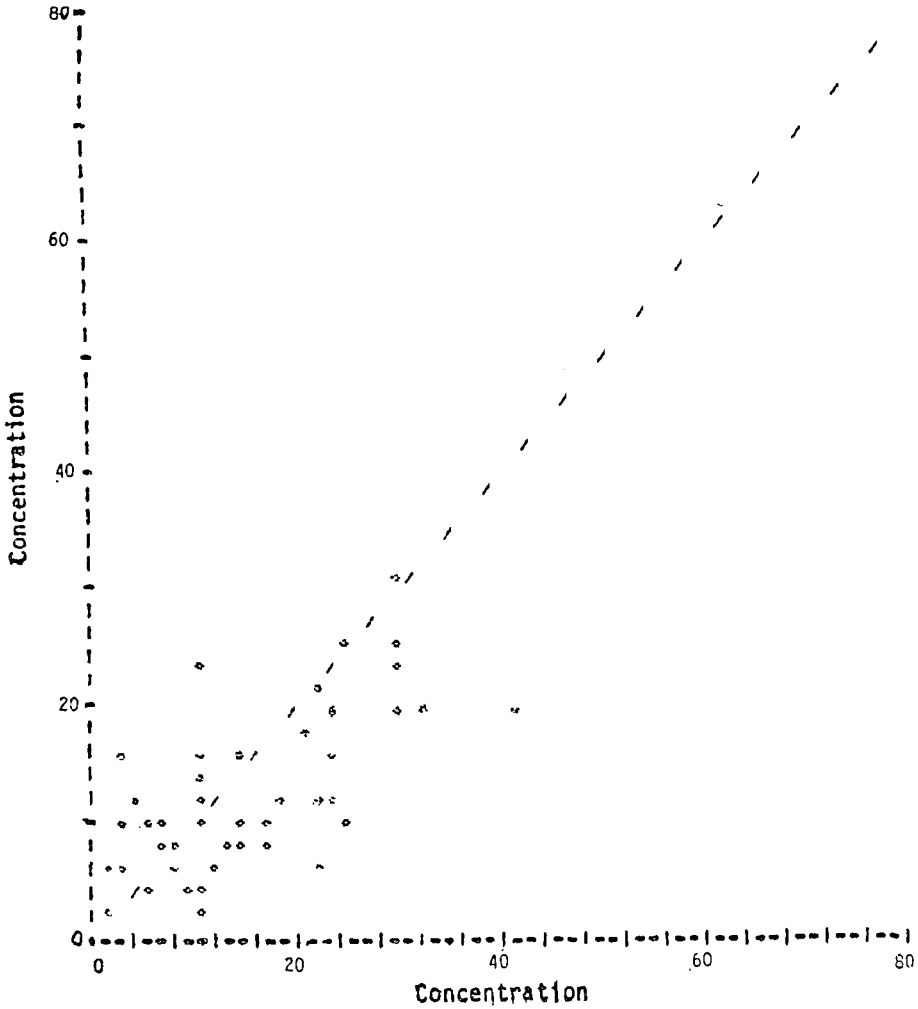

(a) PES--Horizontal Axis = PESC, Vertical Axis = PESM

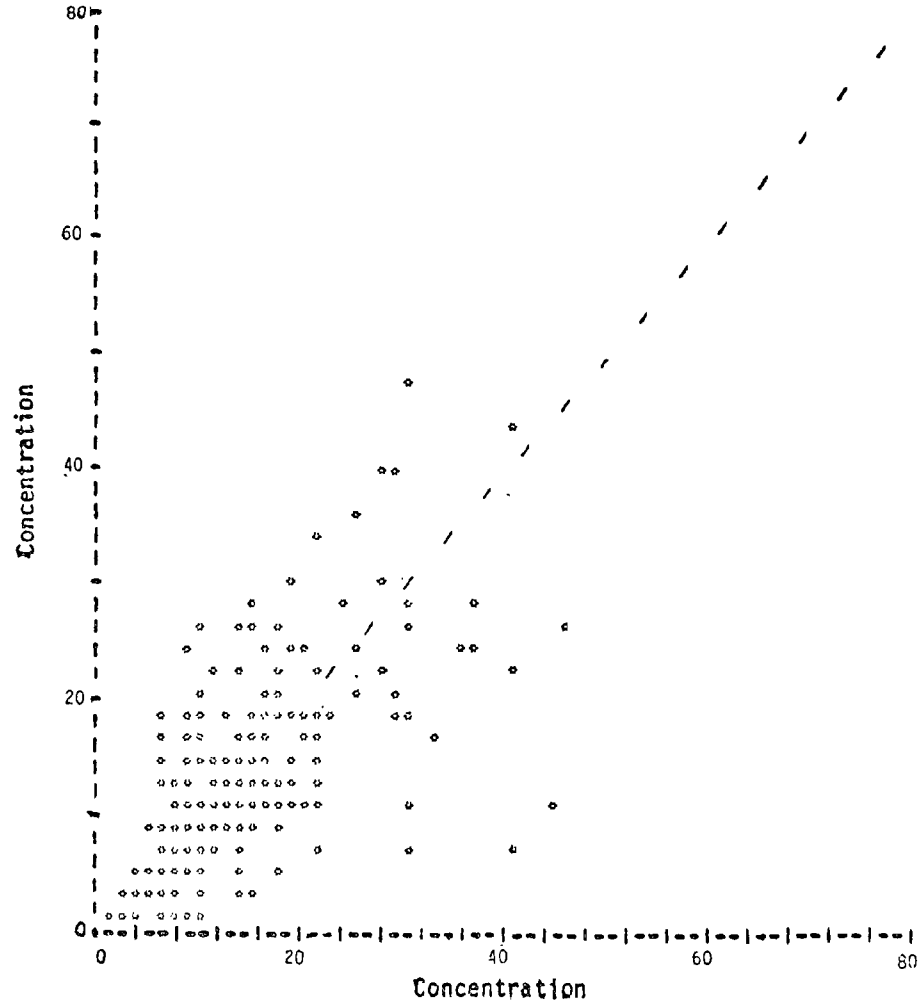

(b) SAI--Horizontal Axis = SAIC, Vertical Axis = SAIM

FIGURE II-4. SCATTER PLOTS FOR THE NO_2 RESULTS

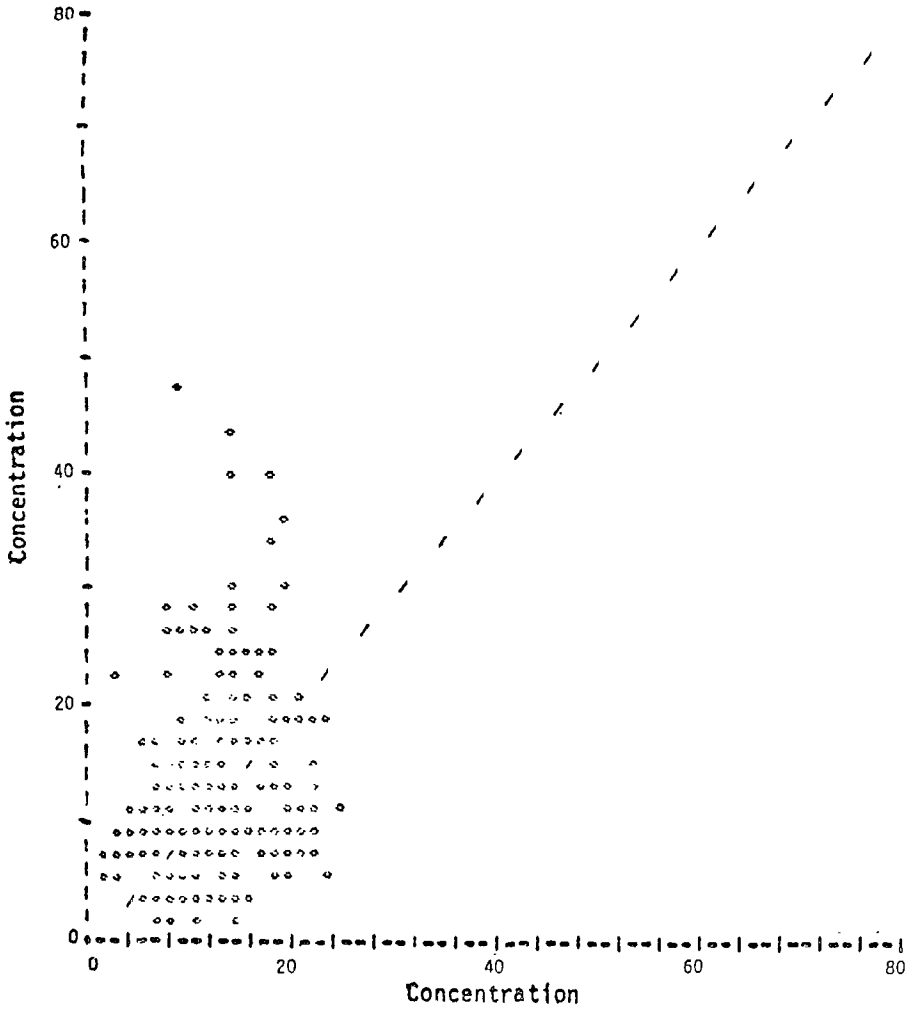

(c) Correlated Station--Horizontal Axis = CORC, Vertical Axis = CORM

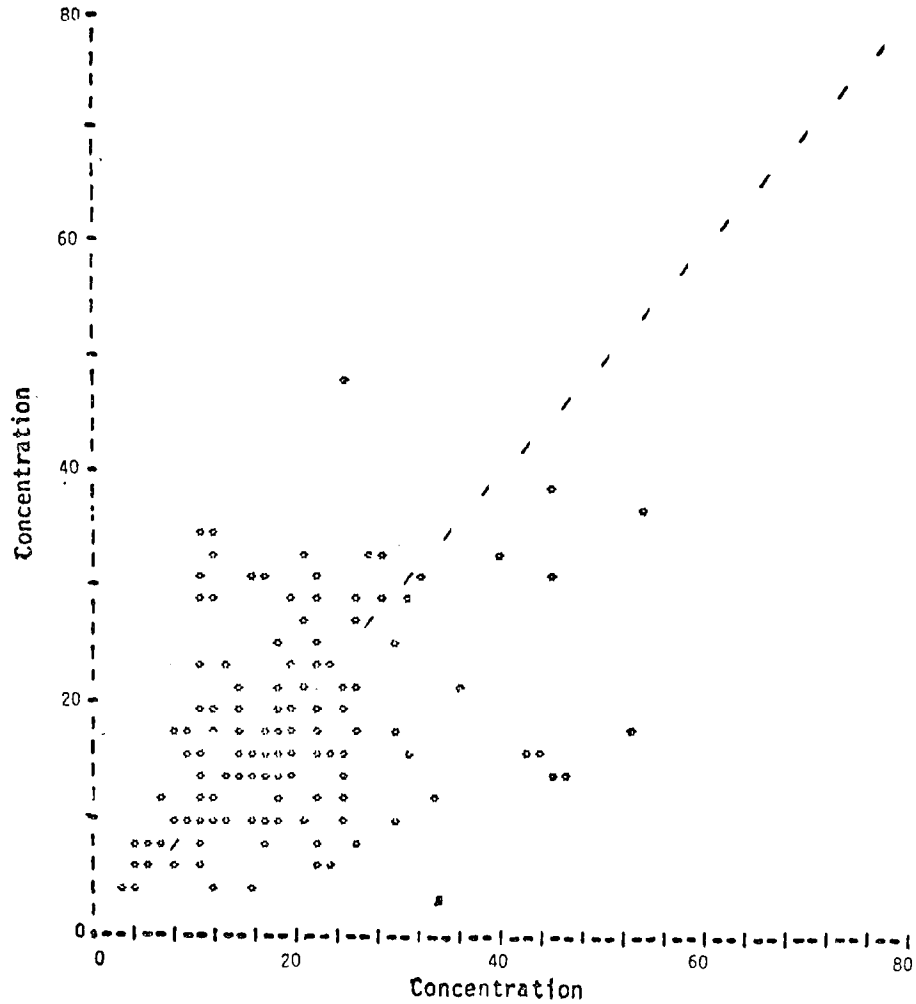

(d) GRC--Horizontal Axis = GRCT, Vertical Axis = GRCI

FIGURE II-4. SCATTER PLOTS FOR THE NO_2 RESULTS (Continued)

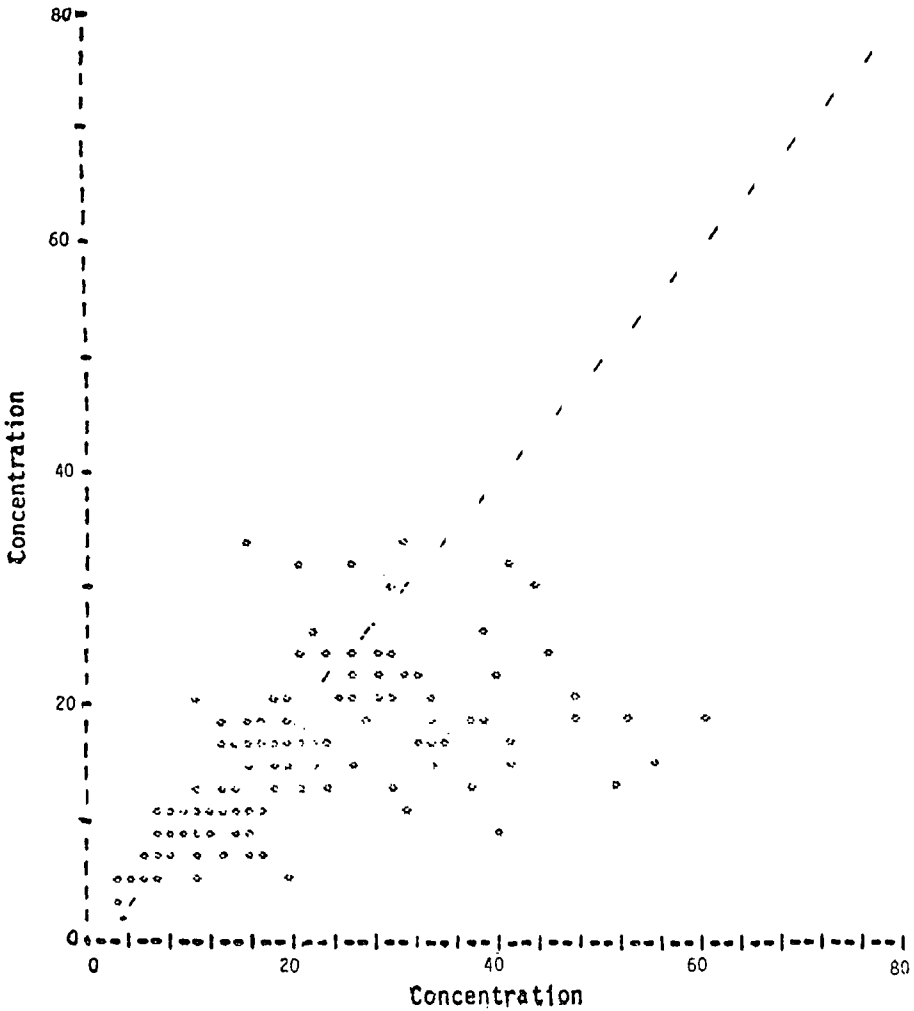

(e) SAI--Horizontal Axis = SAIT, Vertical Axis = SAII

FIGURE II-4. SCATTER PLOTS FOR THE NO_2 RESULTS (Concluded)

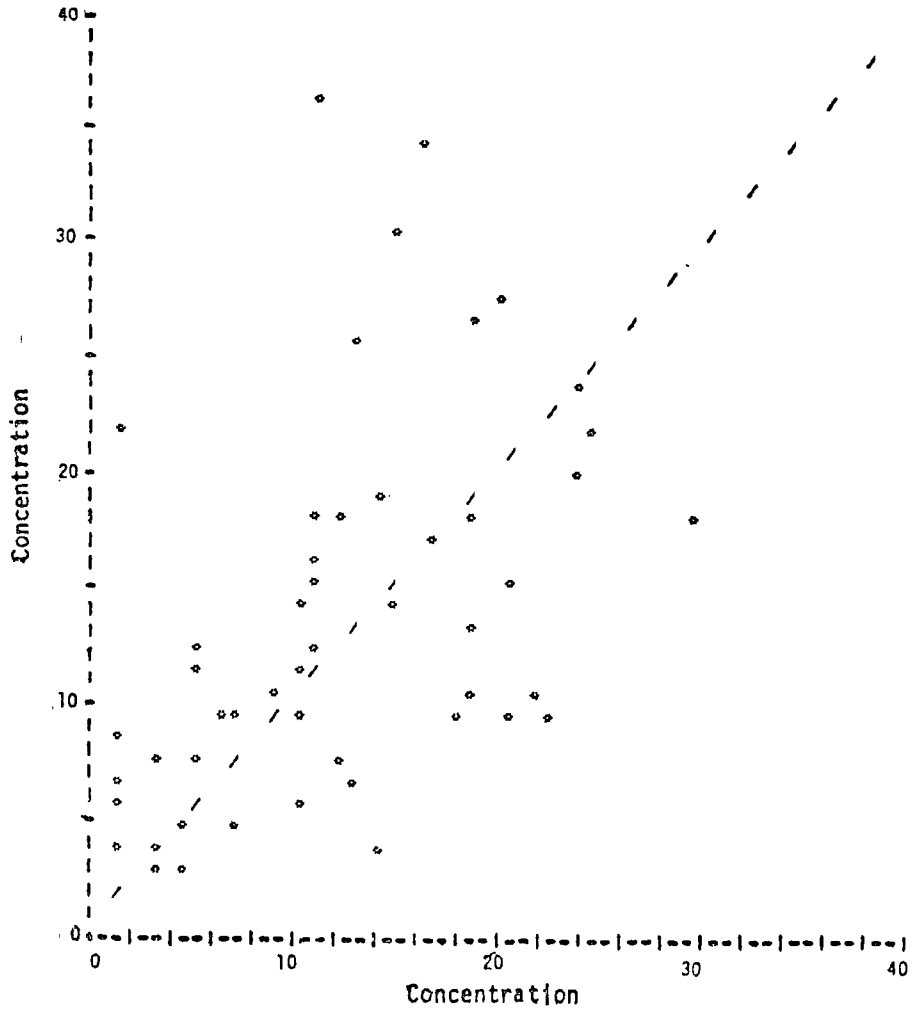

(a) PES--Horizontal Axis = PESC, Vertical Axis = PESM

FIGURE II-5. SCATTER PLOTS FOR THE O_3 RESULTS

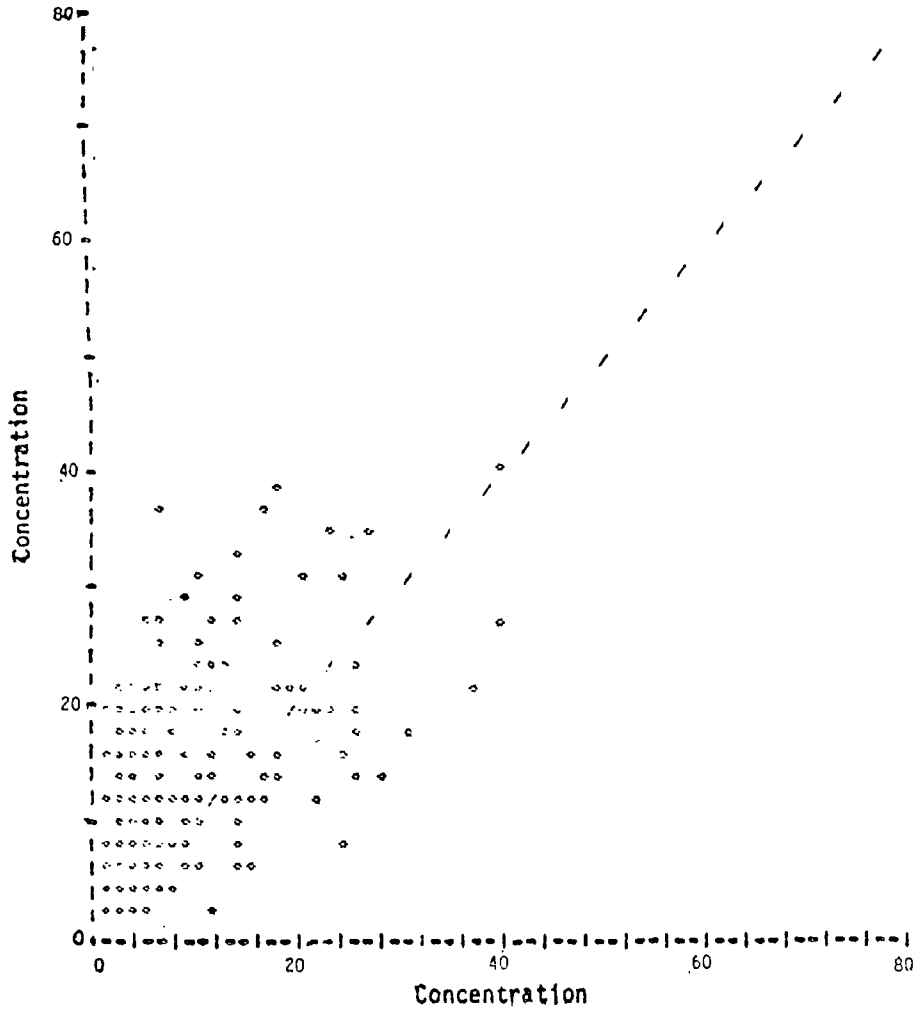

(b) SAI--Horizontal Axis = SAIC, Vertical Axis = SAIM

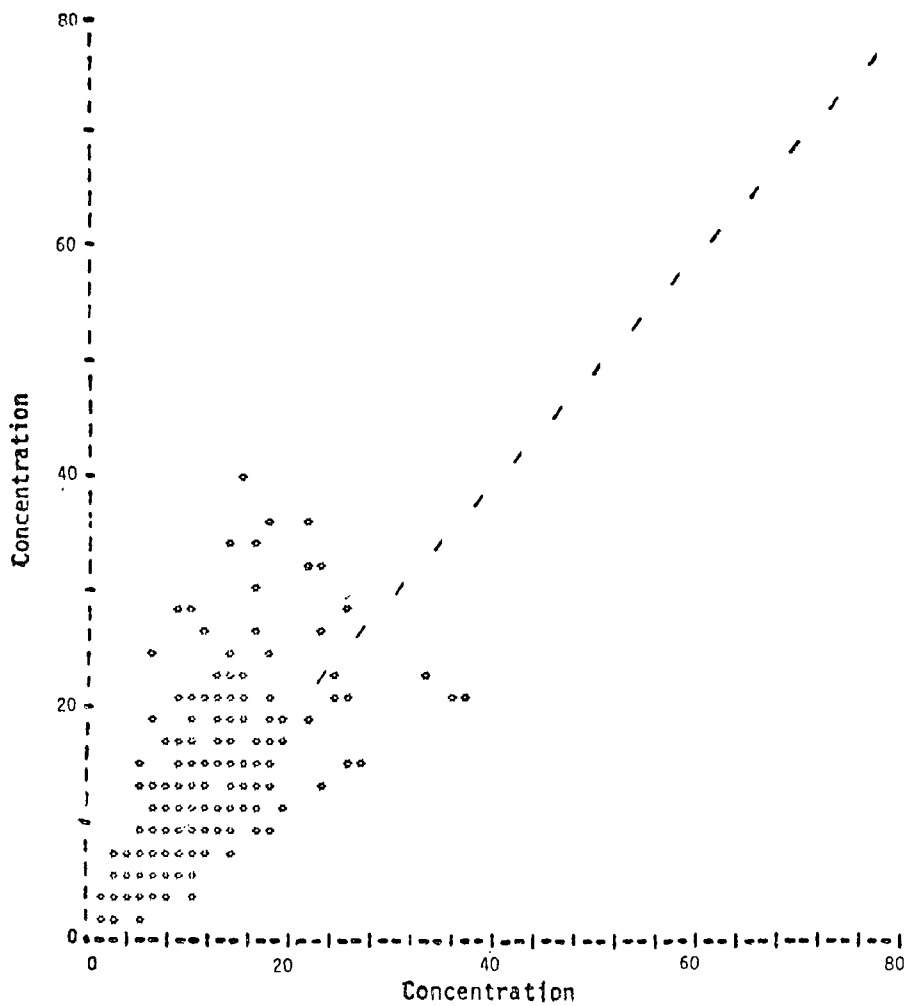

(c) Correlated Station--Horizontal Axis = CORC, Vertical Axis = CORM

FIGURE II-5. SCATTER PLOTS FOR THE O_3 RESULTS (Continued)

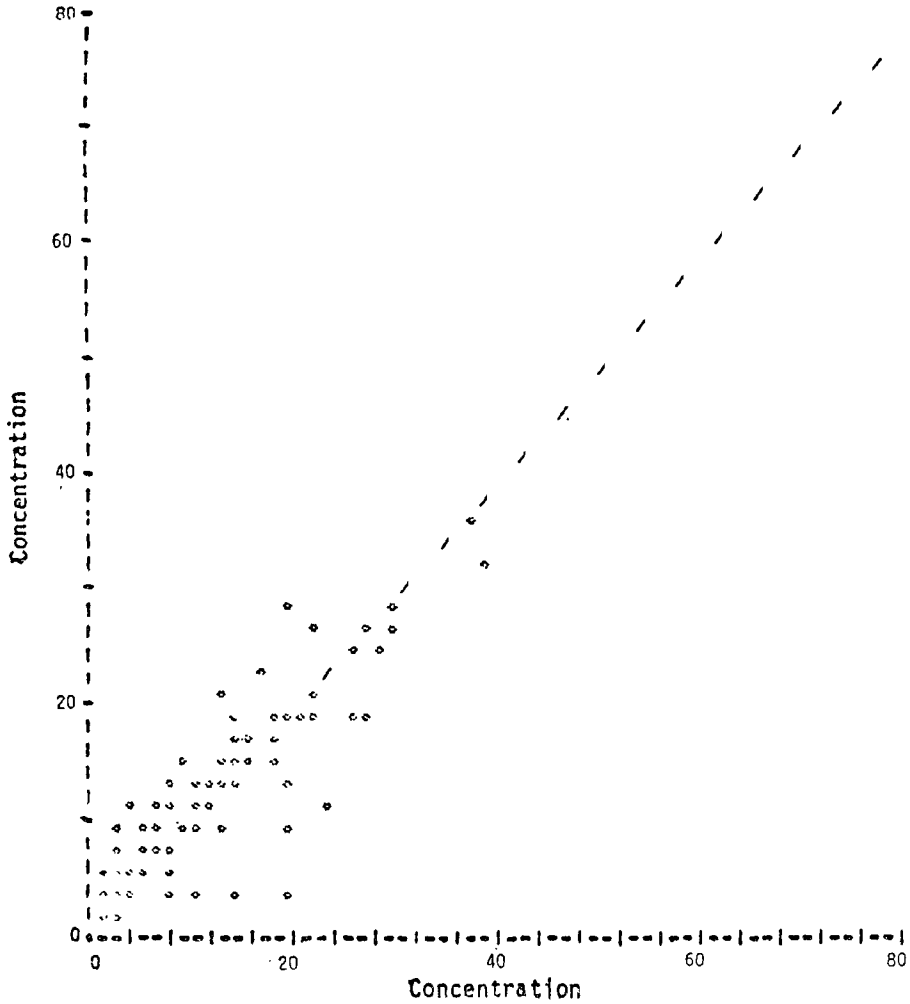

(d) GRC--Horizontal Axis = GRCT, Vertical Axis = GRCI

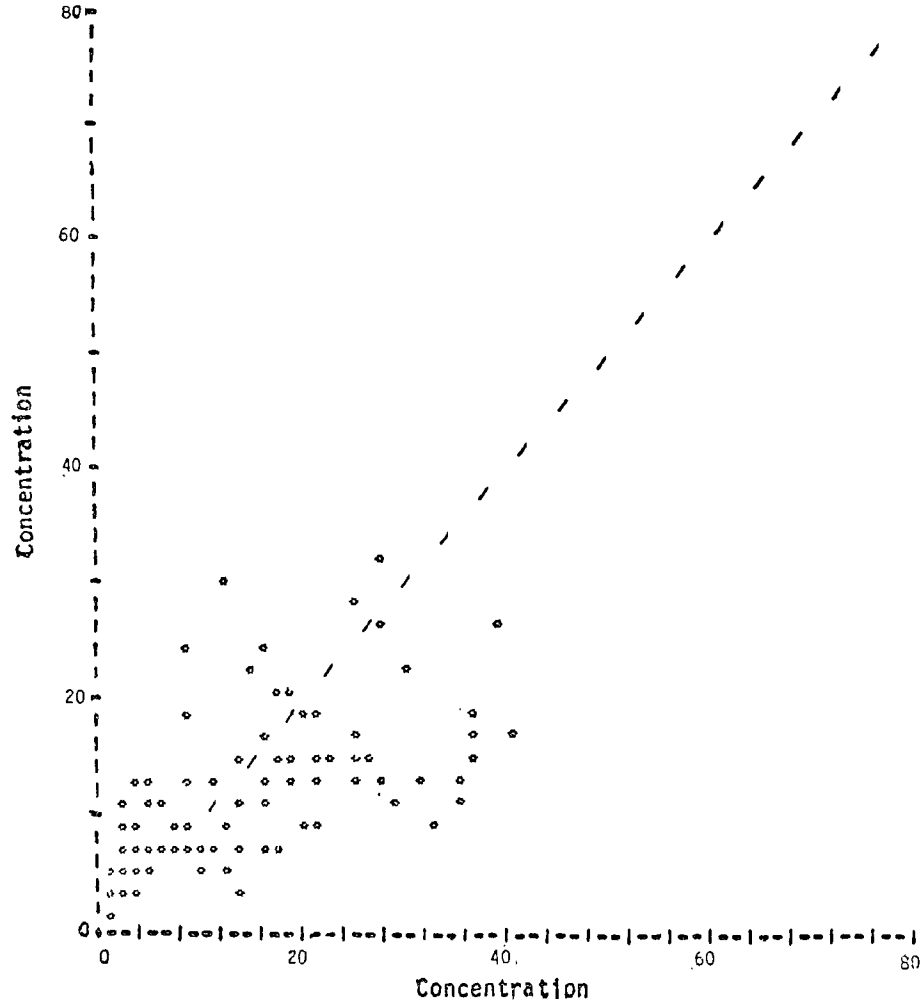

(e) SAI--Horizontal Axis = SAIT, Vertical Axis = SAII

FIGURE II-5. SCATTER PLOTS FOR THE O_3 RESULTS (Concluded)

As in the case of CO, the PES, GRC, and SAI station results for NO_2 (Figure II-4) generally appear at first to be randomly distributed about the 45° line. However, the SAI trajectory results for NO_2 definitely indicate a trend toward measured concentrations smaller than the predicted values. A more detailed examination of the PES, GRC, and SAI station results shows, moreover, that a similar tendency is also present at high observed concentrations (say, greater than 25 pphm). However, there is a definite tendency to underestimate the highest NO_2 concentrations when performing correlated station interpolations.

This last point can be readily explained. As noted in Table II-1, the Burbank monitoring station is located very near a power plant, which provides a strong local source of nitrogen oxides. Peak hour NO_2 concentrations at Burbank are double those of any other station. Since other stations in the neighborhood of Burbank record much lower NO_2 concentrations, the station correlation algorithm cannot calculate the high concentrations at Burbank; this explains the anomalous points in Figure II-4(c) and, to a lesser extent, Figure II-3(c). This is an extreme, but highly effective, example of how nonrepresentative the location of a monitoring station can be. In this instance, only microscale modeling could resolve the problem of disparity in scales.

The trend toward overprediction of NO_2 concentrations by the models is less easily explained. The problems associated with the station measurements and the chemical reaction kinetics of the oxides of nitrogen have been mentioned above. Both are likely contributors to the disparities between measured and predicted nitrogen dioxide concentrations.

The ozone results (Figure II-5) demonstrate a rather striking anomaly. The predictions at the station locations by PES, COR, and SAI are low relative to the measured values, whereas the predictions along the trajectories for GRC and SAI are high relative to the interpolated values. In both cases, the effect is more pronounced for the SAI data. This anomalous behavior

probably reflects the smoothing aspects of the interpolation process, as discussed in detail earlier, and indicates a need for further development in the application of interpolation algorithms.

4. Residuals Analyses

Residuals analyses of the data are presented in Figures II-6 through II-25. Each figure contains four residual plots:

- Histogram--residual value as a function of the number of occurrences of that value.
- Time plot--residual value as a function of the time of day of occurrence of that value.
- Calculated concentration--residual value as a function of the calculated pollutant concentration that gave rise to that value.
- Observed concentration--residual value as a function of the measured pollutant concentration that gave rise to that value.

Each of these types of plots is of potential value in attempting to uncover deficiencies in either the model being evaluated or in the data with which predictions are being compared. The results obtained using each model for the pollutants CO, NO, NO_2, and O_3 are analyzed separately below.

Residuals analyses of the PES data for CO are presented in Figures II-6(a) thrugh II-6(d). A survey of the results given in the histogram of residuals and the plot of residuals as a function of time and predicted concentrations [Figures II-6(a), II-6(b), and II-6(c)] indicates no notable trends in the residuals. However, a definite trend can readily be seen in Figure II-6(d): At high measured concentrations, most of the residuals (calculated minus measured values) are negative. This trend agrees with the discussion presented above of undercalculation of some station values.

The residuals analyses of the SAI station results for CO are given in Figures II-7(a) through II-7(d). Figure II-7(a) shows a definite trend toward

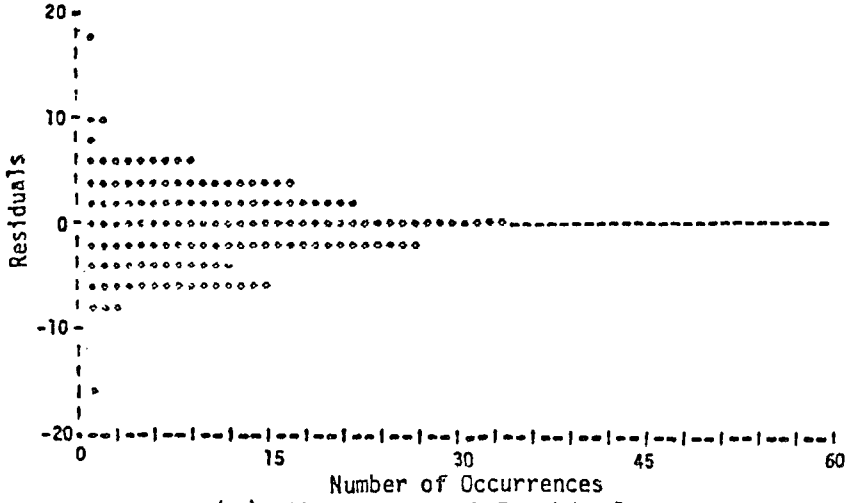

(a) Histogram of Residuals

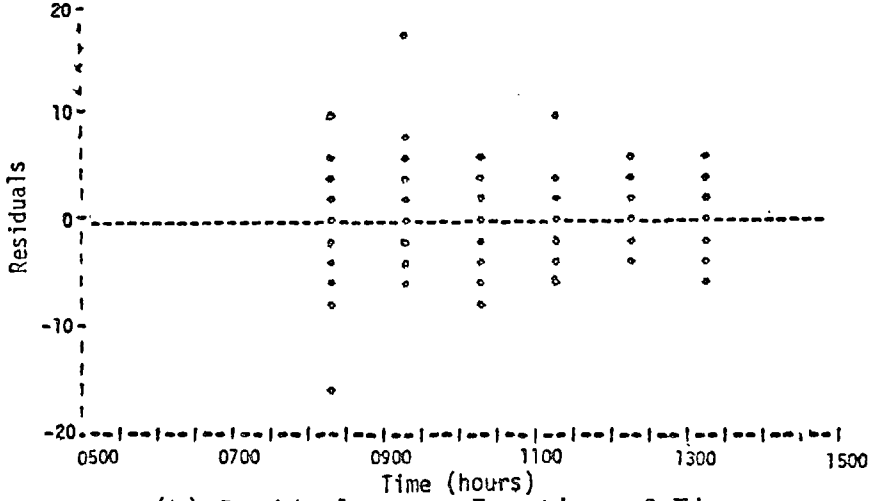

(b) Residuals as a Function of Time

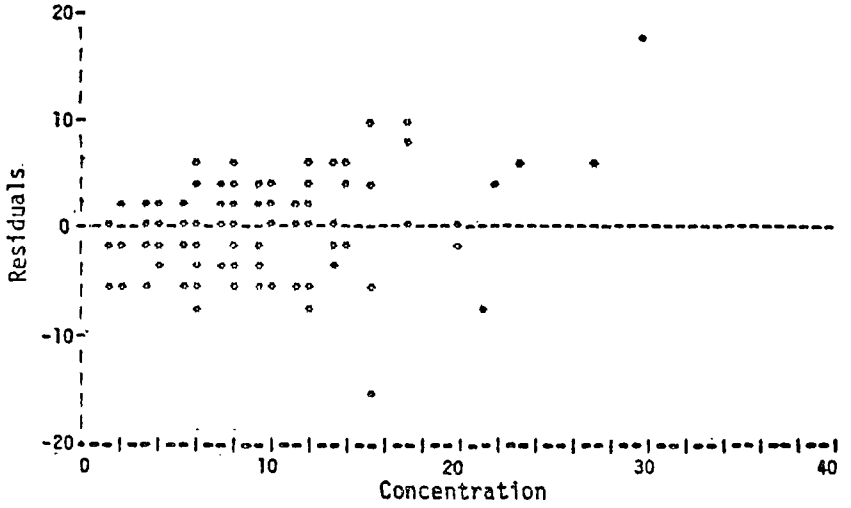

(c) Residuals as a Function of PESC Concentration

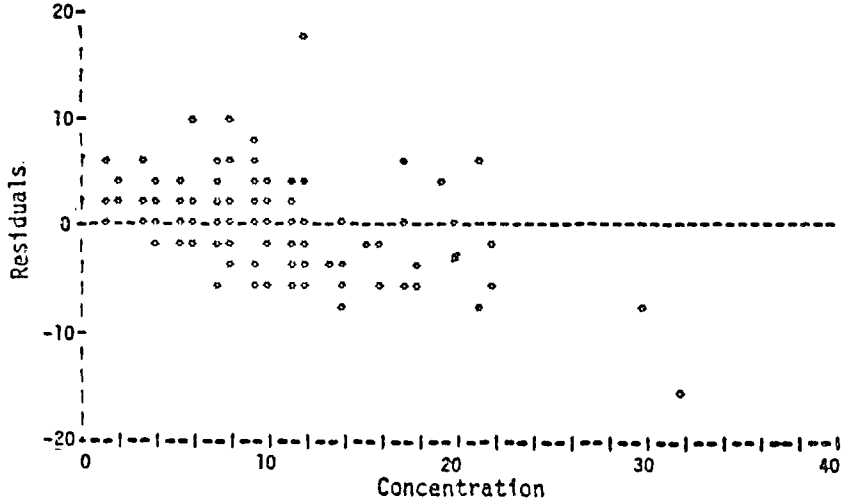

(d) Residuals as a Function of PESM Concentration

FIGURE II-6. RESIDUALS (PESC MINUS PESM) ANALYSES OF THE PES RESULTS FOR CO

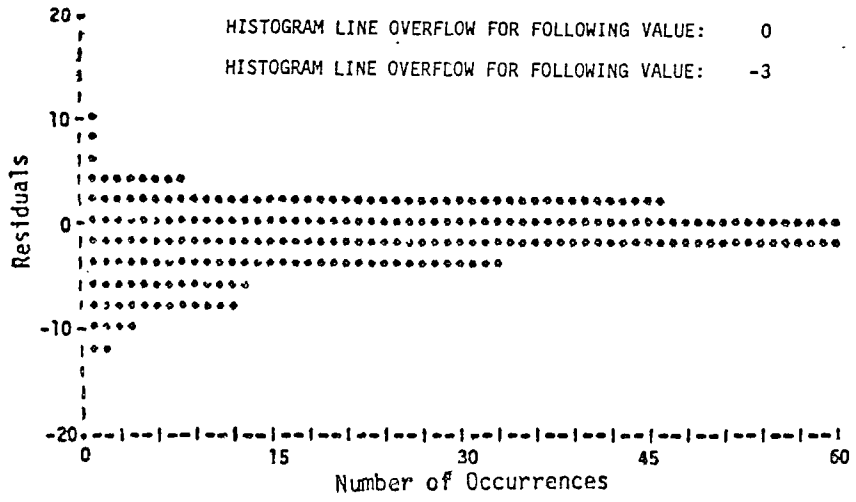

(a) Histogram of Residuals

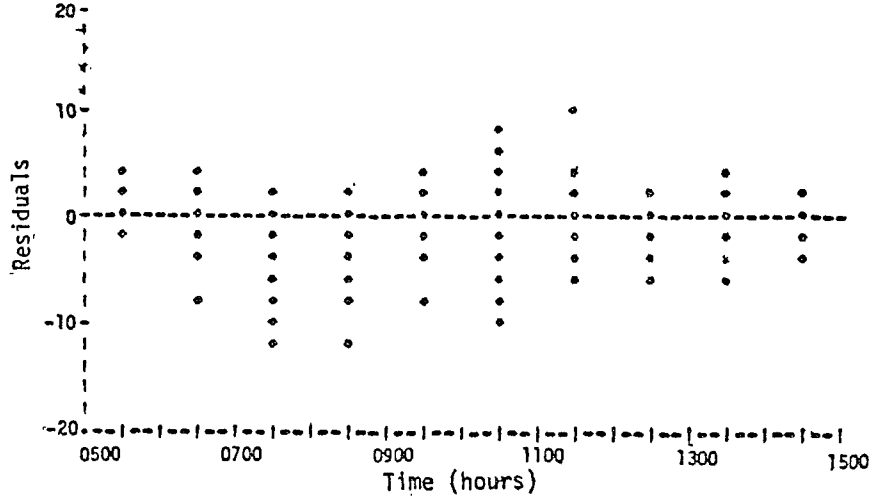

(b) Residuals as a Function of Time

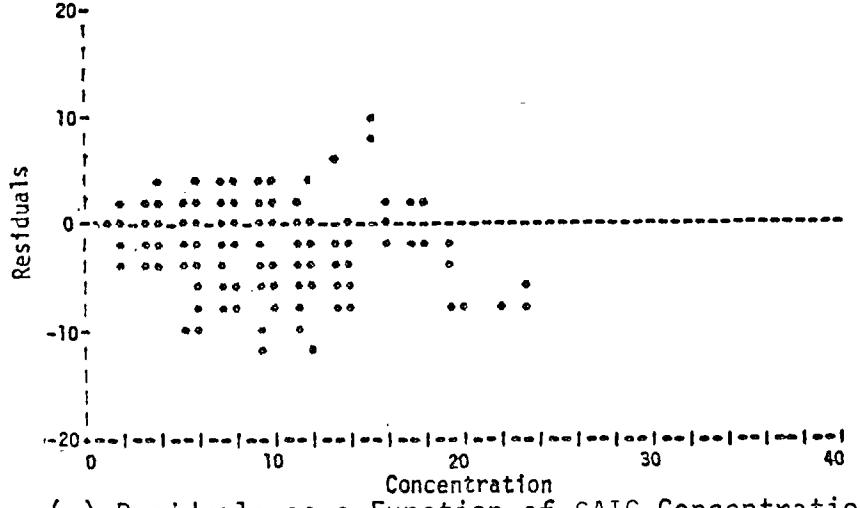

(c) Residuals as a Function of SAIC Concentration

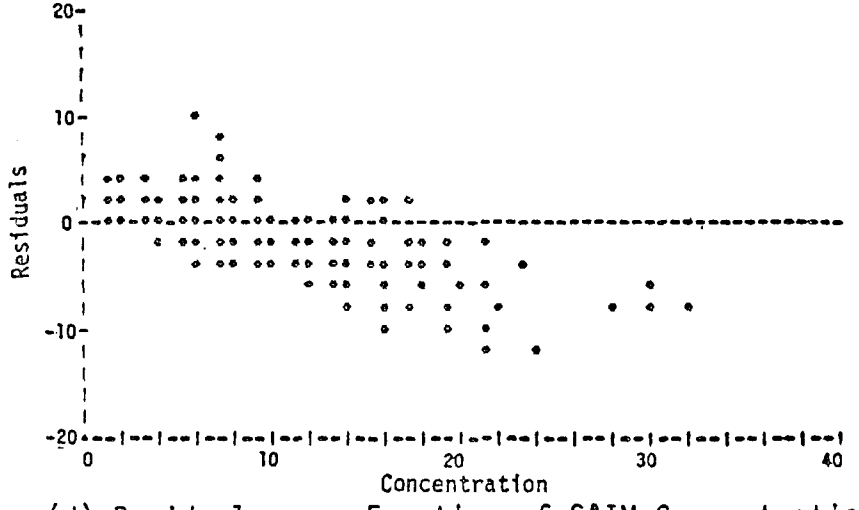

(d) Residuals as a Function of SAIM Concentration

FIGURE II-7. RESIDUALS (SAIC MINUS SAIM) ANALYSES OF THE SAI STATION RESULTS FOR CO

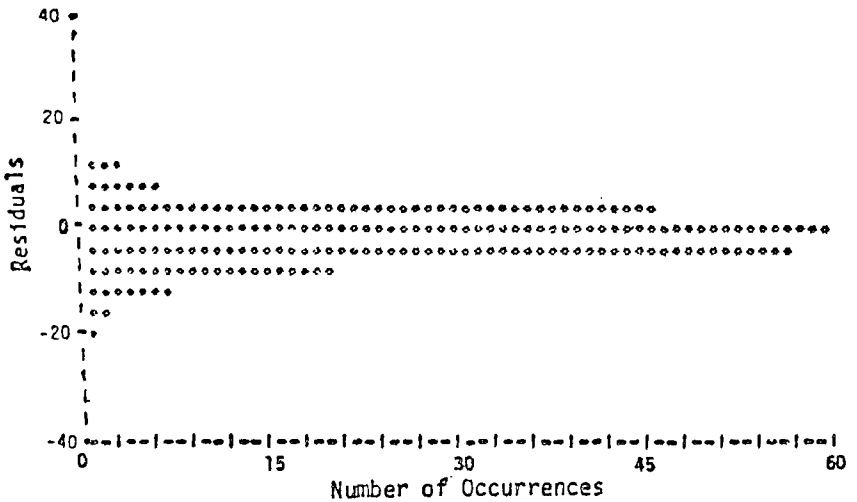

(a) Histogram of Residuals

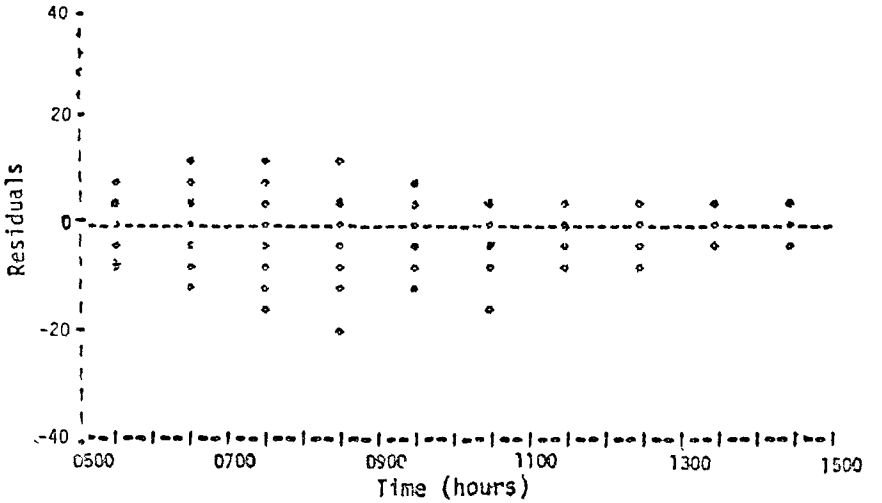

(b) Residuals as a Function of Time

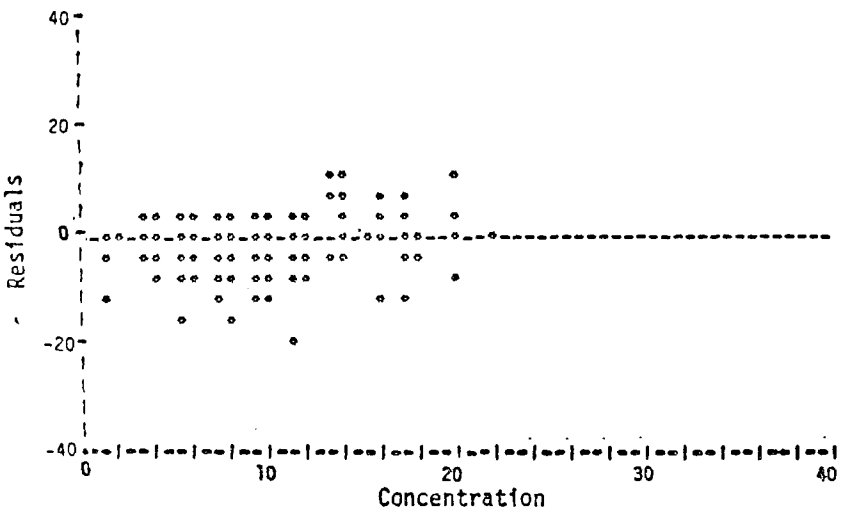

(c) Residuals as a Function of CORC Concentration

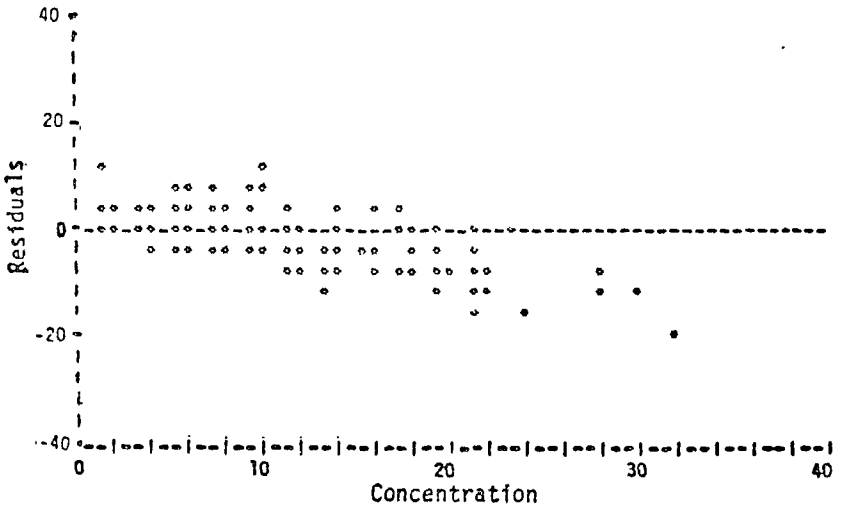

(d) Residuals as a Function of CORM Concentration

FIGURE II-8. RESIDUALS (CORC MINUS CORM) ANALYSES OF THE CORRELATED STATION RESULTS FOR CO

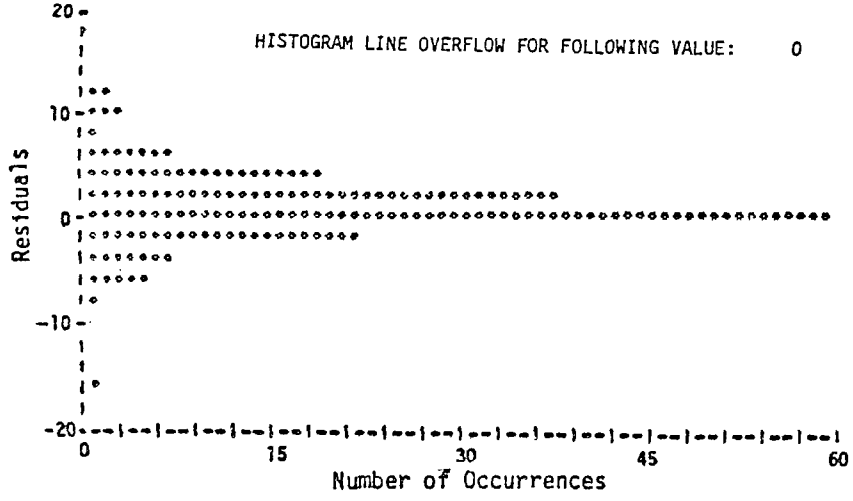

(a) Histogram of Residuals

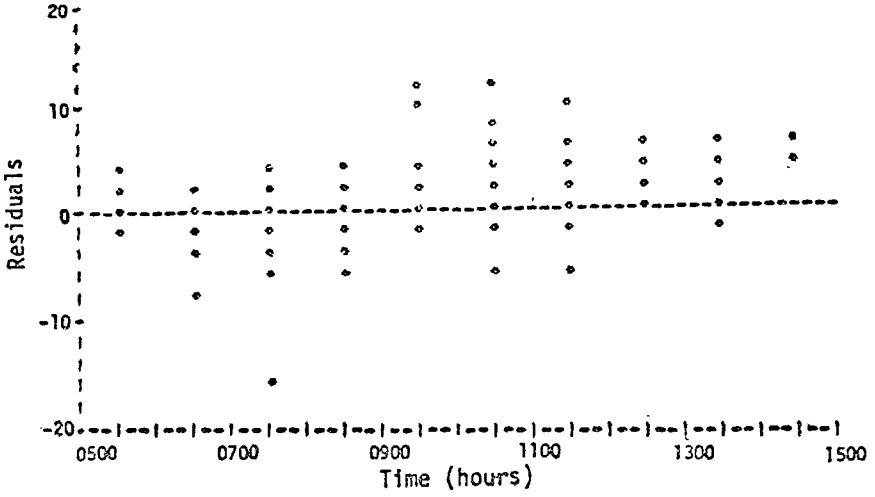

(b) Residuals as a Function of Time

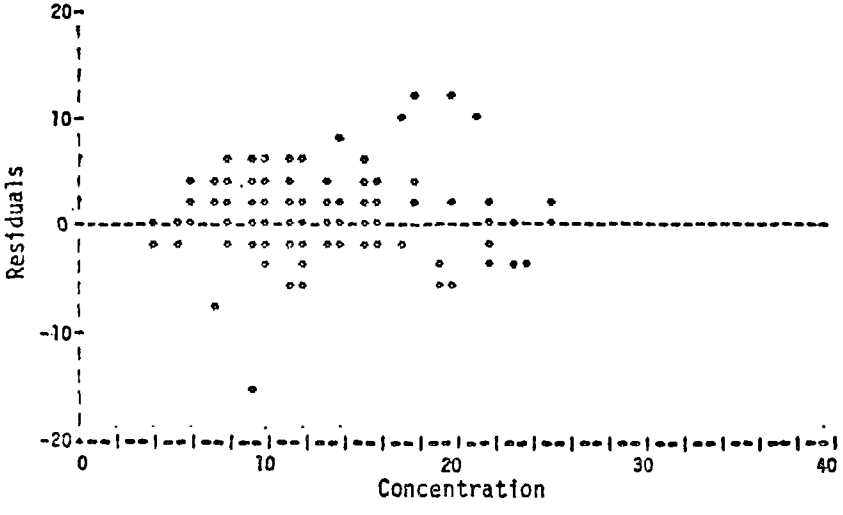

(c) Residuals as a Function of GRCT Concentration

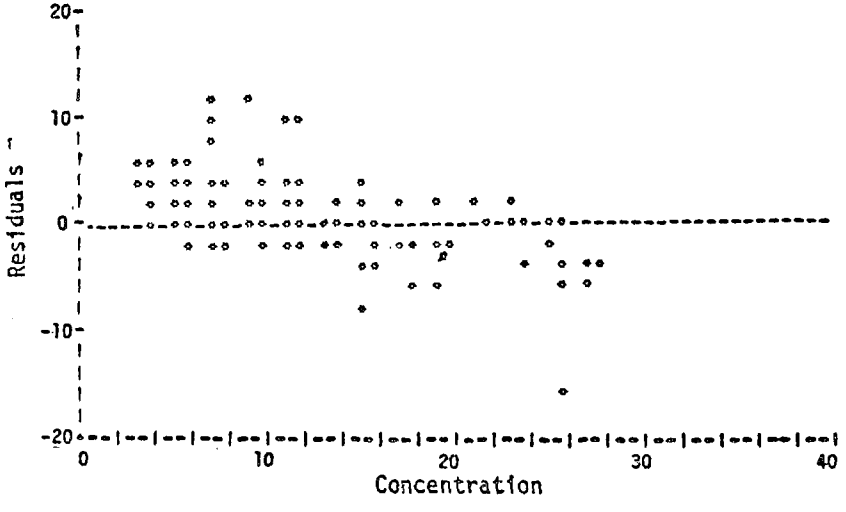

(d) Residuals as a Function of GRCI Concentration

FIGURE II-9. RESIDUALS (GRCT MINUS GRCI) ANALYSES OF THE GRC RESULTS FOR CO

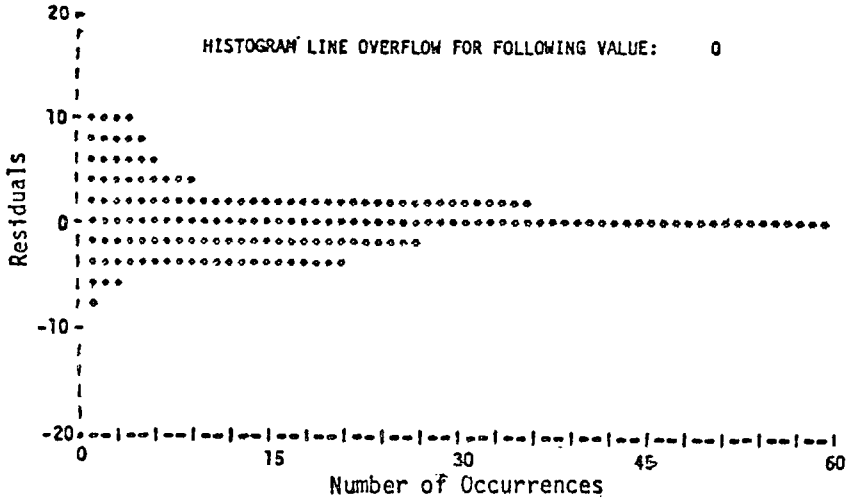

(a) Histogram of Residuals

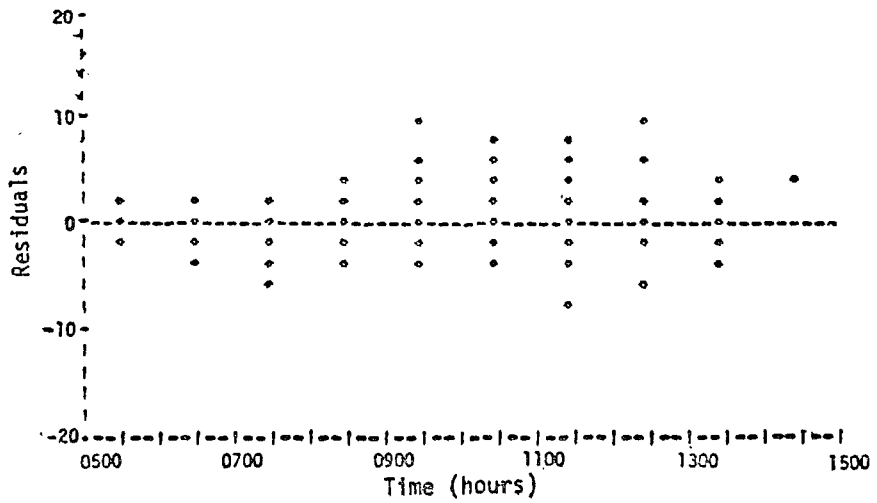

(b) Residuals as a Function of Time

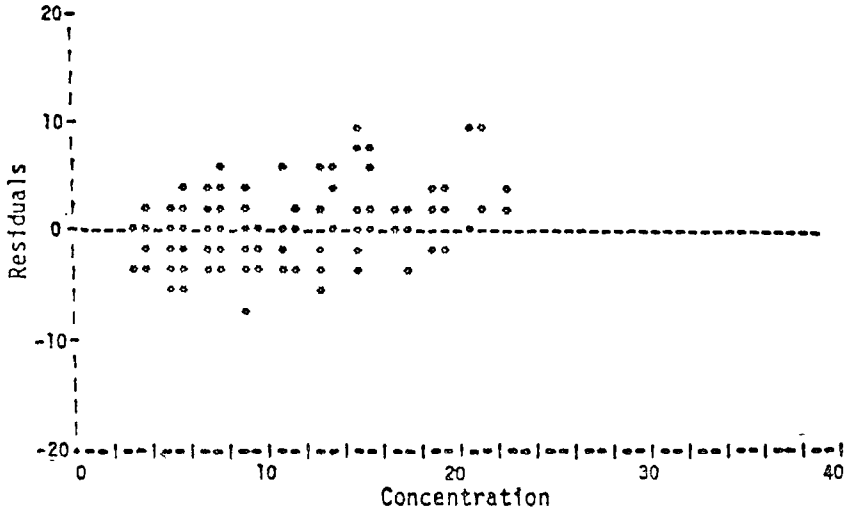

(c) Residuals as a Function of SAIT Concentration

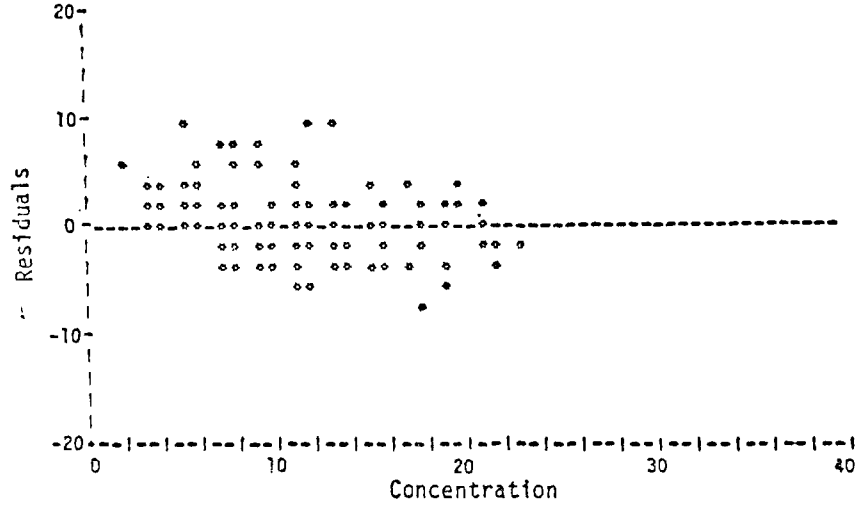

(d) Residuals as a Function of SAII Concentration

FIGURE II-10. RESIDUALS (SAIT MINUS SAII) ANALYSES FOR THE SAI TRAJECTORY RESULTS FOR CO

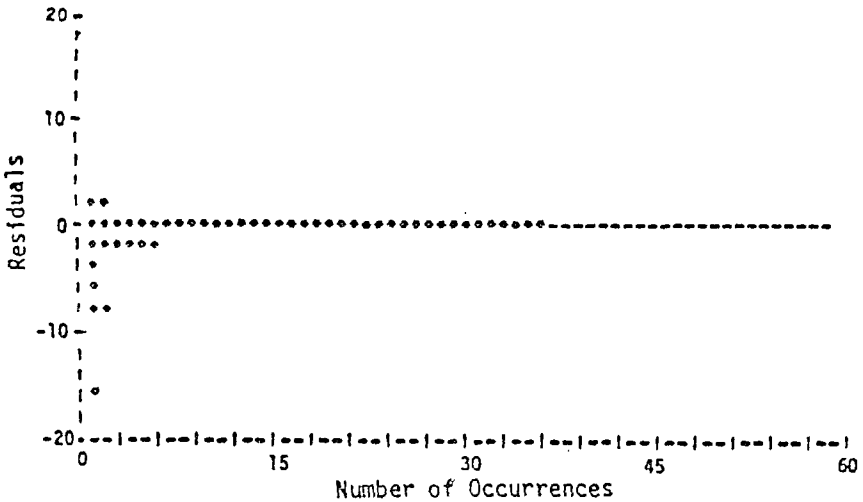

(a) Histogram of Residuals

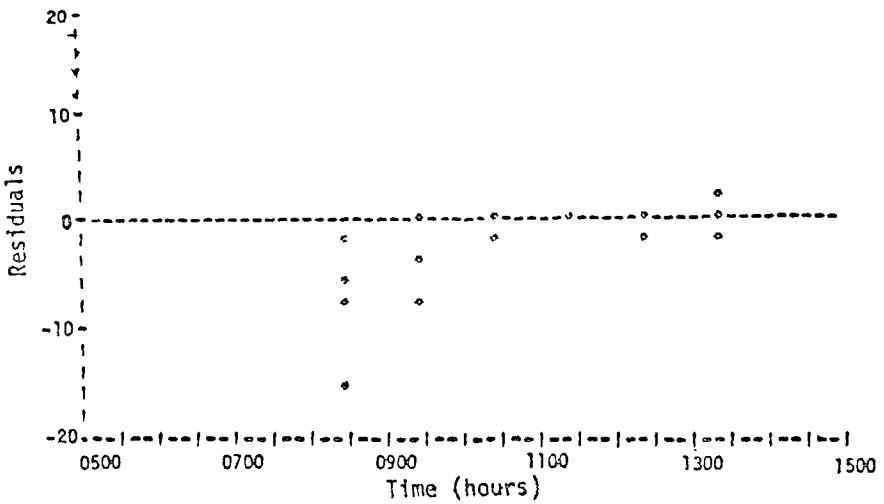

(b) Residuals as a Function of Time

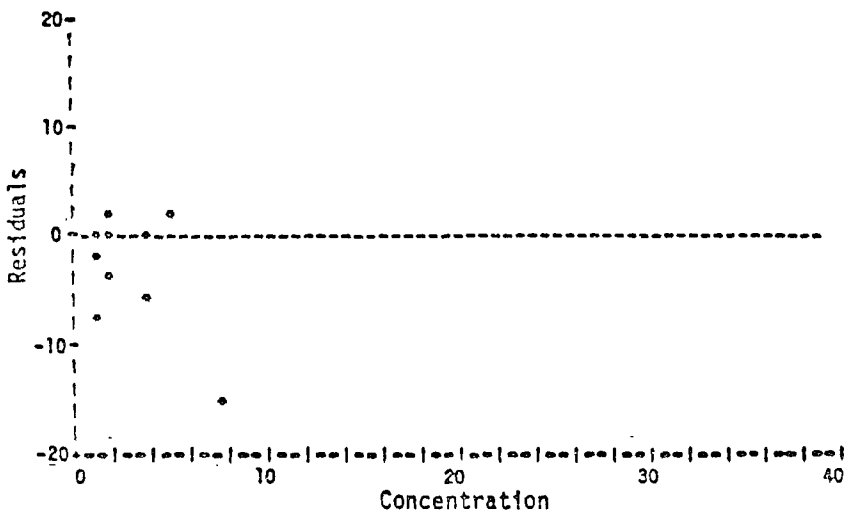

(c) Residuals as a Function of PESC Concentration

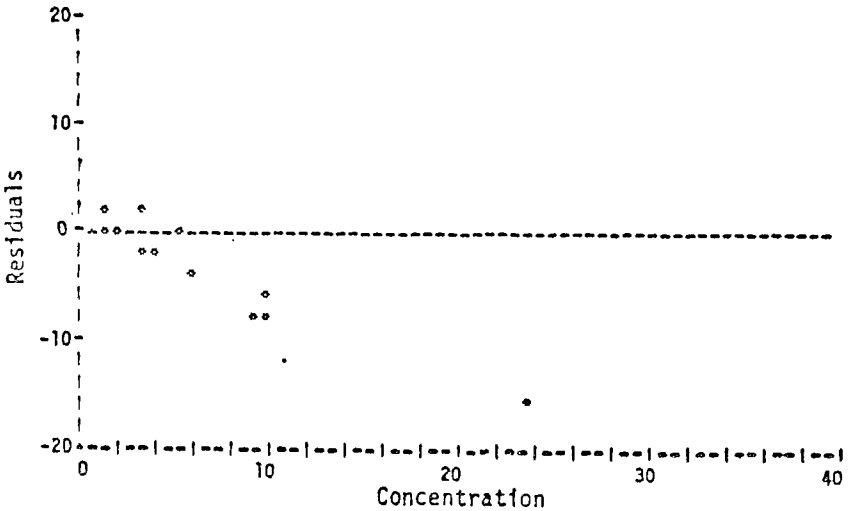

(d) Residuals as a Function of PESM Concentration

FIGURE II-11. RESIDUALS (PESC MINUS PESM) ANALYSES OF THE PES RESULTS FOR NO

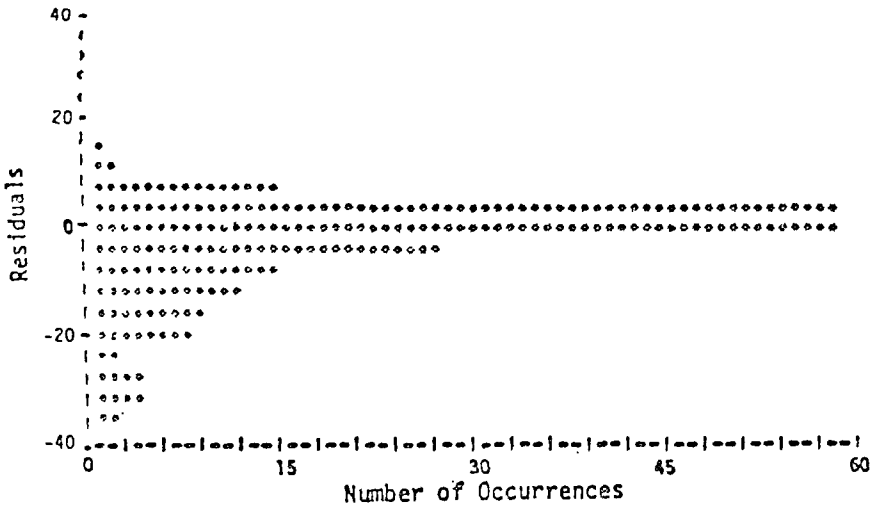

(a) Histogram of Residuals

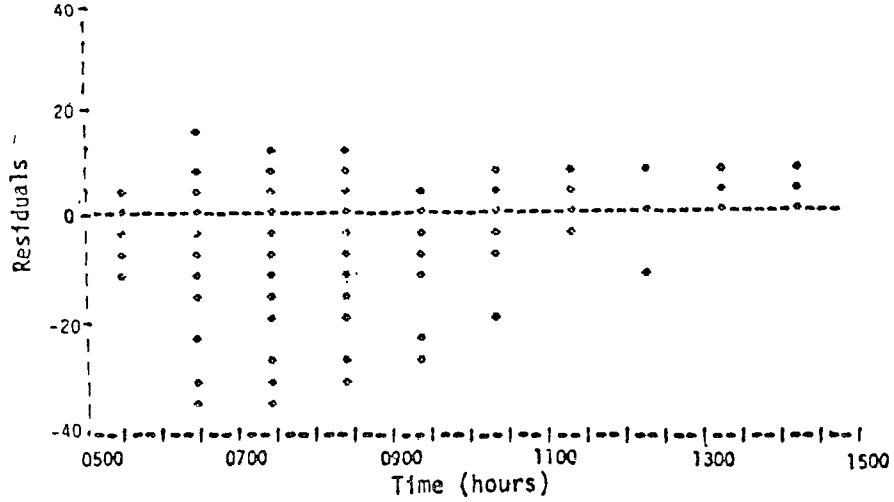

(b) Residuals as a Function of Time

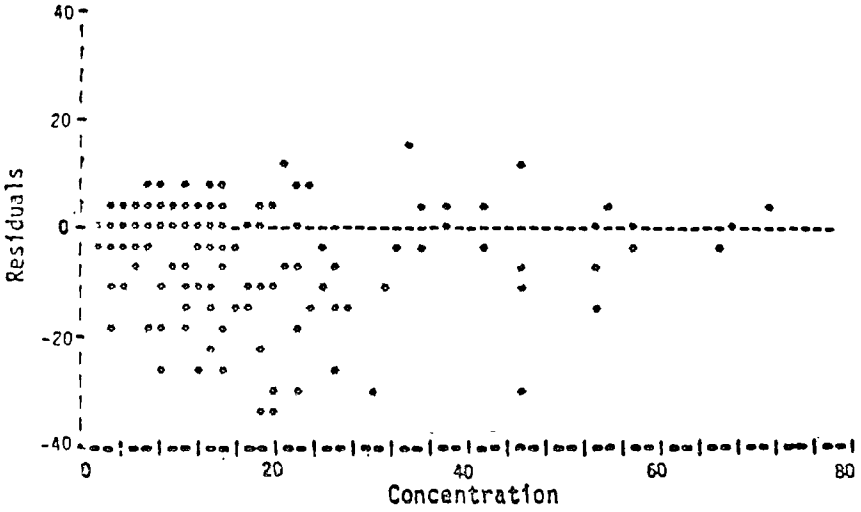

(c) Residuals as a Function of SAIC Concentration

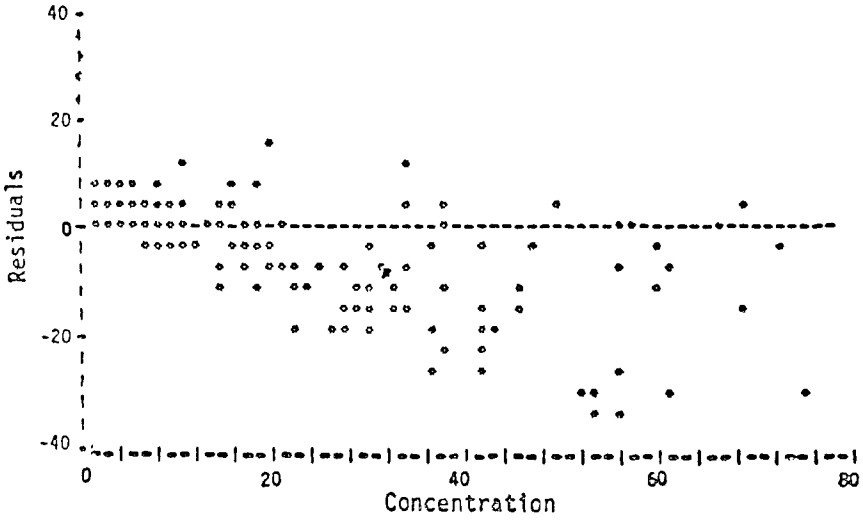

(d) Residuals as a Function of SAIM Concentration

FIGURE II-12. RESIDUALS (SAIC MINUS SAIM) ANALYSES OF THE SAI STATION RESULTS FOR NO

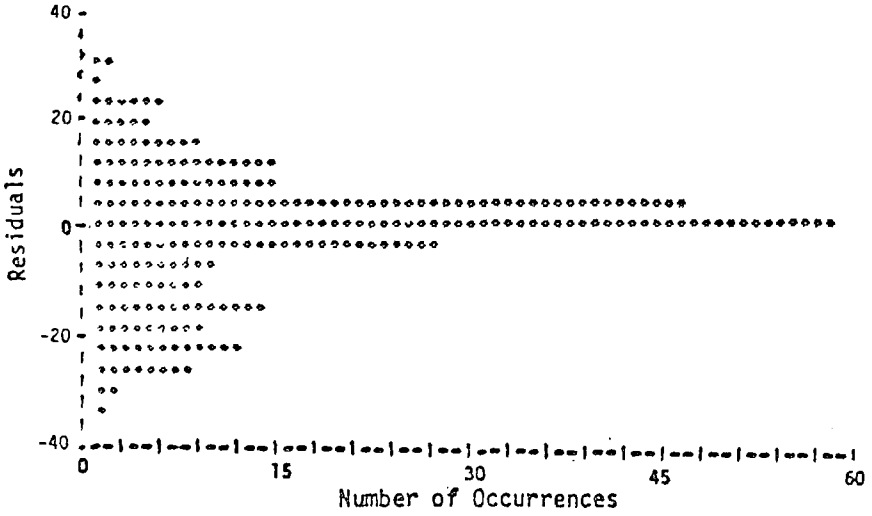

(a) Histogram of Residuals

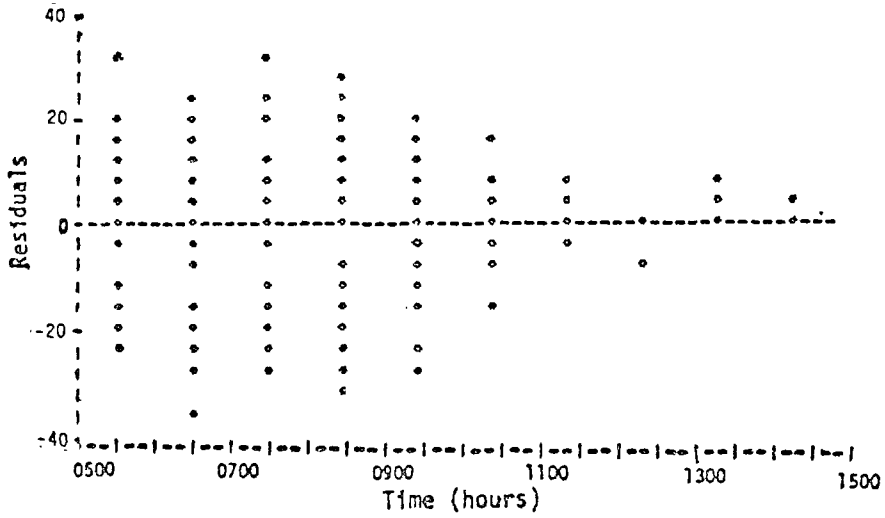

(b) Residuals as a Function of Time

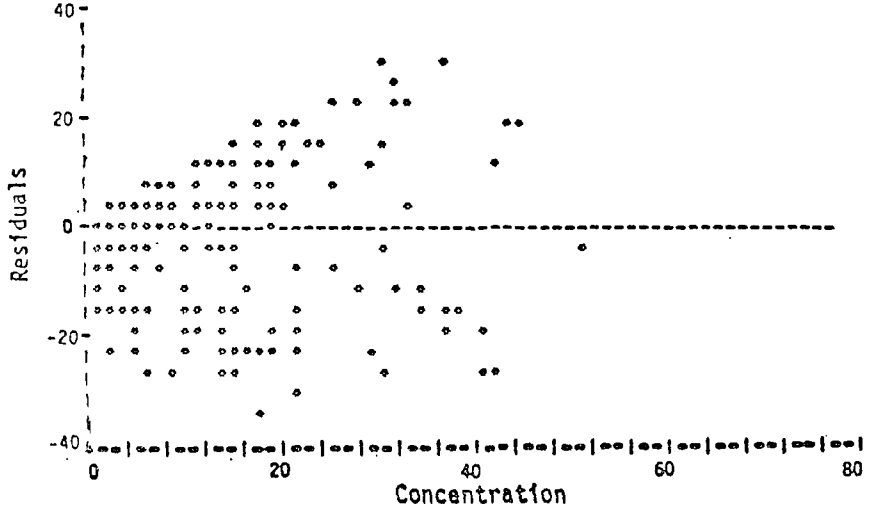

(c) Residuals as a Function of CORC Concentration

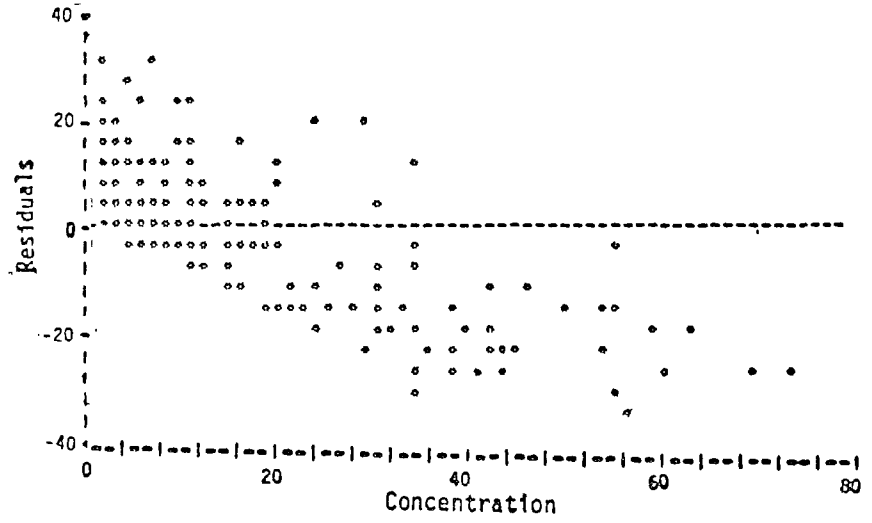

(d) Residuals as a Function of CORM Concentration

FIGURE II-13. RESIDUALS (CORC MINUS CORM) ANALYSES OF THE CORRELATED STATION RESULTS FOR NO

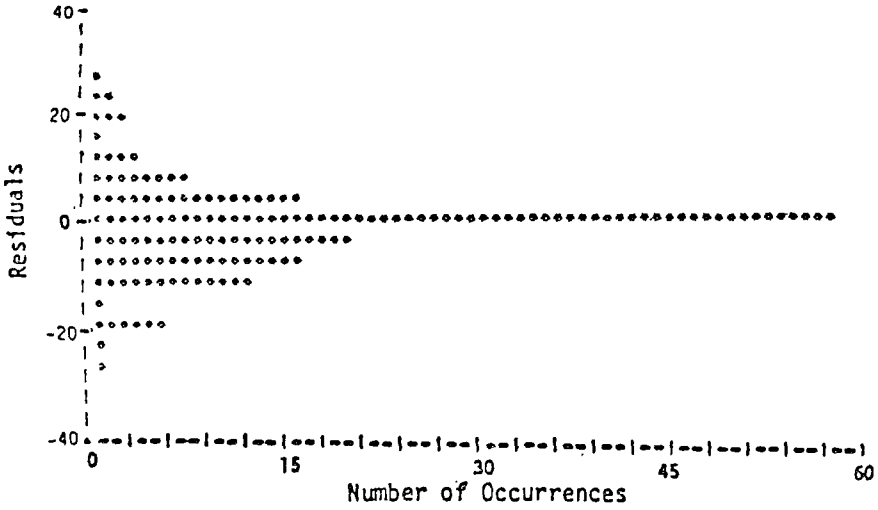

(a) Histogram of Residuals

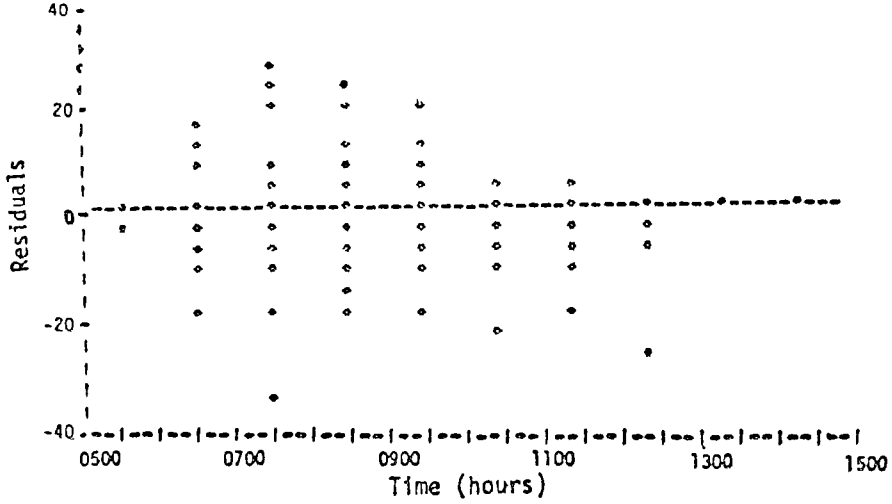

(b) Residuals as a Function of Time

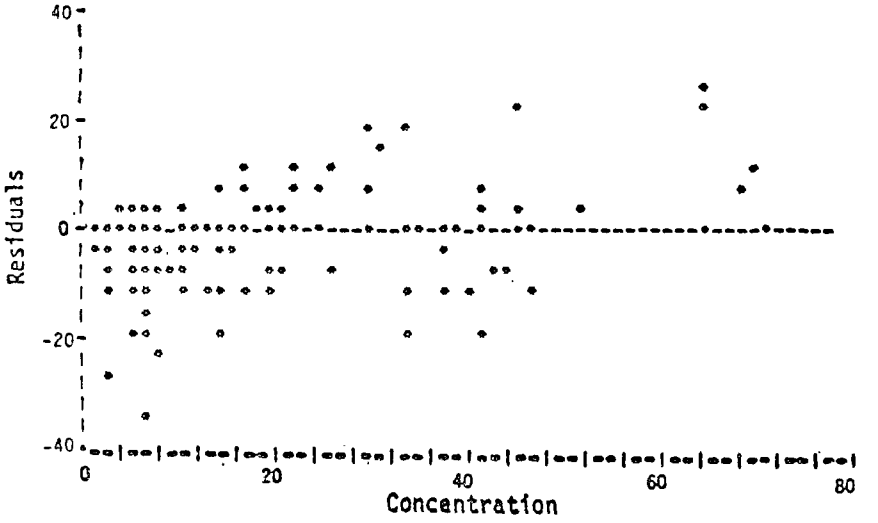

(c) Residuals as a Function of GRCT Concentration

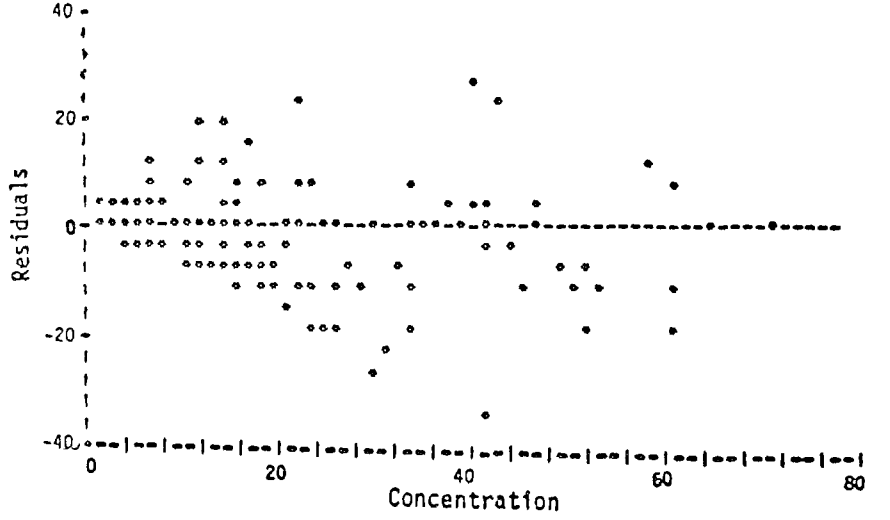

(d) Residuals as a Function of GRCI Concentration

FIGURE II-14. RESIDUALS (GRCT MINUS GRCI) ANALYSES OF THE GRC RESULTS FOR NO

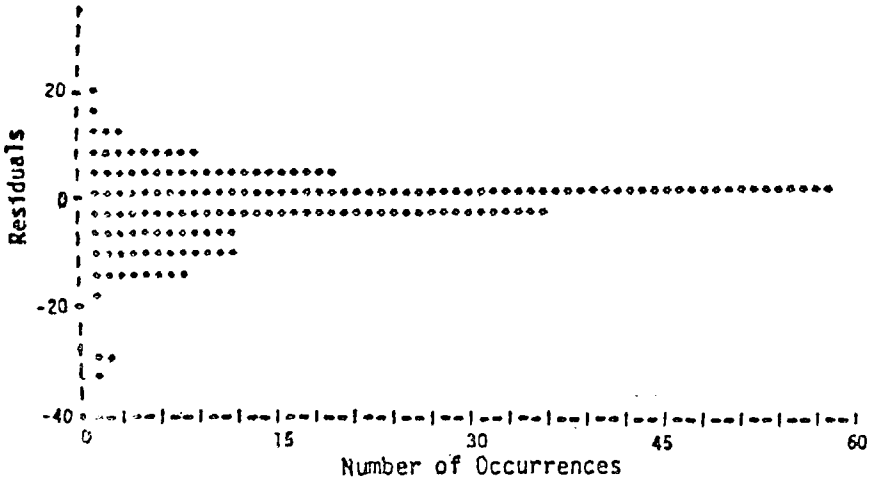

(a) Histogram of Residuals

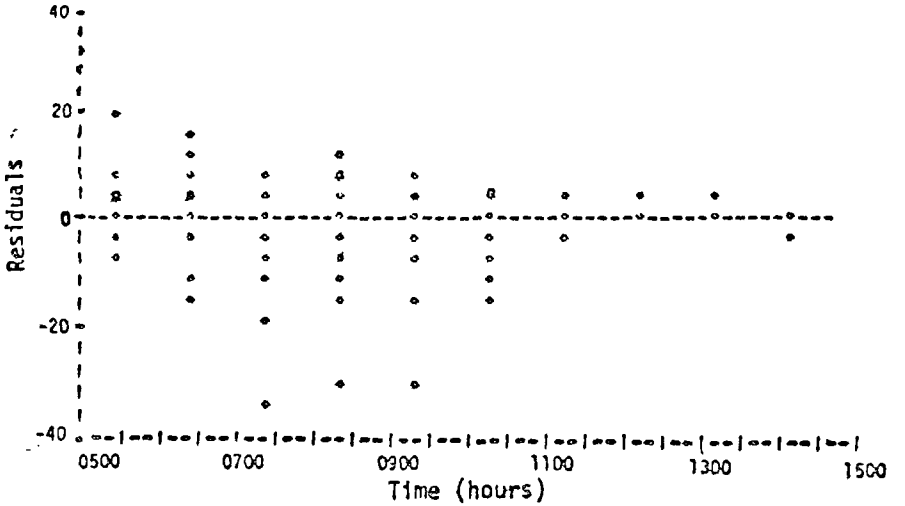

(b) Residuals as a Function of Time

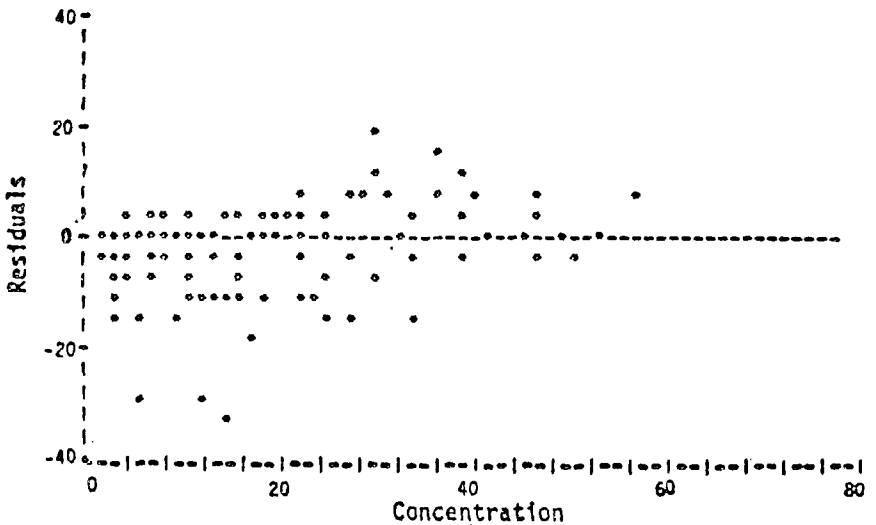

(c) Residuals as a Function of SAIT Concentration

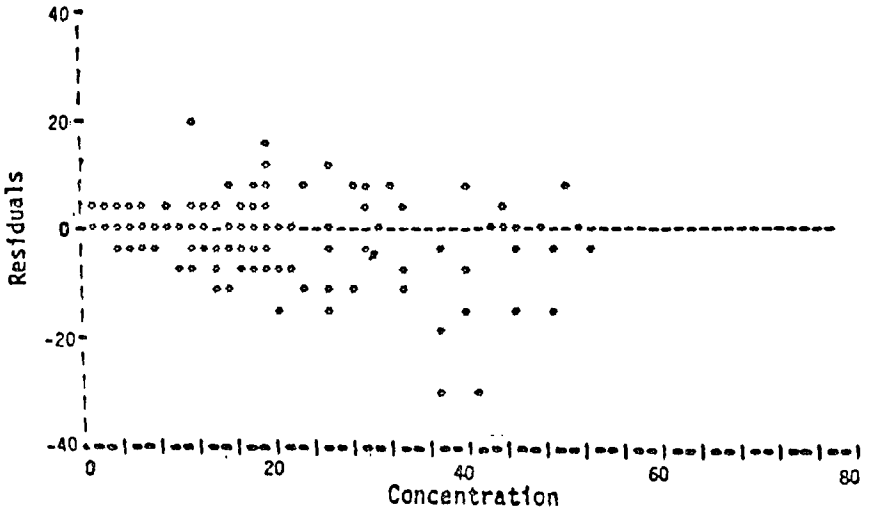

(d) Residuals as a Function of SAII Concentration

FIGURE II-15. RESIDUALS (SAIT MINUS SAII) ANALYSES OF THE SAI TRAJECTORY RESULTS FOR NO

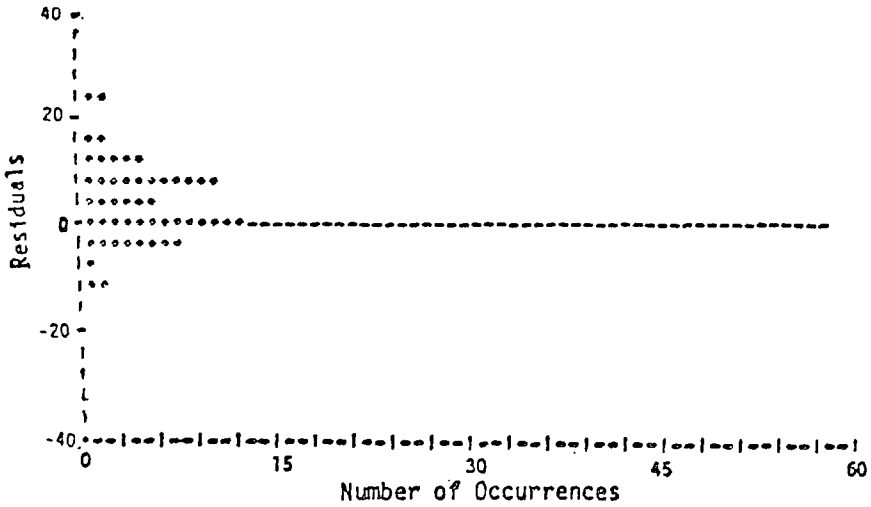

(a) Histogram of Residuals

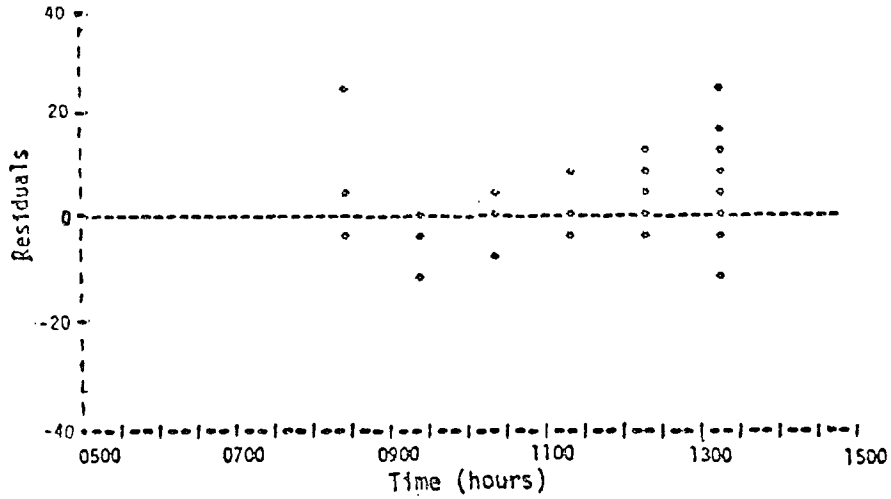

(b) Residuals as a Function of Time

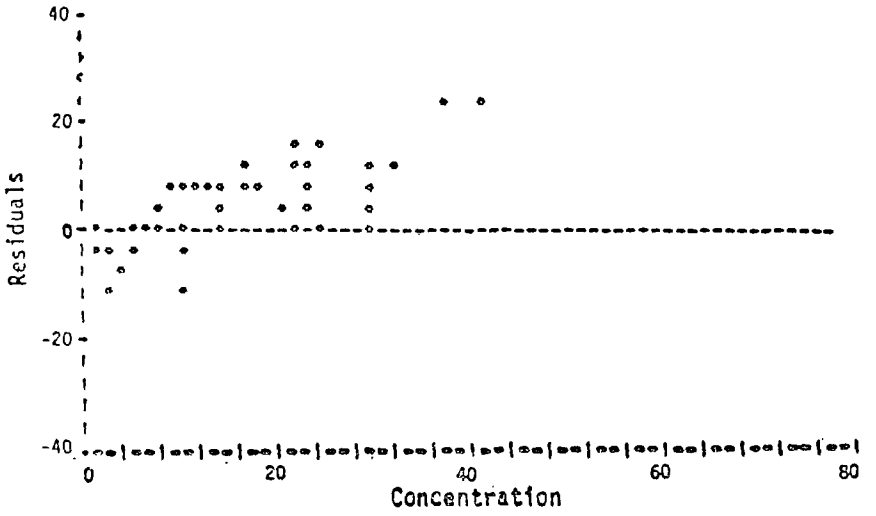

(c) Residuals as a Function of PESC Concentration

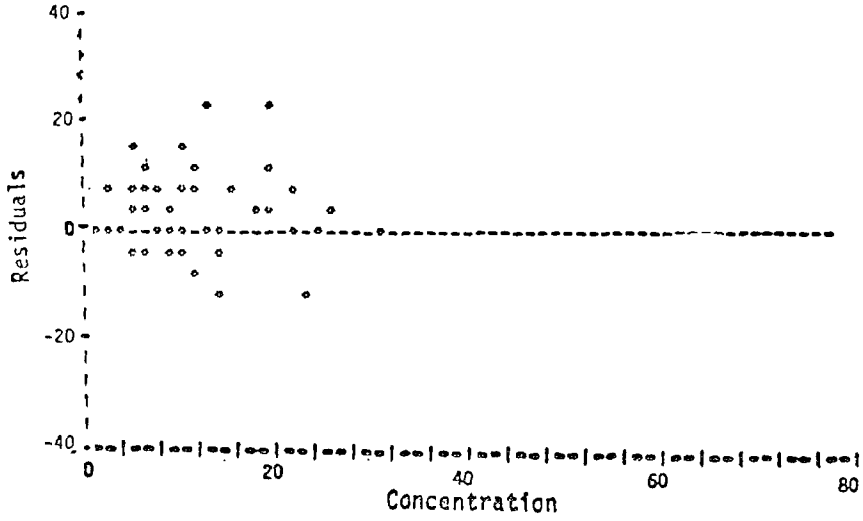

(d) Residuals as a Function of PESM Concentration

FIGURE II-16. RESIDUALS (PESC MINUS PESM) ANALYSES OF THE PES RESULTS FOR NO_2

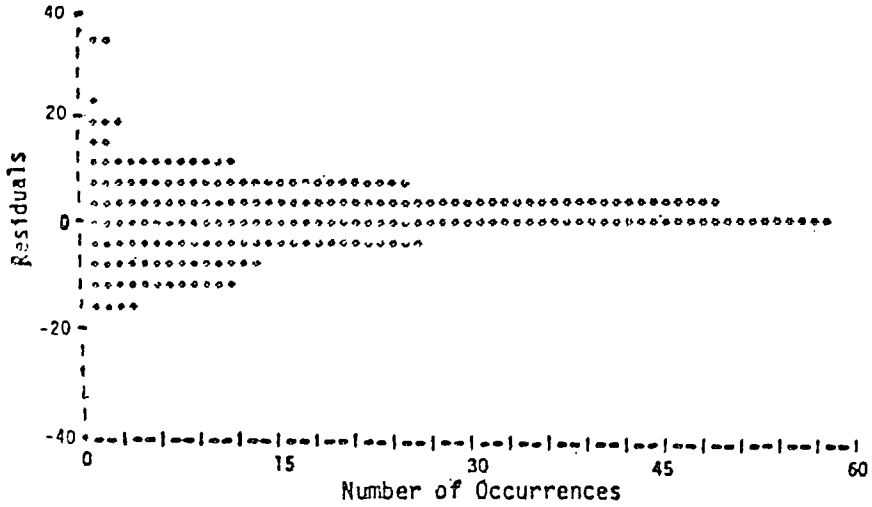

(a) Histogram of Residuals

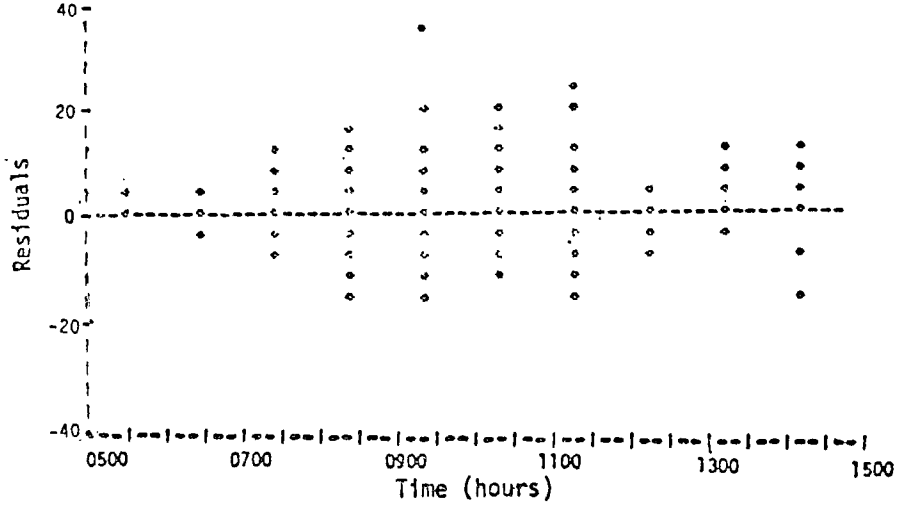

(b) Residuals as a Function of Time

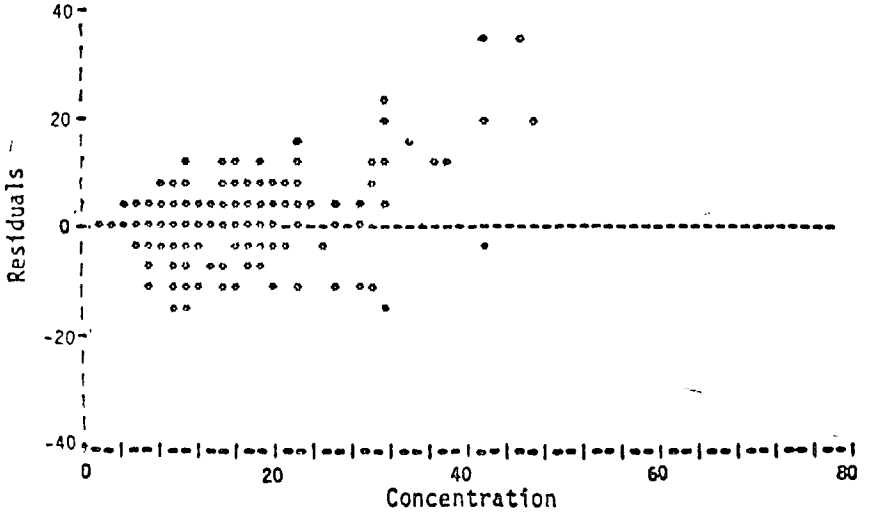

(c) Residuals as a Function of SAIC Concentration

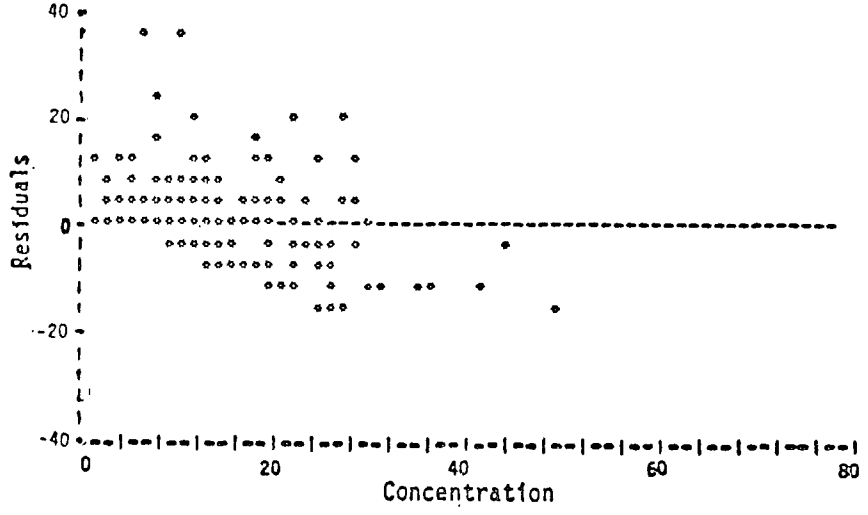

(d) Residuals as a Function of SAIM Concentration

FIGURE II-17. RESIDUALS (SAIC MINUS SAIM) ANALYSES OF THE SAI STATION RESULTS FOR NO_2

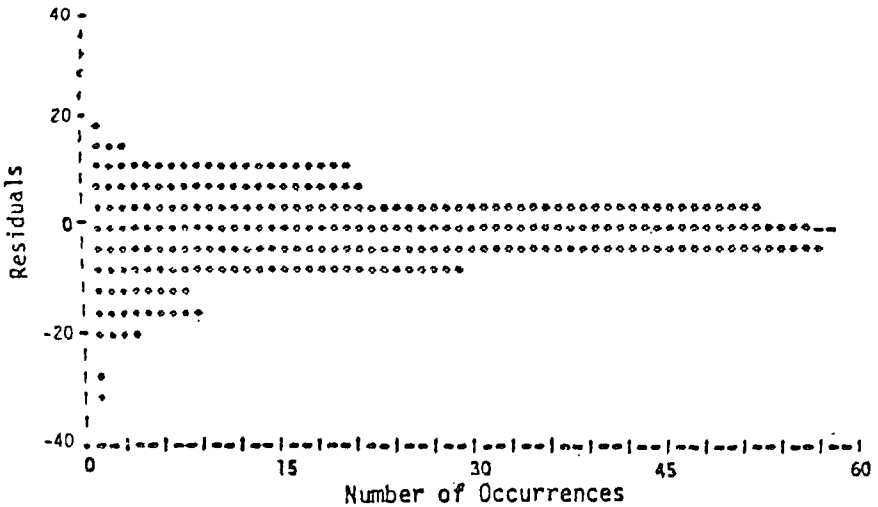

(a) Histogram of Residuals

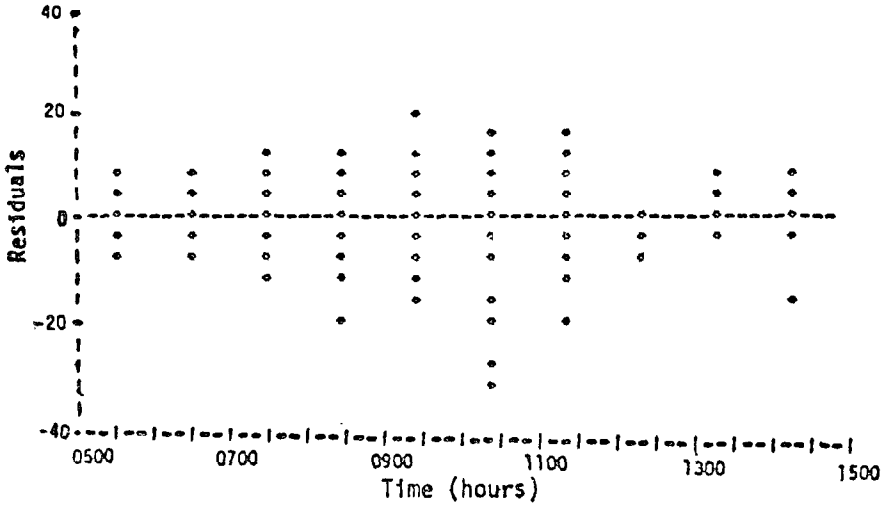

(b) Residuals as a Function of Time

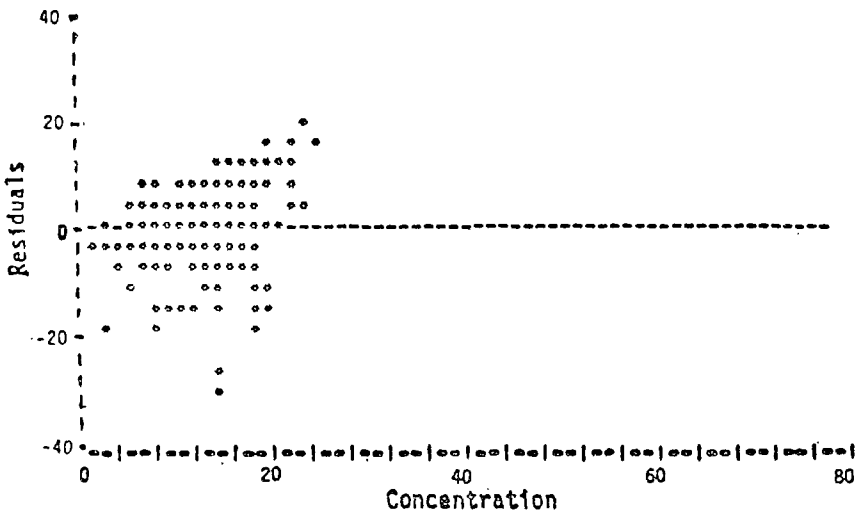

(c) Residuals as a Function of CORC Concentration

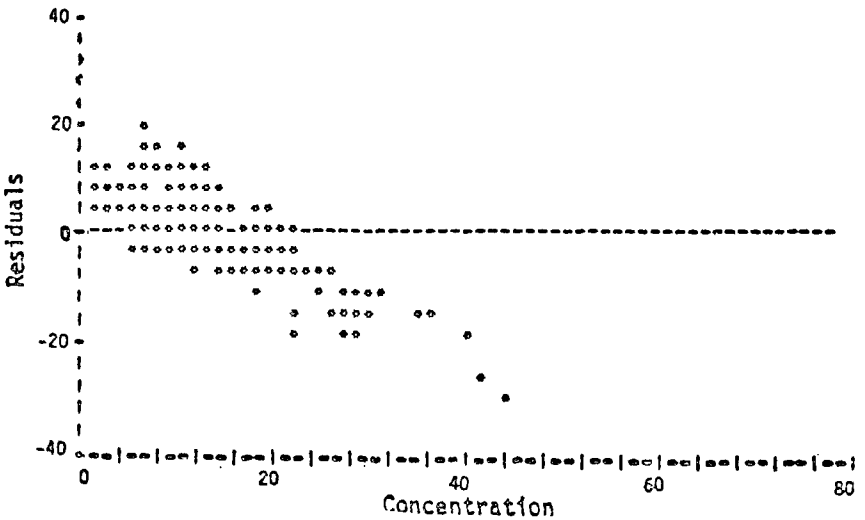

(d) Residuals as a Function of CORM Concentration

FIGURE II-18. RESIDUALS (CORC MINUS CORM) ANALYSES OF THE CORRELATED STATION RESULTS FOR NO_2

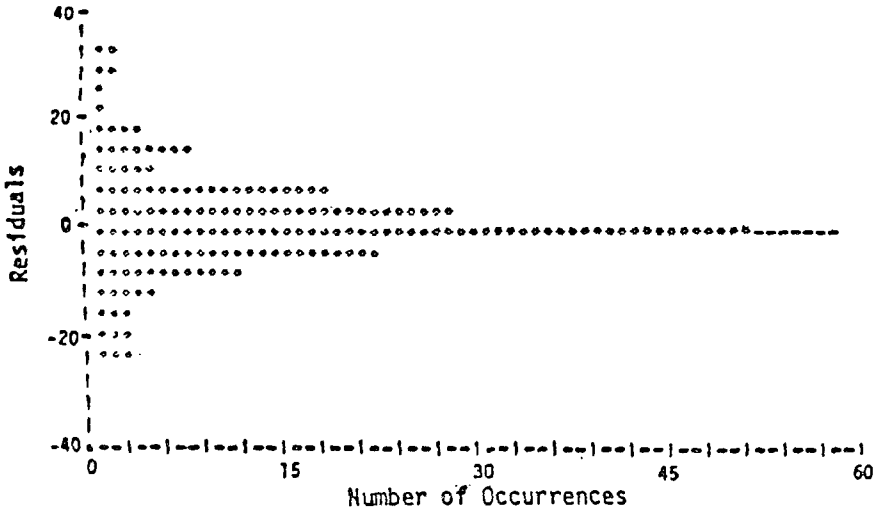

(a) Histogram of Residuals

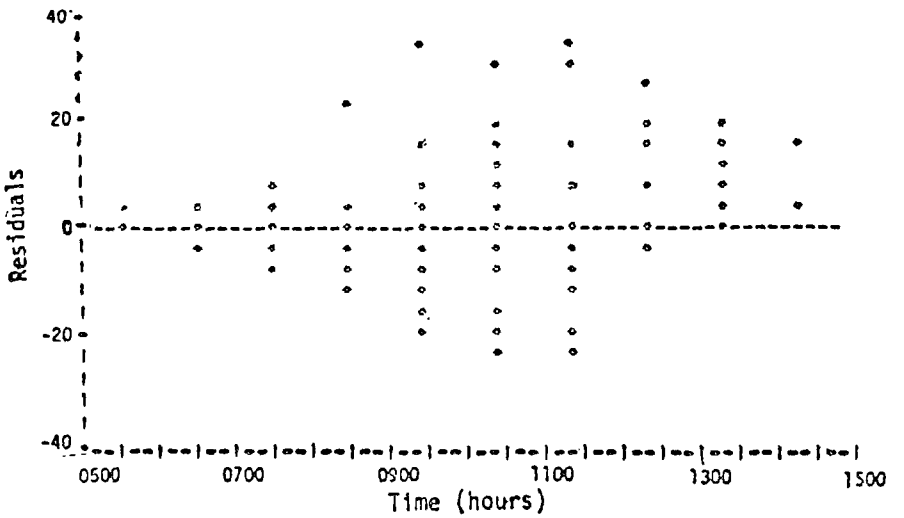

(b) Residuals as a Function of Time

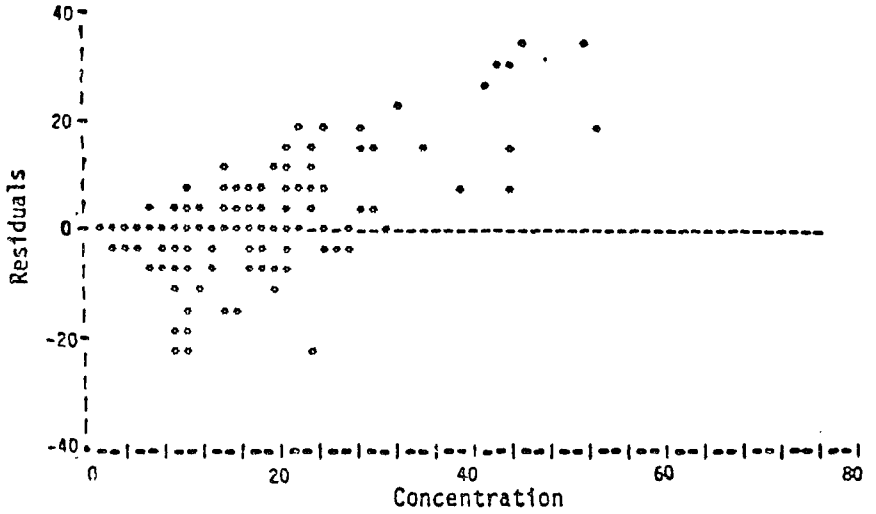

(c) Residuals as a Function of GRCT Concentration

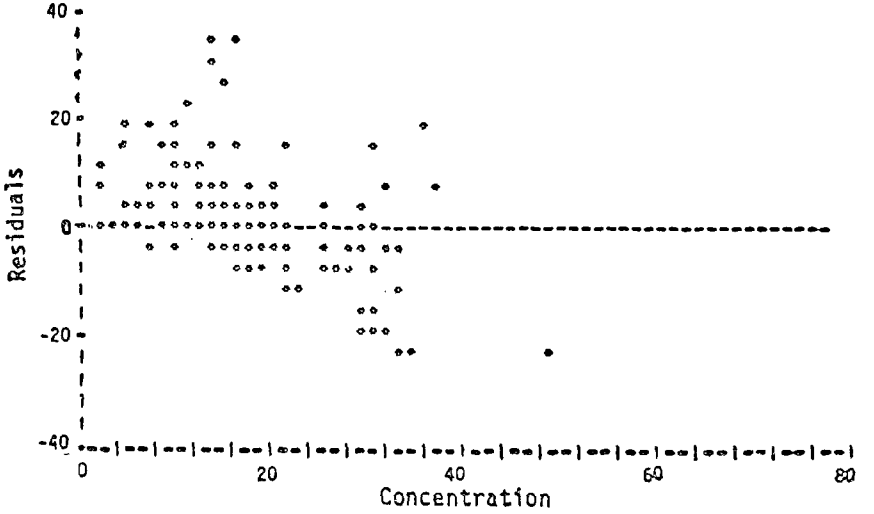

(d) Residuals as a Function of GRCI Concentration

FIGURE II-19. RESIDUALS (GRCT MINUS GRCI) ANALYSES OF THE GRC RESULTS FOR NO_2

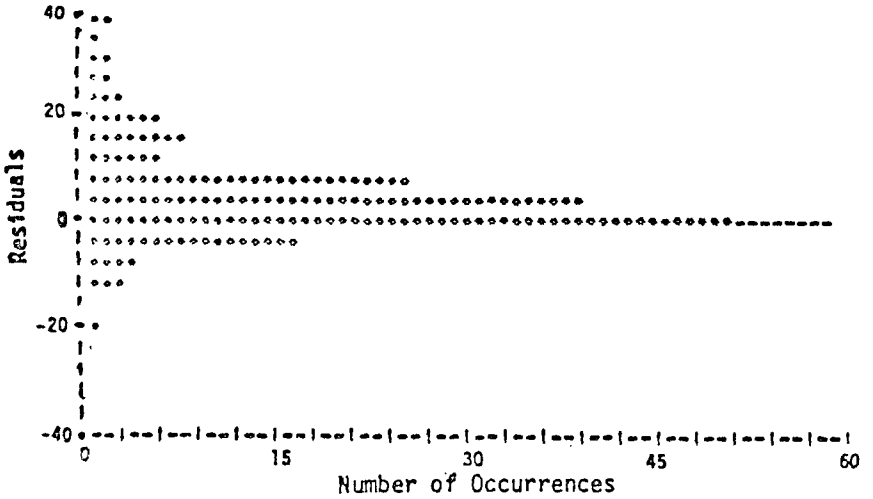

(a) Histogram of Residuals

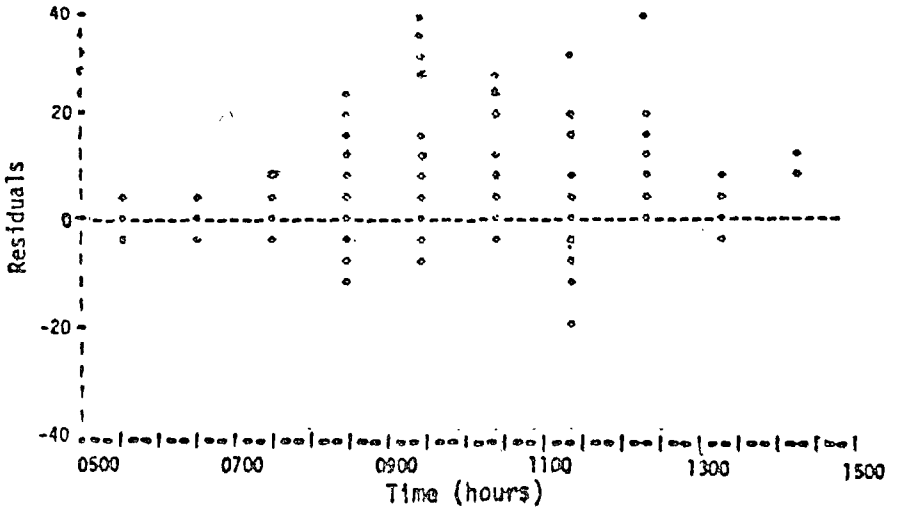

(b) Residuals as a Function of Time

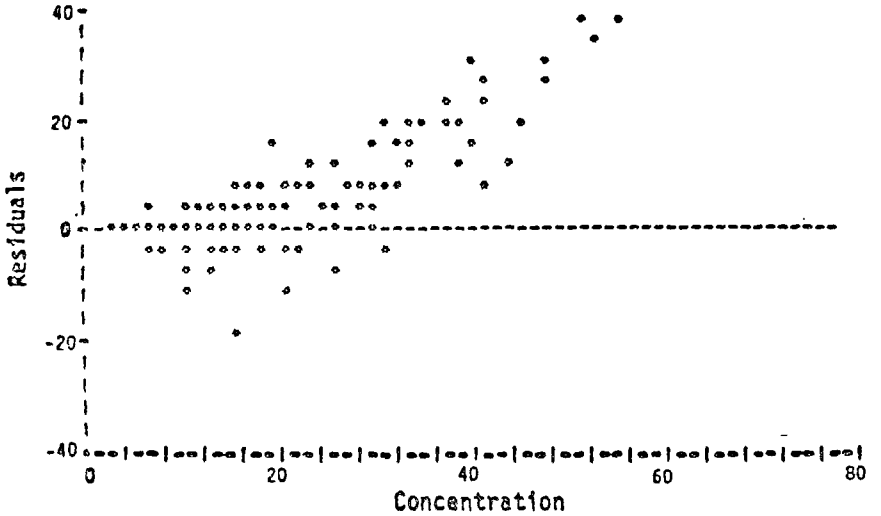

(c) Residuals as a Function of SAIT Concentration

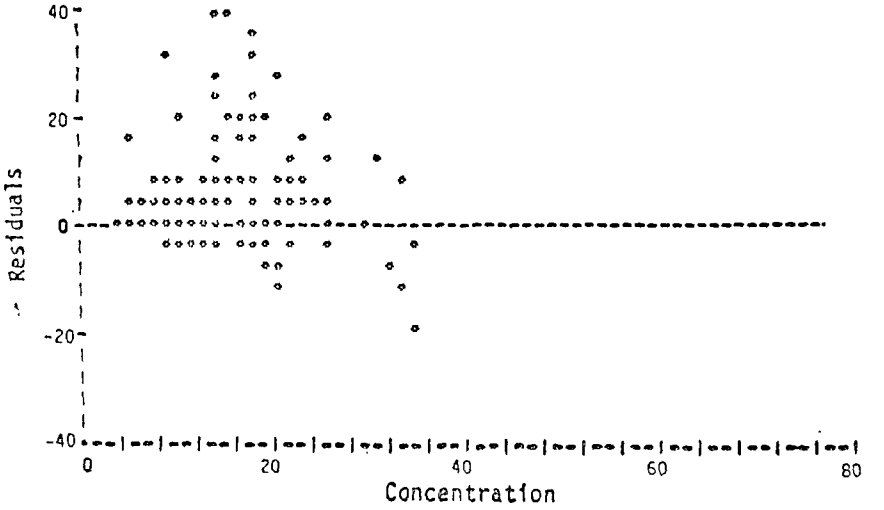

(d) Residuals as a Function of SAII Concentration

FIGURE II-20. RESIDUALS (SAIT MINUS SAII) ANALYSES OF THE SAI TRAJECTORY RESULTS FOR NO_2

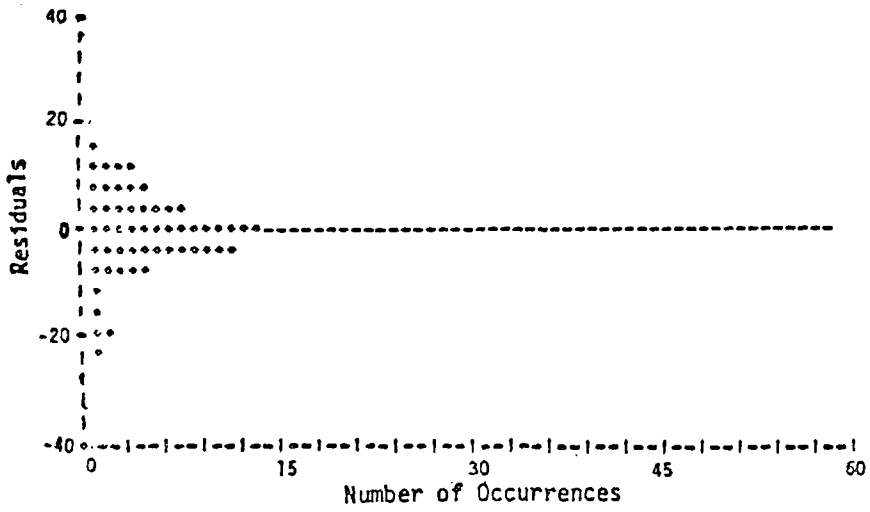

(a) Histogram of Residuals

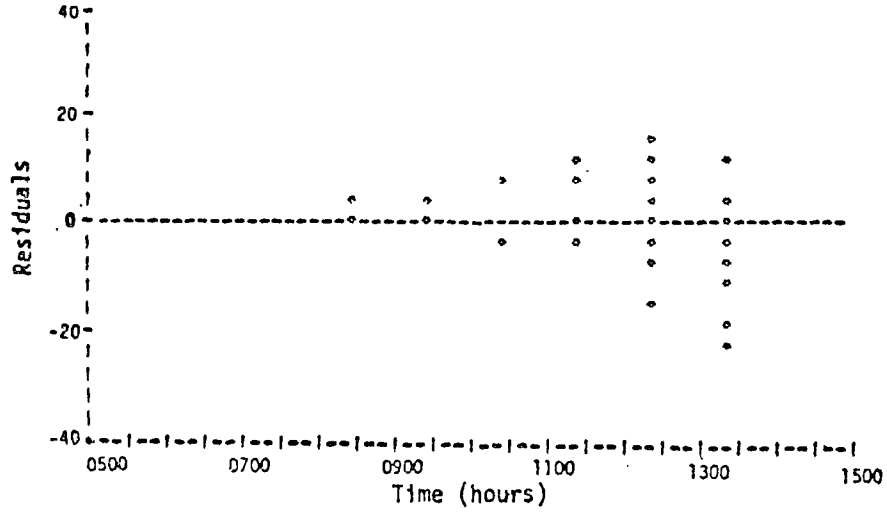

(b) Residuals as a Function of Time

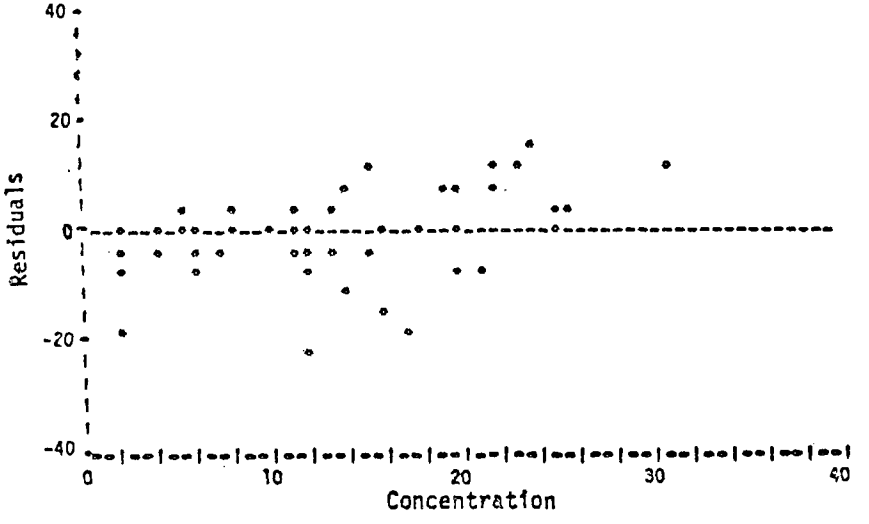

(c) Residuals as a Function of PESC Concentration

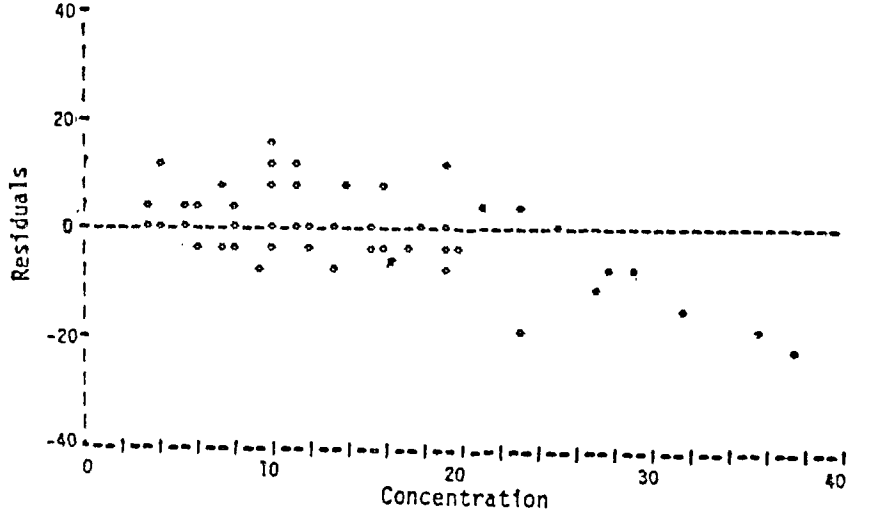

(d) Residuals as a Function of PESM Concentration

FIGURE II-21. RESIDUALS (PESC MINUS PESM) ANALYSES OF THE PES RESULTS FOR O_3

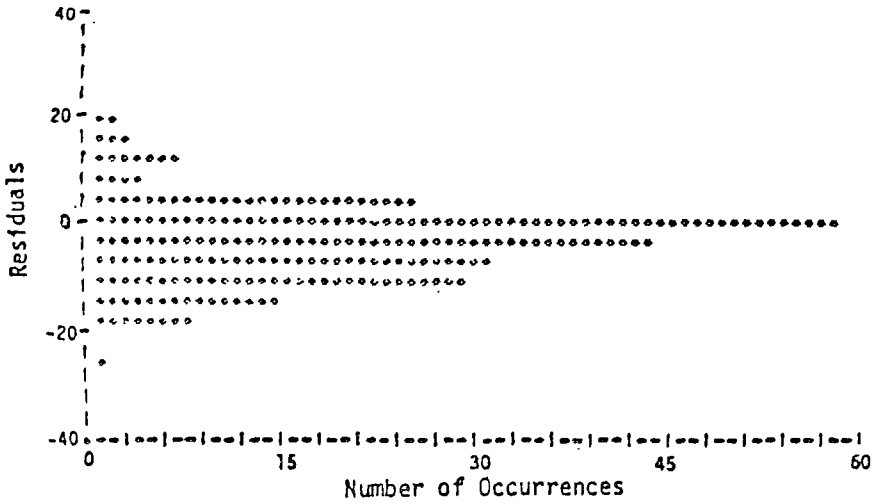

(a) Histogram of Residuals

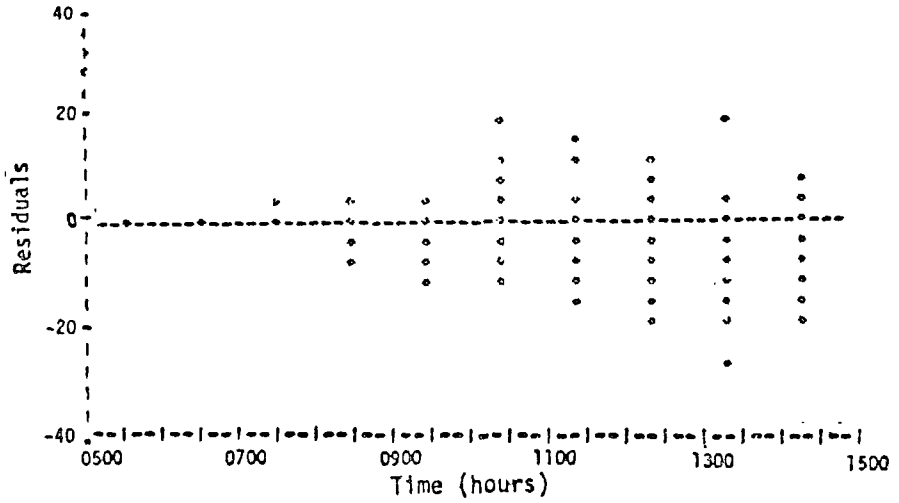

(b) Residuals as a Function of Time

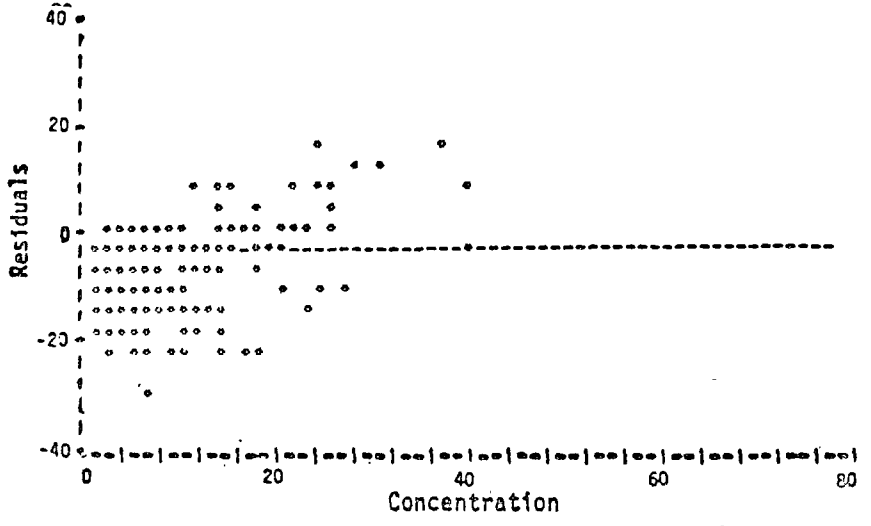

(c) Residuals as a Function of SAIC Concentration

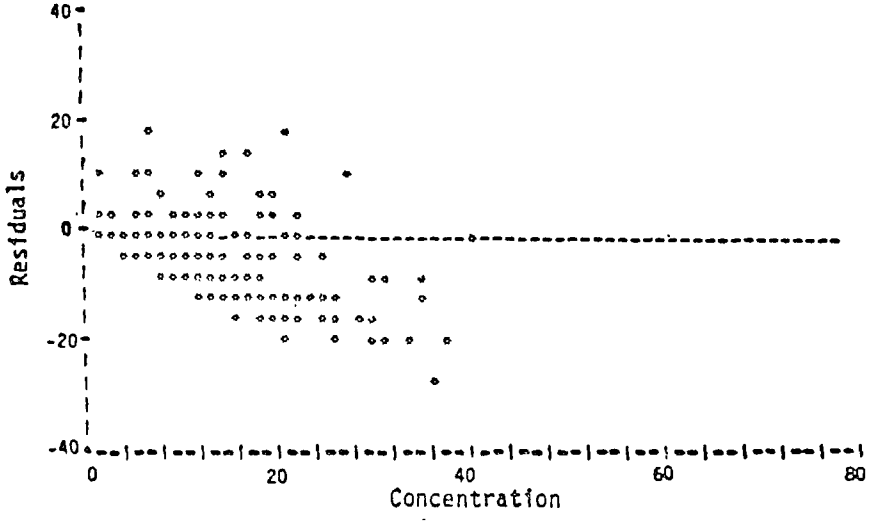

(d) Residuals as a Function of SAIM Concentration

FIGURE II-22. RESIDUALS (SAIC MINUS SAIM) ANALYSES OF THE SAI STATION RESULTS FOR O_3

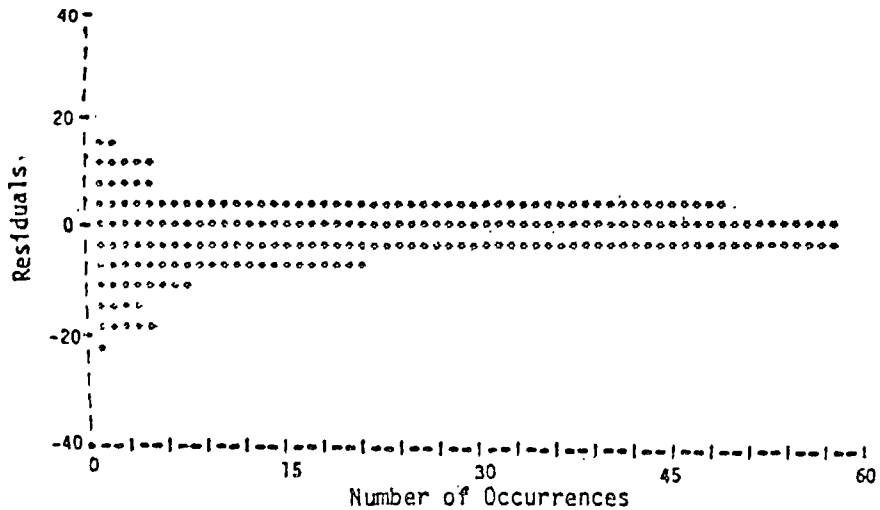

(a) Histogram of Residuals

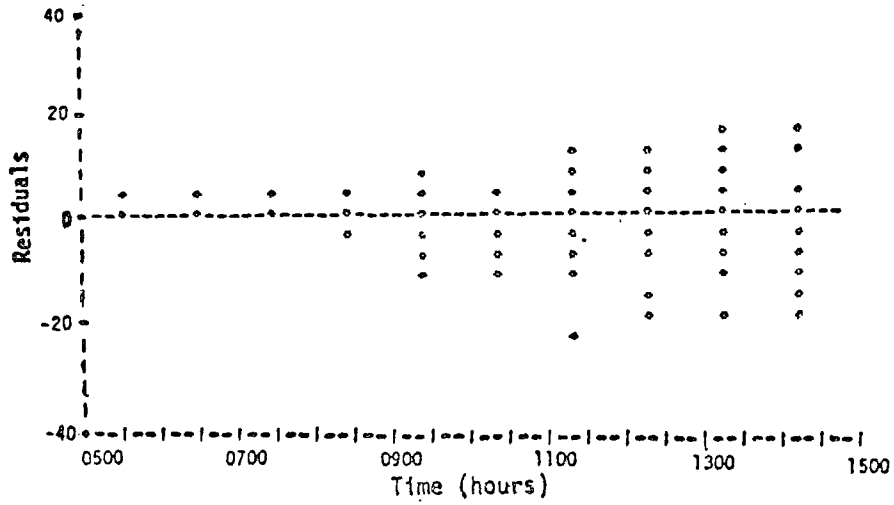

(b) Residuals as a Function of Time

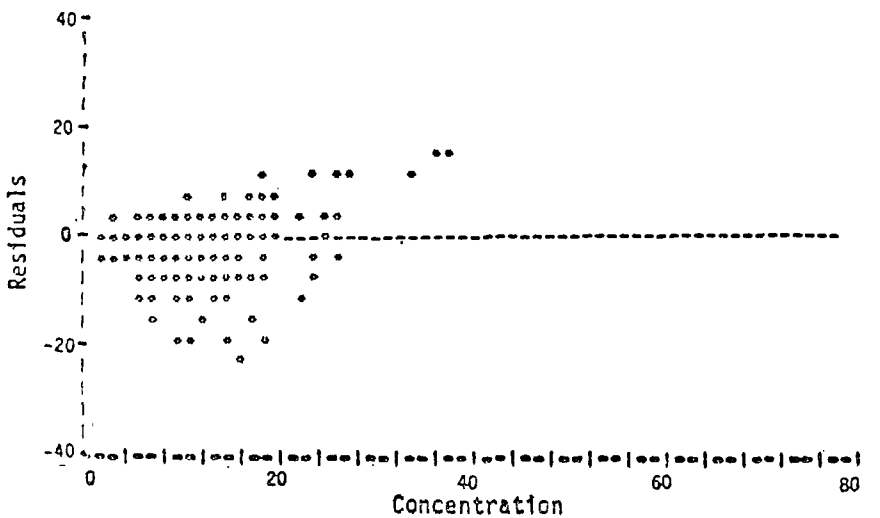

(c) Residuals as a Function of CORC Concentration

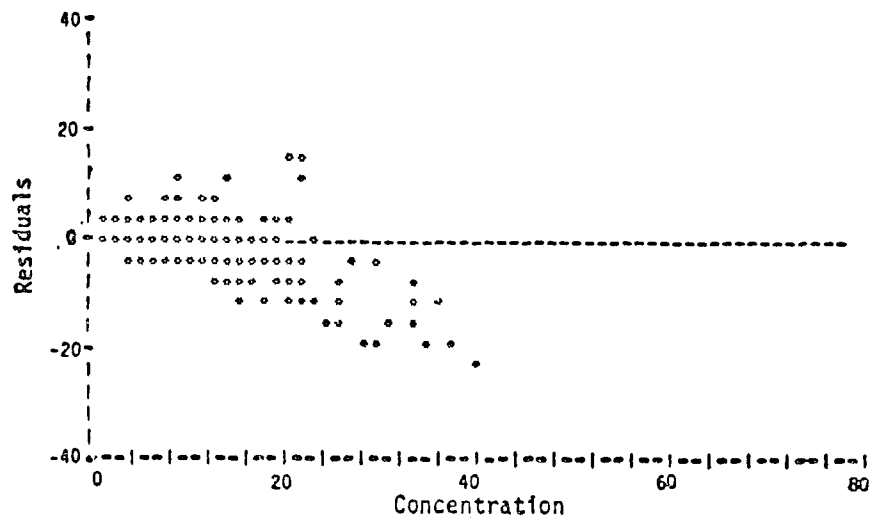

(d) Residuals as a Function of CORM Concentration

FIGURE II-23. RESIDUALS (CORC MINUS CORM) ANALYSES OF THE CORRELATED STATION RESULTS FOR O_3

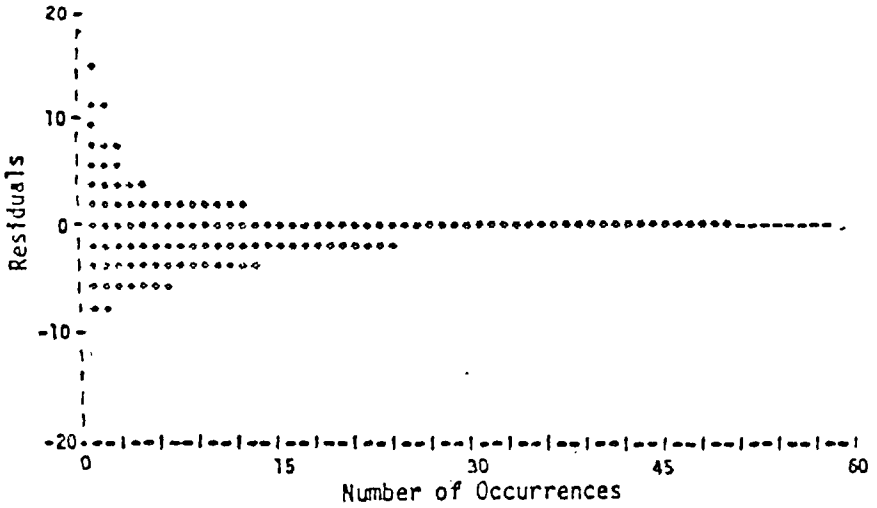

(a) Histogram of Residuals

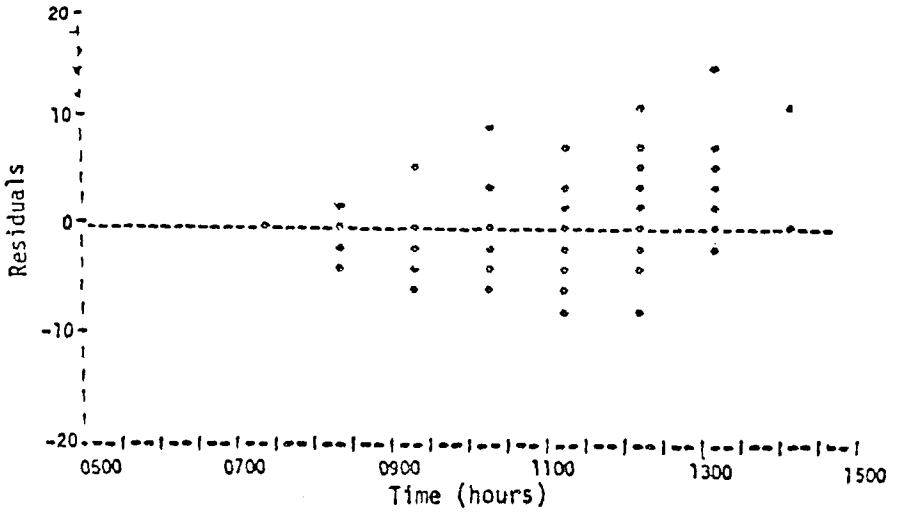

(b) Residuals as a Function of Time

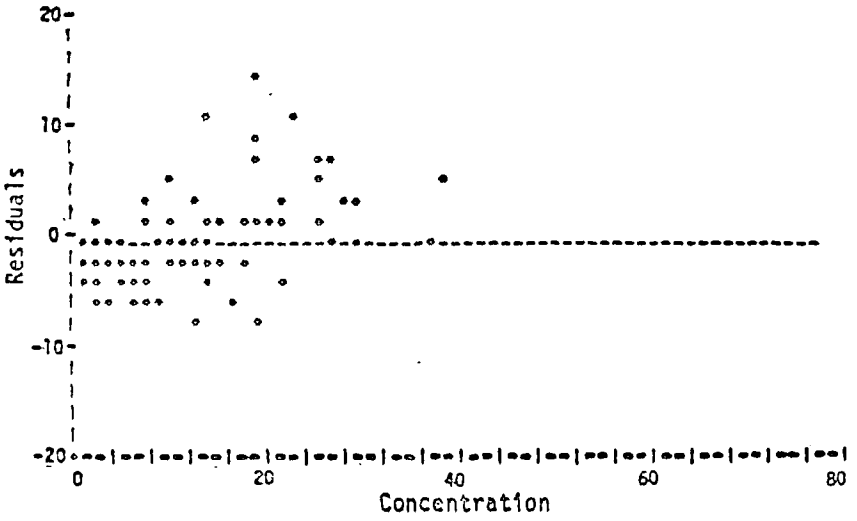

(c) Residuals as a Function of GRCT Concentration

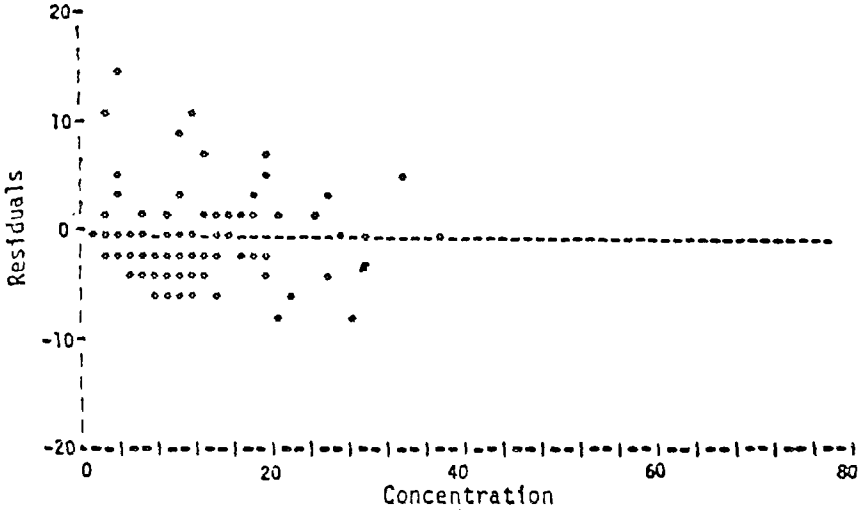

(d) Residuals as a Function of GRCI Concentration

FIGURE II-24. RESIDUALS (GRCT MINUS GRCI) ANALYSES OF THE GRC RESULTS FOR O_3

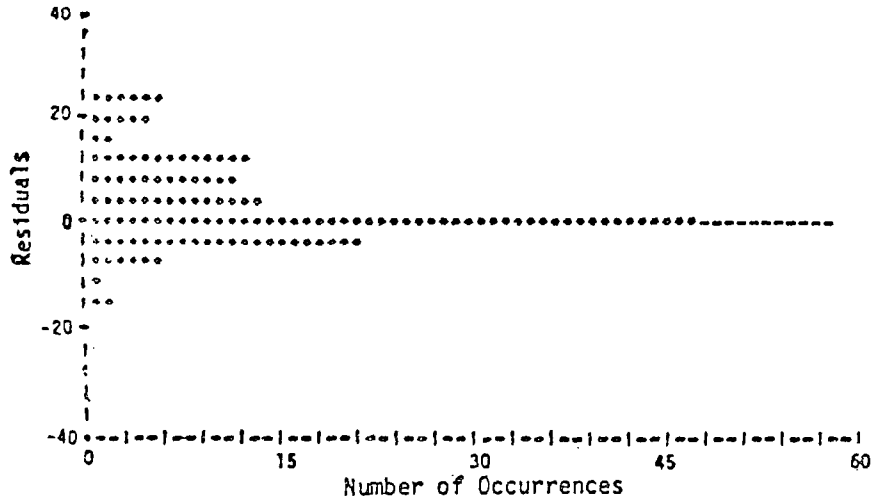

(a) Histogram of Residuals

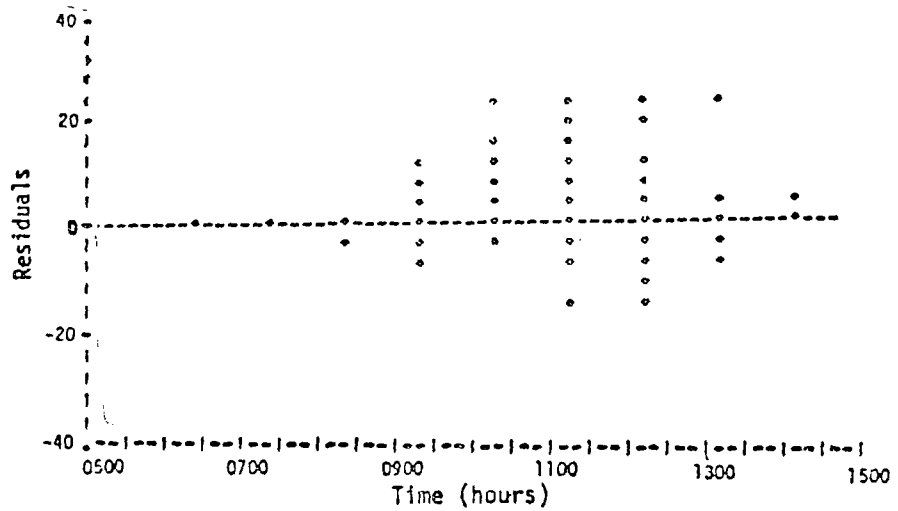

(b) Residuals as a Function of Time

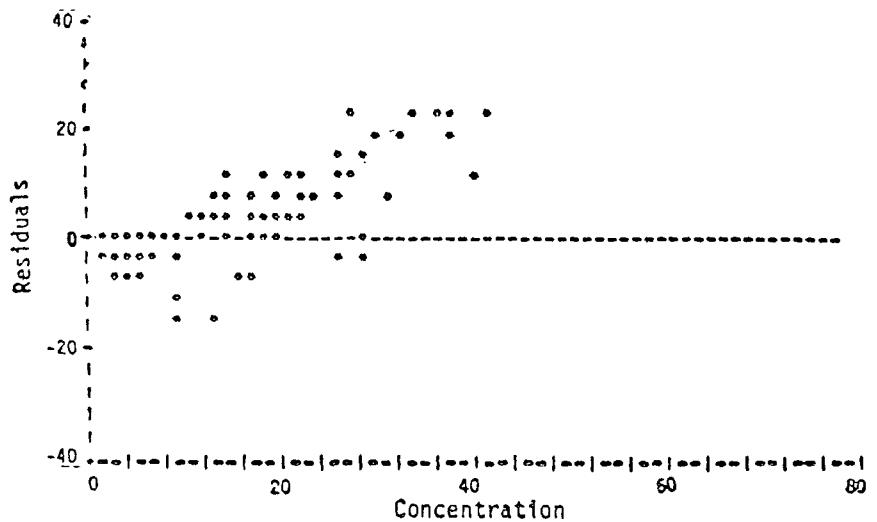

(c) Residuals as a Function of SAIT Concentration

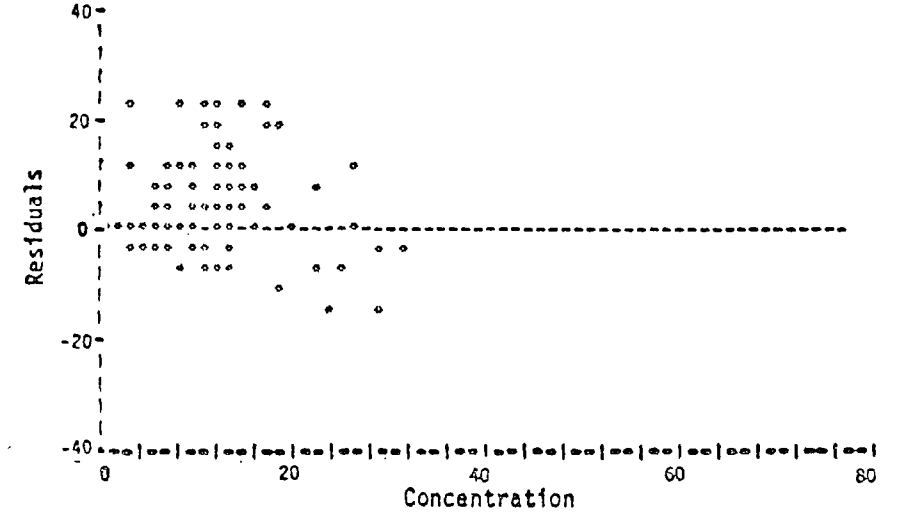

(d) Residuals as a Function of SAII Concentration

FIGURE II-25. RESIDUALS (SAIT MINUS SAII) ANALYSES OF THE SAI TRAJECTORY RESULTS FOR O_3

undercalculation. Further insight can be obtained from Figure II-7(b), which indicates a clear tendency to underpredict during the morning rush hours (0700 to 0900). In Figure II-7(d) the residuals are negative at high measured concentrations, a situation similar to that found for the PES results.

The station correlation results for CO are similar to those for PES, except for a consistent tendency to underpredict [Figure II-8(c)] at almost all concentration levels. This tendency arises from the attempt to calculate particularly high, and probably nonrepresentative, CO concentrations using lower, and probably more representative, concentrations from neighboring stations. A similar effect is present in Figure II-8(d), where the negative residuals at high concentrations also indicate a lack of high-concentration neighbors.

In the residuals analyses of the GRC results [Figures II-9(a) through II-9 (d)], there is a trend toward underprediction during the rush period and a trend toward overprediction in the afternoon [Figure II-9(b)]. This particular behavior in the afternoon does not seem to be present in either the PES or SAI station results [Figures II-6(b) and II-7(b)]. As with the PES and SAI station results discussed previously, Figure II-9(d) points out that the GRC results show underprediction at high measured concentrations.

Finally, an examination of the residuals for the SAI trajectory CO results [Figures II-10(a) through II-10(d)] indicates much less of a tendency to underpredict during the morning rush hours [see Figure II-10(b)], compared with the GRC model and, in general, a weaker bias toward negative residuals.

The residual results for NO (Figures II-11 through II-15) do not reflect the homogeneity that the CO results showed. In the PES results, the histogram [Figure II-11(a)] appears to indicate extremely strong agreement between calculated and measured values. However, almost all of the data reported by PES were for the early afternoon, when NO concentrations have reached their background level of 1 pphm. For the one day when PES carried out calculations for the morning period, the residuals were consistently negative (indicating underprediction), as shown in Figures II-11(b) and II-11(d). Since NO is a primary emissions product, these results probably reflect the problems of disparity in scales and station nonrepresentativeness.

The SAI residuals, for both the station and trajectory model results, show a skewed distribution [Figures II-12(a) and II-15(a)], tending toward either slightly high or markedly low values around zero. The greatest (negative) deviations occurred at mid-morning [Figures II-12(b) and II-15(b)], which was also the time of the highest NO concentration [Figures II-12(d) and II-15(d)]. Afternoon predictions by the SAI model were consistently high, indicating its inadequate treatment of NO/NO_2 kinetics.

The GRC residuals, though they demonstrate a slight bias toward underprediction [Figure II-14(a)], do not exhibit any particular trends as a function of time [Figure II-14(b)] or concentration [Figures II-14(c) and II-14(d)]. The differences between the GRC and SAI trajectory results can most likely be attributed to the differences between the chemical reaction mechanisms used. The station interpolation values are reasonably well distributed, though highly scattered, except in Figure II-13(d), where the interpolation scheme is unable to match the highest measured values. Closer investigation of the data shows that almost all of these high values occur at Burbank; the anomalous location of this station (and the correspondingly high measured values) has already been discussed.

The NO_2 results (Figures II-16 through II-20) show a series of trends opposite to those exhibited by NO. Again, the preponderance of PES data in the early afternoon obscures some of the findings, but the tendency toward overprediction [Figures II-16(a)] is evident.

The SAI and GRC results are similar in that they display a tendency toward overprediction, most noticeably in the late morning hours [Figures II-17(b), II-19(b), and II-20(b)], with a predilection toward gross overprediction at the highest calculated values [Figures II-17(c), II-19(c), and II-20(c)]. This latter trend results in part from a tendency of the GRC and SAI models to predict occasionally the peak in the NO_2 concentration one or two hours earlier than its actual occurrence. Similar behavior is observed in smog chamber simulations and is presumably attributable to the inadequacies of the reaction mechanism.

In contrast, the station correlations do not show any particular trend except underprediction of the largest measured values [Figure II 18(d)]; this again is a result of the juxtaposition of the Burbank measuring station and a neighboring power plant. The SAI station calculations also failed to reflect these high measured values [Figure II-17(d)], though no such trend is noticed for the SAI trajectory results [Figure II-20(d)]. This is a particularly clear-cut example of the problem of disparity in scales.

Ozone is produced in the Los Angeles basin entirely as a result of photochemical reactions. Its concentration rises sharply in the afternoon after a morning "incubation period," because of the complex and relatively slow reaction kinetics involved. Therefore, the trends observed in the O_3 residuals are primary indicators of any systematic bias in the chemical kinetics mechanism of a model.

For the PES results, the histogram [Figure II-21(a)] shows a reasonably even distribution, but the time sequence [Figure II-21(b)] demonstrates that this distribution is achieved through overprediction around midday and an inability to calculate the steep O_3 concentration rise in the afternoon. The concentration plots demonstrate the same behavior: positive residuals at the highest predicted values [Figures II-21(c)] and negative residuals for the highest measured values [Figure II-21(d)].

The SAI station residual plots somewhat parallel those of PES, though the histogram [Figure II-22(a)] is more negatively biased and the midday overprediction [Figure II-22(b)] is less pronounced. The concentration plots [Figures II-22(c) and II-22(d)] again show an inability to reproduce the sharply rising measured O_3 concentrations.

The station correlations are dense and evenly distributed; only at the highest values [Figures II-23(c) and II-23(d)] do the interstation discrepancies become apparent.

The GRC model produced a reasonably even distribution for both the histogram [Figure II-24(a)] and concentration plots [Figures II-24(c) and II-24(d)]. Only the time sequence [Figure II-24(b)] shows evidence of a decided tendency to overpredict; this may be a consequence of the reduction in NO emissions, since excess NO would tend to reduce the O_3 concentration chemically.

The SAI trajectory results are most interesting. Unlike the other three data sets, this histogram [Figure II-25(a)] demonstrates a decided bias toward overprediction, primarily at mid-morning [Figure II-25(c)]. The trend toward underprediction of the highest measured values is not nearly as severe [Figure II-25(d)].

Since the same SAI model was used both to underpredict the station values (Figure II-22) and to overpredict the trajectory values (Figure II-25), it is necessary to find some explanation beyond simple modeling error to explain the discrepancy. A likely rationale for this behavior is the problem of disparity in scales--a problem that would be expected to be especially severe in the case of a slow-forming, fast-reacting pollutant such as ozone. Owing to variations in pollutant concentrations and reaction conditions within the grid squares, the "well-mixed chemical reactor" assumption used in modeling is simply inadequate to represent the actual conditions in the "real world," and resolutions of such discrepancies as that noted in this case must await more widespread application of subgrid models and better knowledge of the chemical mechanisms of smog formation.

E. CONCLUSIONS

In general, it cannot be stated that any of the three models has or has not been validated adequately. The intrinsic difficulties in attempting to use a sparse and incomplete data base, with stations sited at what are, from the modeler's point of view, highly nonrepresentative locations, leave too many unknown factors to identify whether discrepancies are due to modeling error or data inappropriateness. Better tests of the ability of the models to simulate the formation and dispersion of photochemical smog must await the availability of denser, more uniform, and more representative measurements.

Given the above caveat, it is still possible to draw a few general conclusions about the performance of the three models under investigation. All of the models were able to follow the changes in concentration of the major pollutants as a function of time. The shortened time frame and small number of data points offered by PES obviously did not stress the model sufficiently, in the sense that it did not have the opportunity to follow the rise and fall of pollutant concentrations during the early morning hours; thus, its validity remains most in doubt. The GRC model and especially the SAI model were placed in a "higher state of jeopardy" by virtue of their earlier starting times and larger number of runs over more varied conditions. Both performed well with regard to the primary pollutants, CO and NO. The GRC model, "tuned" for ozone at the expense of NO_2, predicted the former well. The SAI model treated NO_2 and ozone equally successfully. None of the models exhibited a particular flair for predicting the highest pollutant concentrations, which are of the greatest interest from a pollution control standpoint. However, those highest concentrations are also the ones most suspect in terms of representativeness. Again, satisfactory validation will ultimately depend on the availability of more suitable data bases.

III. ASSESSMENT OF THE VALIDITY OF AIRSHED MODELS

A. INTRODUCTION

Airshed models can be classified according to the type of coordinate system used: fixed coordinate (grid) or moving coordinate (trajectory). Grid models are based on a coordinate system that is fixed with respect to the ground; hence, they are commonly referred to as Eulerian models. Trajectory models "attach" their coordinate system to a hypothetical vertical air column that moves horizontally with the advective wind; they are often called Lagrangian models. Since the coordinate system used is one of the basic differences among first generation photochemical air pollution models, one of the first tasks that should be undertaken in the development of a second generation model is a careful examination of the range and conditions of validity of each of these modeling approaches. Such an assessment is necessary to determine which type of model (or combination of models) provides a more suitable basis for the development of a second generation model.

In each of these two modeling approaches, we can phenomenologically identify the sources of inaccuracies. First, we consider the trajectory model. This formulation is based on the concept of a hypothetical vertical air column that must maintain its integrity as it moves through the airshed. For several reasons, this model may not be valid under certain conditions in the turbulent atmospheric boundary layer. In the planetary boundary layer, both the magnitude and the direction of the wind vary with height. Therefore, strictly speaking, an air column cannot possibly remain vertical as it is being advected by the wind over the time periods commonly of interest Errors introduced by the assumption of a vertical air column are determined by such factors as the wind profile in the vertical direction, the size of the air column and the transverse distance it travels, and the concentration gradients in the horizontal direction.

Another possible source of errors in the trajectory model is the way in which the trajectories are obtained. Conventionally, these trajectories are computed from wind measurements made by a network of ground stations. The question naturally arises as to whether a network of fixed wind stations can provide the trajectories of air colmns in a turbulent atmosphere. As shown in Appendix A, two types of "Lagrangian" average velocities can be formed, and, depending on the turbulent statistics, they can be quite different. Dyer (1973) estimated values for many hypothetical cases and found that the two velocities can differ under certain circumstances by more than 50 percent. If this is the case, then which, if either, of these two velocities equals the corresponding "Eulerian" velocity registered by a fixed wind station? Apparently, fundamental difficulties exist in the construction of the trajectories used in the Lagrangian model.

Second, we consider the grid model. The primary source of errors associated with this type of model arises in the discretization of the spatial coordinates. Consideration of both computational time and available core memory usually limits the amount of cells in each direction to a number of the order of 50 or less. Unfortunately, in the advective transport of material across the grid system, such a relatively small number of grids produces the undesired effect of pseudo-diffusion. This is evident in the following illustration, which shows that the concentration distribution, as represented by a grid model, has been artificially smoothed.

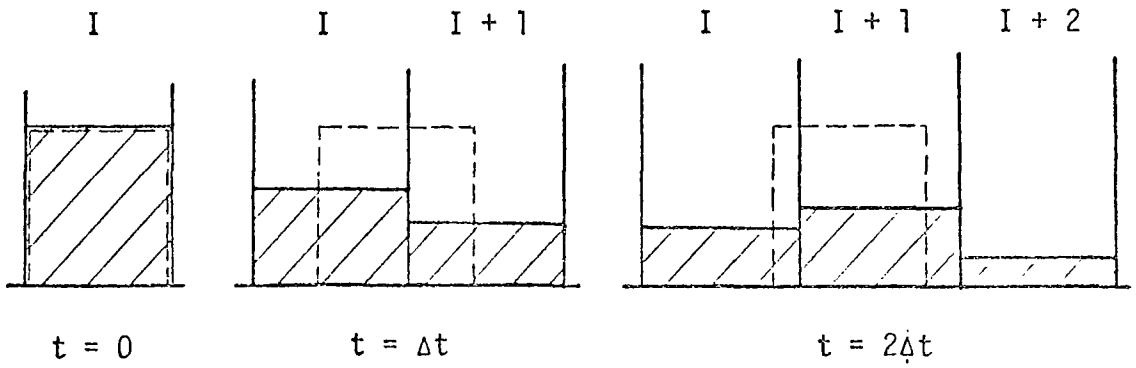

Both the fixed-coordinate grid model and the trajectory model, as shown in Figure III-1, are based on the diffusion equation, which in turn can be derived from a very general model, referred to here as the basic model. The essential assumption upon which the diffusion equation for species that react linearly--and, hence, the grid and trajectory models--are based, is that the kernel Q in the basic model is Gaussian. This is true, however, only for the case of homogeneous, stationary turbulence (Monin and Yaglom, 1971). Further assumptions must be made in deriving the grid and the trajectory models. Solution of the grid model requires finite differencing, whereas formulation of the trajectory model involves neglect of the spatial derivatives. Therefore, a study that examines the validity of the airshed models can be divided into the following two tasks:

- Evaluation of the validity of the diffusion equation.
- Determination of the magnitudes of the errors in the solution of the diffusion equation under the assumptions made in the grid and the trajectory models.

The evalution of the validity of the diffusion equation has been examined by many investigators (e.g., Lamb and Seinfeld, 1973). However, only qualitative results have been obtained with regard to the conditions that must be met in applying the equation. Since these conditions involve the statistics of atmospheric turbulence and linearity or nonlinearity of photochemical reaction terms in the equations of continuity, quantitatively stated conditions for the validity of the diffusion equation under realistic situations are extremely difficult, if not impossible, to obtain. Therefore, despite our suggestions of a scheme at the outset of this task to assess the validity of the diffusion equation for certain restricted cases, we later decided to omit this evaluation altogether in the present study for two reasons:

- It would have required considerably more time and effort than we could devote.

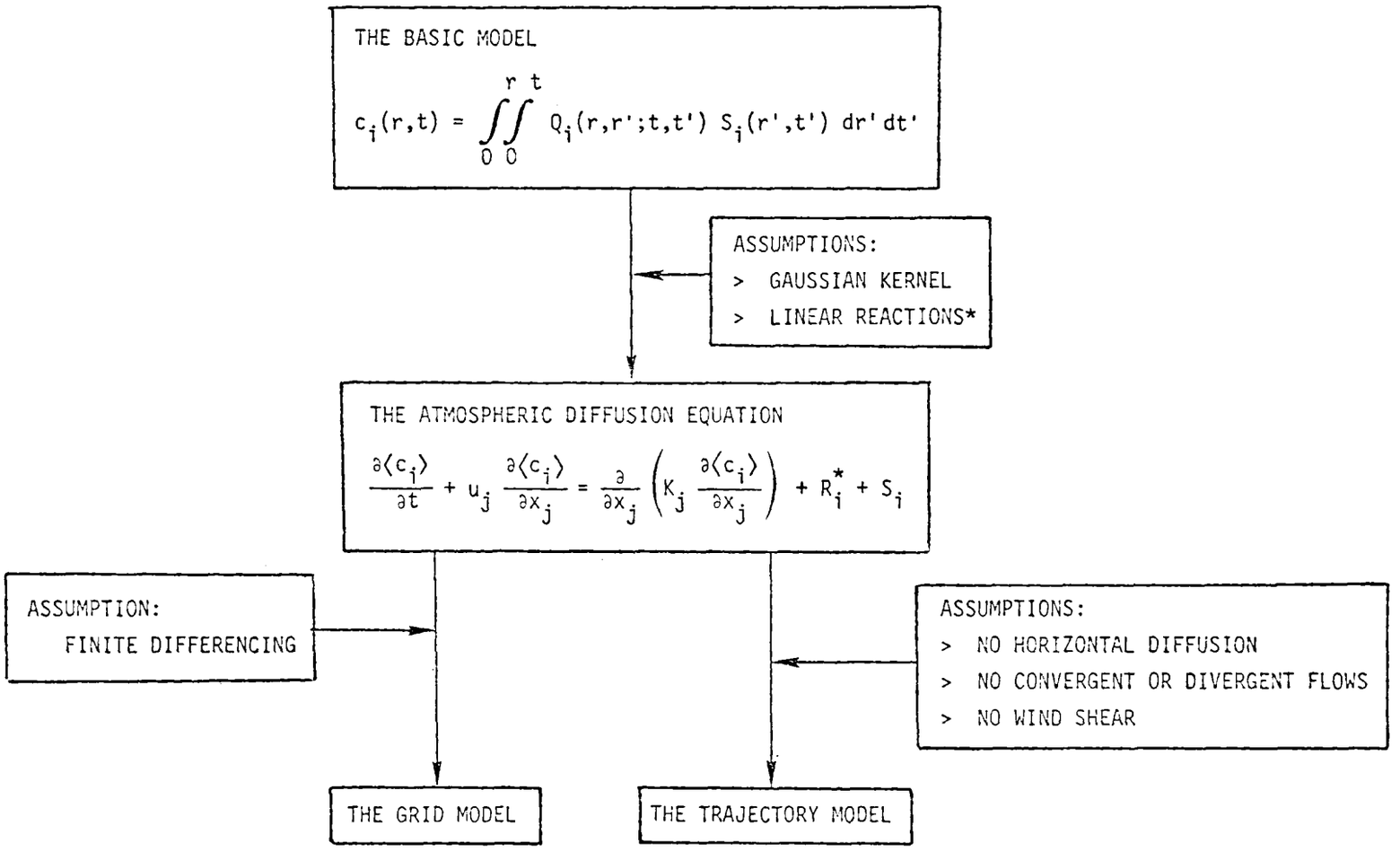

*However, if one considers the atmospheric diffusion equation to be derived phenomenologically, the reactions therein may not necessarily be linear.

FIGURE III-1. DIAGRAM OF THE BASIC RELATIONSHIPS IN THE VALIDITY STUDY

> Cases for which analytic solutions can be obtained (such as homogeneous, stationary turbulence, linear reactions) and, thus, cases for which model evaluation can be undertaken, may be too restrictive to be of practical interest.

Consequently, we chose to restrict the scope of the validity study in this contract effort to the second task: assessment of the validity of the grid and trajectory models when compared with the diffusion equation.

In the next section, we present a theoretical analysis of the errors in the trajectory and grid models. This evaluation takes the form of a direct examination of the basic mathematical formulation inherent in each of these two approaches. In spite of the rigor of this theoretical analysis, it yielded only qualitative, or order-of-magnitude, estimates. To provide a quantitative assessment, we carried out a numerical experiment, which we describe in Section C. Although they are still limited to two-dimensional cases, accurate comparisons can be made for many realistic situations. Section D presents the results of these comparisons for the trajectory model, and Section E, for the grid model. Section F summarizes our conclusions regarding the relative merits of these two models.

B. A THEORETICAL ANALYSIS OF THE VALIDITY OF THE AIRSHED MODELS

The most direct approach to investigating the difference between the fixed-coordinate grid model and the moving-trajectory model is to compare the mathematical equations upon which the two classes of models are based. As we stated earlier, we chose the atmospheric diffusion equation as the common basis of comparison. By invoking the assumption of eddy diffusivity we can write the most general diffusion equation describing the transport, diffusion, and chemical reaction processes that take place in the atmosphere as follows:

$$\frac{\partial c_i}{\partial t} + u\frac{\partial c_i}{\partial x} + v\frac{\partial c_i}{\partial y} + w\frac{\partial c_i}{\partial z} = \frac{\partial}{\partial x}\left(K_H \frac{\partial c_i}{\partial x}\right) + \frac{\partial}{\partial y}\left(K_H \frac{\partial c_i}{\partial y}\right) + \frac{\partial}{\partial z}\left(K_V \frac{\partial c_i}{\partial z}\right) + R_i + S_i$$

$$i = 1, 2, \ldots, N, \qquad \text{(III-1)}$$

where c_i is the mean concentration of species i; R_i is the average reaction rate and S_i is the emission rate for the species i; u, v, and w are the average velocity components of the wind; and K_H and K_V are the horizontal and vertical diffusivities, respectively.

As we subsequently show, both the grid and the trajectory models are derivatives of Equation (III-1) with the application of further--and thus more restrictive--assumptions. In the following two subsections, we attempt to evaluate the relative merits of each of these two classes of modeling approaches, but first we derive the appropriate form of the model equations for the two models. By comparing these model equations with the atmospheric equation (III-1), we identify the deficiencies of each of the modeling approaches.

1. The Trajectory Model

Despite the basically Eulerian nature of the atmospheric diffusion equation, we can derive the modeling equation for trajectory models from Eq. (III-1). As we stated earlier, the trajectory model attempts to describe, using a coordinate system that moves along a surface level wind trajectory, physical processes that influence pollutant concentrations. Toward this end, we can introduce the following general transformation of variables in Eq. (III-1):

$$\begin{aligned} \xi &= \xi(x,y,t) \quad , \\ \eta &= \eta(x,y,t) \quad , \\ z &= z \quad , \\ t &= t \quad , \end{aligned} \tag{III-2}$$

where the functional forms of ξ and η are to be determined from the trajectories. Invoking the chain rule to yield the derivatives, substituting these derivatives in Eq. (III-1), and rearranging some terms, we obtain

$$\frac{\partial c}{\partial t} = K_H \left\{ \left[\left(\frac{\partial \xi}{\partial x}\right)^2 + \left(\frac{\partial \xi}{\partial y}\right)^2 \right] \frac{\partial^2 c}{\partial \xi^2} + 2 \left[\left(\frac{\partial \eta}{\partial x}\right)\left(\frac{\partial \xi}{\partial x}\right) + \left(\frac{\partial \eta}{\partial y}\right)\left(\frac{\partial \xi}{\partial y}\right) \right] \frac{\partial^2 c}{\partial \xi \partial \eta} \right.$$

$$\left. + \left[\left(\frac{\partial \eta}{\partial x}\right)^2 + \left(\frac{\partial \eta}{\partial y}\right)^2 \right] \frac{\partial^2 c}{\partial \eta^2} + \left(\frac{\partial^2 \xi}{\partial x^2} + \frac{\partial^2 \xi}{\partial y^2} \right) \frac{\partial c}{\partial \xi} + \left(\frac{\partial^2 \eta}{\partial x^2} + \frac{\partial^2 \eta}{\partial y^2} \right) \frac{\partial c}{\partial \eta} \right\}$$

$$- \left(\frac{\partial \xi}{\partial t} + u \frac{\partial \xi}{\partial x} + v \frac{\partial \xi}{\partial y} \right) \frac{\partial c}{\partial \xi} - \left(\frac{\partial \eta}{\partial t} + u \frac{\partial \eta}{\partial x} + v \frac{\partial \eta}{\partial y} \right) \frac{\partial c}{\partial \eta}$$

$$- w \frac{\partial c}{\partial z} + \frac{\partial}{\partial z} \left(K_V \frac{\partial c}{\partial z} \right) + R + S \qquad \text{(III-3)}$$

To the extent that the atmospheric diffusion equation is a valid description of the physical processes under consideration, Eq. (III-3) is still the "exact" equation describing the concentration changes relative to a moving coordinate system. We compare below Eq. (III-3) with the most general form of the modeling equations that have been adopted in the trajectory approach,*

$$\frac{\partial c}{\partial t} = \frac{\partial}{\partial z} \left(K_V \frac{\partial c}{\partial z} \right) + R + S \quad , \qquad \text{(III-4)}$$

---

* Regardless of the size of its base area, we have considered the hypothetical air column to be horizontally homogeneous. Thus, the pollutant concentrations within the cell depend only on the distance above the ground, z, and the time of travel, t, of the air column. If we assume further that K-theory is valid, we can derive Eq. (III-4) phenomenologically for the variation of the mean concentration in the air column.

along a trajectory specified by

$$\frac{\partial \xi}{\partial t} + \bar{u}\frac{\partial \xi}{\partial x} + \bar{v}\frac{\partial \xi}{\partial y} = 0 \quad ,$$

$$\frac{\partial \eta}{\partial t} + \bar{u}\frac{\partial \eta}{\partial x} + \bar{v}\frac{\partial \eta}{\partial y} = 0 \quad , \qquad \text{(III-5)}$$

where $\bar{u} \equiv u(x,y,z_R,t)$ and $\bar{v} \equiv v(x,y,z_R,t)$ represent the surface wind* used to construct the trajectory. Term-by-term comparisons of Eqs. (III-3), (III-4), and (III-5) immediately disclose the following:

- The horizontal diffusion terms, i.e., the first group of terms with the common multiplication factor K_H, are neglected in the trajectory models. As is clear from the terms in the braces in Eq. (III-3), horizontal diffusion can be neglected theoretically, in general, only in the trivial case in which the concentration field is constant throughout the entire region of interest. However, strong localized sources, such as freeways and power plants, are commonplace in any airshed. Consequently, the concentration field generally is far from constant. Thus, in the validity study of trajectory models, the effect of the exclusion of horizontal diffusion terms must be considered.
- The vertical component of the wind has been altogether neglected in the conventional trajectory models. The occurrence of convergent flows in an urban area due to many factors, such as the urban heat island effect, certainly makes this assumption unrealistic.
- As shown in Eq. (III-3), terms involving the first spatial derivatives, $\partial c/\partial \xi$ and $\partial c/\partial \eta$, vanish only if

---

* The surface wind is typically taken to be that at a height of 10 m; i.e., $z_R = 10$ m.

$$\frac{\partial \xi}{\partial t} + u \frac{\partial \xi}{\partial x} + v \frac{\partial \xi}{\partial y} = 0 \quad ,$$

$$\frac{\partial \eta}{\partial t} + u \frac{\partial \eta}{\partial x} + v \frac{\partial \eta}{\partial y} = 0 \quad , \qquad \text{(III-6)}$$

where, in general, $u = u(x,y,z,t)$ and $v = v(x,y,z,t)$. A comparison of Eqs. (III-5) and (III-6) shows that in the trajectory model, it is further assumed that

$$u = \overline{u} \quad ,$$
$$v = \overline{v} \quad . \qquad \text{(III-7)}$$

This assumption implies that only a constant horizontal wind field at a reference height, z_R, can be incorporated in the trajectory model. In other words, the vertical variability of the horizontal wind is suppresssed in the trajectory modeling approach. As we show later, the effect of suppressing vertical variations of horizontal wind on the predicted concentrations can be quite substantial.

In the preceding discussion, we have identified the sources of errors associated with the trajectory modeling approach; the remaining task is to establish the magnitudes of errors so that the range of validity of the trajectory model can be determined. In principle, this task can be accomplished by evaluating the magnitudes of the respective error terms under commonly occurring circumstances. In practice, the multiplicity of possible conditions or combinations of conditions that can take place in an urban atmsophere render this approach impracticable. Furthermore, only qualitative, or order-of-magnitude, estimates can be obtained. For these reasons, we propose an alternative approach in Section C: assessment of the trajectory model through numerical experiments.

2. The Grid Model

Although the representations of the various terms in the atmospheric diffusion equation can all be accommodated in a grid model, the model can be considered as the discrete analog of Eq. (III-1). In the process of discretization,* inaccuracies are unfortunately introduced. These inaccuracies are usually discussed in terms of the order of truncation terms. As an illustration of this type of analysis, consider the following simple form of Eq. (III-1) containing only the time-dependent and x-direction advective terms:

$$\frac{\partial c}{\partial t} + U_0 \frac{\partial c}{\partial x} = 0 \quad , \tag{III-8}$$

with a constant reference velocity U_0. Suppose we choose the following difference equation, from a first-order scheme, to approximate Eq. (III-8):

$$\frac{C_j^{n+1} - C_j^n}{\Delta t} + \frac{U_0}{\Delta x}\left(C_j^n - C_{j-1}^n\right) = 0 \quad . \tag{III-9}$$

Then we can carry out a Taylor series expansion about the time-space point

---

* In the present investigation, we focused our attention on only the finite difference method, in which the coordinates are discretized. In the particle-in-cell technique, the pollutants masses are discretized, and different types of difficulties are introduced. Nevertheless, this method is a viable procedure that can also be classified as a grid modeling approach.

(n,j) to obtain

$$\frac{\partial c}{\partial t} + U_0 \frac{\partial c}{\partial x} = \left[\frac{U_0 \Delta x}{2} \left(1 - \frac{U_0 \Delta t}{\Delta x} \right) \right] \frac{\partial^2 c}{\partial x^2} + \text{Higher Order Terms.} \qquad \text{(III-10)}$$

Comparing Eq. (III-8) with Eq. (III-10), we find that all the terms on the right-hand side are introduced through discretization. The lowest order term of these, having the form of a second-order spatial derivative, can be mathematically characterized as a diffusion process. This term is therefore often called "numerical," "pseudo," or "artificial" diffusion..

For the finite difference scheme to be stable, the diffusion coefficient must be positive. This restriction leads to the famous Courant condition for stability:

$$\frac{U_0 \Delta t}{\Delta x} < 1 \quad . \qquad \text{(III-11)}$$

Thus, it is apparent from this simple analysis that the primary source of errors arising from adoption of the grid model is associated with the introduction of an undesirable diffusion term, which is always positive. The presence of this additional diffusion term masks the true diffusion and, of course, introduces inaccuracies.

Although the type of analysis present above is useful in revealing some insights into the critical problems involved in adopting finite difference approximations, its use in practical problems is, nevertheless, very limited. In the first place, extension of such an analysis to the full three-dimensional, nonlinear problem would probably be too complicated to lead to useful conclusions

For example, even in the simple case we discussed above, a similar expansion for a variable velocity would generate terms proportional to $\partial U_0/\partial x$ in the set of artificial diffusion terms. Whether the additional terms would tend to alleviate the artificial diffusion problem, however, would depend on the sign and magnitude of the acceleration term. Furthermore, the result of this type of analysis can be stated, at best, in terms of order-of-magnitude expressions. Although the analysis shows that the higher order truncation terms always vanish when higher order finite difference schemes are used, this phenomenon does not necessarily imply that these schemes are more suitable. A notorious example can be found in airshed modeling: Near localized sources, higher order schemes predict unreasonable negative concentrations, whereas simple first-order schemes do not. In view of these deficiencies, we concluded that the inaccuracies in the grid model could be more profitably assessed through the numerical experiments dicussed in the next section.

C. ASSESSING THE VALIDITY OF AIRSHED MODELS THROUGH NUMERICAL EXPERIMENTS

We have explored the validity of both the trajectory model and the grid model by examining the formulae from which the two classes of models are derived. As shown in Figure III-1, the atmospheric diffusion equation was the common basis for comparison. By recognizing mathematical terms that have been incorrectly (though, in some cases, unavoidably) introduced or neglected in each of these two modeling approaches, we can identify the sources of errors. We list these sources below:

> Trajectory model sources
  - Neglect of horizontal mixing across the boundaries of the parcel.
  - Neglect of the vertical component of the wind velocity (the movement of the parcel is two-dimensional).
  - Assumption that the entire parcel moves with a wind velocity that is invariant with height.

> Grid model source--"Numerical" diffusion introduced by finite differencing

Although errors of each type can be estimated by evaluating the magnitudes of the relevant terms under commonly occurring conditions, quantitative estimates are, nevertheless, difficult to obtain. The remaining portion of this section is, therefore, devoted to a description of a numerical experiment that provides a means for assessing the absolute errors.

The major components of the numerical experiment consist of the following three steps:

(1) Find the exact solution of the atmospheric diffusion equation for some well-defined hypothetical cases. These cases should be carefully chosen so that they are as general and as realistic as possible. In addition, they must include, at a minimum, one or more of the key ingredients noted earlier. However, these cases should be sufficiently simple that analytic solutions to the atmospheric diffusion equation can be obtained.

(2) Exercise the trajectory or the grid model for these hypothetical cases, and compare the differences between the analytic solutions and the predictions of each model.

(3) Compare these results for variations in each parameter over a range of values that may occur in a real atmosphere, so that the range of validity of each of these two modeling approaches can be ascertained.

To examine the importance of the various effects that we mentioned earlier, we need to include, where possible, in the atmospheric diffusion equation the following terms, taken one or more at a time for evaluative purposes:

Term	Effect to be Evaluated
Horizontal diffusion	Neglect of horizontal diffusion
Vertical convection	Convergent or divergent flow
Vertical variations of the horizontal wind speed	Wind shear
Time-dependent and advection terms	Numerical errors

It should be evident from the preceding discussion that the hypothetical cases can be of no greater complexity than a two-dimensional, time-dependent formulation if analytical solutions are to be derived. Unlike the modeling of turbulent flow, where fundamental differences can exist between two- and three-dimensional turbulence, this assumption of two-dimensionality does not unduly affect the conclusions of a validity study. Furthermore, since meteorological parameters are of primary importance in the validity study of different modeling approaches, we also assumed that the chemical-reaction and volume-source terms are absent in Eq. (III-1). Thus, we considered the following equation in the present study:

$$\frac{\partial c}{\partial t} + u \frac{\partial c}{\partial x} + w \frac{\partial c}{\partial y} = \frac{\partial}{\partial x}\left(K_H \frac{\partial c}{\partial x}\right) + \frac{\partial}{\partial z}\left(K_Z \frac{\partial c}{\partial z}\right) \quad . \tag{III-12}$$

Although Eq. (III-12) is a considerably simplified form of the atmospheric diffusion equation, general solutions still cannot be found for arbitrarily specified wind speeds, diffusivities, and boundary conditions. We carried out a limited effort to examine existing analytic solutions (usually special cases) that were relevant to the present study. Table III-1 summarizes the results. As Table III-1 shows, none of the cases for which analytical solutions had been obtained contains all the ingredients that are necessary to assess both the trajectory and the grid models. Compromises must thus be made, such as considering only special cases that isolate certain effects that are neglected in either the trajectory model or the grid model. Table III-2 summarizes the cases considered in this study.

D. THE VALIDITY OF THE TRAJECTORY MODEL

This section examines, to the extent possible, the individual errors committed through the neglect of horizontal diffusion, vertical wind, and wind shear in the trajectory model. As a basis of evalution, we compare the analytic solution for each of the first six cases listed in Table III-2 with the corresponding prediction of the trajectory model.

TABLE III-1

EXACT SOLUTIONS TO THE DIFFUSION EQUATION

$$\frac{\partial c}{\partial t} + u\frac{\partial c}{\partial x} + w\frac{\partial c}{\partial z} = \frac{\partial}{\partial x}\left(K_H\frac{\partial c}{\partial x}\right) + \frac{\partial}{\partial z}\left(K_V\frac{\partial c}{\partial z}\right).$$

Investigator	Type of Source	∂/∂t	u	w	K_H	K_V
Roberts (1923)	Line and point source	Yes	0	0	K	K_V
	Line source	No	U	0	K	K_V
Calder (1949)	Line source	No	Uz^m	0	0	$K_V z^n$
Smith (1957)	Elevated point source	No	$U(z + h)^{1/2}$	0	$K(z + h)^{1/2}$	$K_V(z + h)^{1/2}$
	Elevated line source	No	$U(z + h)^{\alpha}$	0	0	$K_V(z + h)^{1-\alpha}$
Smith (1957)	Ground-level line source	No	U	W	0	Case 1 $K_V(H \quad z)z, \quad 0 \le z < H$ $\frac{\partial c}{\partial z} = 0, \quad z \quad H$ Case 2 $K_V z, \quad 0 \le z \le 1/2H$ $K_V(H - z), \quad 1/2H \le z \le H$ $\frac{\partial c}{\partial z} = 0, \quad z \quad H$
Smith (1957)	Ground-level line source	No	U	W_z	0	$K_V z^{-\alpha}, \quad 0 \le z \le H$ $\frac{\partial c}{\partial t} \quad 0, \quad z \quad H$
Monin (1959)	Elevated line source	Yes	0	0	0	$Kv_* z, \quad z < \lvert L\rvert$ $Kv_* L, \quad z < \lvert L\rvert$
Yordanov (1965)	Elevated point source	No	$U_1 z^m, \quad z < \lvert L\rvert$ $U_2, \quad z > \lvert L\rvert$	0	0	$K_1 z, \quad z < \lvert L\rvert$ $K_2 z^{4/3}, \quad z > \lvert L\rvert$
Yordanov (1968)	Elevated point source	Yes	0	0	0	Case 1 $K_1 z^n, \quad z < a\lvert L\rvert$* $K_1(aL)^{n-(3/4)} z^{3/4}, \quad z > a\lvert L\rvert$ Case 2 $K_1 z^n, \quad z < a\lvert L\rvert$† $K_1(aL)^n, \quad z > a\lvert L\rvert$†
Walters (1969)	Ground-level line source	No	U	0	K-z	$K_V z$
Dilley and Yen (1971)	Ground-level line source	No	$(U - ax)\left(\frac{z}{z_1}\right)^m$	$\frac{az}{m+1}\left(\frac{z}{z_1}\right)^m$	0	$K_V\left(\frac{z}{z_1}\right)^n$
Calder (1971)	Line and point source	No	Uz^m	0	$K\text{-}z^{\alpha}$	$K_V z^{\beta}$

* Unstable atmosphere.

† Stable atmosphere.

TABLE III-2

SUMMARY OF THE CASES CONSIDERED IN THE VALIDITY STUDY

Type of Assessment	Type of Sources	Model Equation	Comments
Trajectory model			
The effect of neglecting horizontal diffusion	Instantaneous, ground-level line source	$\frac{\partial c}{\partial t} + U\frac{\partial c}{\partial x} = K_H\frac{\partial^2 c}{\partial x^2} + \frac{\partial}{\partial z}\left(K_V\frac{\partial c}{\partial z}\right)$ U - constant K_H = constant $K_V = \bar{K}_1 z^n$	See Section C-1-a
	Continuous, ground-level line source	$U\frac{\partial c}{\partial x} = K_H\frac{\partial^2 c}{\partial x^2} + \frac{\partial}{\partial z}\left(K_V\frac{\partial c}{\partial z}\right)$ K_H $\bar{K}_0 z$ K_V $\bar{K}_1 z$	See Section C-1-b and Walters (1969)
	Time- and space-varying ground-level area source	$\frac{\partial c}{\partial t} + U\frac{\partial c}{\partial x} = K_H\frac{\partial^2 c}{\partial x^2} + \frac{\partial}{\partial z}\left(K_V\frac{\partial c}{\partial z}\right)$ U constant K_H constant K_V $\bar{K}_1 z^n$	See Section C-1-c
The effect of neglecting vertical wind	Continuous, ground-level crosswind line source	$u\frac{\partial c}{\partial x} + w\frac{\partial c}{\partial z} = \frac{\partial}{\partial z}\left(K_V\frac{\partial c}{\partial z}\right)$ u - $(U_1$ $ax)\left(\frac{z}{z_1}\right)^m$ w $\frac{az}{m+1}\left(\frac{z}{z_1}\right)^m$ K_V $\bar{K}_1\left(\frac{z}{z_1}\right)^n$	See Section C-2 and Dilley and Yen (1971)
The effect of neglecting wind shear	Continuous, ground-level crosswind line source	$u(z)\frac{\partial c}{\partial x} = \frac{\partial}{\partial z}\left(K_V\frac{\partial c}{\partial z}\right)$ $u(z)$ $u_1\left(\frac{z}{z_1}\right)^m$ K_V $K_1\left(\frac{z}{z_1}\right)^m$	See Section C-3-a
	Time- and space-varying ground-level area source	$u(z)\frac{\partial c}{\partial x} = \frac{\partial}{\partial z}\left(K_V\frac{\partial c}{\partial z}\right)$ $u(z)$ $u_1\left(\frac{z}{z_1}\right)^m$ $K_V = K_1\left(\frac{z}{z_1}\right)^n$	See Section C-3-b
Grid model			
The effect of numerical errors	Time- and space-varying ground-level area source	$\frac{\partial c}{\partial t} + U\frac{\partial c}{\partial x} = K_H\frac{\partial^2 c}{\partial x^2} + \frac{\partial}{\partial z}\left(K_V\frac{\partial c}{\partial z}\right)$ U = constant K_H constant K_V = constant	See Section D

1. The Effect of Horizontal Diffusion

We first consider two physical situations that provide, in effect, upper and lower bounds on the errors induced in the trajectory model. The first is that of an instantaneous line source at ground level in an atmosphere with a uniform wind blowing in the x-direction. The second is that of a continuous line source at ground level in a similar atmosphere. In the dispersion of a puff from an instantaneous release, horizontal dispersion, in the absence of wind shear, can be expected to play a key role in spreading out the cloud. For a continuously emitting source, concentration gradients in the direction of the mean wind are substantially smaller than those for an instantaneous release. Thus, a comparison of the concentrations predicted by the trajectory model with the actual concentrations provides upper and lower bounds on the errors committed by not including horizontal diffusion. To provide a more realistic assessment, we consider next the impact on the induced errors of an urban-type source distribution--a time- and space-varying area source.

a. Instantaneous Line Sources

We can derive the mean concentration resulting from an instantaneous line source under the conditions of a constant crosswind, U, and a constant horizontal diffusivity, K_H, from a simplified form of Eq. (III-12):

$$\frac{\partial c}{\partial t} + U \frac{\partial c}{x} = K_H \frac{\partial^2 c}{\partial x^2} + \frac{\partial}{\partial z}\left(K_V \frac{\partial c}{\partial z}\right) \quad . \tag{III-13}$$

By invoking the coordinate transformations,

$$\xi = x - Ut \quad ,$$

$$\rho = z \quad ,$$

$$\tau = t \quad ,$$

we obtain for Eq. (III-13)

$$\frac{\partial c}{\partial \tau} = K_H \frac{\partial^2 c}{\partial \xi^2} + \frac{\partial}{\partial \rho}\left(K_V \frac{\partial c}{\partial \rho}\right) \quad . \tag{III 14}$$

We can write the appropriate initial and boundary conditions as

$$c(\xi,\rho,0) = Q_\ell \delta(\xi)\delta(\rho) \quad , \tag{III-15}$$

$$c(\xi,\rho,\tau) = 0 \quad , \quad \xi \to \pm\infty \quad , \tag{III-16}$$

$$-K_V \frac{\partial}{\partial \rho} = 0 \quad , \quad \rho = 0 \quad , \tag{III-17}$$

$$c(\xi,\rho,\tau) = 0 \quad , \quad \rho \to \infty \quad , \tag{III-18}$$

where c is the mean concentration, in $g \cdot m^{-3}$, and Q_ℓ is the mass of pollutant emitted per unit width in the y-direction, in $g \cdot m^{-1}$. The problem defined by Eqs. (III-14) through (III 18) describes the two-dimensional dispersion of a puff of inert contaminant relative to its horizontal center of mass in a horizontally and vertically homogeneous atmosphere.

We can express the solution of Eq. (III-14) in the form

$$c(\xi,\rho,\tau) = X(\rho,\tau) \exp\left[-\frac{\xi^2}{f(\rho,\tau)}\right] \quad . \tag{III-19}$$

We define the zeroth and second moments, respectively, of $c(\xi,\rho,\tau)$ as follows:

$$c_0(\rho,\tau) = \int_{-\infty}^{\infty} c(\xi,\rho,\tau)\, d\xi \quad , \tag{III-20}$$

$$c_2(\rho,\tau) = \int_{-\infty}^{\infty} c(\xi,\rho,\tau)\xi^2 d\xi \quad , \tag{III-21}$$

where c_0 and c_2 have units of $g\cdot m^{-2}$ and g, respectively. We can express $f(\rho,\tau)$ and $X(\rho,\tau)$ in terms of c_0 and c_2,

$$f = \frac{2c_2}{c_0} \quad , \tag{III-22}$$

$$X = c_0 \left(\frac{c_0}{2\pi c_2}\right)^{\frac{1}{2}} \quad . \tag{III-23}$$

The zeroth moment, $c_0(\rho,\tau)$, satisfies

$$\frac{\partial c_0}{\partial \tau} = \frac{\partial}{\partial \rho}\left(K_V \frac{\partial c_0}{\partial \rho}\right) \quad , \tag{III-24}$$

$$c_0(\rho,0) = Q_\ell \delta(\rho) \quad , \tag{III-25}$$

$$-K_V \frac{\partial c_0}{\partial \rho} = 0 \quad , \quad \rho = 0 \quad , \tag{III-26}$$

$$c_0(\rho,\tau) = 0 \quad , \quad \rho \to \infty \quad . \tag{III-27}$$

The solution of Eq. (III-24), subject to Eqs. (III-25) through (III-27) and $K_V = \overline{K}_1 \rho^n$, is

$$c_0(\rho,\tau) = \frac{Q_\ell}{(2-n)^{\frac{n}{2-n}}\,\Gamma\left(\frac{1}{2-n}\right)(\overline{K}_1\tau)^{\frac{1}{2-n}}} \exp\left[-\frac{\rho^{2-n}}{(2-n)^2\,\overline{K}_1\tau}\right] \quad . \tag{III-28}$$

The second moment, c_2, satisfies

$$\frac{\partial c_2}{\partial \tau} = \frac{\partial}{\partial \rho}\left(K_V \frac{\partial c_2}{\partial \rho}\right) + 2K_H c_0 \quad , \tag{III-29}$$

$$c_2(\rho,0) = 0 \quad , \tag{III-30}$$

$$-K_V \frac{\partial c_2}{\partial \rho} = 0 \quad , \quad \rho = 0 \quad , \tag{III-31}$$

$$c_2(\rho,\tau) = 0 \quad , \quad \rho \to \infty \quad . \tag{III-32}$$

In addition to $K_V = \bar{K}_1 \rho^n$, we set K_H = constant. The solution of Eq. (III-29) subject to Eqs. (III-30) through (III-32) is

$$c_2(\rho,\tau) = \frac{2K_H Q_\ell \tau^{\frac{1-n}{2-n}}}{(2-n)^{\frac{n}{2-n}} \Gamma\left(\frac{1}{2-n}\right) \bar{K}_1^{\frac{1}{2-n}}} \exp\left[-\frac{\rho^{2-n}}{(2-n)^2 \bar{K}_1 \tau}\right] \quad . \tag{III-33}$$

Using Eqs. (III-22), (III-23), (III-28), and (III-33), we can obtain the solution of Eq. (III-14):

$$c(\xi,\rho,\tau) = \frac{\frac{Q_\ell}{(4\pi K_H \tau)^{\frac{1}{2}}}}{(2-n)^{\frac{n}{2-n}} \Gamma\left(\frac{1}{2-n}\right)\left(\bar{K}_1 \tau\right)^{\frac{1}{2-n}}} \exp\left[-\frac{\xi^2}{4K_H \tau} - \frac{\rho^{2-n}}{(2-n)^2 \bar{K}_1 \tau}\right] \quad . \tag{III-34}$$

The ground-level concentration at the centroid of the puff is

$$c(0,0,\tau) = \frac{\dfrac{Q_\ell}{(4\pi K_H \tau)^{\frac{1}{2}}}}{(2-n)^{\frac{n}{2-n}}\,\Gamma\left(\dfrac{1}{2-n}\right)\left(\bar{K}_1\tau\right)^{\frac{1}{2-n}}} \quad . \tag{III-35}$$

We can consider Eqs. (III-34) and (III-35) as the "exact" expressions for the mean concentration in the puff, and we can compare them with corresponding expressions derived from the trajectory model.

We now proceed to develop the form of the trajectory model applicable to the description of the dispersion of an instantaneous release. We have denoted the actual mean concentration of a pollutant from such a release by $c(\xi,\rho,\tau)$ in the case of a line source; c is expressed in units of $g\cdot m^{-3}$, and the instantaneous source, in units of $g\cdot m^{-1}$. The concentration $\tilde{c}(\rho,\tau)$, derived using the trajectory model, is also in the customary units of $g\cdot m^{-3}$. Thus, for inert contaminants and no elevated sources, the governing equation and associated initial and boundary conditions become, for an instantaneous release,

$$\frac{\partial \tilde{c}(\rho,\tau)}{\partial \tau} = \frac{\partial}{\partial \rho}\left(K_V \frac{\partial \tilde{c}}{\partial \rho}\right) \quad , \tag{III-36}$$

$$\tilde{c}(\rho,0) = Q_A \delta(\rho) \quad , \tag{III-37}$$

$$-K_V \frac{\partial \tilde{c}}{\partial \rho} = 0 \quad , \quad \rho = 0 \quad . \tag{III-38}$$

$$\tilde{c}(\rho,\tau) = 0 \quad , \quad \rho \to \infty \tag{III-39}$$

where the proper source strength, Q_A, in Eq. (III 37) is expressed in units of $g \cdot m^{-2}$, i.e., an instantaneous area source. The key problem, then, in formulating the trajectory model for an instantaneous source is to relate the true source strength $Q(g \cdot m^{-1}]$ in the case of a line source) to the source strength Q_A $(g \cdot m^{-2})$ in Eq. (III-37). For an instantaneous line source, the source strength Q_A in Eq. (III-37) is related to the actual strength Q_ℓ by

$$Q_A = \frac{Q_\ell}{\ell} \quad , \tag{III-40}$$

where ℓ is a length in the x-direction over which the actual source is averaged. Because of the necessity of using $g \cdot m^{-3}$ as the concentration unit in both descriptions, the true instantaneous strengths must be spatially averaged in the trajectory model. We show subsequently that this averaging is unnecessary for continuous sources.

We can obtain the solution of Eqs. (III-36) through (III-39), with $K_V = \bar{K}_1 \rho^n$, from Eq. (III-28), with Q_ℓ from Eq. (III-40):

$$\tilde{c}(\rho,\tau) = \frac{Q_A}{(2-n)^{\frac{1}{2-n}} \Gamma\left(\frac{1}{2-n}\right)\left(\bar{K}_1 \tau\right)^{\frac{1}{2-n}}} \exp\left[-\frac{\rho^{2-n}}{(2-n)^2 \bar{K}_1 \tau}\right] \quad . \tag{III-41}$$

We can express the measure of the deviation of $c(0,\tau)$ from $c(0,0,\tau)$ in Eqs. (III-35), (III-40), and (III-41) by their ratio:*

---

*A similar analysis of an instantaneous, ground-level point source reveals that the ratio of the ground-level concentration predicted by the trajectory model to the actual concentration is

$$\gamma = \frac{4K_H \tau}{A} \quad .$$

$$\gamma = \frac{\left(4\pi K_H\right)^{\frac{1}{2}}}{\ell} \quad . \qquad \text{(III-42)}$$

Figure III-2 presents a plot of this ratio for three values of $4\pi K_H/\ell^2$ commonly encountered in an urban scale problem. As Figure III-2 shows, for small τ, $\gamma < 1$, the trajectory model underpredicts the ground concentrations, whereas for large τ, $\gamma > 1$, the trajectory model overpredicts the ground concentrations. The explanation for this result is as follows. The ratio γ, as given by Eq. (III-42), can be viewed as the ratio of two length scales: that associated with horizontal turbulent diffusion and that characteristic of the spatial averaging of the emissions. Initially, the spreading of the pollutant cloud varies approximately as the square root of the time. Therefore, at this stage, the spread is not sufficient to compensate for the influence of the artificial spatial averaging of emissions; consequently, near the source, the trajectory model tends to predict concentrations that are too low. After a substantial amount of time has elapsed, the effect of horizontal diffusion overtakes the effect of the spatial averaging of the emissions, and the trajectory model begins to overpredict. In summary, for an instantaneous release, the trajectory model is most accurate when the two characteristic lengths are comparable.

In most applications of the trajectory model, continuous (rather than instantaneous) sources are considered. Thus, the above analysis represents an unnecessarily severe test of the validity of the trajectory model insofar as the effect of horizontal diffusion is concerned.

b. Continuous Line Sources

We now consider the case of a continuous ground-level crosswind line source with a constant mean wind speed that is independent of height. Since

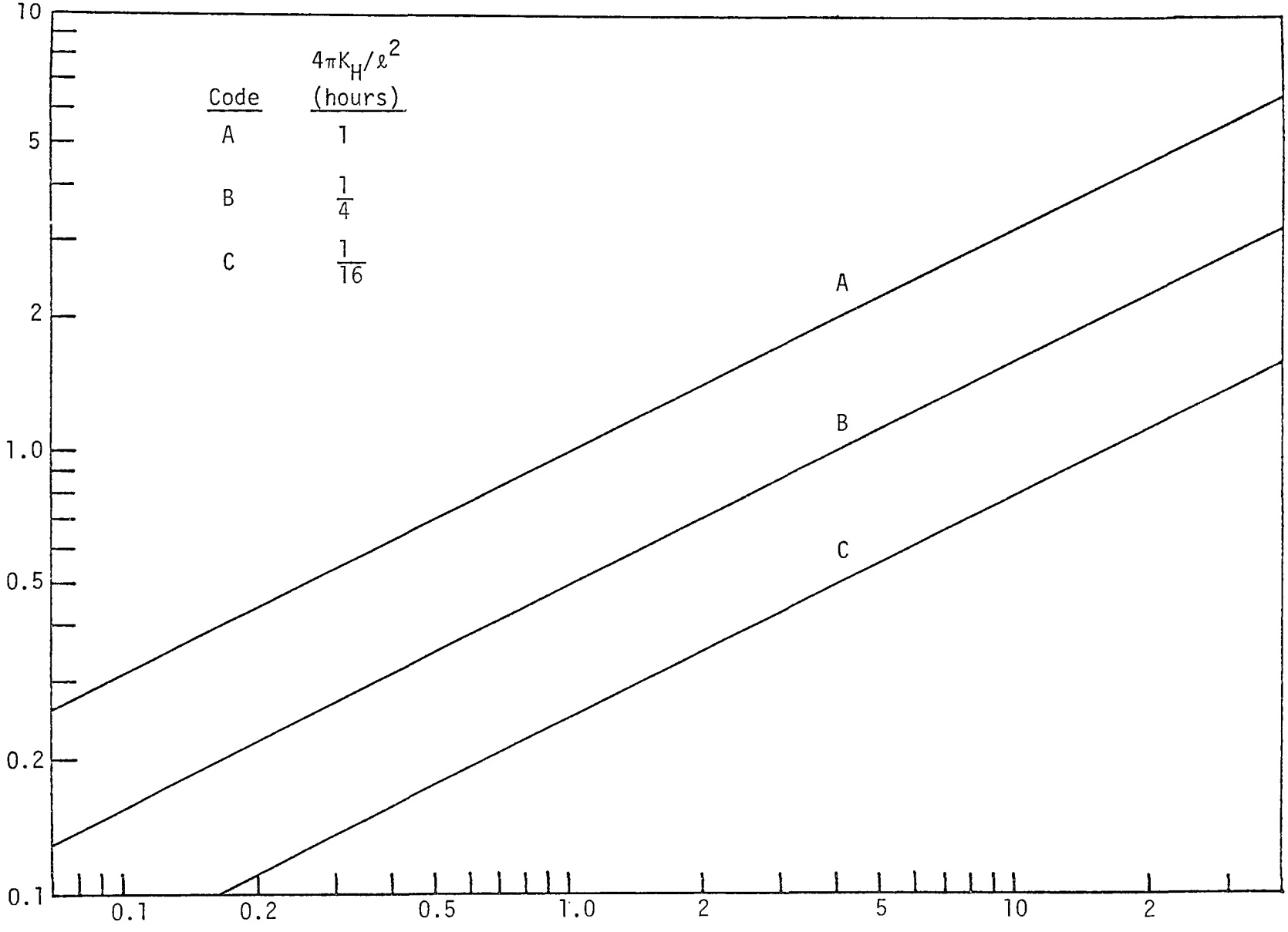

FIGURE III-2. THE EFFECT OF NEGLECTING HORIZONTAL DIFFUSION ON THE TRAJECTORY MODEL PREDICTIONS (FOR INSTANTANEOUS LINE SOURCES)

our main purpose in considering this case is to assess the effect of horizontal diffusion, the basic equation governing the concentration distribution, in (x,z) coordinates, is

$$U \frac{\partial c(x,z)}{\partial x} = K_H \frac{\partial^2 c}{\partial x^2} + \frac{\partial}{\partial z}\left(K_V \frac{\partial c}{\partial z}\right) \quad , \tag{III-43}$$

$$c(x,z) = 0 \quad , \quad x \to \pm\infty \quad , \tag{III-44}$$

$$c(x,z) = 0 \quad , \quad z \to \infty \quad , \tag{III-45}$$

$$c \to \infty \quad , \quad x,z \to 0 \quad , \tag{III-46}$$

$$-K_V \frac{\partial c}{\partial z} = 0 \quad , \quad z = 0 \quad , \quad x \neq 0 \quad , \tag{III-47}$$

$$\int_{-\infty}^{\infty} \left(-K_V \frac{\partial c}{\partial z}\right) dx = q_\ell \quad , \tag{III-48}$$

where $c(x,z)$ is expressed in $g \cdot m^{-3}$ and q_ℓ represents the pollutant flux for a line source (in $g \cdot m^{-1}\ sec^{-1}$).

Walters (1969) solved the case in which $K_H = \bar{K}_0 z$ and $K_V = \bar{K}_1 z$:

$$c(x,z) = \frac{q_\ell}{\bar{K}_1 \left(1 + e^{-\lambda\pi}\right)} \frac{\exp\left[-\lambda \tan^{-1}\left(\mu \frac{z}{x}\right)\right]}{\left(x^2 + \mu^2 z^2\right)^{\frac{1}{2}}} \quad , \tag{III-49}$$

where $\lambda = U/(\bar{K}_0 \bar{K}_1)^{1/2}$, and $\mu = (\bar{K}_0/\bar{K}_1)^{1/2}$. When horizontal diffusion is neglected in Eq. (III-43), the result is

$$c(x,z) = \frac{q_\ell}{\bar{K}_1 x} \exp\left(-\frac{Uz}{\bar{K}_1 x}\right) \quad . \tag{III-50}$$

Equations (III-49) and (III-50) provide a comparison of the effect of neglecting horizontal diffusion with the effect of including it (see Walters, 1969). When $\mu(z/x) << 1$, i.e., when $\mu(z/x)$ is sufficiently close to the ground, the functional dependence of c on x and z is the same in the two cases. However, the ratio of the predicted magnitudes of the concentration varies from unity (when $\overline{K}_0 = 0$) to 2 (when $\overline{K}_0 \to \infty$). Walters also determined the conditions under which horizontal diffusion cannot be neglected when predicting the mean concentration from a continuous line source.

To employ the trajectory model for a continous source, we must convert the downwind distance x into travel time τ. In this case, $x = U\tau$, since the velocity is uniform. The trajectory model is defined by Eqs. (III-36) through (III-39). In relating the trajectory model to the continuous source problem, we note that the proper source strength Q_A in Eq. (III-37) is in units of $g \cdot m^{-2}$, whereas the actual source strength q_ℓ is in units of $g \cdot m^{-1}$ sec^{-1} Thus, it is necessary to convert the steady-state diffusion problem into an unsteady-state problem to employ the trajectory model. If we let

$$Q_A = \frac{q_\ell}{U} \quad , \tag{III-51}$$

then Q_A has the appropriate units of an instantaneous source. In effect, we need not define an area associated with the column, since Q_A represents the mass of material emitted over the time it takes the wind to travel 1 meter.

Using Eq. (III-51) as the emission strength in Eq. (III-37), we obtain the following solution of Eqs. (III-36) through (III-39) for the simple case of $n = 1$:

$$c(\rho,\tau) = \frac{q_\ell}{\overline{K}_1 U\tau} \exp\left(-\frac{\rho}{\overline{K}_1 \tau}\right) \quad . \tag{III-52}$$

Equation (III-52) is merely Eq. (III-50) with x replaced by $U\tau$ and z replaced by ρ. The ratio of the mean ground-level concentration predicted by the trajectory model to the "exact" value can be obtained by replacing

x and z in Eq. (III-49) by U_τ and ρ, respectively, and by dividing the resulting expression into Eq. (III-52) after setting $\rho = 0$ in each expression. Thus,

$$\gamma = 1 + e^{-\lambda\pi} \quad . \tag{III-53}$$

Since typical values of λ in the atmosphere range from 0.75 to 500, a reasonable upper bound on the magnitude of the error introduced into trajectory model predictions when horizontal diffusion is not included is

$$\gamma - 1 < 10\% \quad .$$

It is therefore clear that, for the case of linearly varying diffusivities, we can neglect horizontal diffusion with little error.

c. Time- and Space-Varying Line Sources

The previous two sections highlight certain omissions in the trajectory model. However, these examples are somewhat idealized when compared with situations in which one might actually use a trajectory model. Conditions that one might commonly encounter include:

> Distributed sources that emit continuously and vary with time.
> Diffusivity-height relationships that are not linear.

To assess the performance of the trajectory model in situations other than those explored thus far, we consider here a continuous, ground-level area source under conditions of constant wind speed and vertical turbulent diffusivity varying as a power law function of altitude.

Equation (III-34) gives the mean concentration from an instantaneous ground-level line source with a uniform mean wind. In that equation, Q_ℓ is in units of $g \cdot m^{-1}$. We now wish to consider the case in which the ground-

level emissions are distributed over the strip $0 \leq x \leq L$. We examine first an instantaneous area source. If we assume that the original source strength is distributed over the strip $0 \leq x \leq L$, then the instantaneous area source strength Q_A, in $g \cdot m^{-2}$, is

$$Q_A = \frac{dQ_\ell}{dx} \quad . \tag{III-54}$$

The concentration resulting from an infinitesimal line source of strength $Q_A\, d\alpha$ located at $x = \alpha$ is, from Eq. (III-34),

$$dc(s,z,t) = \frac{\dfrac{Q_A d\alpha}{\left(4\pi K_H t\right)^{\frac{1}{2}}}}{(2-n)^{\frac{n}{2-n}}\, \Gamma\left(\frac{1}{2-n}\right)\left(\bar{K}_1 t\right)^{\frac{1}{2-n}}}$$

$$\cdot \exp\left[-\frac{(x - Ut - \alpha)^2}{4K_H t} - \frac{z^{2-n}}{(2-n)^2\, \bar{K}_1 t}\right] \tag{III-55}$$

Thus, the concentration resulting from the instantaneous area source of width L and unit length is

$$c(x,z,t) = \frac{\left(4\pi K_H t\right)^{-\frac{1}{2}}}{(2-n)^{\frac{n}{2-n}}\, \Gamma\left(\frac{1}{2-n}\right)\left(\bar{K}_1 t\right)^{\frac{1}{2-n}}} \exp\left[-\frac{z^{2-n}}{(2-n)^2\, \bar{K}_1 t}\right]$$

$$\cdot \int_0^L \exp\left[-\frac{(x - Ut - \alpha)^2}{4K_H t}\right] Q_A\, d\alpha \quad , \tag{III-56}$$

where we have allowed Q_A to vary with location. In addition, for a continuous ground-level area source, where $q_A = \Delta Q_A / \Delta t$ and varies in time ($g \cdot m^{-2}\ sec^{-1}$),

the concentration is

$$c(x,z,t) = \frac{1}{(2-n)^{\frac{n}{2-n}}\,\Gamma\left(\frac{1}{2-n}\right)} \int_0^t \frac{\left[4\tau K_H(t-\beta)\right]^{-\frac{1}{2}}}{\left[\bar{K}_1(t-\beta)\right]^{\frac{1}{2-n}}}$$

$$\cdot \exp\left[-\frac{z^{2-n}}{(2-n)^2\,\bar{K}_1(t-\beta)}\right] \int_0^L \exp\left\{-\frac{[x-(Ut-\beta)-\alpha]^2}{4K_H(t-\beta)}\right\}$$

$$\cdot qA(\alpha,\beta)\,d\alpha\,d\beta \quad . \qquad \text{(III-57)}$$

Note we can derive this equation from Eq. (III-56) by applying the principle of superposition.

We can obtain the corresponding solution for the trajectory model from Eq. (III-41), which gives the mean concentration from an instantaneous source of strength Q_A. To consider sources of strength $q_A(\tau)$ (in $g \cdot m^{-2}$ sec^{-1}), we invoke the principle of superposition. Integrating over time the concentration resulting from an instantaneous source $q_A\,d\beta$ released at time $\tau = \beta$ gives

$$\tilde{c}(\rho,\tau) = \frac{1}{(2-n)^{\frac{n}{2-n}}\,\Gamma\left(\frac{1}{2-n}\right)} \int_0^\tau \frac{q_A(\beta)}{\left[\bar{K}_1(\tau-\beta)\right]^{\frac{1}{2-n}}}$$

$$\cdot \exp\left[\frac{\rho^{2-n}}{(2-n)^2\,\bar{K}_1(\tau-\beta)}\right] d\beta \quad . \qquad \text{(III-58)}$$

We obtained the spatial and temporal distributions of the emissions used for the present study from the emission pattern of carbon monoxide for a horizontal strip of Los Angeles (see Figures III-3 and III-4). Mathematically expressed, this type of pattern is the summation of a series of rectangular step functions:

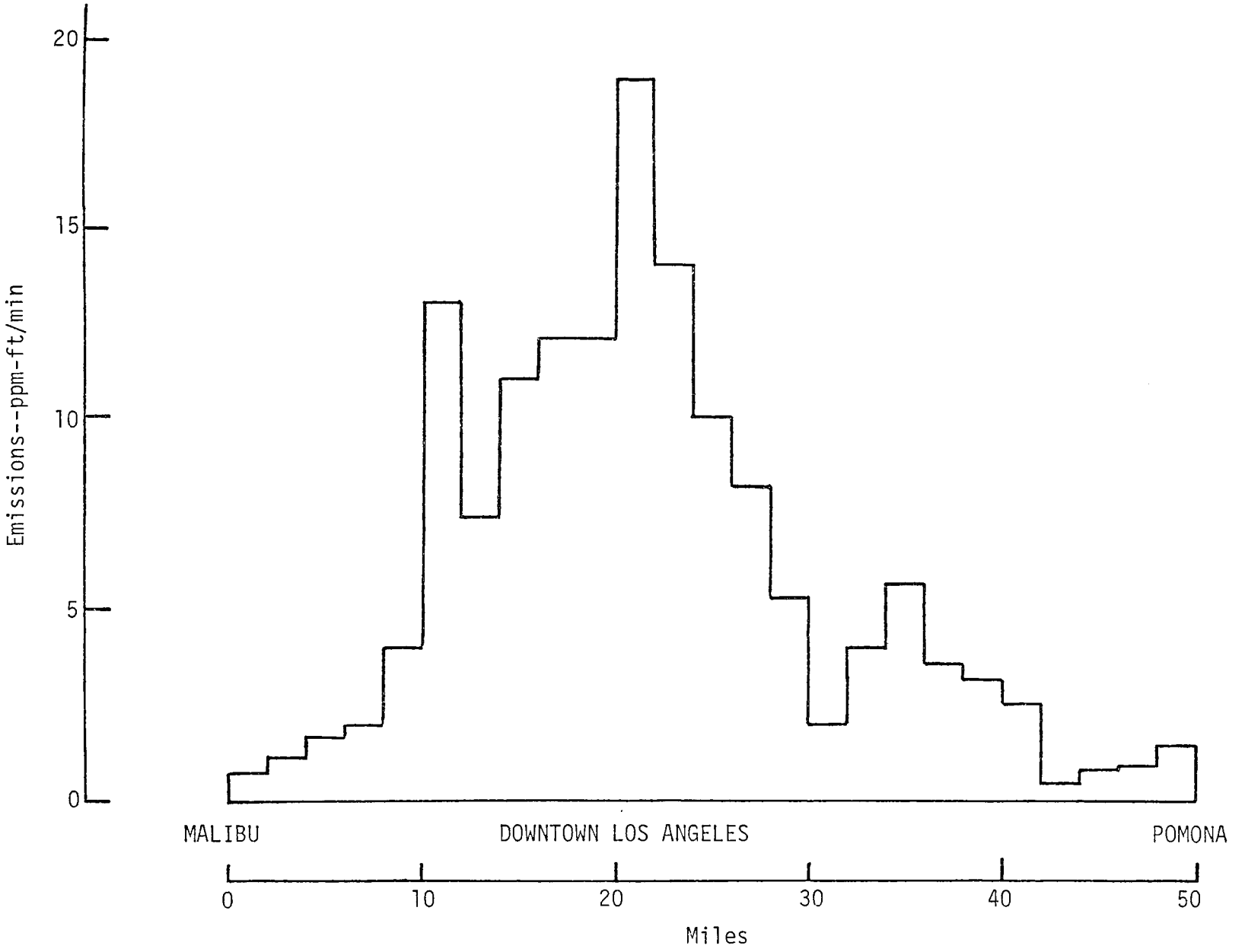

FIGURE III-3. SPATIAL DISTRIBUTION OF CARBON MONOXIDE EMISSIONS (10:00 A.M. PST)

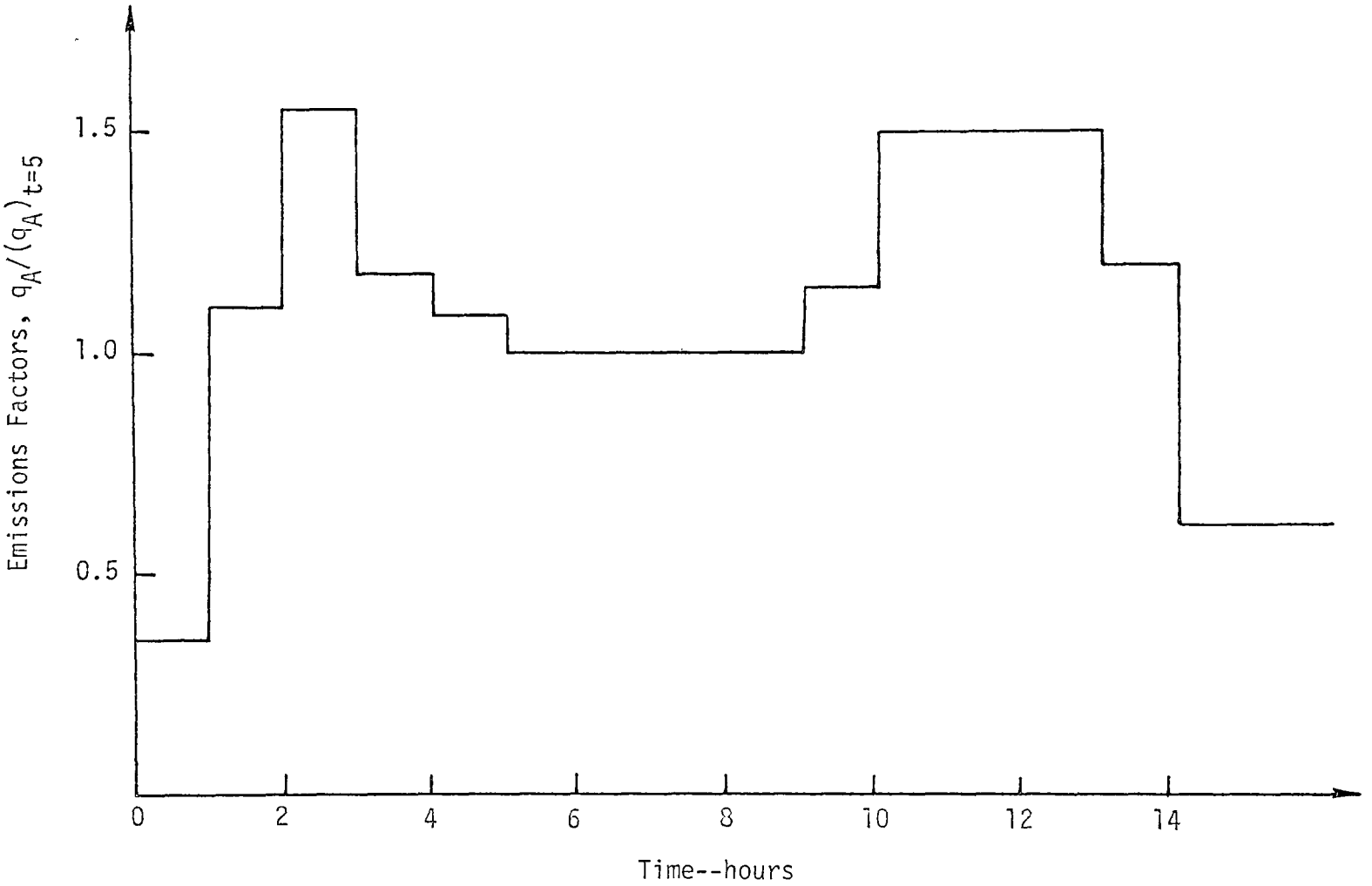

FIGURE III-4. TEMPORAL DISTRIBUTION OF CARBON MONOXIDE EMISSIONS

$$q_A = \sum_{i=1}^{N} f_i(t) \quad , \tag{III-59}$$

where

$$f_i(t) = \begin{cases} E_i(t), \text{ a constant, for } i\Delta x > x > (i-1)\Delta x, \\ 0 \text{ elsewhere,} \end{cases}$$

and where

N = the total number of grid points (25),

Δx = the grid spacing,

$E_i(t)$ = the magnitude of emission flux strength from grid point i at time t.

Under the assumption of a step function for the spatial distribution of emissions, as described above, we can reduce the double integral on the right-hand side of Eq. (III-57) to a single integral:

$$c(x,z,t) = \frac{(2-n)^{-\frac{n}{2-n}}}{2\Gamma\left(\frac{1}{2-n}\right)} \int_0^t \frac{\exp\left[-\dfrac{z^{2-n}}{(2-n)^2\,\overline{K}_1(t-\beta)}\right]}{\left[\overline{K}_1(t-\beta)\right]^{\frac{1}{2-n}}}$$

$$\cdot \left(\sum_{i=1}^{N} E_i(\beta) \left\{ \operatorname{erf}\left[\frac{x-(i-1)\Delta x - U(t-\beta)}{\sqrt{4K_H(t-\beta)}}\right] \right.\right.$$

$$\left.\left. - \operatorname{erf}\left[\frac{x - i\Delta x - U(t-\beta)}{\sqrt{4K_H(t-\beta)}}\right] \right\} \right) d\beta \quad . \tag{III-60}$$

The integrals in Eq. (III-58) and (III-60) unfortunately exhibit singular behavior near the upper limit of the integration. Thus, the achievement of results that are acceptably accurate would require extremely fine meshes. For example, using numerical techniques to evaluate either integral [Eq. (III-58) or Eq. (III-60)] with a relative error less than ε, we find that the total number of mesh points required is on the order of

$$M \approx \varepsilon^{-\frac{2-n}{1-n}} .$$

For $n = 0$ and $\varepsilon = 0.1$ percent, the required number is a staggering 10^6. However, we can remove this difficulty by elongating the time axis in accordance with the following coordinate transformations:

$$\lambda = (\tau - \beta)^{\frac{1-n}{2-n}} \qquad \text{for Eq. (III-58)}$$

or

$$\lambda = (t - \beta)^{\frac{1-n}{2-n}} \qquad \text{for Eq. (III-60).}$$

Equations (III-58) and (III-60) subsequently become

$$\tilde{c}(\rho,\tau) = \frac{(2-n)^{\frac{2(1-n)}{2-n}}}{(1-n)\,\Gamma\left(\frac{1}{2-n}\right)\bar{K}_1^{\frac{1}{2-n}}} \cdot \int_0^{\tau^{\frac{1-n}{2-n}}} q_A(\lambda) \cdot \exp\left[-\frac{\rho^{2-n}}{(2-n)^2\,\bar{K}_1\lambda^{\frac{2-n}{1-n}}}\right] d\lambda \quad , \qquad \text{(III-61)}$$

and

$$c(x,z,t) = \frac{(2-n)^{\frac{2(1-n)}{2-n}}}{2(1-n)\,\Gamma\left(\frac{1}{2-n}\right)\bar{K}_1^{\frac{1}{2-n}}} \cdot \int_0^{t^{\frac{1-n}{2-n}}} \exp\left[-\frac{z^{2-n}}{(2-n)^2\,\bar{K}_1\lambda^{\frac{2-n}{1-n}}}\right]$$

$$\cdot \left(\sum_{i=1}^{N} E_i(\lambda) \left\{ \operatorname{erf}\left[\frac{x - (i-1)\Delta x - U\lambda^{\frac{2-n}{1-n}}}{\sqrt{4K_H \lambda^{\frac{2-n}{2(1-n)}}}} \right] \right.\right.$$

$$\left.\left. - \operatorname{erf}\left[\frac{x - i\Delta x - U\lambda^{\frac{2-n}{1-n}}}{\sqrt{4K_H \lambda^{\frac{2-n}{2(1-n)}}}} \right] \right\} \right) d\lambda \quad . \qquad \text{(III-62)}$$

We evaluated these integrals using Simpson's rule.

We performed calculations for several different sets of conditions representing typical or extreme conditions observed in urban atmospheres. We computed the ratios γ of the ground concentrations predicted by the "exact" solution to the ground concentrations predicted by the trajectory model. Figure III-5 shows these ratios as a function of release time of the air parcels in the trajectory model. Although Figure III-5 shows that the effect of neglecting horizontal diffusion increases with increasing horizontal diffusivity and vertical wind shear and with decreasing wind speeds, the absolute magnitudes of the errors are rather small--apparently less than 10 percent.

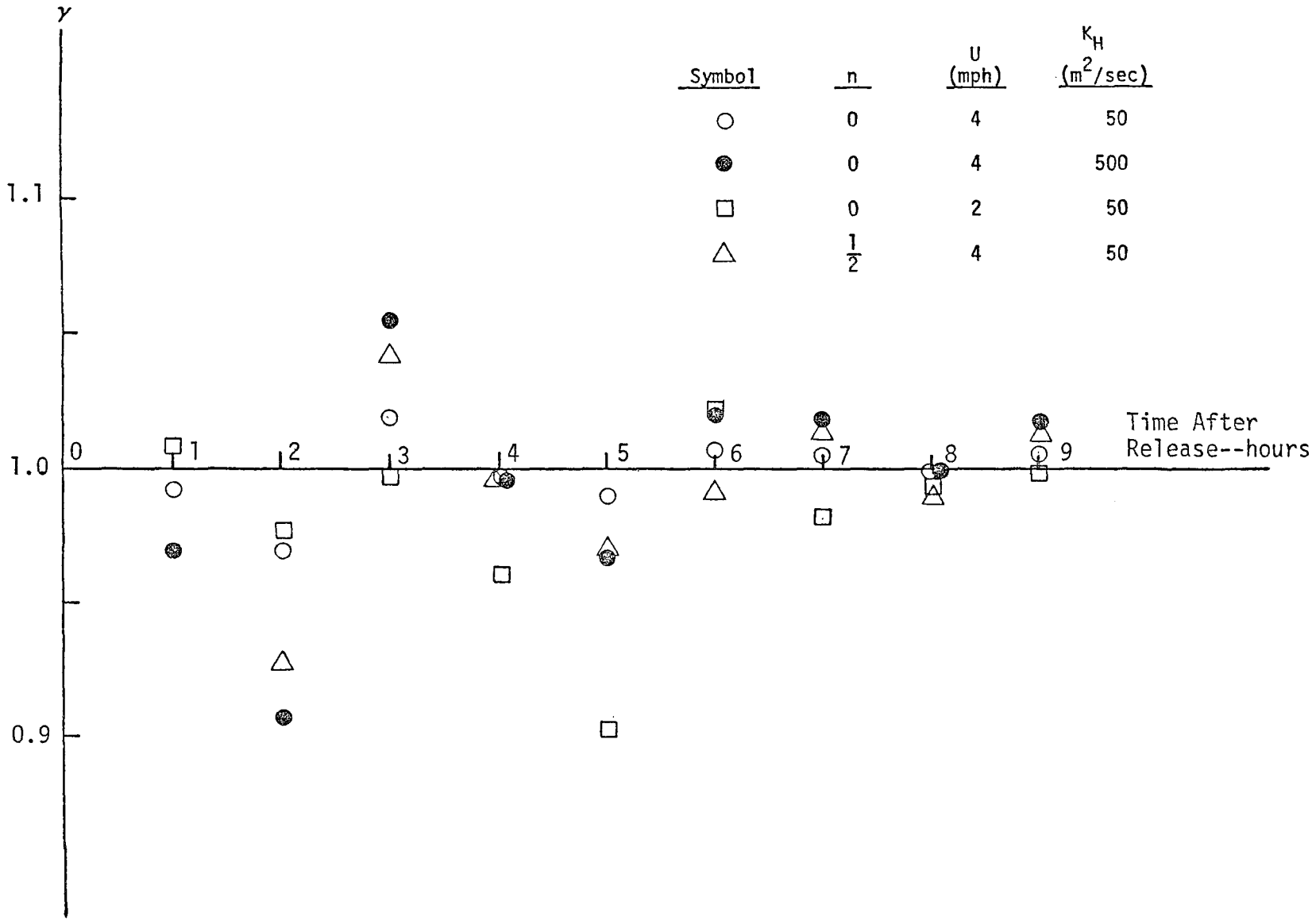

FIGURE III-5. THE EFFECT OF NEGLECTING HORIZONTAL DIFFUSION ON THE TRAJECTORY MODEL PREDICTIONS (FOR URBAN-TYPE SOURCES)

Thus, we concluded that, for all practical purposes, the neglect of horizontal diffusion in the trajectory model is unimportant when compared with other uncertainties in airshed modeling.

2. The Effect of Vertical Winds

Convergent and divergent flows are not uncommon in many urban areas. Channeled by local topography, two air flows having opposite direction can clash to produce a strong convergent flow, such as that characterizing the famous San Fernando convergent zone in Los Angeles. Hot or cool spots in an urban area can also create local convergent or divergent flows. As we indicated earlier, existing trajectory models invoke the assumption that the vertical component of the wind field can be neglected. (We note that although this assumption is commonly made, it is not necessary.) This section assesses the errors committed as a result of neglecting the vertical wind in the trajectory model.

Dilley and Yen (1971) studied a continuous ground-level crosswind line source emitting into an atmosphere in which the wind consists of a local convergent flow (with both horizontal and vertical components) superimposed on a horizontal wind, which also varies with height. We chose this case, illustrated in the following sketches, as a basis for studying the effect of neglecting the vertical wind on the predictions of a trajectory model.

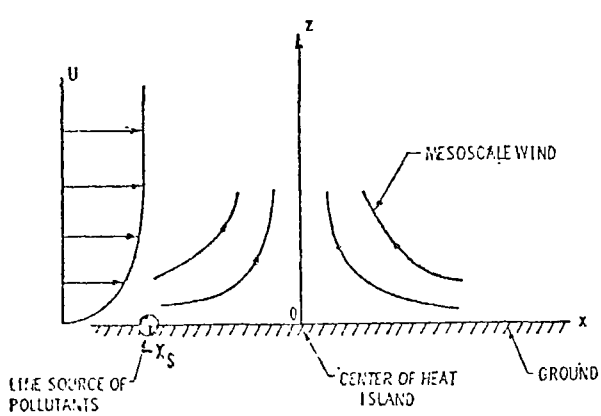

The equation governing the pollutant concentration can be written as

$$(u_1 - ax)\left(\frac{z}{z_1}\right)^m \frac{\partial c}{\partial x} + \frac{az}{m+1}\left(\frac{z}{z_1}\right)^m \frac{\partial c}{\partial z} = \frac{\partial}{\partial z}\left[K_1\left(\frac{z}{z_1}\right)^n \frac{\partial c}{\partial z}\right] \quad , \qquad \text{(III-63)}$$

subject to the usual condition for a continuous ground-level line source at $x = -x_s$, $x_s > 0$. As shown by Dilly and Yen (1971), the solution of Eq. (III-63) is

$$c(x,z) = \frac{(m - n + 2)\, z_1^r\, q_\ell}{\Gamma(s)} \cdot \left\{ \frac{a}{(m+1)(m-n+2)\, K_1 \left[(u_1 - ax_s)^{\frac{1}{s}} - (u_1 - ax)^{\frac{1}{s}}\right]} \right\}^s \cdot \exp\left\{ - \frac{a(u_1 - ax)^{\frac{1}{s}}\, z^{m-n+2}}{(m+1)(m-n+2) z_1^{m-n} K_1 \left[(u_1 - ax_s)^{\frac{1}{s}} - (u_1 - ax)^{\frac{1}{s}}\right]} \right\} \quad ,$$

(III-64)

where $m - n + 1 > 0$, $u_1 - ax > 0$, and

$$r = \frac{m + n}{m - n + 2} \quad ,$$

$$s = \frac{m + 1}{m - n + 2} \quad .$$

Equation (III-41) gives the trajectory model applicable to this situation. The basic difficulty, however, in comparing Eqs. (III-41) and (III-64) is to relate the parcel travel time, τ, to the downwind distance, x. Let us assume that the parcel velocity, U, for the trajectory model is $u_1 - ax$, i.e., the parcel velocity at the reference altitude z_1. It follows that the location of an air parcel that was at s_x at $\tau = 0$ is

$$x(\tau) = \frac{u_1}{a} + \left(x_s - \frac{u_1}{a}\right) e^{-a\tau} \quad . \tag{III-65}$$

Thus, the travel time, τ, is related to the downwind distance, x, as follows:

$$\tau = \frac{1}{a} \ell n \left[\frac{u_1 - ax_s}{u_1 - ax}\right] \quad . \tag{III-66}$$

As in the previous line source examples, the appropriate source strength, Q_A, for use in the trajectory model is related to the actual continuous emission rate, q_ℓ, as follows:

$$Q_A = \frac{q_\ell}{U} \quad .$$

The solution is thus given by Eq. (III-41) with Q_A replaced by q_ℓ/U.

Therefore, the mean concentration predicted by the trajectory model is

$$c(x,z) = \frac{\dfrac{q_\ell}{u_1 - ax}}{(2-n)^{\frac{n}{2-n}} \Gamma\left(\dfrac{1}{2-n}\right) \bar{K}_1^{\frac{1}{2-n}} \cdot \left[\dfrac{1}{a} \ell n \left(\dfrac{u_1 - ax_s}{u_1 - ax}\right)\right]^{\frac{1}{2-n}}}$$

$$\cdot \exp\left[-\frac{az^{2-n}}{(2-n)^2 \bar{K}_1 \ell n \dfrac{u_1 - ax_s}{u_1 - ax}}\right] \quad . \tag{III-67}$$

Given Eqs. (III-64) and (III-67), we can now complete the ratio of the predicted ground-level concentrations in which we are interested. The ratio is

$$\gamma = \frac{\tilde{c}(x,0)}{c(x,0)}$$

$$= \frac{\Gamma(s)(m+1)^{s}(m-n+2)^{2-1}}{(2-n)^{\frac{n}{2-n}}\,\Gamma\left(\frac{1}{2-n}\right)}\ \zeta^{-2p}\cdot\frac{1}{\psi}\cdot\left(1-\psi^{\frac{1}{s}}\right)^{s}\cdot\left[\ell n\left(\frac{1}{\psi}\right)\right]^{-\frac{1}{2-n}}, \qquad \text{(III-68)}$$

where

$$p = \frac{m(1-n)}{(m-n+2)(2-n)} ,$$

and

$$\zeta = \frac{z_1}{\sqrt{\frac{K_1}{a}}} ,$$

$$\psi = \frac{u_1 - x}{\frac{u_1}{a} - x_s} .$$

This equation shows that the deviation of the trajectory model predictions from the exact solutions is a function of two dimensionless distances. The first, τ, is a nondimensional form of the reference height, the elevation at which the wind is used to compute the trajectory; the second, ψ, is a nondimensional horizontal distance. The values of ψ vary continuously from 1 to 0 as the air parcel travels from the source point $x - x_s$ to a location where a reverse flow begins to appear ($x = u_1/a$) and beyond which the solutions developed above no longer apply. We computed the ratio γ for a family of the parameters m and n and for three values of ζ. Figure III-6 presents the results.

From a study of Figures III-6(a) through III-6(h), many interesting observations emerge concerning the effect of neglecting the vertical wind component in a trajectory model. As shown in Figures III-6(a) and III-6(b), the ratio γ is independent of ζ if either $m = 0$ or $n = 1$, i.e., the choice of a reference height becomes immaterial if the atmosphere possesses either a constant diffusivity profile or a wind field that varies linearly with height. For either case, it is clear that the trajectory model always overpredicts the ground-level concentrations, and the deviations increase as the trajectories move downwind of the source. Furthermore, the deviations increase with a decreasing exponent in a power law diffusivity profile or an increasing exponent in the power law wind profile. For a general combination of m and n, Figures III-6(c) through III-6(h) show that the ratio γ depends on the choice of the reference height. The trajectory model predictions increase with decreasing reference height. The ratio γ, however, always increases as the distance from the source point increases, indicating an accumulation of pollutants due to the lack of vertical transport by the vertical component of the wind in the trajectory model.

The most significant conclusion that can be drawn from the above analysis is that, for meteorological conditions typical of those observed in urban environments, the value of γ can vary greatly (i.e., by an order of magnitude), particularly at distances far from the point of release. This implies that, with the exception of the special case of a vanishing vertical

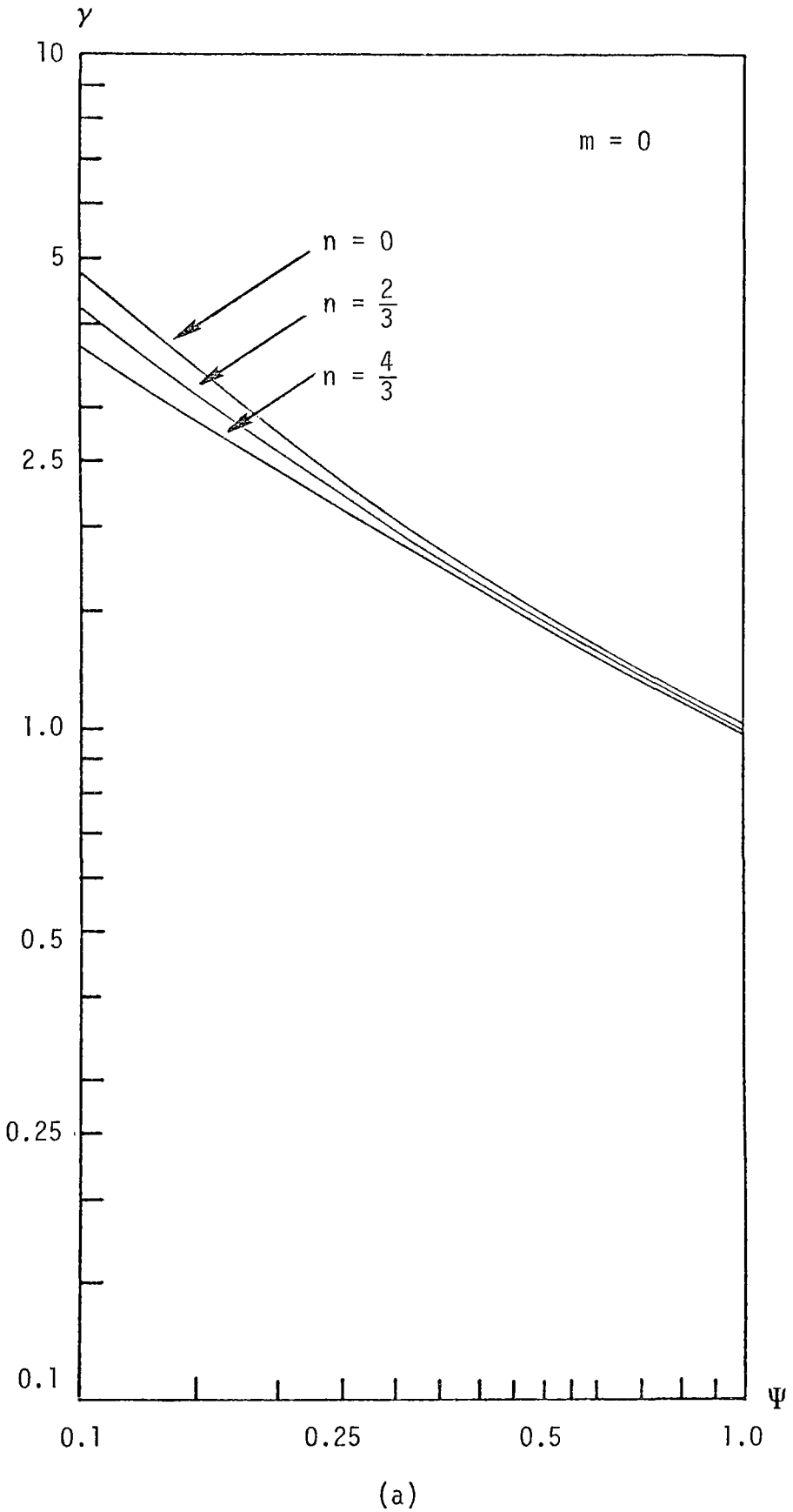

(a)

FIGURE III-6. THE EFFECT OF VERTICAL WIND ON THE TRAJECTORY MODEL PREDICTIONS

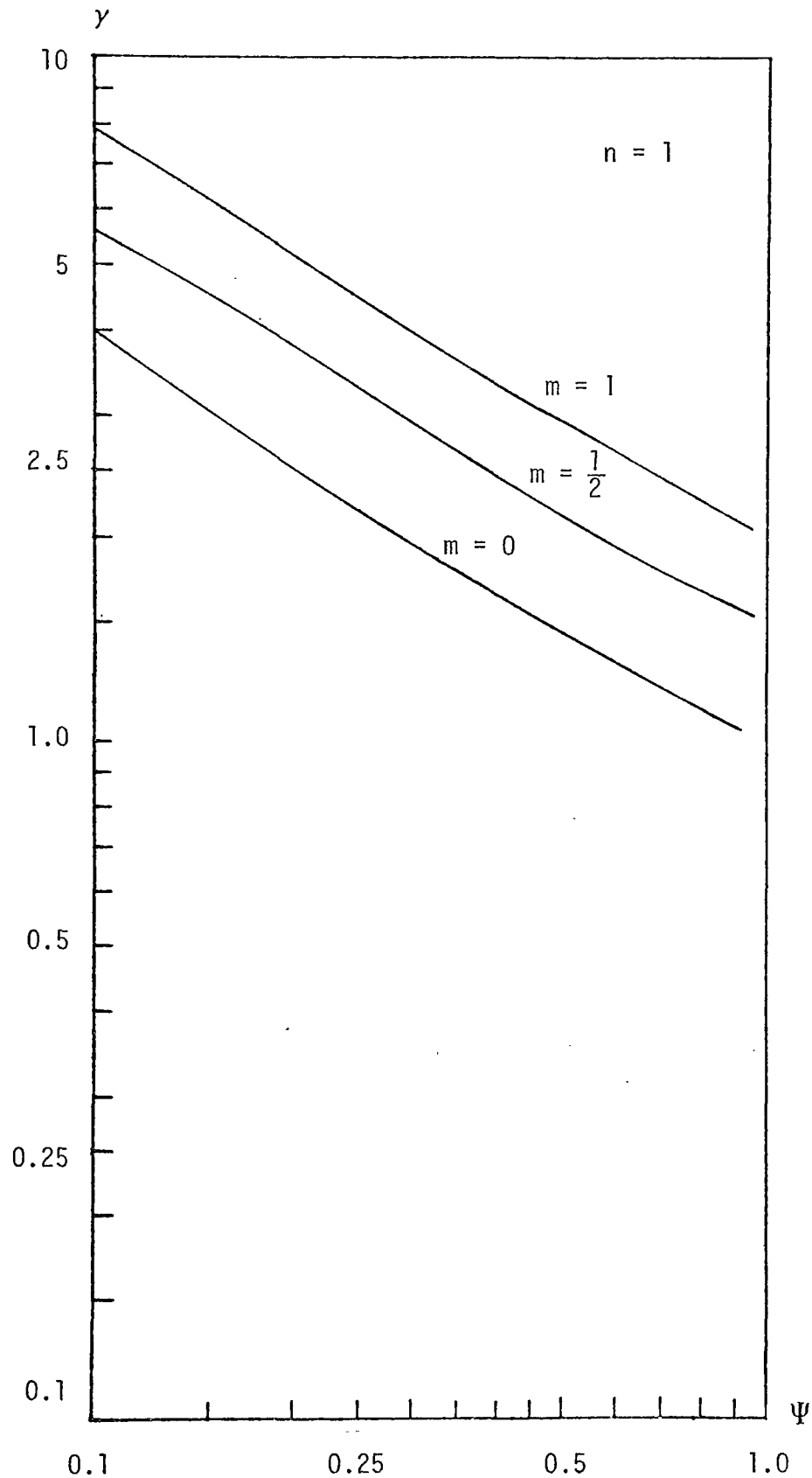

(b)

FIGURE III-6. THE EFFECT OF VERTICAL WIND ON THE TRAJECTORY MODEL PREDICTIONS (Continued)

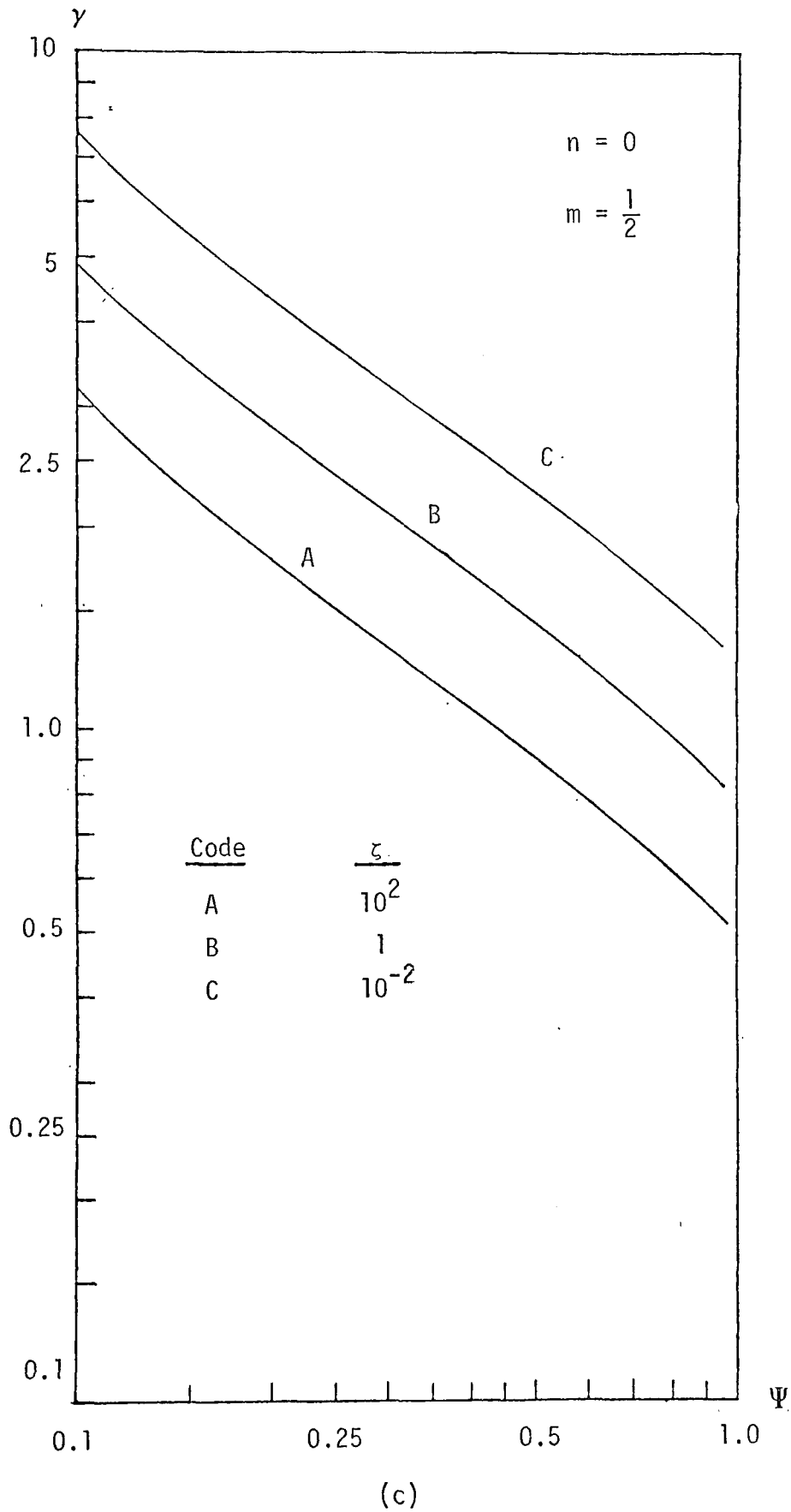

(c)

FIGURE III-6. THE EFFECT OF VERTICAL WIND ON THE TRAJECTORY MODEL PREDICTIONS (Continued)

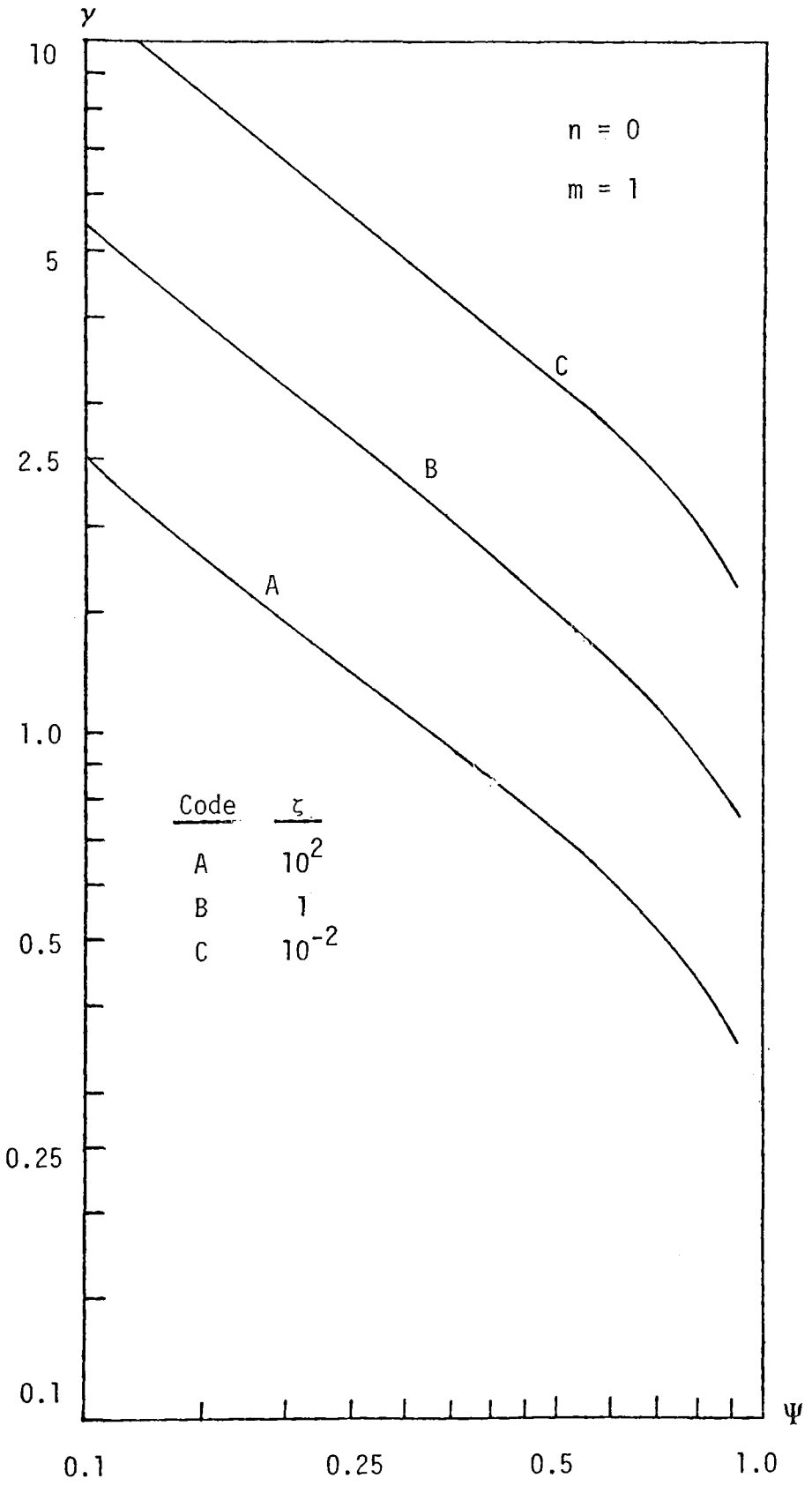

(d)

FIGURE III-6. THE EFFECT OF VERTICAL WIND ON THE TRAJECTORY MODEL PREDICTIONS (Continued)

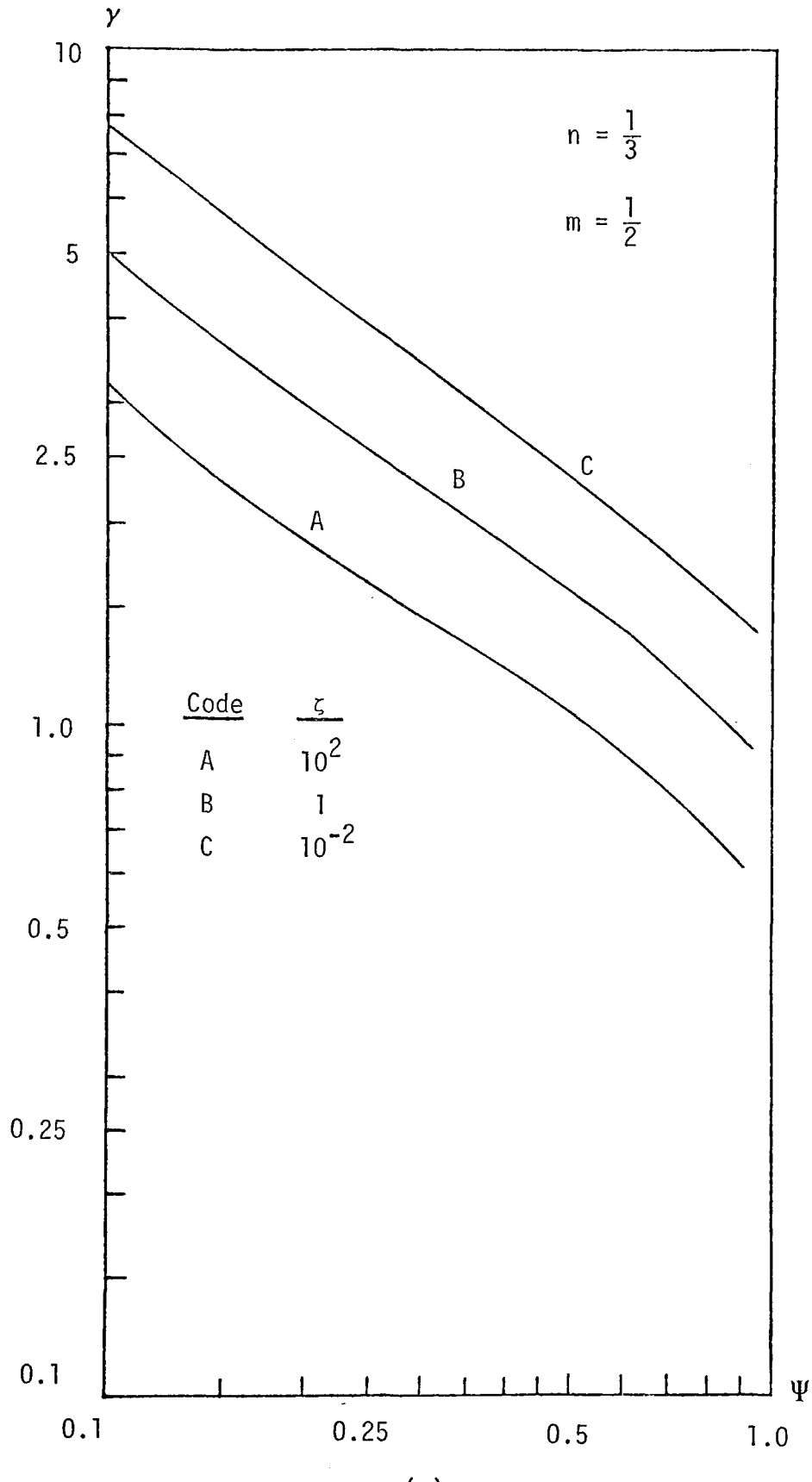

(e)

FIGURE III-6. THE EFFECT OF VERTICAL WIND ON THE TRAJECTORY MODEL PREDICTIONS (Continued)

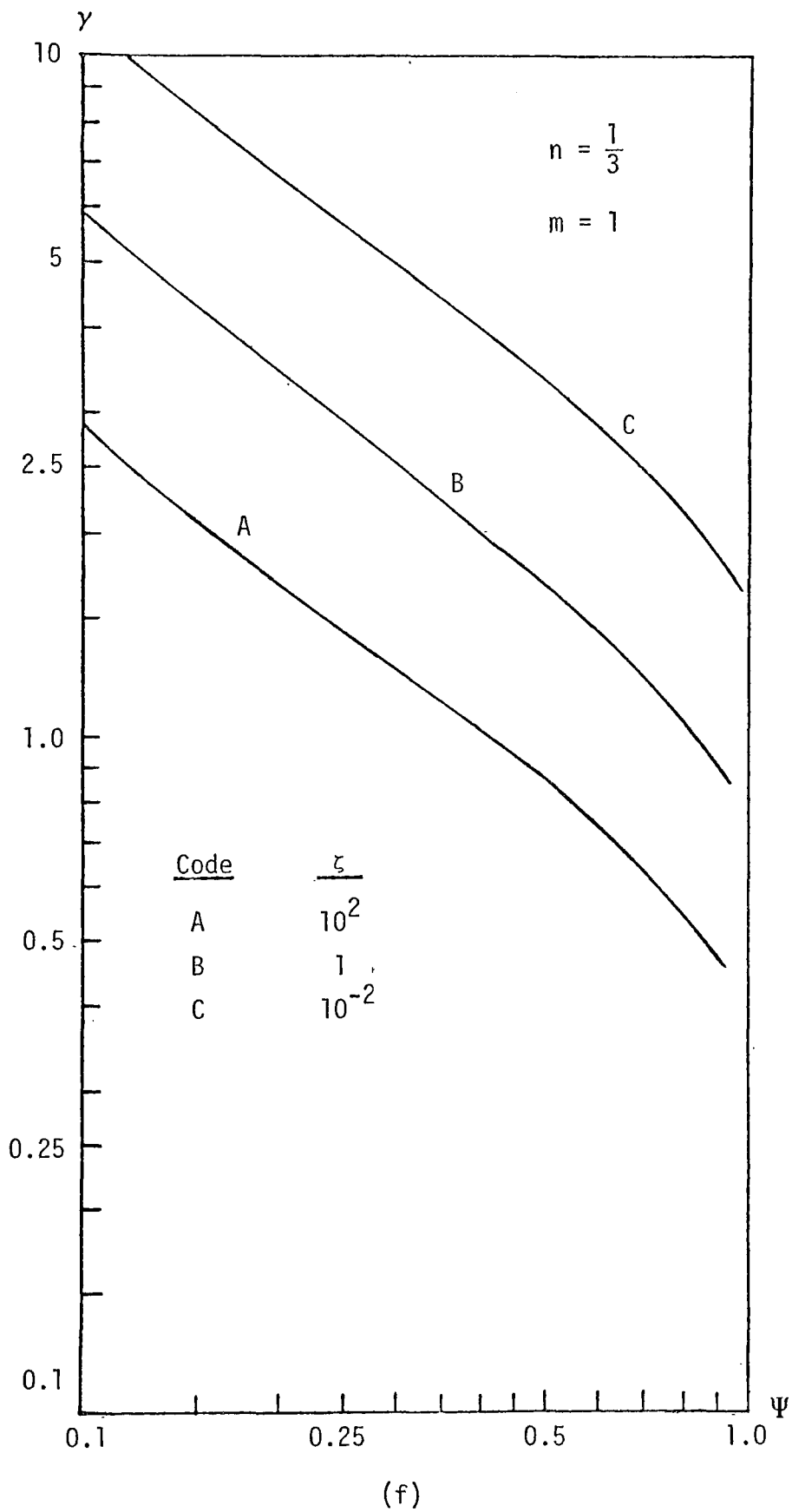

(f)

FIGURE III-6. THE EFFECT OF VERTICAL WIND ON THE TRAJECTORY MODEL PREDICTIONS (Continued)

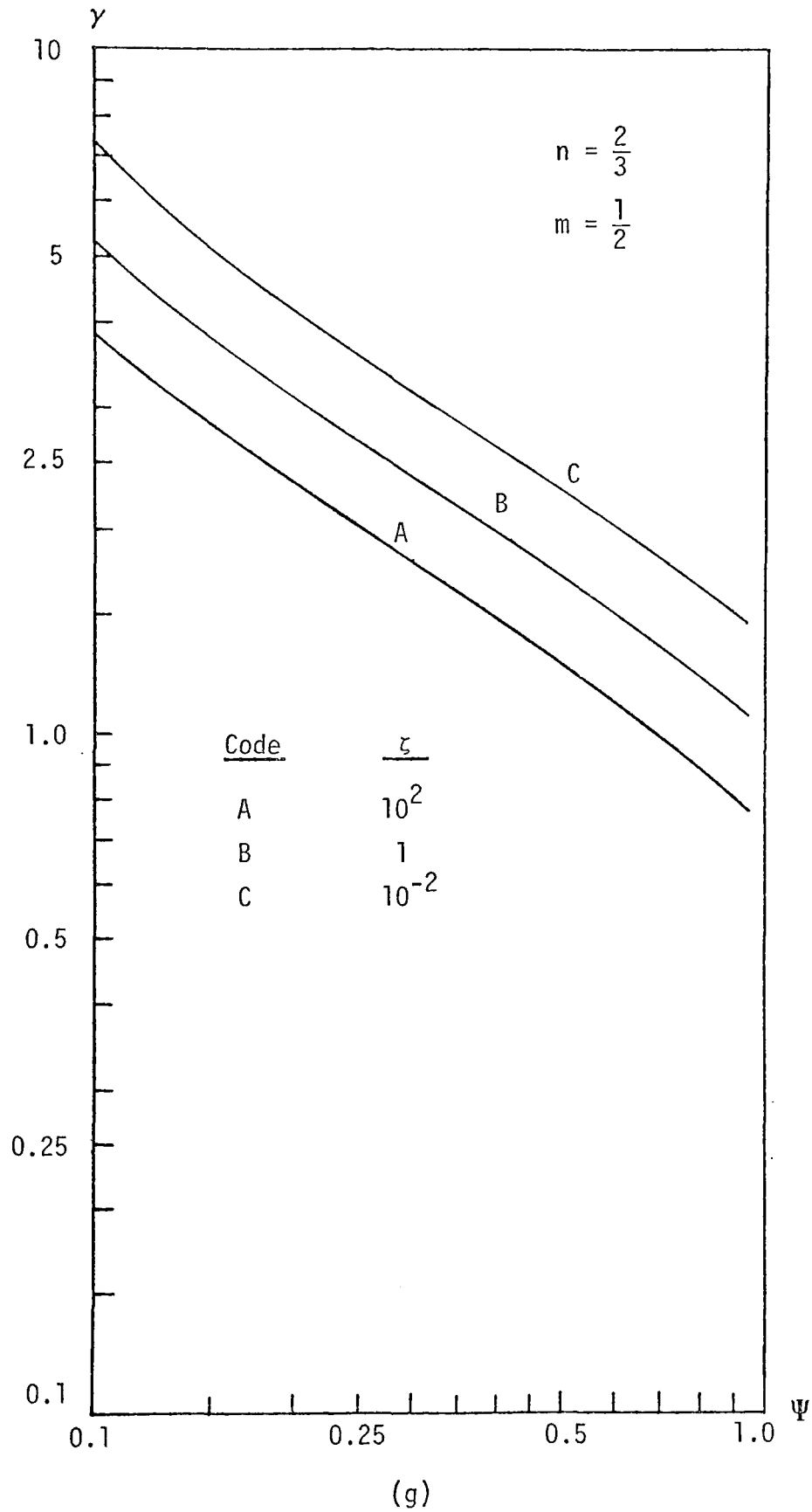

(g)

FIGURE III-6. THE EFFECT OF VERTICAL WIND ON THE TRAJECTORY MODEL PREDICTIONS (Continued)

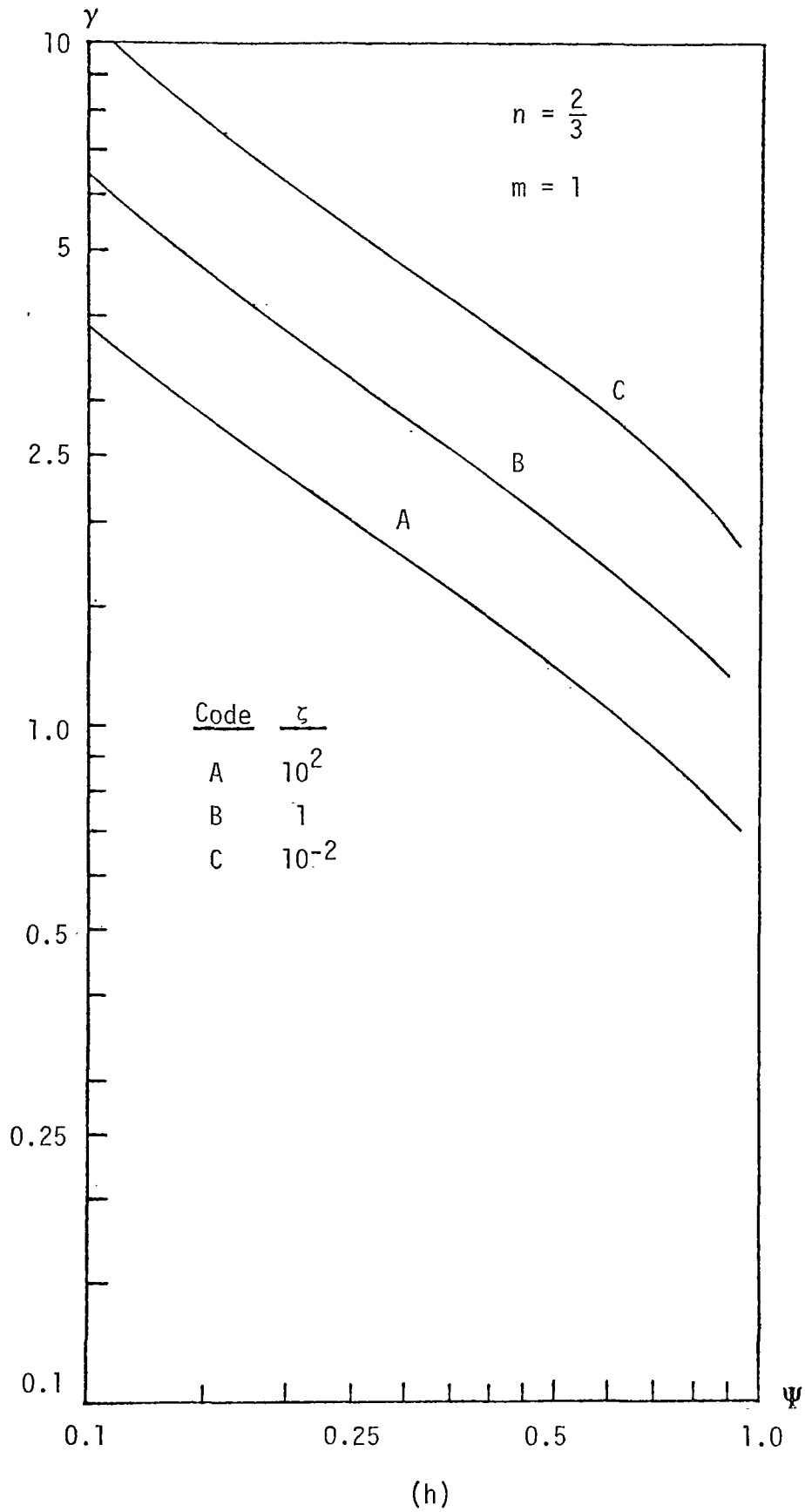

FIGURE III-6. THE EFFECT OF VERTICAL WIND ON THE TRAJECTORY MODEL PREDICTIONS (Concluded)

wind* (i.e., $a \to 0$ and $\psi \to 1$), the neglect of the vertical wind can cause gross errors in the predictions of pollutant concentrations.

3. The Effect of Wind Shear

As we mentioned earlier, the case of a horizontal wind that varies with height cannot be properly handled by a trajectory model because, intrinsically, only one horizontal wind at any location can be used to compute the movement of the air column. We assess here the errors incurred as a result of this assumption. We consider two different cases: (1) a simple, crosswind continuous line source and (2) a more realistic urban-type (distributed) source. As shown in Figure III-7, we allowed the wind speed and vertical turbulent diffusivity in both cases to vary with altitude according to the following power laws:

$$u = u_1 \left(\frac{z}{z_1} \right)^m \quad , \tag{III-69}$$

$$K = K_1 \left(\frac{z}{z_1} \right)^n \quad . \tag{III-70}$$

---

*Convergence in an urban area, as we emphasized earlier, is by no means small. For example, a change of more than 1 mph over a 1 mile distance is quite common. If we use the two-dimensional continuity equation to estimate the convergence, we obtain

$$a \simeq \frac{\Delta w}{\Delta z} \simeq - \frac{\Delta u}{\Delta x} \sim \frac{1 \text{ mph}}{1 \text{ mile}} = 1 \text{ hr}^{-1} \sim 3 \times 10^{-4} \text{ sec}^{-1} \quad ,$$

which agrees with measurements made by Ackerman (1974).

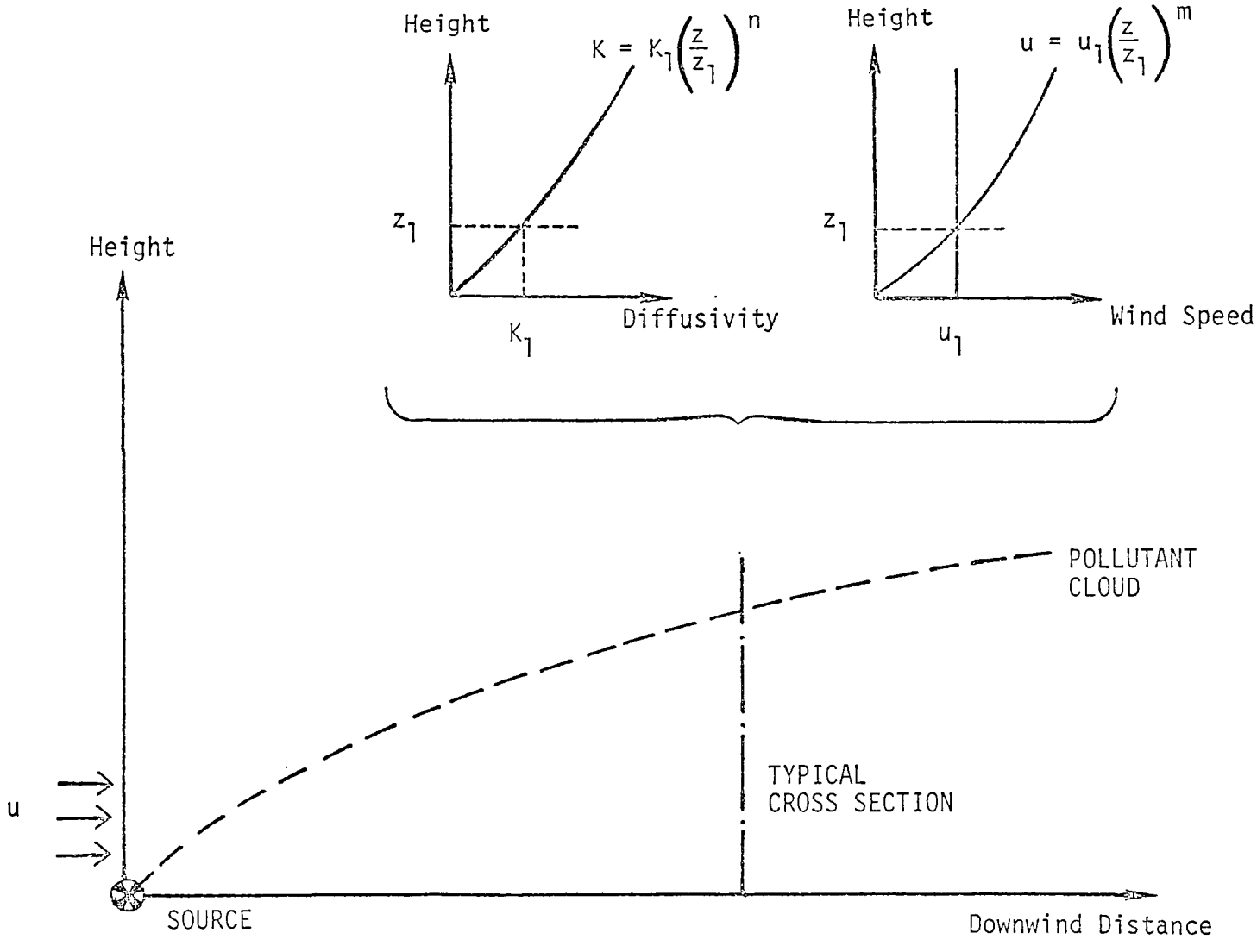

FIGURE III-7. ASSESSING THE EFFECT OF WIND SHEAR

a. A Continuous Line Source

The well-known Roberts solution (Monin and Yaglom, 1971) gives the mean concentration downwind of a continuous ground-level line source in an atmosphere with a power law wind speed and vertical diffusivity profile:

$$c(x,z) = \frac{(m - n + 2)z_1^r Q_\ell}{u_1 \Gamma(s)} \left[\frac{u_1}{(m - n + 2)^2 K_1 x} \right]^s \cdot \exp \left[- \frac{u_1 z^{m-n+2}}{(m - n + 2)^2 K_1 z_1^{m-n} x} \right] , \qquad \text{(III-71)}$$

where

$$m - n + 1 \geq 0^*$$

and

$$r = \frac{m + 1}{m - n + 2} ,$$

$$s = \frac{m + 1}{m - n + 2} .$$

*Monin and Yaglom (1971) appear to have incorrectly quoted $m - n + 2 > 0$. A more stringent condition, $m - n + 1 \geq 0$, is needed to satisfy the condition that the flux is zero along the x-axis (except at the origin).

For the trajectory model, we assume that the air parcel moves with the wind speed at the reference height u_1 as we have defined before. Then, from Eq. (III-41), the solution is

$$\tilde{c}(\rho,\tau) = \frac{\frac{q_\ell}{u_1}}{(2-n)^{\frac{n}{2-n}}\,\Gamma\left(\frac{1}{2-n}\right)\left(K_1\tau\right)^{\frac{1}{2-n}}} \exp\left[-\frac{\rho^{2-n}}{(2-n)^2\,\bar{K}_1\tau}\right] \quad . \tag{III-72}$$

To compare the two solutions, we let $x = u\tau$ and $z = \rho$ in Eq. (III-71) and set $\rho = 0$ in both equations. We then obtain the ratio of the trajectory model solution to the exact solution:

$$\gamma = \frac{\Gamma(s)(m-n+2)^{2s-1}}{(2-n)^{\frac{n}{2-n}}\,\Gamma\left(\frac{1}{2-n}\right)} \cdot \eta^{\rho} \quad , \tag{III-73}$$

where

$$\rho = \frac{m(1-n)}{(m-n+2)(2-n)} \quad ,$$

$$\eta = \left(\frac{K_1}{z_1^2}\right)\tau \quad .$$

We evaluated the ratio γ over a wide range of values of m and n as a function of the dimensionless time η (see Figure III-8). The results show that the predictions of a trajectory model that neglects the variation of

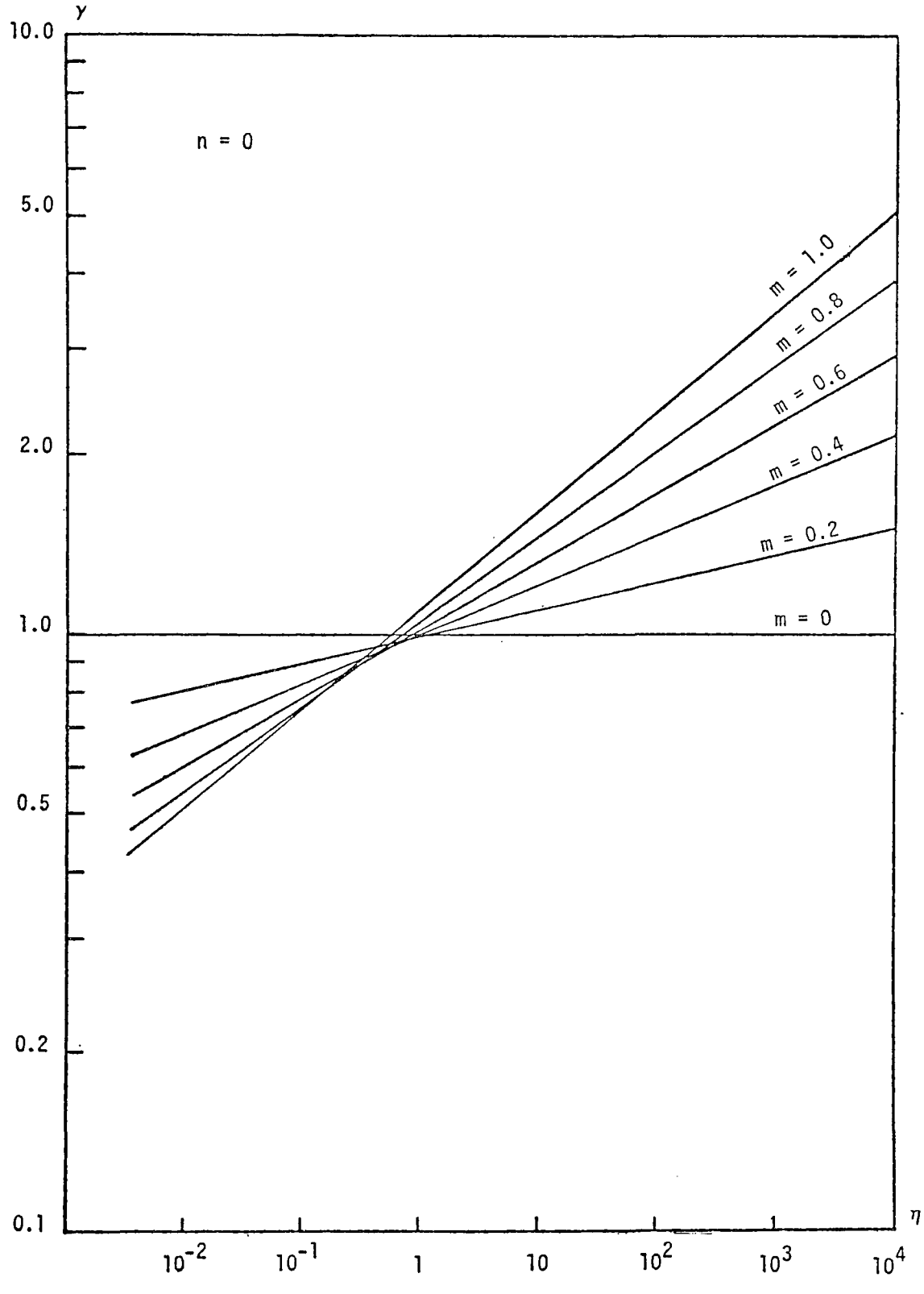

(a)

FIGURE III-8. THE EFFECT OF WIND SHEAR ON TRAJECTORY MODEL PREDICTIONS (FOR LINE SOURCES)

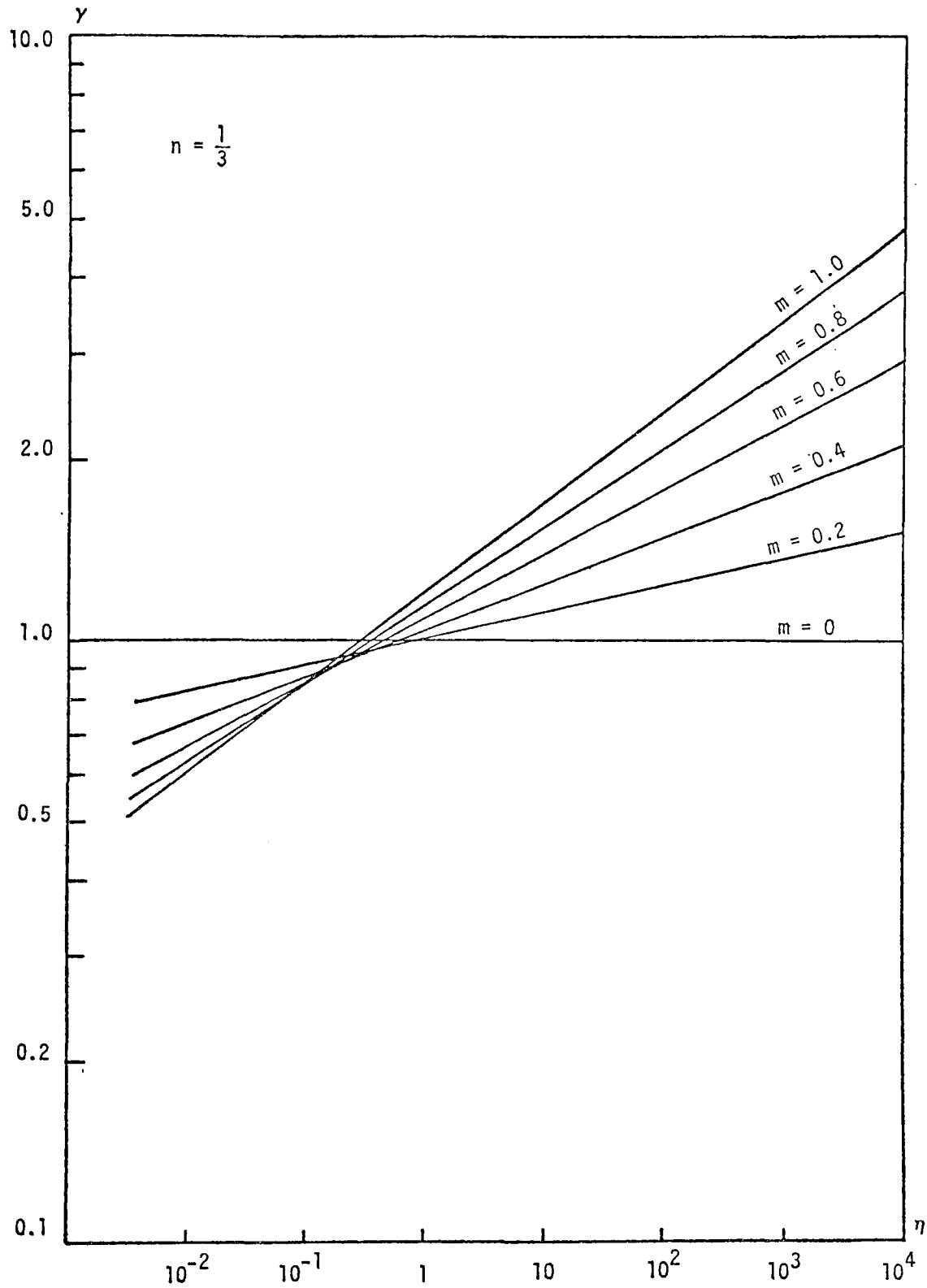

(b)

FIGURE III-8. THE EFFECT OF WIND SHEAR ON TRAJECTORY MODEL PREDICTIONS (FOR LINE SOURCES) (Continued)

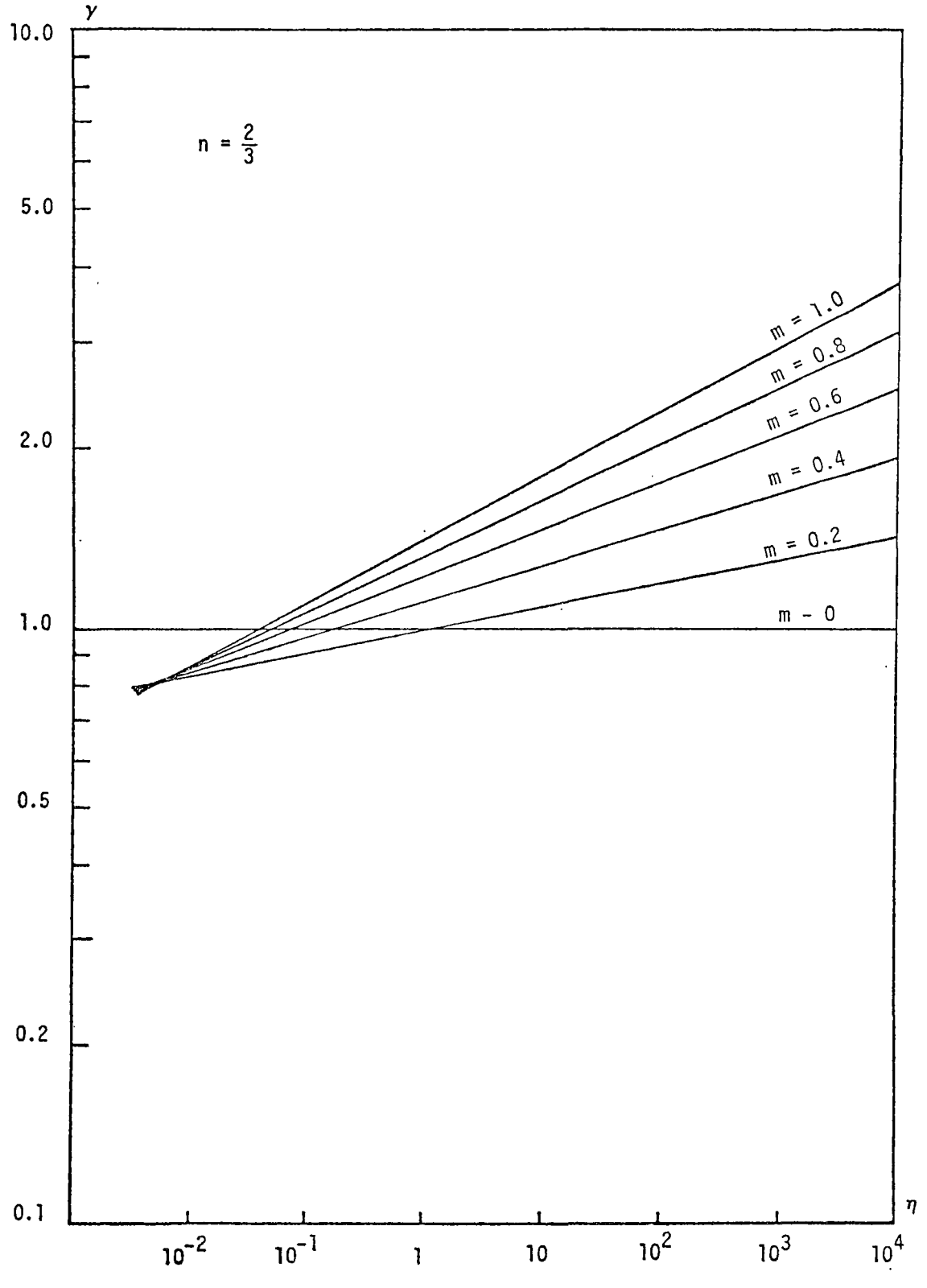

(c)

FIGURE III-8. THE EFFECT OF WIND SHEAR ON TRAJECTORY MODEL PREDICTIONS (FOR LINE SOURCES) (Continued)

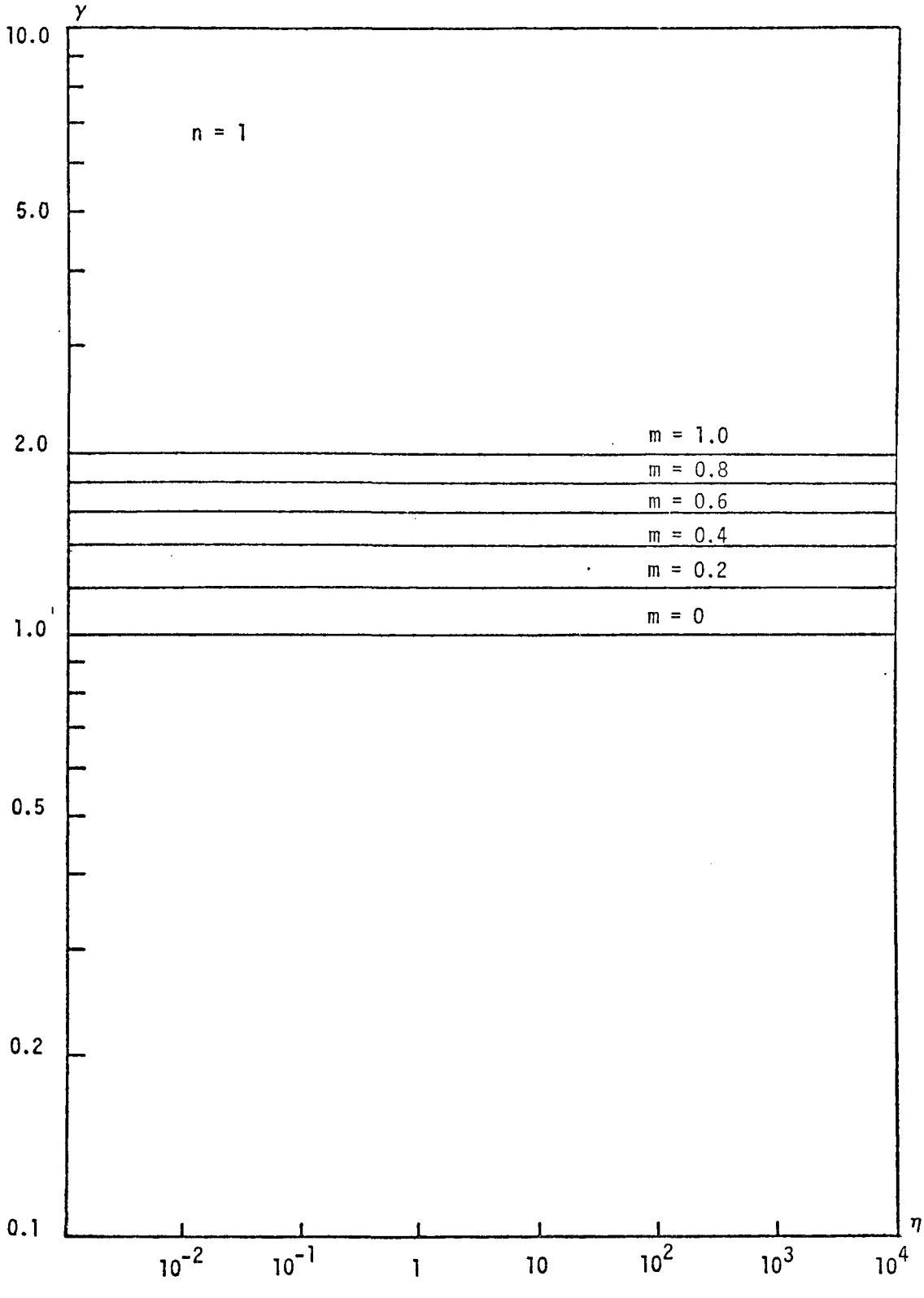

(d)

FIGURE III-8. THE EFFECT OF WIND SHEAR ON TRAJECTORY MODEL PREDICTIONS (FOR LINE SOURCES) (Continued)

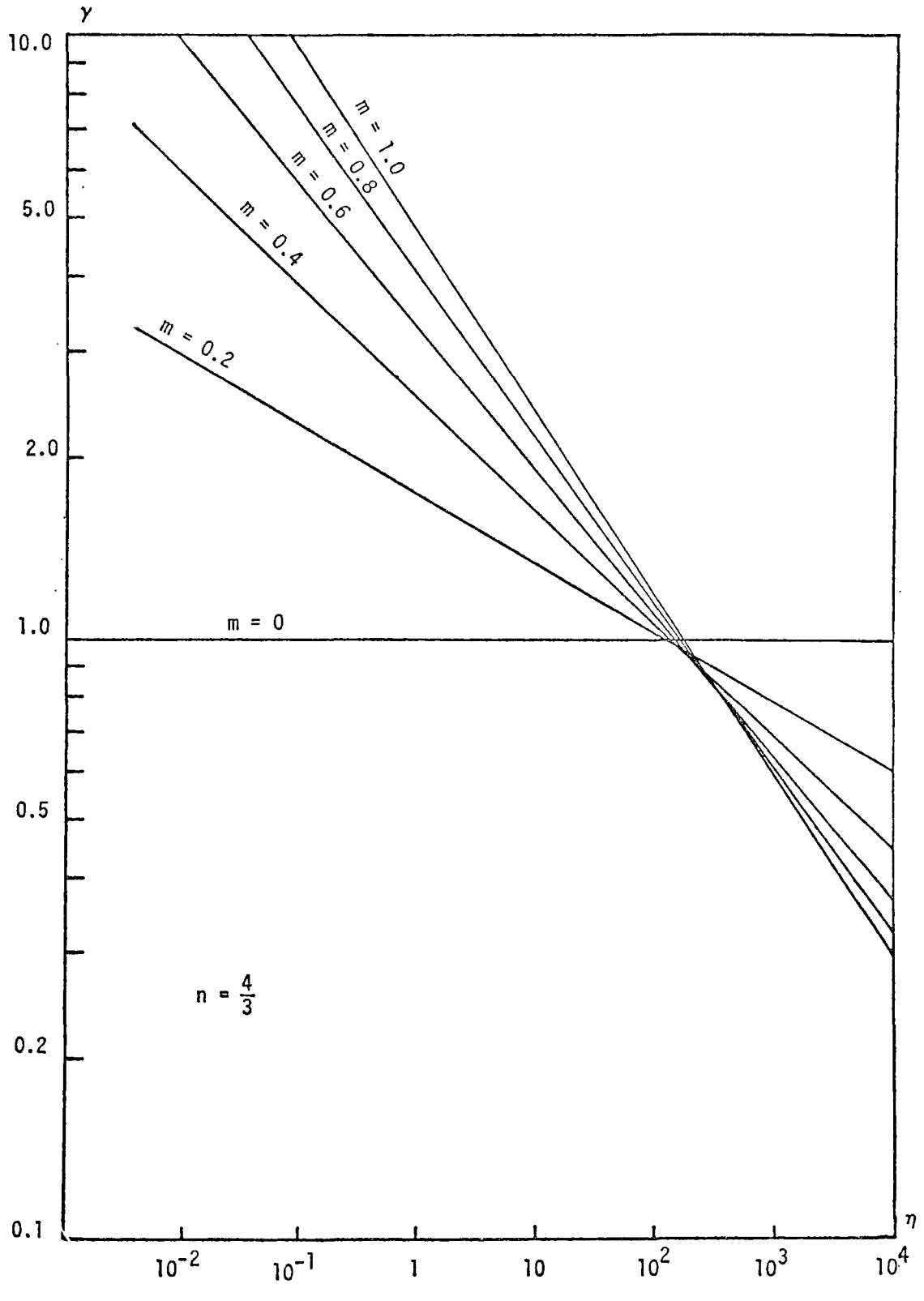

(e)

FIGURE III-8. THE EFFECT OF WIND SHEAR ON TRAJECTORY MODEL PREDICTIONS (FOR LINE SOURCES) (Concluded)

horizontal wind with height can be affected not only by the shape of the wind profile (as expressed by the exponent m), but also by the shape of the diffusivity profile (as expressed by the exponent n). With the exception of a linear diffusivity profile, Figure III-8(d), the performance of the trajectory model deteriorates with increasing time. The effect of a nonuniform wind profile on the trajectory model predictions is such that the atmosphere acts as if an imaginary emission source were introduced when its diffusivity variation is less than linear and as if an imaginary sink were introduced when its diffusivity variation is greater than linear.

To obtain a quantitative assessment of the trajectory model in real situations, we conducted a literature survey to estimate the possible values of m and n in an urban atmosphere. As discussed in Appendix B, we found that the ranges of values for m and n likely to occur in an urban atmosphere are 0.2 ~ 0.4 for m and ~ 1 for n.

If we let $K_1 = 1\ m^2\ sec^{-1}$ and $z_1 = 10$ m, a real time ranging from 1-1/2 minutes to 3 hours corresponds to a change of 1 to 100 in η. Figure III-8 indicates that over the ranges of m and n specified above, the trajectory model can be in error by more than 50 percent for the time span indicated as a result of the neglect of shear effects alone.

b. A Continuous Areal Source

The second case we consider here is an emission source that varies with location--a more realistic situation in an urban area.

Using assumptions identical to those made in the first case, we can obtain the solutions for the exact model and the trajectory model by applying the principle of superposition to Eqs. (III-71) and (III-72):

$$c(x,z) = \frac{(m - n + 2)z_1^{\Gamma}}{u_1 \Gamma(s)} \left[\frac{u_1}{(m - n + 2)^2 K_1} \right]^s \int_0^x \frac{q_A(\alpha)}{(x - \alpha)^s}$$

$$\cdot \exp \left[- \frac{u_1 z^{m-n+2}}{(m - n + 2)^2 K_1 z_1^{m-n} (x - \alpha)} \right] d\alpha \quad ,$$

and

$$c(\rho,\tau) = \frac{1}{u_1 (2 - n)^{\frac{n}{2-n}} \Gamma\left(\frac{1}{2 - n}\right) \overline{K}_1^{\frac{1}{2-n}}} \cdot \int_0^{\tau} \frac{q_A(\lambda)}{(\tau - \lambda)^{\frac{1}{2-n}}}$$

$$\cdot \exp \left[- \frac{\rho^{2-n}}{(2 - n)^2 \overline{K}_1 (\tau - \lambda)} \right] d\lambda \qquad \text{(III-74)}$$

Again, singular behavior exists near the upper limit of the integration, and coordinate transformations similar to the ones we discussed earlier must be invoked. We evaluated the resulting integrals using Simpson's rule. We used the same step-wise emissions pattern described in Section D-2. Figure III-9 shows the results for a wide range of values of m and n.

The significance of the ordinate γ is the same as that defined earlier; it is the ratio of the prediction of the trajectory model to that of the exact model. Figures III-9(a) through III-9(e) clearly demonstrate that, under conditions that are likely to occur in an urban atmosphere, the errors incurred as a result of the neglect of variations in horizontal wind with height can be quite substantial. For instance, using the set of values

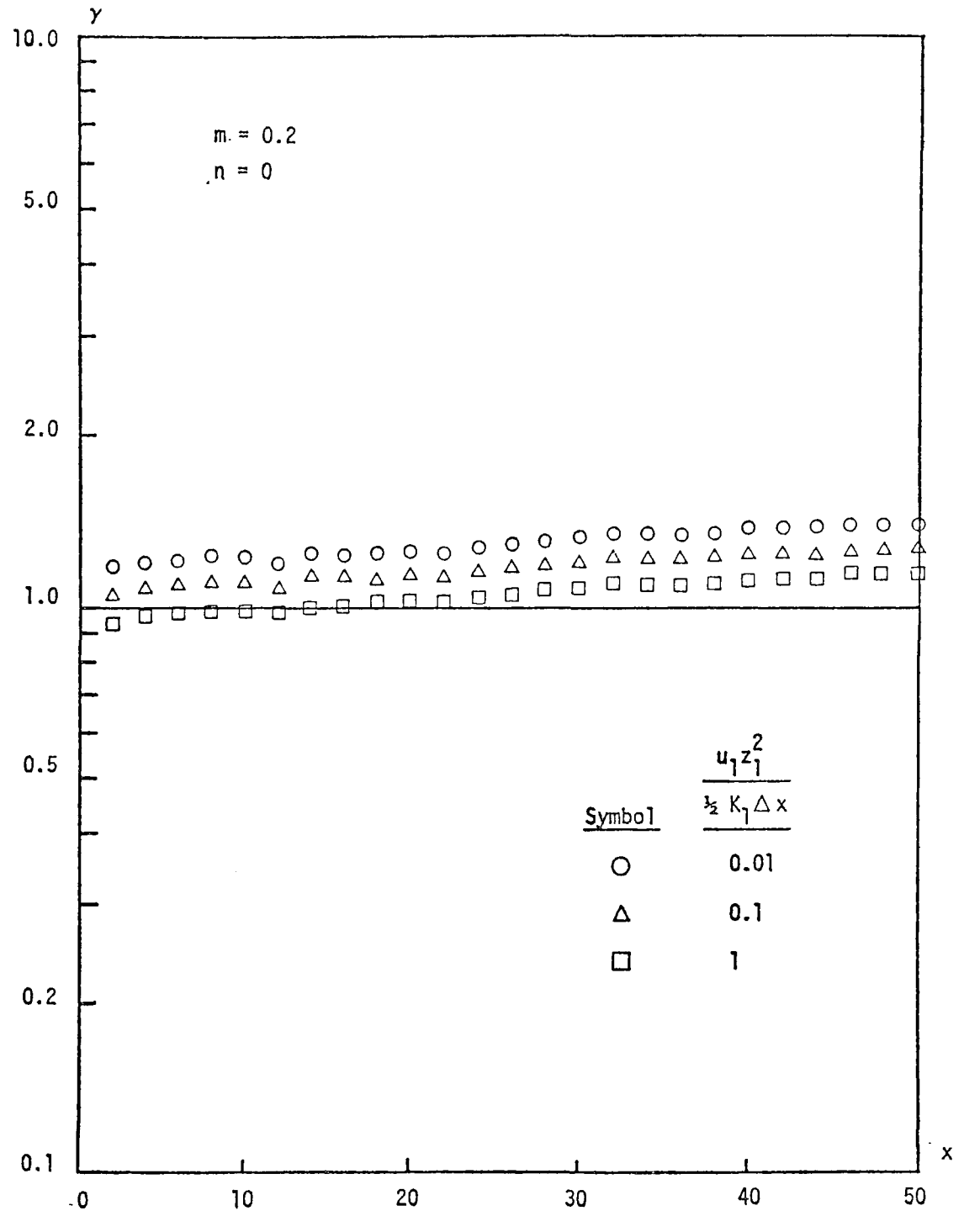

(a)

FIGURE III-9. THE EFFECT OF WIND SHEAR ON TRAJECTORY MODEL PREDICTIONS (FOR AREAL SOURCES)

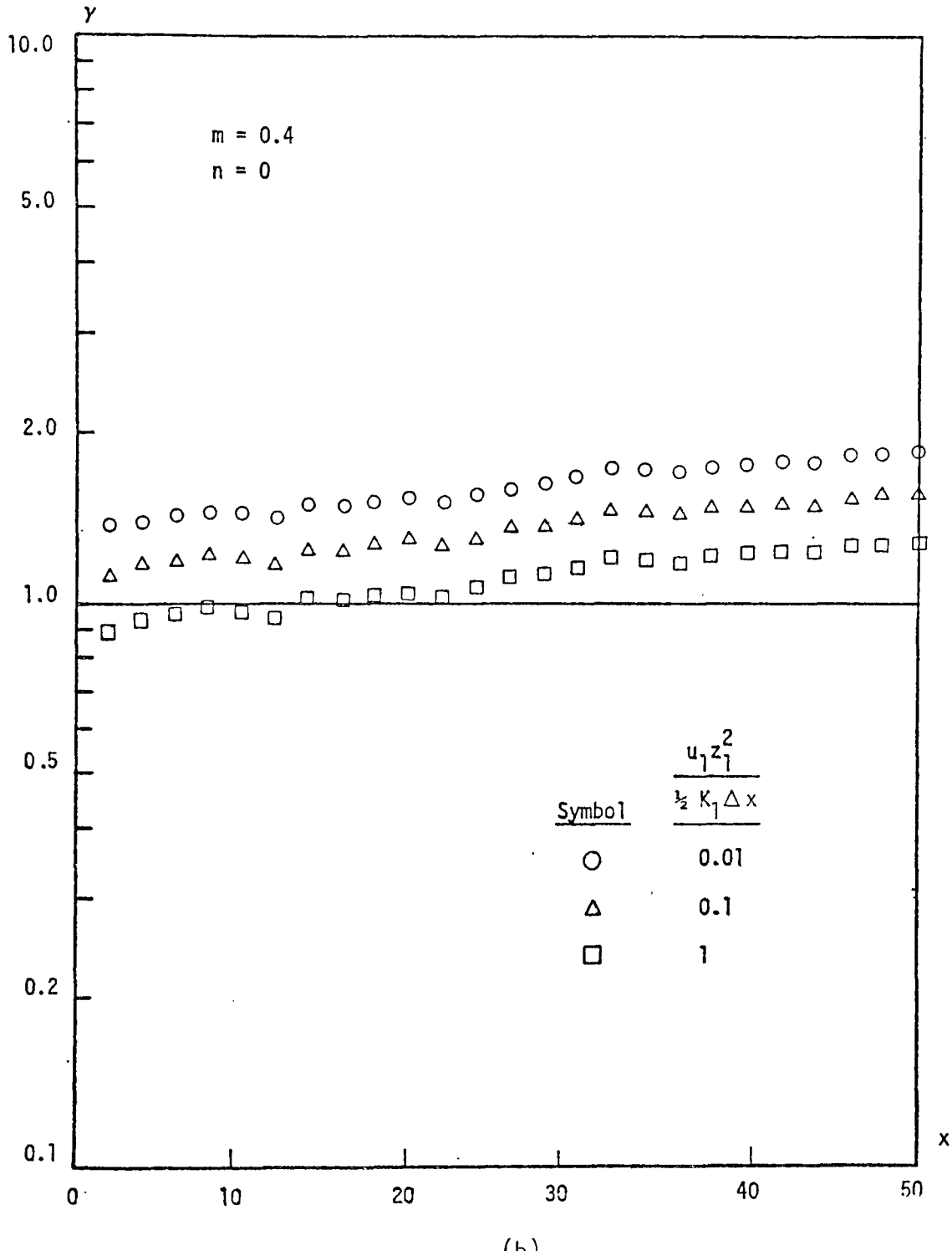

(b)

FIGURE III-9. THE EFFECT OF WIND SHEAR ON TRAJECTORY MODEL PREDICTIONS (FOR AREAL SOURCES) (Continued)

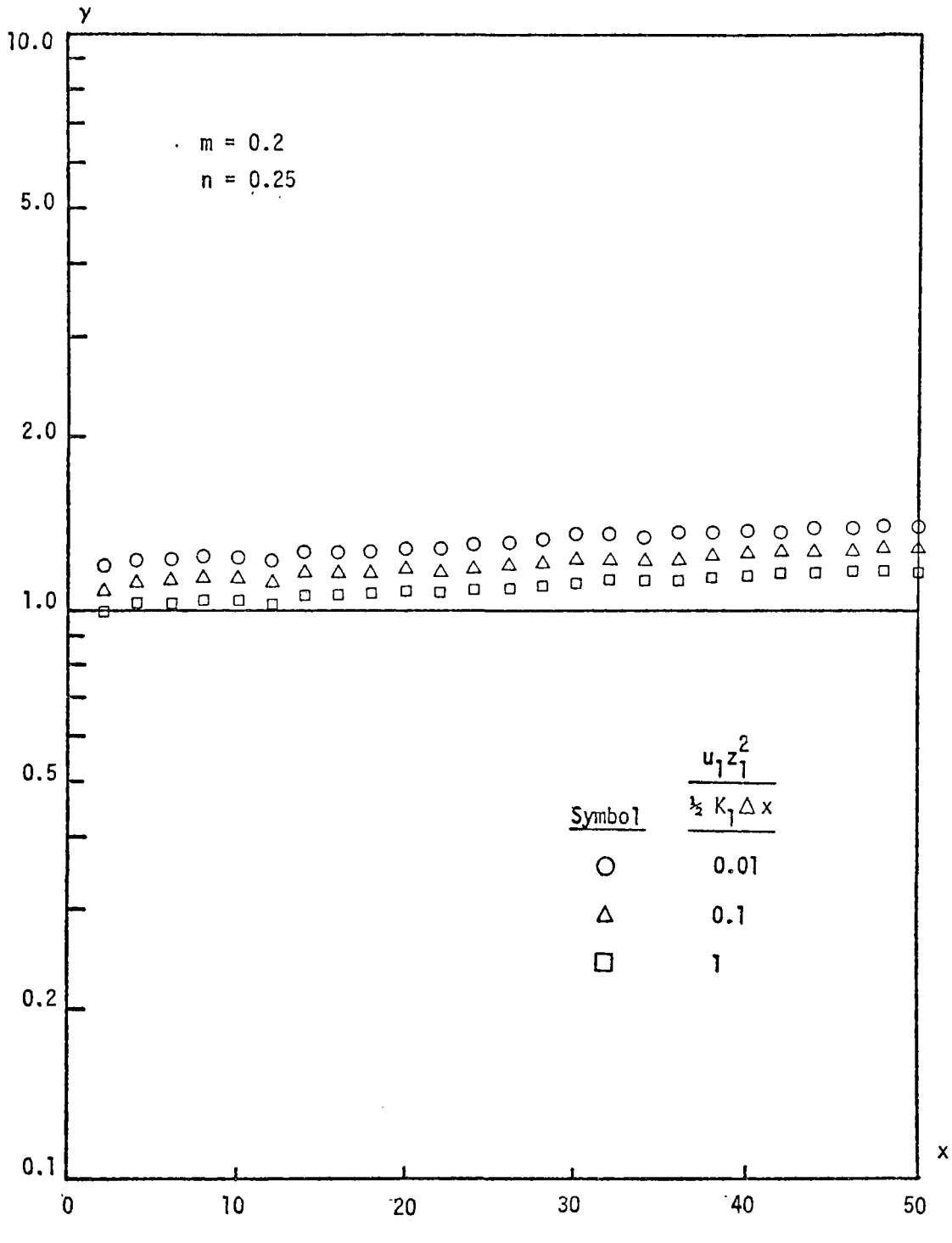

(c)

FIGURE III-9. THE EFFECT OF WIND SHEAR ON TRAJECTORY MODEL PREDICTIONS (FOR AREAL SOURCES) (Continued)

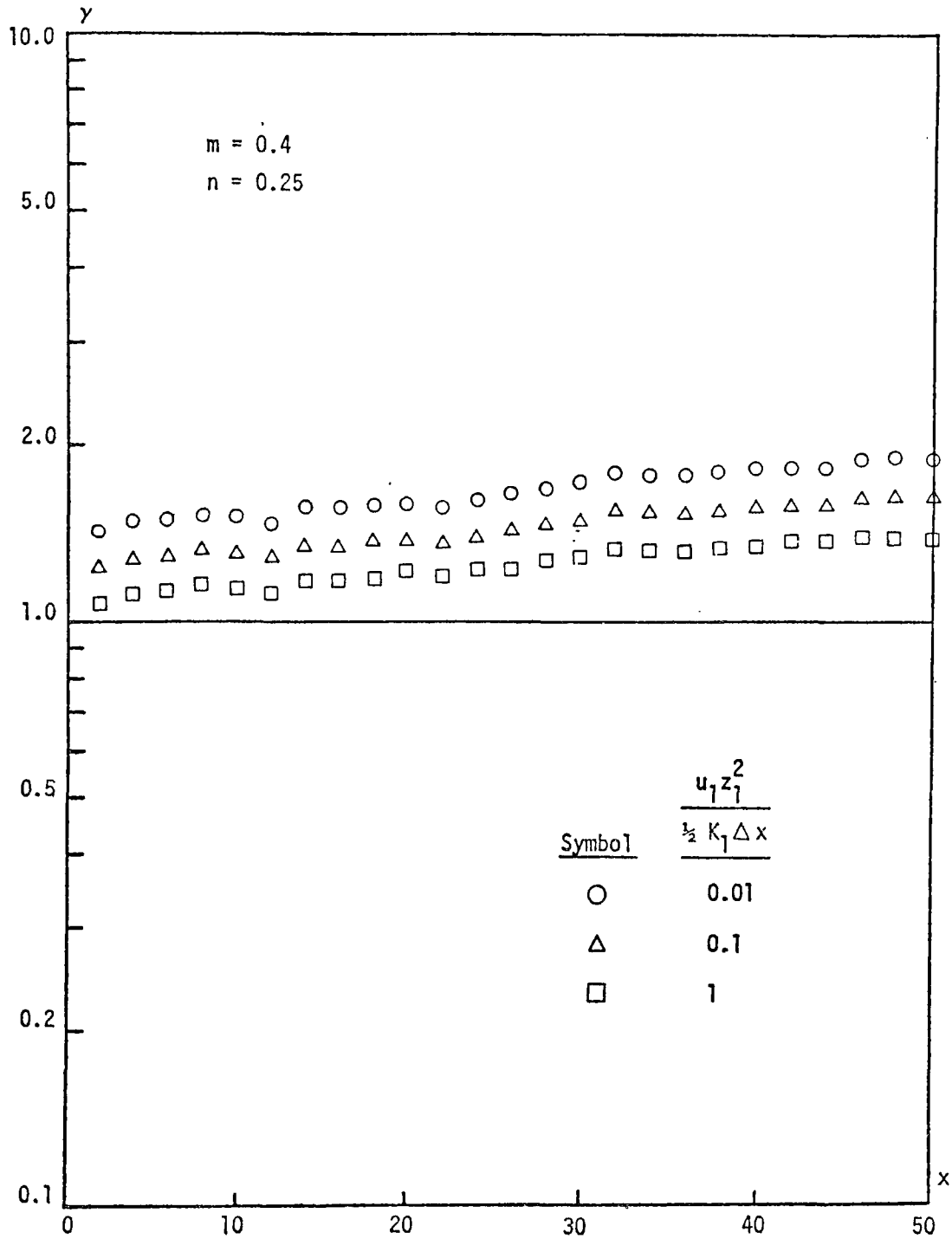

(d)

FIGURE III-9. THE EFFECT OF WIND SHEAR ON TRAJECTORY MODEL PREDICTIONS (FOR AREAL SOURCES) (Continued)

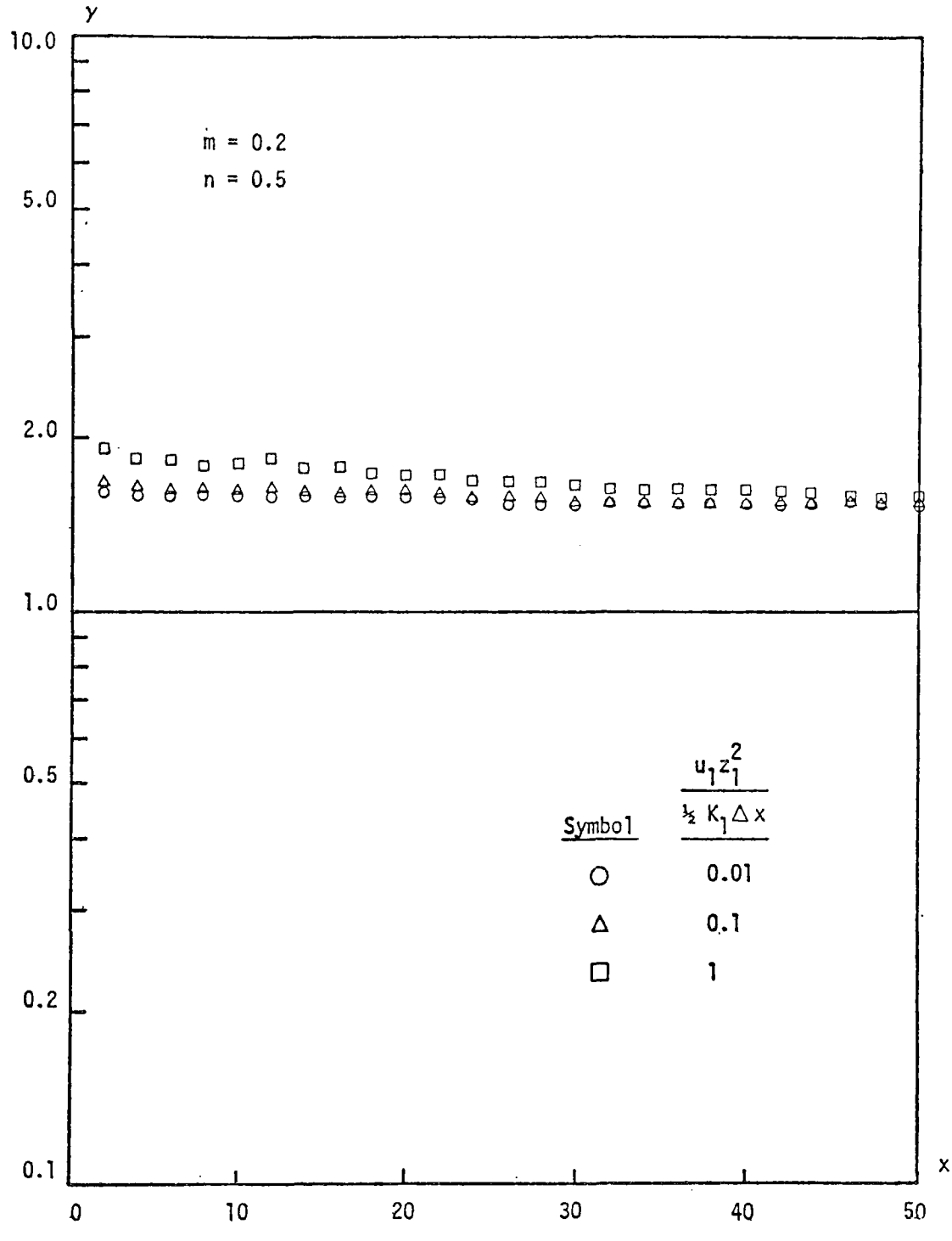

(e)

FIGURE III-9. THE EFFECT OF WIND SHEAR ON TRAJECTORY MODEL PREDICTIONS (FOR AREAL SOURCES) (Continued)

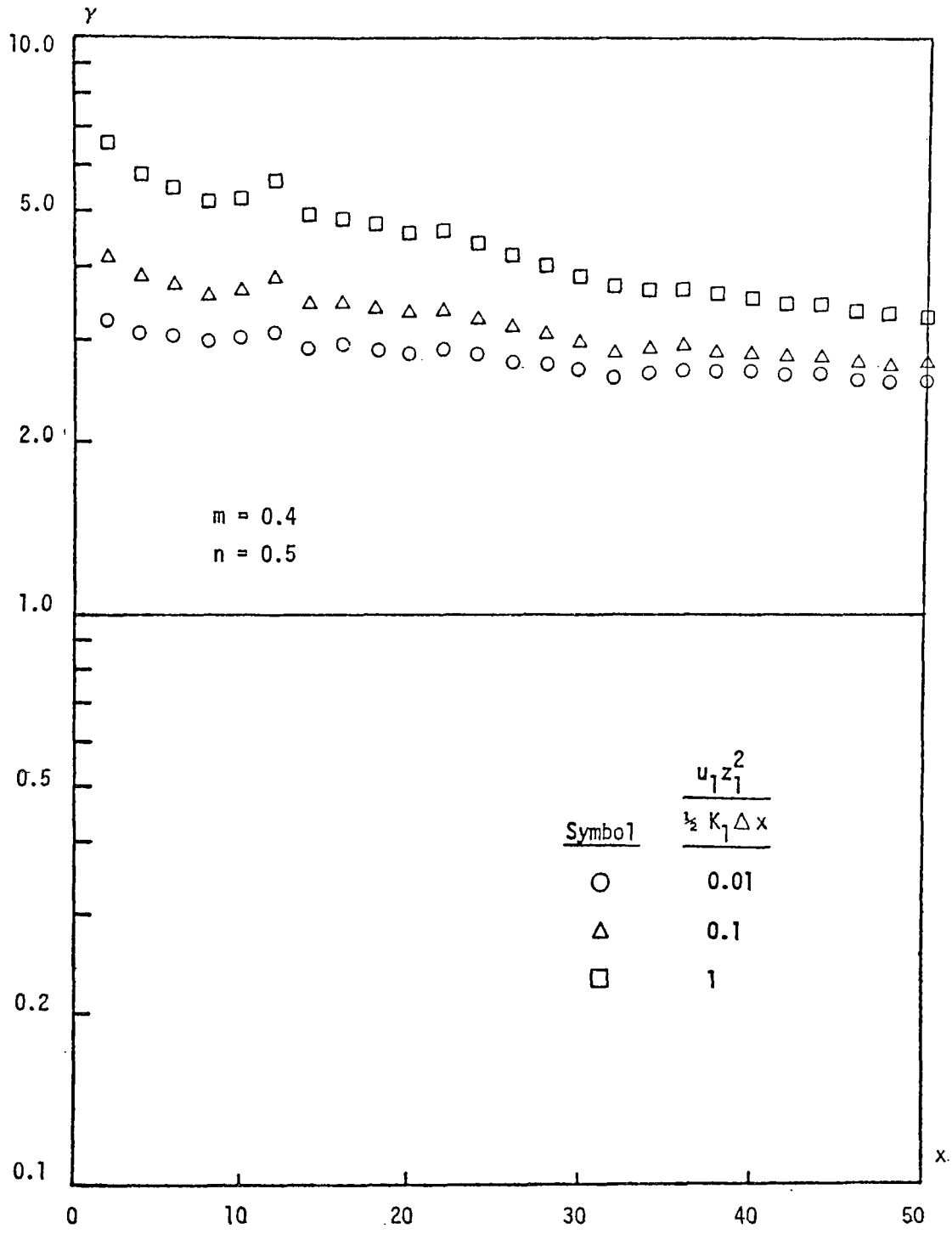

(f)

FIGURE III-9. THE EFFECT OF WIND SHEAR ON TRAJECTORY MODEL PREDICTIONS (FOR AREAL SOURCES) (Concluded)

$$u_1 = 1.5 \text{ m sec}^{-1} ,$$

$$z_1 = 10 \text{ m}$$

$$K_1 = 1 \text{ m}^2 \text{ sec}^{-1} ,$$

$$\Delta x = 3 \times 10^3 \text{ m} ,$$

we obtain a dimensionless number of 0.1 for $u_1 z_1^2/(1/2)K_1 \Delta x$; therefore, the set of points represented by triangles in Figures III-9(a) through III-9(e) is applicable. The corresponding values of γ then show that the trajectory model can overpredict the ground-level concentrations by more than 50 percent.

E. THE VALIDITY OF THE GRID MODEL--THE EFFECT OF NUMERICAL ERRORS

As we have pointed out in Section B, numerical errors generated using a grid model arise primarily in the process of discretizing the atmospheric diffusion equation, which is generally in a differential form. Two major aspects of a grid model are crucial in the determination of the magnitudes of numerical errors. The first is the choice of the cell size and the corresponding time interval. Although a decrease in the cell size and time interval ideally results in a decrease in the magnitudes of numerical errors generated using a grid approach, a compromise must be made between the cell size and time interval on one hand and the computing time and availability of data on the other (Seinfeld, 1970). Unfortunately, this results in a set of cell sizes producing numerical errors that are by no means insignificant. The second aspect of a grid model that affects the numerical errors is the type of numerical scheme that is used to represent the governing equation. There are probably as many numerical schemes as there are numerical models, and their performances vary greatly as the conditions of their applications change. However, they have one thing in common: None of them are perfect representations under all conditions. The objective here is not to evaluate the relative

merit of each of these numerical schemes. Rather, it is to estimate quantitatively the magnitudes of numerical errors generated using a grid model under realistic conditions. To avoid compounding the issue, we did not use fancy or sophisticated numerical schemes. Instead, we used a second-order difference scheme developed by Price et al. (1966) and a simple first-order difference scheme. Thus, the results derived in this section can be viewed as the upper bounds on numerical errors committed as a result of discretization.

The methodology we describe here to assess the numerical errors generated by a grid model is the same as the one we used to assess the inaccuracies of trajectory models. First, we obtained analytical solutions for certain specific but realistic cases. Then, we exercised a grid model to provide the corresponding predicted concentrations under similar conditions. Finally, we compared the two sets of numbers. All of the cases considered in this study, as prescribed by Eq. (III-12), were two-dimensional (crosswind) and time-dependent. We assumed that the wind speed and diffusivities (both horizontal and vertical components) were constant. Furthermore, we adopted step-wise emission patterns, as described in Eq. (III-59), under these conditions. The exact solution is

$$c(x,z,t) = \frac{1}{2\sqrt{\pi K_1}} \int_0^t \frac{1}{\sqrt{t-\beta}} \cdot \exp\left[-\frac{z^2}{4K_1(t-\beta)}\right] \cdot \left(\sum_{i=1}^{N} E_i(\beta) \left\{ \operatorname{erf}\left[\frac{x - (i-1)\Delta x - U(t-\beta)}{4K_H(t-\beta)}\right] - \operatorname{erf}\left[\frac{x - i\Delta x - U(t-\beta)}{4K_H(t-\beta)}\right] \right\} \right) d\beta \quad . \qquad \text{(III-75)}$$

Again, the removal of the singularities at the upper limit of the integral required coordinate transformations.

The grid model that was the subject of the present investigation uses two differencing schemes to represent Eq. (III-12): a first-order differencing scheme,

$$C_i^{n+1} = C_i^n - \frac{U\Delta t}{\Delta x}(C_i - C_{i-1}) + \frac{K_H \Delta t}{\Delta x^2}\left(C_{i-1}^n - 2C_i^n + C_{i+1}^n\right) \quad , \quad \text{(III-76)}$$

and the second-order differencing scheme developed by Price (1966),

$$C_i^{n+1} = C_i^n - \frac{U\Delta t}{2\Delta x}\left(3C_i^n - 2C_{i-1}^n - C_{i-2}^n\right) + \frac{K_H \Delta t}{\Delta x^2}\left(C_{i-1}^n - 2C_i^n + C_{i+1}^n\right) \quad . \quad \text{(III-77)}$$

The first-order scheme is the simplest and the most primitive of all finite difference schemes. Thus, the results probably represent the worst case insofar as the generation of errors as a result of discretization is concerned. Since Price's scheme is a higher order method, it is presumably more accurate. In addition, it has the desirable property of suppressing the prediction of negative concentrations of reactive pollutants in regions where sharp concentration gradients exist. We computed the ratios of the ground concentrations predicted using the grid model, i.e., Eq. (III-76) or Eq. (III-77), to those predicted using the exact solution, i.e., Eq. (III-75).

Using a realistic spatial and temporal emission pattern as shown in Figures III-3 and III-4, along with the second-order finite difference scheme (Price et al., 1966) in the grid model, we plotted the ratio γ in Figure III-10 for the following case:

$$u = 4 \text{ mph}$$

$$K_H = 50 \text{ m}^2 \text{ sec}^{-1} \quad .$$

Several interesting observations concerning the accuracy of the grid model emerge from a close scrutiny of Figure III-10. First, the numerical

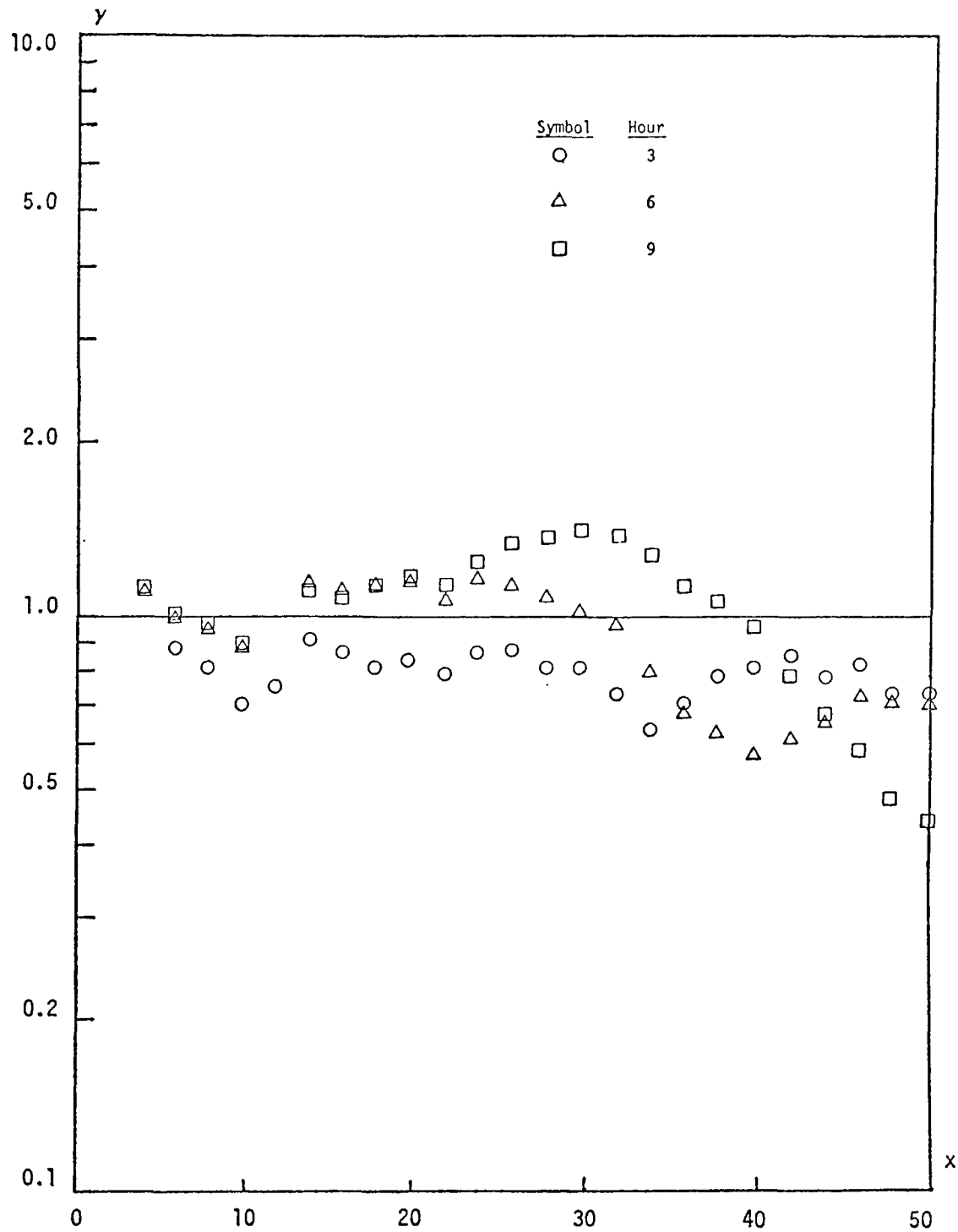

FIGURE III-10. THE EFFECT OF NUMERICAL ERRORS ON GRID MODEL PREDICTIONS: RESULTS USING THE FIRST-ORDER FINITE DIFFERENCE SCHEME (WIND SPEED = 4 MPH)

errors associated with the grid model apparently exhibit a wave-like behavior. The wave trains emanating from the upwind edge of the modeling region (which experiences a step jump in emissions) appear to be amplified both in amplitudes and in phase angles as the simulation time increases. After a nine-hour simulation, numerical errors can be an unbearable ±50 percent for many downwind locations. However, the difference scheme selected strongly influences the numerical errors generated using a grid model. To demonstrate this aspect, we tested the simpler--and thus more inaccurate--first-order difference scheme. As shown in Figure III-11, the resultant wave-like error propagation has amplitudes significantly higher than those for the second-order case.

As we discussed earlier, numerical errors also depend upon a complex matrix of physical parameters in the simulation. In the present study, we explored some of the more important ones. Since the numerical errors generated by the grid model originate primarily from inhomogeneities in the concentration distributions, spatial variations of the emissions undoubtedly have a strong effect on the performance of the model. Instead of using the realistic spatial emission pattern shown in Figure III-3, we used the smooth pattern shown in Figure III-12. With all other conditions identical to those in the numerical studies discussed in the preceding paragraph, we tested the second-order finite difference scheme. The results, plotted in Figure III-13, show that the errors are bounded by ±20 percent, a value more tolerable than the ±50 percent variation mentioned above.

We then explored the effect of the physical horizontal diffusion on the accuracy of the grid model. In this study, we increased the value of the horizontal diffusivity, K_H, by a factor of 10 (to 500 m^2 sec^{-1}) over that used in previous cases. This value probably represents an upper bound for K_H for urban-scale airshed models. The effect of this change, as established by comparing the results shown in Figure III-10 and III-14, was minimal. Figure III-15 shows the effect of varying the wind speed, under the same conditions as those used for Figure III-10, except that the wind speed was decreased to 2 mph. This change resulted in considerable improvement (the error bounds

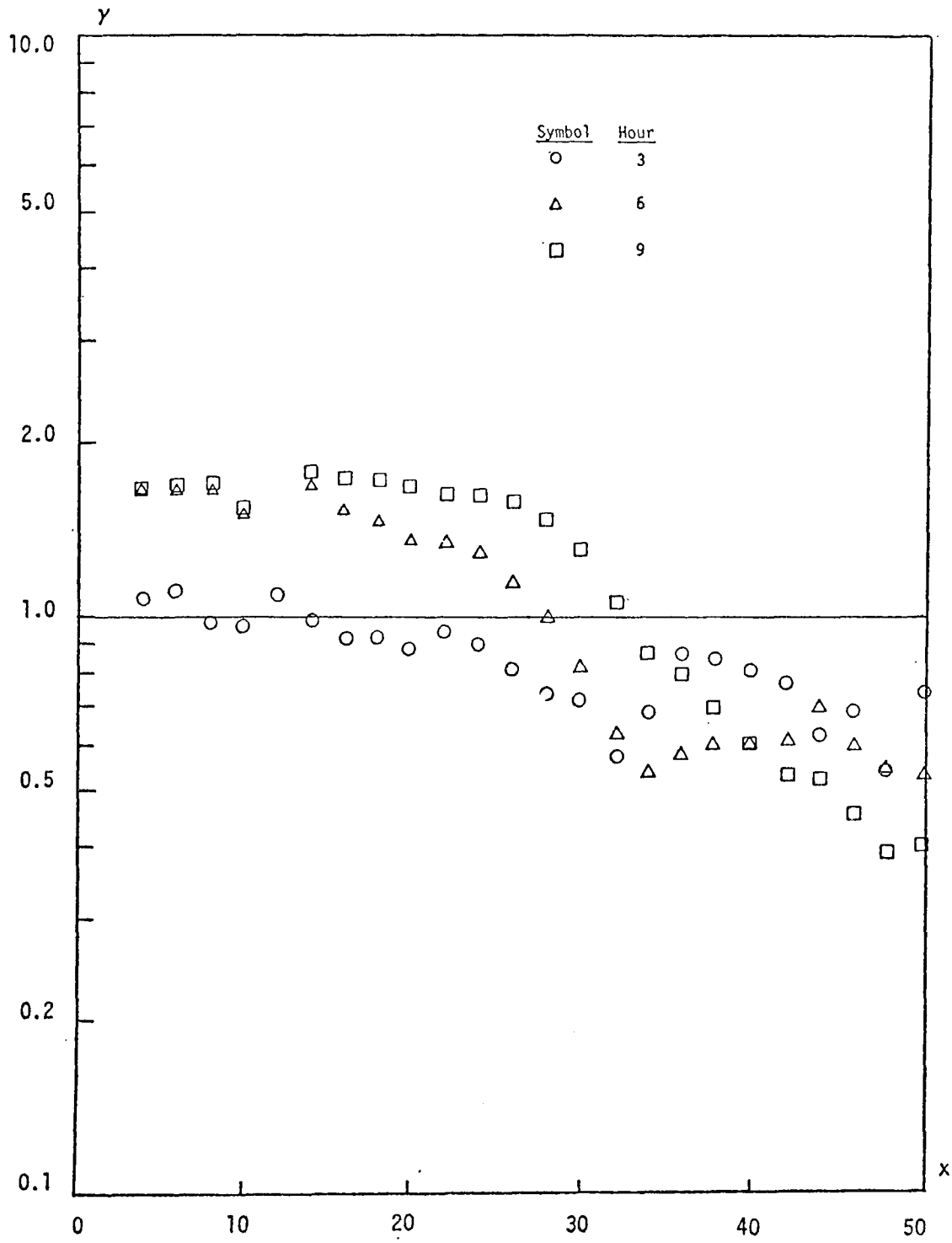

FIGURE III-11. THE EFFECT OF NUMERICAL ERRORS ON GRID MODEL PREDICTIONS: RESULTS USING THE SECOND-ORDER FINITE DIFFERENCE SCHEME AND REALISTIC SPATIAL AND TEMPORAL EMISSION PATTERNS

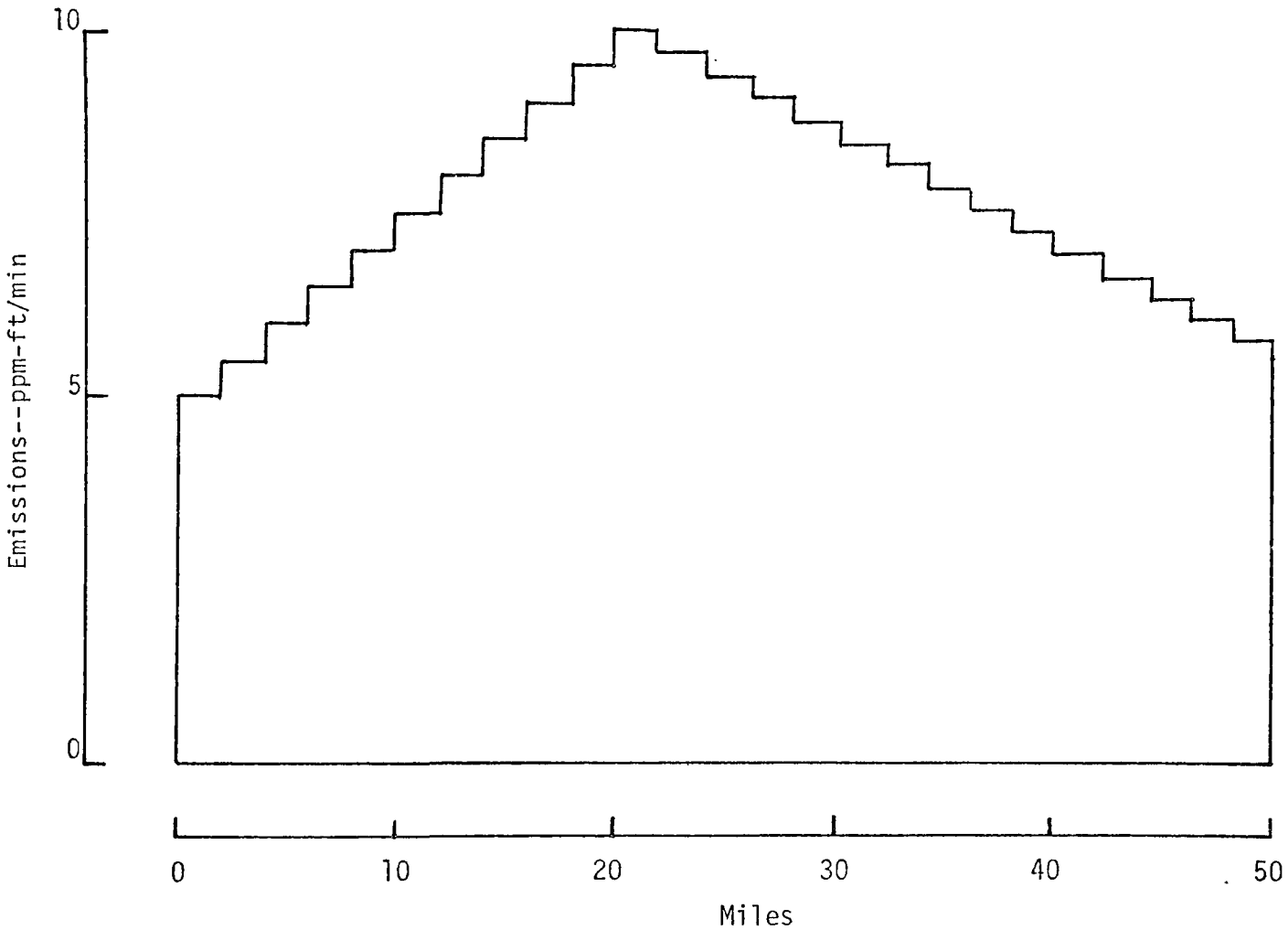

FIGURE III-12. A SMOOTH PATTERN OF POLLUTANT EMISSIONS

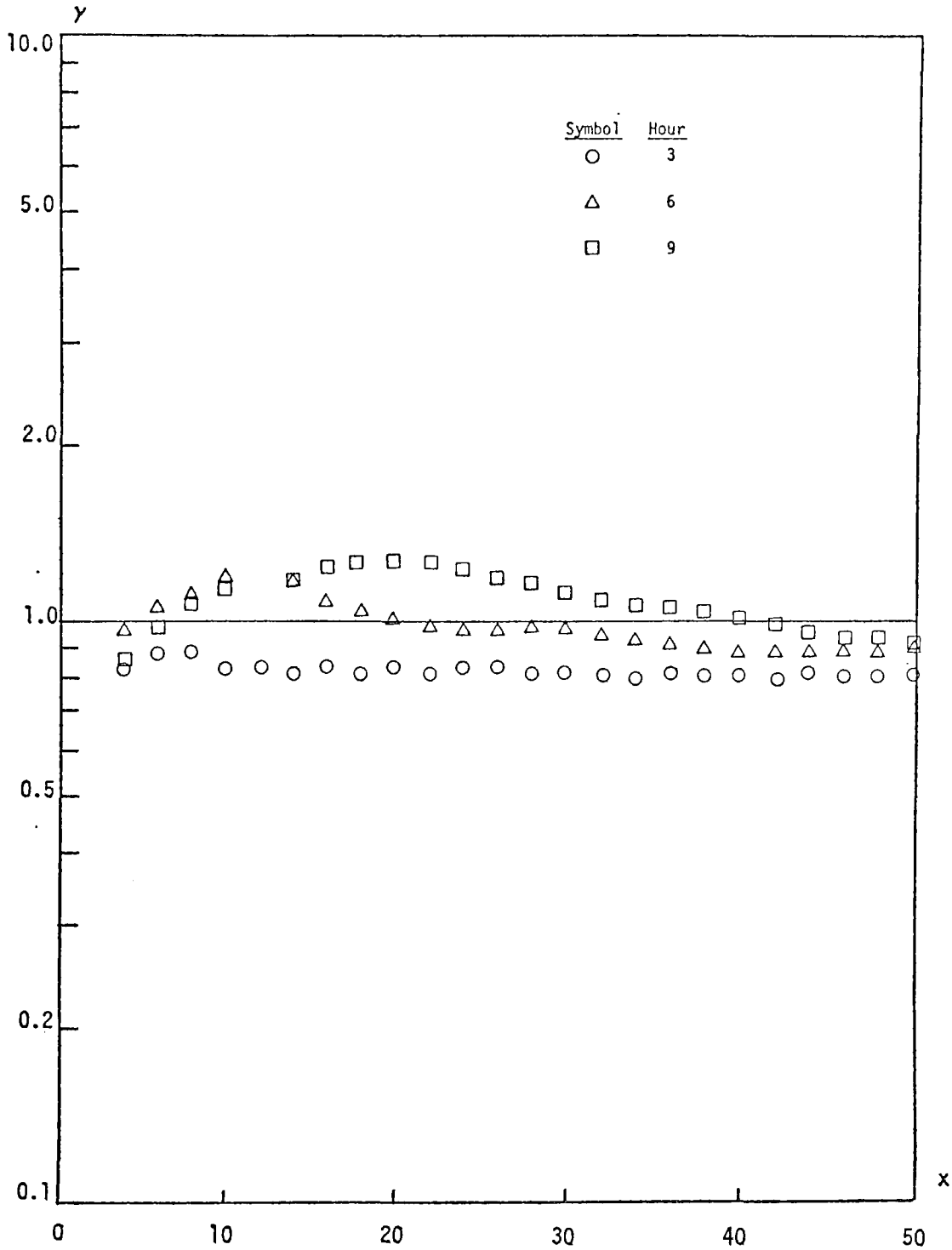

FIGURE III-13. THE EFFECT OF NUMERICAL ERRORS ON GRID MODEL PREDICTIONS: RESULTS USING THE SECOND ORDER FINITE DIFFERENCE SCHEME AND SMOOTH SPATIAL AND TEMPORAL EMISSION PATTERNS

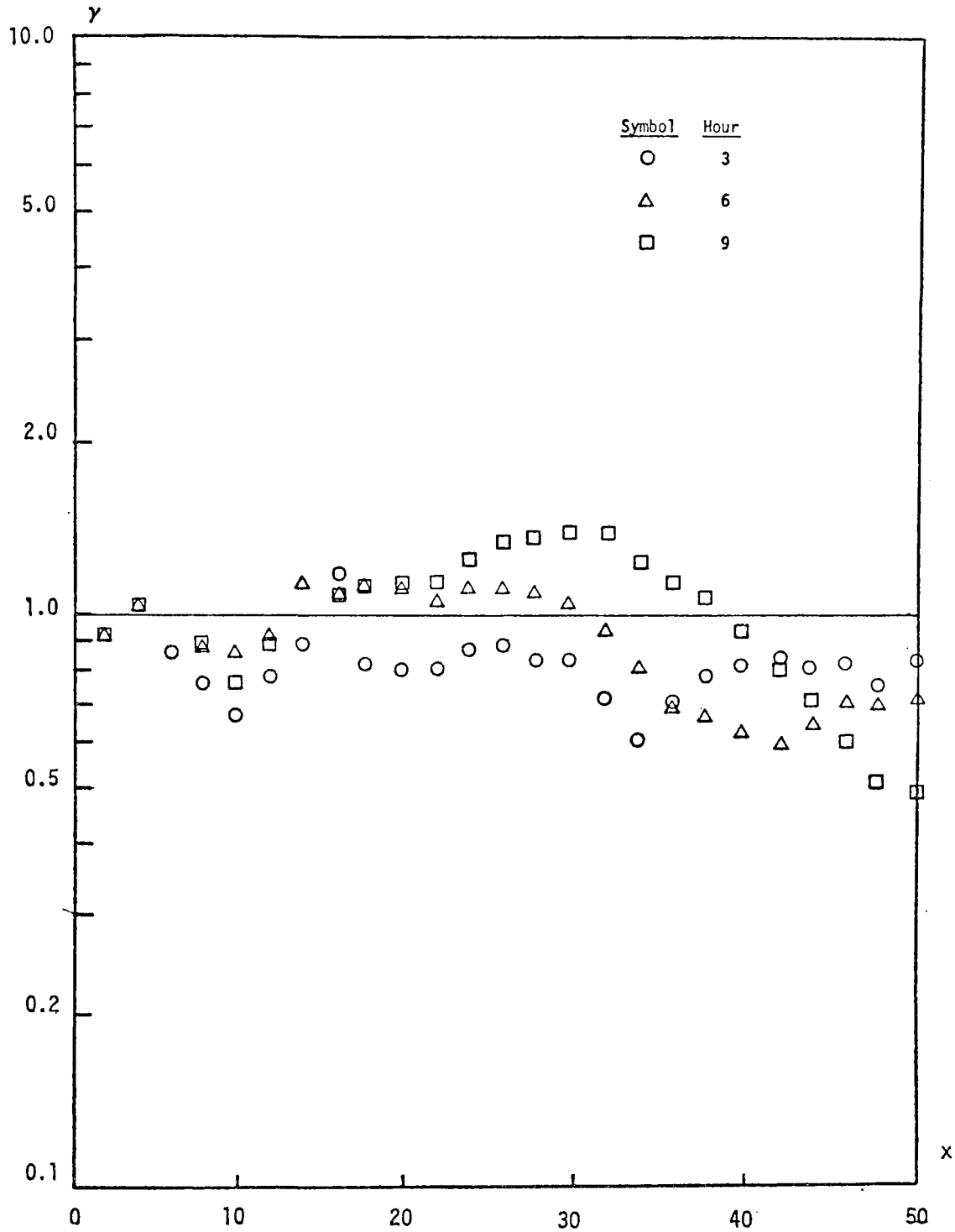

FIGURE III-14. THE EFFECT OF NUMERICAL ERRORS ON GRID MODEL PREDICTIONS: RESULTS UNDER THE SAME CONDITIONS AS THOSE OF FIGURE III-10, EXCEPT FOR AN INCREASE IN HORIZONTAL DIFFUSION

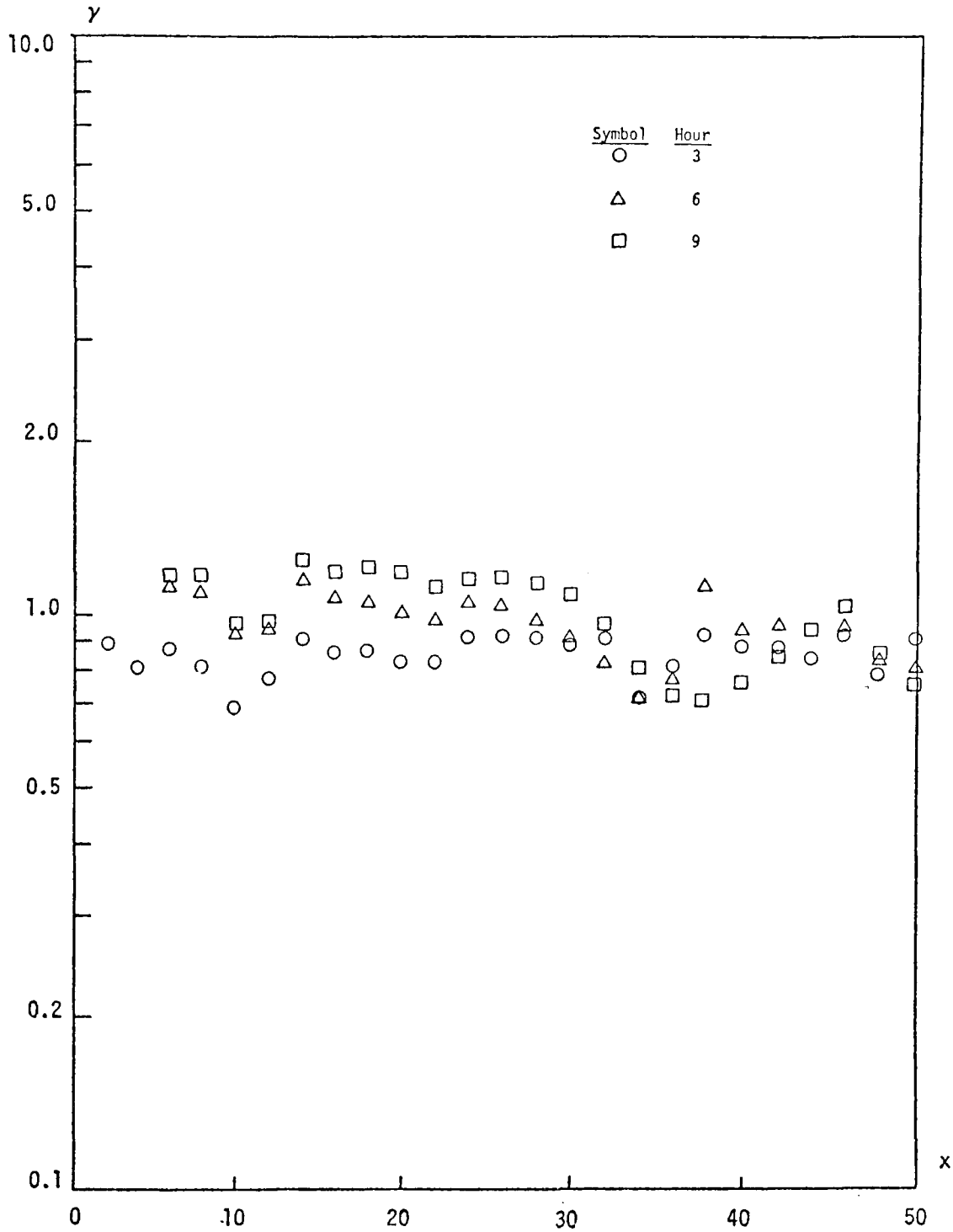

FIGURE III-15. THE EFFECT OF NUMERICAL ERRORS ON GRID MODEL PREDICTIONS: RESULTS UNDER THE SAME CONDITIONS AS THOSE OF FIGURE III-10, EXCEPT FOR A REDUCTION IN WIND SPEED

are ±25 percent, a reduction of one-half from the 4 mph case), in agreement with the qualitative conclusions drawn from the linear analysis we described earlier.

F. CONCLUSIONS AND RECOMMENDATIONS

We investigated the validity of urban airshed models that use either a trajectory approach or a grid approach through comparisons of exact solutions of the atmospheric diffusion equation, for simple but realistic cases, with the corresponding predictions of the trajectory or grid model. Despite our lengthy exposition in the previous sections, the question of the validity of urban airshed models is by no means completely resolved. For example, we only superficially treated the effect of numerical methods used in solving the grid model equations. Because of a lack of time, we did not explore the use of sophisticated, higher order finite difference techniques and the variation of time and spatial step sizes. For example, we did not include the particle-in-cell method, a viable numerical scheme that can be classified as a grid model (Sklarew, 1971), in this study at all. With regard to the trajectory model, we did not address such questions as the uncertainties in obtaining a Lagrangian wind velocity in a turbulent atmosphere (see Appendix A) or the inaccuracies arising from the variation of the horizontal shape of the air column (conventional trajectory modelers assume the shape is invariable).* Nevertheless, many useful quantitative estimates concerning the range of applicability of these two classes of models under various conditions of atmospheric stability, wind shear, and source configuration emerged from this study.

In our assessment of the trajectory model, we found (as expected) that the exchange of material at the boundary of the air parcel as a result of horizontal diffusion is not important. However, we showed that the effect

---

* In the present study, we did not consider this aspect because, rigorously speaking, we assumed that the trajectory model has a zero base area.

of neglecting the vertical wind component is quite significant, depending on (among other things) the strength of the convergence. This limitation does not severely restrict the utility of the trajectory model because, conceptually, we can easily include the vertical transport term in a model that also includes the vertical diffusion term (e.g., see Eschenroeder, 1972). The most detrimental conclusion drawn regarding the trajectory model relates to the neglect of wind shear: For wind profiles typically observed in an urban area, the trajectory model predictions can be in error by an order of magnitude when shear effects are not taken into account.

We also assessed the inaccuracies in the grid model due to finite differencing under realistic conditions. Many interesting results emerged, including the wave-like propagation of numerical errors. The shape of the error wave, which grows with simulation time, depends on such parameters as the spatial variability of the concentration field, the wind speed, the spatial (or temporal) step sizes, and the differencing scheme used in the grid model. Our study has further shown that, using an uncentered second-order difference scheme, the results of a nine-hour simulation produced by a grid model are probably acceptable if the spatial variations in emissions are relatively modest, the wind relatively low (~2 mph), or both. For more demanding situations, in terms of the conditions that apply and the length of time being simulated, a search for a more suitable finite difference scheme is warranted [e.g., the material-conserving computation procedure developed by Egan and Mahoney (1972) or the spectral method that has been actively developed over the past few years by Orszag (1970, 1971) and Orszag and Israeli (1974)].

We note, however, that the judgment we have made above regarding the effect of numerical errors on long-period grid model predictions may be too severe for inert species, such as CO. In urban air pollution, concentrations of most of the primary air pollutants characteristically drop to insignificantly low levels during the early afternoon (1 p.m. to 2 p.m.) as a result of extensive ground heating by sunlight and the ensuing inversion breakup. If the model simulation were to start at sunrise (about 5 a.m. or 6 a.m.), it would reach the nine-hour mark around 2 p.m. Although the effect of

numerical errors would be intolerable by then, the low levels of the primary air pollutants, fortunately, would make the consequence more bearable. For instance, the CO levels in Los Angeles in the afternoon are typically 3 to 5 ppm; a 50 percent error in the concentration levels amounts to merely 2 ppm, an acceptable error. This may explain why error generation and propagation did not strongly affect the multiple-day runs recently performed by Systems Applications.

IV SENSITIVITY STUDY OF THE SAI URBAN AIRSHED MODEL

A. INTRODUCTION

The formation of air pollution in an urban airshed is the result of a complex chain of events. First, for all air pollutants, the levels of contaminant concentrations depend on the emissions sources, which, in an urban area, consist of a matrix of ground-based areal sources and volumetric sources aloft, with widely varying effluent compositions, emissions rates, and other emissions characteristics. Second, after the pollutants are released into the air, they are influenced by the turbulent motion of the atmosphere: They are carried downstream by a mean transport wind, and they are diffused in all directions by turbulent eddies. Concentration levels at any receptor point depend not only on the synoptic-scale and mesoscale meteorology, but also on the modifications of air motion caused by the local topography in the vicinity of the receptor point. Thus, it is difficult to enumerate all of the parameters that may affect the eventual distribution of air pollutants. Finally, compounding the difficulties, secondary pollutants are produced through chemical reactions of primary (or emitted) pollutants in an urban atmosphere. The rate of transformation depends on the intensity of solar radiation and on local concentration levels and, consequently, on all of the parameters delineated above. It is therefore clear that the primary task of modeling photochemical air pollution consists of sifting through the myriad of physical parameters and selecting only several of the more important ones to include in the model.

The process of developing an airshed model thus inevitably involves a trial-and-error approach. First, a primitive model is developed. Its predictions are then evaluated, either by comparing them with observations, if adequate data are available, or by theoretically assessing their validity. The objective of these evaluation processes is to identify the sources of

errors or inadequacies in the primitive model. Hopefully, based on these findings, improvements to the model can be made.

In this process of model development, the study of the sensitivity of the model plays a vital role. Ideally, the sensitivity study should be preceded by a validity study to affirm that all parameters necessary to simulate urban air pollution have been included in the model. The sensitivity study should be followed by an analysis of the model predictions to establish the cause-effect relationship between the input conditions and the model predictions. Through its variations of input parameters within the range of physical reality, the sensitivity study serves as a vehicle for examining the responses of the model. The goal of such an analysis is to assess the influence of each parameter on the prediction of air quality. More specifically, such a study seeks to achieve the following objectives:

> To assess the importance of a given input parameter so that decisions can then be made as to whether this parameter should be retained in the model. In the event that this parameter is to be neglected, the analysis can provide an error bound for neglecting it.
> To determine the necessity of including the temporal or spatial variation of a physical parameter once its importance has been established.
> To estimate the required accuracy of a given parameter so that appropriate arrangements can be made to meet these requirements, or, correspondingly, to assess the effect of a parameter with a given level of uncertainty.
> To enhance existing knowledge of the role played by each parameter so that explanations can be offered in those cases in which model predictions differ from observational data.
> To aid in the construction of a repro-model by choosing a proper combination of input parameters.

In view of these diversified objectives and the complexities of the urban airshed model itself, the successful execution of a sensitivity study is not a simple or straightforward undertaking. A well-planned program is needed to extract the maximum possible information at a given level of effort. This chapter describes our sensitivity study of the SAI urban airshed model.

Section B presents the design of the sensitivity study. Section C summarizes our effort to extract useful information from the unavoidably massive collection of computer printout comprising the output of the study. Section D discusses the overall sensitivity of the SAI urban airshed model and presents our conclusions and recommendations.

B. DESIGN OF THE SENSITIVITY STUDY

A sensitivity study can be defined as a numerical experiment to assess the effect of varying one or more input parameters in a model under controlled but realistic conditions. Thus, in essence, the execution of a sensitivity study may be no more than a series of modeling exercises with different sets of input data. The complexities of SAI's urban airshed model, however, make this job rather tedious, if not difficult. Careful plans were therefore necessary to ensure the achievement of the intended goals summarized above. In this section, we discuss two key elements in carrying out our sensitivity analysis: the detailed planning of the cases we considered and the selection of the criteria we used in the analysis of the sensitivity of the SAI model.

1. Plans for Carrying Out the Sensitivity Study

As the subject for analysis, we chose the SAI urban airshed (grid) model (Reynolds et al., 1973; Roth et al., 1974; Reynolds et al., 1974), primarily because the limited resources available for this project prohibited exploration of the sensitivities of both a grid model and a trajectory model. Of

these two approaches, the grid model offers the advantage of conveniently providing basin-wide coverage and, consequently, a richer information base. Furthermore, resource limitations also prevented us from studying more than one base case.

We selected a late summer day in Los Angeles, September 29, 1969, as the base case for the study. This day was not only a typical smoggy day, but also one that has been extensively measured and studied. For a comprehensive description of the aerometric data collected on this day and of the corresponding predictions obtained using the SAI urban airshed model, we refer the reader to Reynolds et al. (1974).

Having chosen an appropriate model and a base case, we then faced the problem of selecting the test cases. In the following subsections, we briefly describe the input parameters chosen, the reasons for their selection, and the ways in which they were varied. Table III-1 presents a summary of the cases explored in this study.

a. Surface Wind

Our interest in varying the surface wind field was twofold: to examine both the accuracy and the sensitivity of the model. First, we wanted to assess the effect of uncertainties in the wind speed and wind direction measurements on the airshed model predictions. Second, we wished to determine the response of the airshed model predictions to systematic changes in wind speed. For the first task, we randomly varied both the wind speed and the wind direction by an amount characteristic of the uncertainty in measuring or reporting this quantity: 1 mph for the wind speed and 1 point (= 22.5°) for the wind direction. For the second task, we systematically increased or decreased the measured wind speed by a fixed percentage. We explored four cases: -50 percent, -25 percent, +25 percent, and +50 percent.

b. Diffusivity

We considered both the horizontal and the vertical diffusivities. For the horizontal diffusivity, we used two extreme values: 0 and 500 m^2 sec^{-1}.

Table IV-1

SUMMARY OF THE CASES INVESTIGATED IN THE SENSITIVITY STUDY

Input Parameter	Variations	Comment
Wind direction	Station measurements* randomly perturbed by 0 or $\pm 22.5^{o}$	See Section C-1-a
	Values at each grid point† randomly perturbed by 0 or $\pm 22.5^{o}$	See Section C-1-a
Wind speed	Station measurements* randomly perturbed by 0 or ± 1 mph	See Section C-1-b
	Values at each grid point† randomly perturbed by 0 or ± 1 mph	See Section C-1-b
	Station measurements* decreased by 50%	See Section C-2
	Station measurements* decreased by 25%	See Section C-2
	Station measurements* increased by 25%	See Section C-2
	Station measurements* increased by 50%	See Section C-2
Horizontal diffusivity	Decreased§ to 0	See Section C-3-a
	Increased§ to 500 m^2 sec^{-1}	See Section C-3-a
Vertical diffusivity	Decreased** to 0.5 m^2 sec^{-1}	See Section C-3-b
	Increased** to 50 m^2 sec^{-1}	See Section C-3-b
Mixing depth	Decreased by 25%	See Section C-4
	Increased by 25%	See Section C-4
Radiation intensity	Decreased by 30%	See Section C-5
	Increased by 30%	See Section C-5
Emission rate	Decreased by 15%	See Section C-6
	Increased by 15%	See Section C-6

* The station measurements were subsequently interpolated, using techniques described in Liu et al. (1973).

† These values were obtained from manually prepared wind data; see Reynolds et al. (1974).

§ A value of 50 m^2 sec^{-1} was used in the base case.

** A value of 5 m^2 sec^{-1} was used in the base case.

Our objective was to determine whether the horizontal diffusion term should be retained in the model and whether numerical diffusion is an important source of error. We decreased and increased the value of the vertical diffusivity from the one used in the base case by an order of magnitude to examine the effect on the predicted air quality.

c. Mixing Depths

Our objective in this case was to assess the effect of varying the mixing depth. Toward this end, we uniformly decreased or increased the values used in the base case, which change with time and location, by 25 percent, the amount that may represent the error bounds in the determination of the mixing depth.

d. Radiation Intensity

For photochemical air pollutants, the light intensity, or the closely related photolysis rate constant, is the most important parameter in delineating the chemical evolution of these species (Hecht et al., 1973). We decreased and increased this rate constant by 30 percent.

e. Emissions Rate

Contaminant concentrations in an airshed undoubtedly depend directly on the rates of emissions from pollutant sources. We uniformly varied the emissions rates used in the base case by +15 percent and -15 percent, values chosen because they may be characteristic of uncertainties in the emissions rate derivation.

2. Criteria for Assessing the Sensitivity of the SAI Model

The second problem we faced in designing the sensitivity study was the selection of appropriate criteria for assessing the impact on the

predicted air quality of variations in parameter magnitudes for each of the cases delineated above. In view of the large amount of output from the SAI urban airshed model, the choice was neither unique nor straightforward. For example, an 11-hour simulation of the full SAI model furnished nearly 30,000 data points for the ground-level concentrations alone. Consequently, even if we had been concerned only with the ground-level concentrations, we would have had to consider 30,000 pairs of data for each of the cases discussed earlier. It would have been not only impossible, but also overly specific to analyze them individually. Thus, we had to find ways to sort out this large collection of data so that proper cause-effect relationships among the variables could be established. Many conceivable schemes for aggregating predictions exist. In the following subsections, we describe those we considered to be the most suitable.

a. Basin-Wide Averages

The first type of criterion we considered was basin-wide averages. We designated the ground-level concentrations from the base-case and test-case predictions (both were one-hour averages) by $c_{i,j}^{m,n}$ and $\tilde{c}_{i,j}^{m,n}$, respectively, where m denotes the pollutant species; i and j are the horizontal location (N is the total number of locations); and n represents the hour. Then we formulated the following criteria to assess the difference between the two sets of data.

> Average deviation:

$$\bar{D}^{m,n} = \frac{1}{N}\left[\sum_i \sum_j \left(\tilde{c}_{i,j}^{m,n} - c_{i,j}^{m,n}\right)\right] \qquad \text{(IV-1)}$$

> Average absolute deviation:

$$|\bar{D}|^{m,n} = \frac{1}{N}\left[\sum_i \sum_j \left(\left|\tilde{c}_{i,j}^{m,n} - c_{i,j}^{m,n}\right|\right)\right] \qquad \text{(IV-2)}$$

> Average relative deviation:*

$$|\bar{d}|^{m,n} = \frac{1}{N}\left[\sum_i \sum_j \left(\frac{|\tilde{c}^{m,n}_{i,j} - c^{m,n}_{i,j}|}{c^{m,n}_{i,j}}\right)\right] \qquad \text{(IV-3)}$$

> Standard deviation:

$$\sigma^{m,n} = \sqrt{\frac{1}{N}\left[\sum_i \sum_j \left(\tilde{c}^{m,n}_{i,j} - c^{m,n}_{i,j}\right)^2\right]} \qquad \text{(IV-4)}$$

As is clear from these definitions, the criteria given above provide an average measure of the effect to be assessed. Thus, they are most likely to be successful in detecting systematic trends between the two sets of data. For instance, they can be used if the effect of increasing the wind speed by some amount (say, 50 percent) is to be assessed. However, these criteria are obviously inadequate for assessments of local changes. For example, using these averages, it would be difficult to detect the large local changes that are observed when the wind direction is randomly disturbed. In this case, the local maxima might have been shifted markedly, but the overall average effect would be very small.

---

* Although we label this the "average relative deviation," it should more properly be called the "average relative absolute deviation." We made no attempt to calculate an actual average relative deviation,

$$\bar{d}^{m,n} = \frac{1}{N}\left[\sum_i \sum_j \left(\frac{\tilde{c}^{m,n}_{i,j} - c^{m,n}_{i,j}}{c^{m,n}_{i,j}}\right)\right] ,$$

because we felt that it would not add significantly to the set of criteria listed.

b. Local Maximum Deviations

The second type of criterion that we considered was derived by identifying the largest deviation at any of the N locations in the grid. Mathematically, this can be expressed as

$$D^{m,n}_{max} = \tilde{c}^{m,n}_{\alpha,\beta} - c^{m,n}_{\alpha,\beta} \quad , \tag{IV-5}$$

where (α,β) is located by finding $\max_{i,j} \left(|\tilde{c}^{m,n}_{i,j} - c^{m,n}_{i,j}| \right)$, or as

$$d^{m,n}_{max} = \frac{\tilde{c}^{m,n}_{\mu,\nu} - c^{m,n}_{\mu,\nu}}{c^{m,n}_{\mu,\nu}} \quad , \tag{IV-6}$$

where (μ,ν) is located by finding $\max_{i,j} \left[\left(|\tilde{c}^{m,n}_{i,j} - c^{m,n}_{i,j}| \right) / c^{m,n}_{i,j} \right]$.

It is apparent that these criteria are considerably more sensitive than the basin-wide averages. For example, the following trivial inequalities can be written:

$$|D^{m,n}_{max}| \geqslant |\overline{D}|^{m,n} \quad ,$$

$$|d^{m,n}_{max}| \geqslant |\overline{d}|^{m,n} \quad .$$

c. Deviations at the Local Maxima

A third type of criterion was obtained by first locating the maxima in the base case and then calculating the deviation at that location. Formally, such criteria are defined by

$$G^{m,n} = \tilde{c}^{m,n}_{I,J} - c^{m,n}_{I,J} \quad , \tag{IV-7}$$

$$g^{m,n} = \frac{\tilde{c}^{m,n}_{I,J} - c^{m,n}_{I,J}}{c^{m,n}_{I,J}} \quad , \tag{IV-8}$$

where

$$c^{m,n}_{I,J} = \max_{i,j} \left(c^{m,n}_{i,j} \right) \quad ,$$

and

$$\tilde{c}^{m,n}_{I,J} = \max_{i,j} \left(c^{m,n}_{i,j} \right) \quad .$$

One would expect that the third type of criterion would be more sensitive than the first, and certainly less sensitive than the second.

Of these three types of criteria, we used one or more as indices to measure the effect in each of the individual cases we delineated earlier. We based our choice upon the appropriateness and significance of a particular criterion for the specific case of interest. The following section discusses the nature of these considerations.

C. ANALYSIS OF THE SENSITIVITY OF THE SAI MODEL

In this section, we report the results of our analysis of the sensitivity of the SAI urban airshed model. We explored each of the cases listed in Table IV-1 using the criteria discussed in Section B-2 as the basis for evaluation and comparison. We describe below the effects on the model predictions of varying the input parameters.

1. The Effect of Random Perturbations in the Wind Field

We investigated three types of variations in the wind field: random changes in the wind direction, random changes in the wind speed, and systematic changes in the wind speed. We used the first two types to assess the effect of errors in measuring wind direction and wind speed and the third, to evaluate the response of the model to variations in wind speed (i.e., assessment of sensitivity).

a. Wind Direction

In the past, we have used two different methods to prepare the wind field, one of the primary input parameters in the SAI urban airshed model. Although both of them use measurements from a network of ground-level monitoring stations, the first method involves manually smoothing, interpolating, and processing measurement data, whereas the second one provides for automatic performance of these tasks (Liu et al., 1973). In the present study, we varied both manually and automatically prepared wind fields to test the effect of random changes in wind direction. For the manually prepared wind field, we randomly varied wind direction in each cell of the grid by -1, 0, or +1 point.* For the automated wind field, we randomly varied the measured wind direction at each of the monitoring stations by -1, 0, or +1 point; we then automatically interpolated the data to provide the wind direction for each cell.

---

*One point is equivalent to 22.5°, which is typically the unit used in reporting wind direction.

Using the new wind field, we carried out simulations for each of these two variable cases and compared the results with the base case. We considered only carbon monoxide, an inert species, because the accuracy of meteorological parameters was of primary concern in this particular investigation. Figures IV-1 and IV-2 show the results of the calculated average deviations, $\overline{D}$, and the standard deviations, σ. The deviations tend to be negative, as is quite evident in the case where we varied the manually prepared wind field, because randomly disturbing the wind direction is tantamount to incorporating an artificially created horizontal diffusion (see Appendix C). Thus, one would expect the effect to be much greater than it is for the automated wind field, since the manually prepared wind field is characterized by greater randomness. This expectation is confirmed for the latter case by the larger magnitudes of both the average and standard deviations (see Figures IV-1 and IV-2).

The magnitudes of the average and standard deviations also indicate that, on a basin-wide average, the effect is minimal. For example, the maximum values are tabulated below:

Type of Wind Field	$\lvert\overline{d}\rvert_{max}$ (percent)	σ_{max} (ppm)
Manually prepared	6.9%	0.62
Automated	4.9	0.33

However, the deviations in individual cells may not be small. For instance, the largest deviations in the grid in terms of concentration units and percentage are shown in Table IV-2. As this table shows, the local maxima can be quite significant. Thus, although the net effect of randomly varying the wind direction does not greatly influence the basin-wide average concentrations, large local deviations can arise because the random changes in wind direction result in the shuffling of the peak concentrations within the basin. The magnitudes of these local deviations

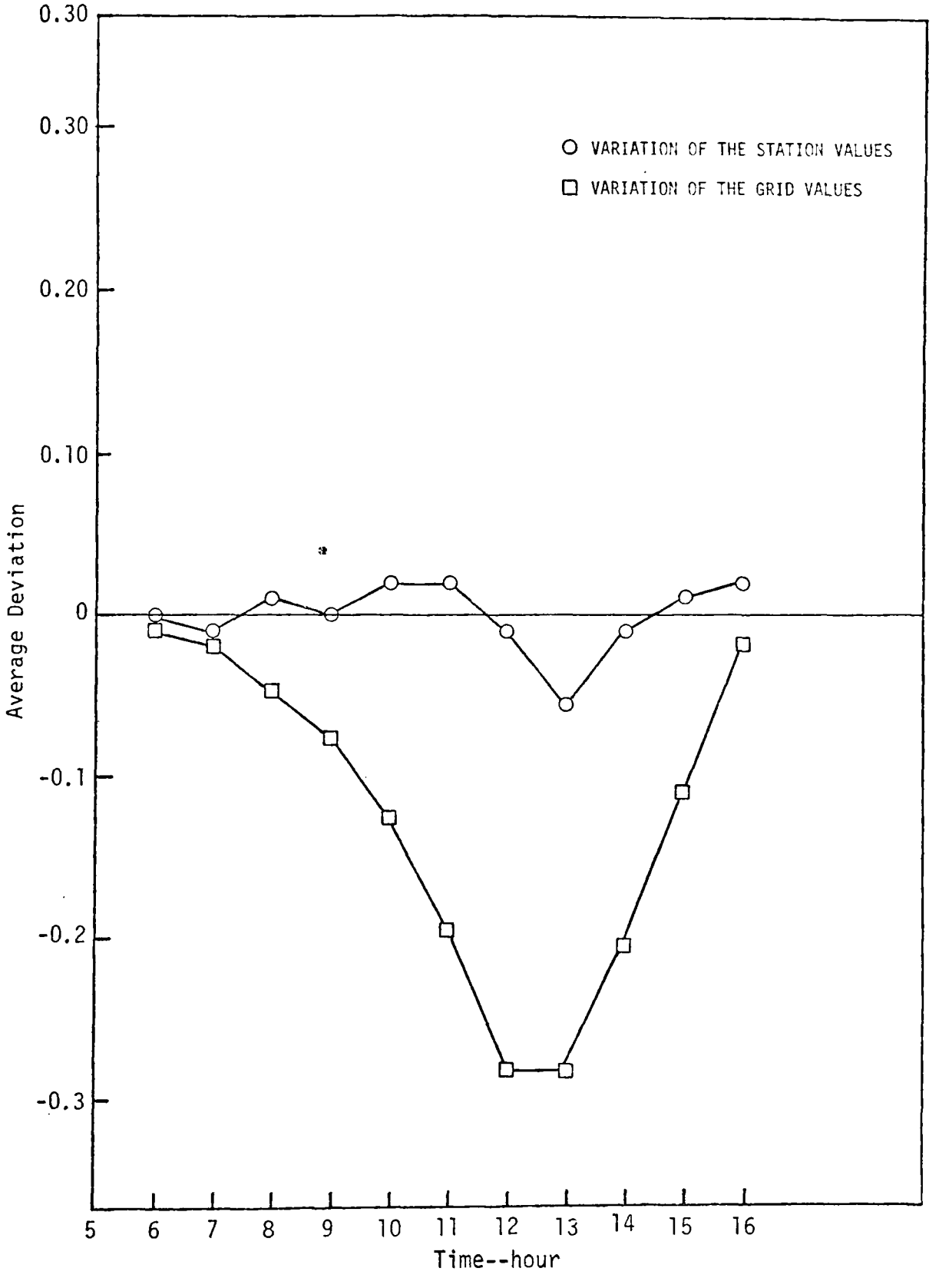

FIGURE IV-1. THE EFFECT--EXPRESSED AS AVERAGE DEVIATIONS--OF RANDOM PERTURBATIONS IN WIND DIRECTION

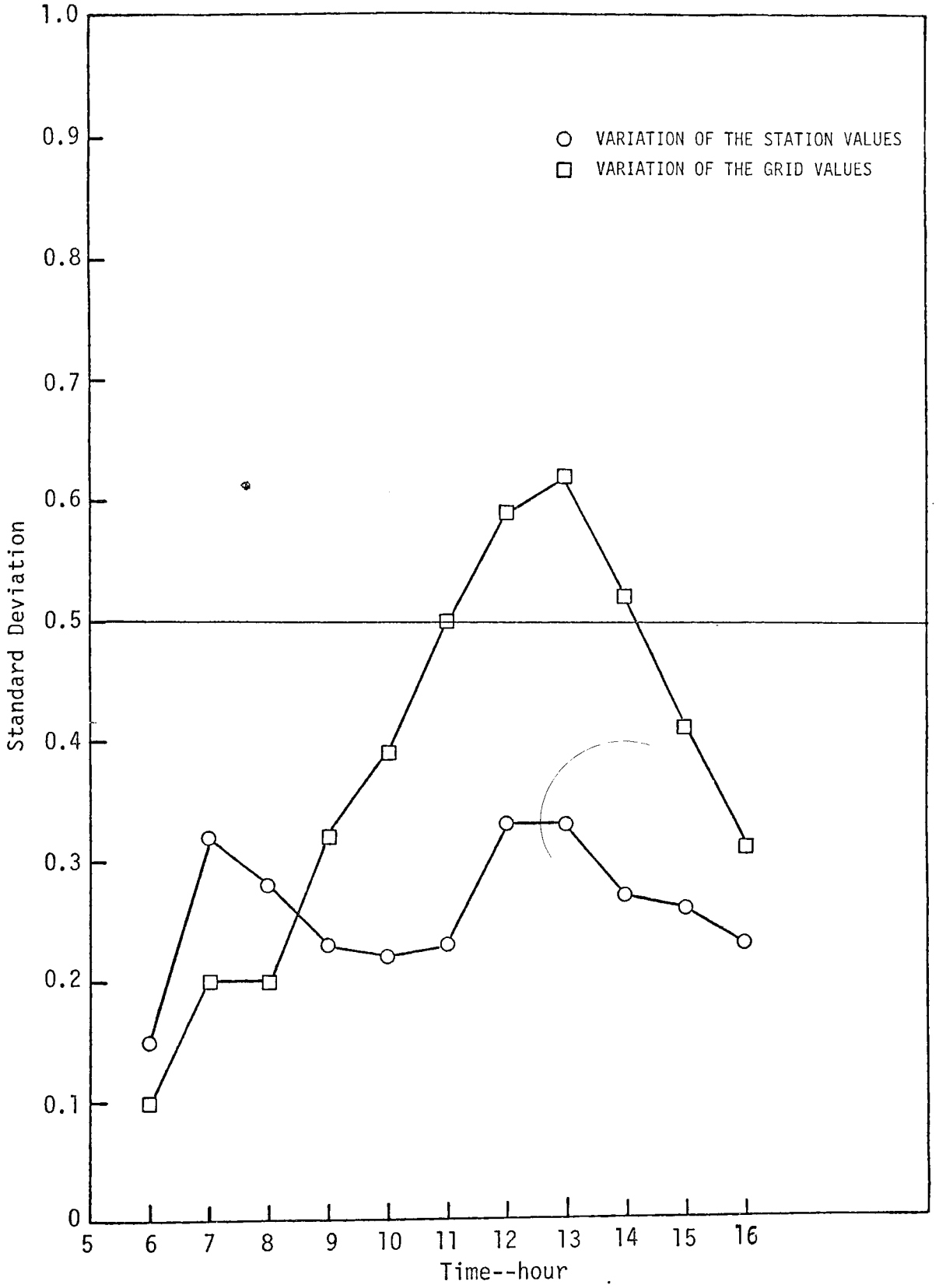

FIGURE IV-2. THE EFFECT--EXPRESSED AS STANDARD DEVIATIONS--OF RANDOM PERTURBATIONS IN WIND DIRECTION

Table IV-2

THE LARGEST DEVIATIONS IN THE GRID GENERATED BY RANDOMLY VARYING THE WIND DIRECTION

(a) $|D_{max}|$ in ppm

	Hour										
Type of Wind Field	6	7	8	9	10	11	12	13	14	15	16
Manually prepared	0.52	1.11	1.09	1.88	1.92	2.07	2.02	2.75	2.81	2.31	1.44
Automated	0.93	1.55	1.26	1.31	0.92	0.86	1.75	1.15	0.77	0.87	0.88

(b) $|d_{max}|$ in Percentages

	Hour										
Type of Wind Field	6	7	8	9	10	11	12	13	14	15	16
Manually prepared	5.9%	10.1%	8.6%	13.8%	17.2%	20.6%	22.4%	28.9%	35.3%	34.0%	49.3%
Automated	8.7	15.1	10.5	14.8	13.6	20.7	29.4	20.8	34.3	40.6	32.4

(which generally increase with time) can reach 40 to 50 percent after 11 hours of simulation; these values appear to match the magnitude of numerical errors typically found in grid airshed models (Liu and Seinfeld, 1974).

b. Wind Speed

To test the effect of uncertainties in the wind speed measurements on the model predictions, we carried out an analysis similar to that discussed above. However, this time we randomly varied the wind speed (in each cell in the case of the manually prepared wind field and at each monitoring site in the case of the automated wind field) by -1, 0, or +1 mph.

As shown in Figures IV-3 and IV-4, although the magnitudes are generally lower compared with the corresponding cases of variations in wind direction, the following trends are still noticeable:

> The average deviations are always negative, manifesting a smoothing process. In other words, a random variation in wind speed is equivalent to an artificially created horizontal diffusion.
> The changes due to varying the manually prepared wind field are more pronounced than those caused by varying the automated wind field. Again, the reason for this effect is that the former case has a higher degree of randomness.
> The effects of changes in wind speeds on the basin-wide average, as shown in Figures IV-3 and IV-4 are very small. The maximum values are as follows:

Type of Wind Field	$\lvert\bar{d}\rvert_{max}$ (percent)	σ_{max} (ppm)
Manually prepared	4.9%	0.45
Automated	2.6	0.27

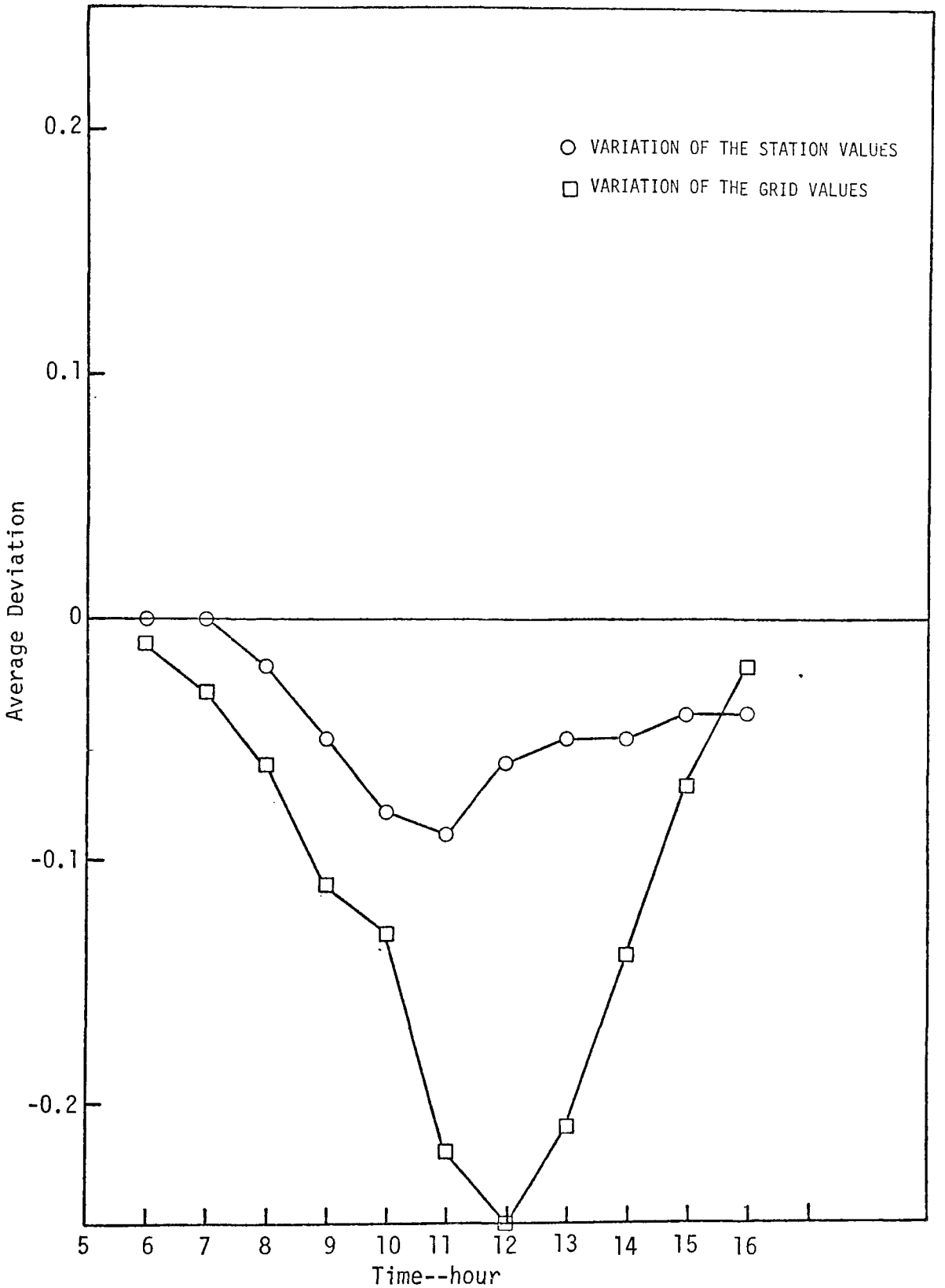

FIGURE IV-3. THE EFFECT--EXPRESSED AS AVERAGE DEVIATIONS--
OF RANDOM PERTURBATIONS IN WIND SPEED

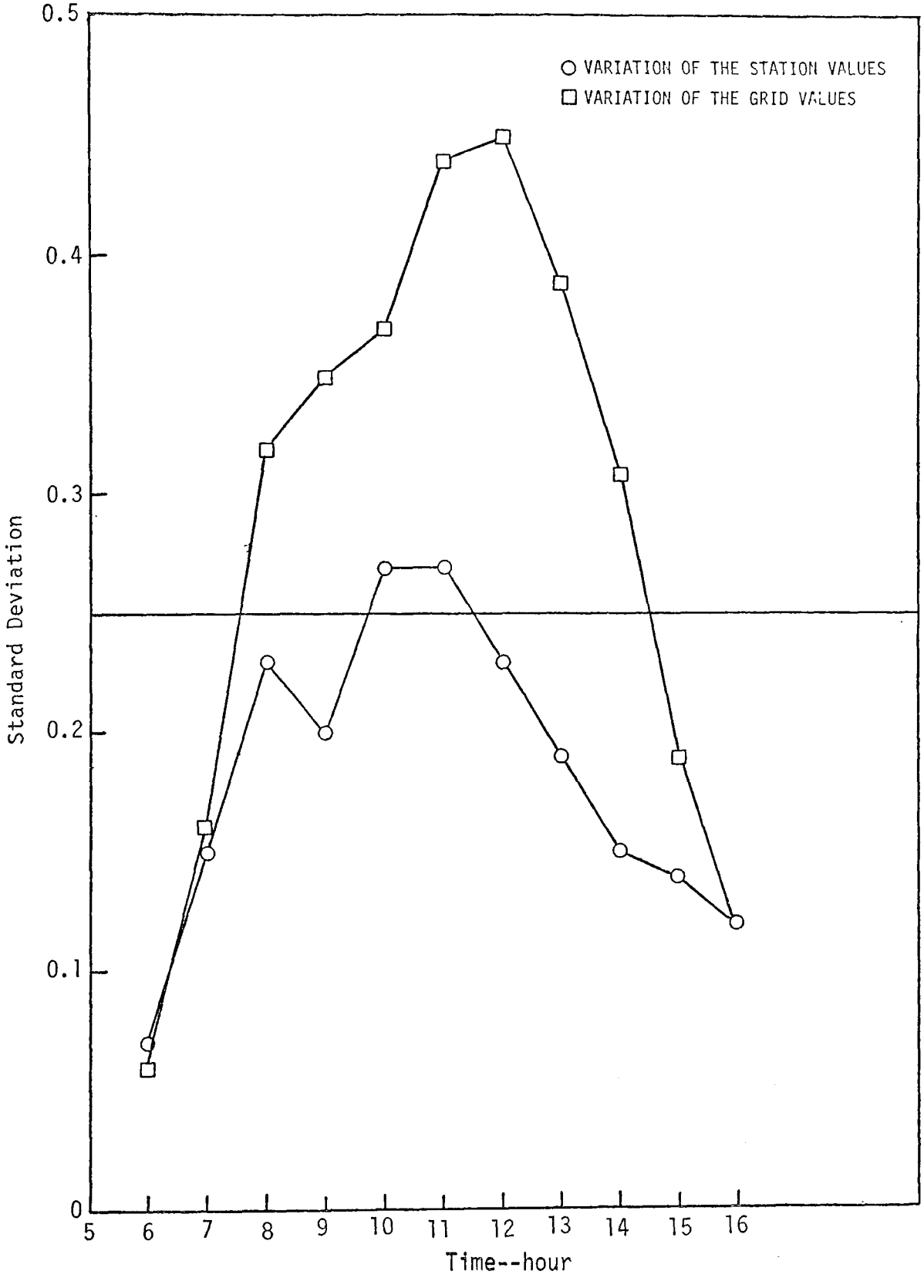

FIGURE IV-4. THE EFFECT--EXPRESSED AS STANDARD DEVIATIONS--OF RANDOM PERTURBATIONS IN WIND SPEED

> Because of the dislocation of the peak concentrations, the local maximum deviations, as tabulated in Table IV-3, remain large; the magnitudes are considerably smaller than those that resulted when the wind direction was randomly varied.

To demonstrate the effect of random variations in both wind direction and wind speed, we plotted Figure IV-5, which shows the relative changes at the locations of maxima for the base case. Although there appears to be no discernible trend in the signs (either positive or negative) of the deviations, changes due to random perturbations in wind direction (indicated by circles) are strongly related to changes due to perturbations in wind speed (indicated by triangles). This is indeed surprising, since the magnitudes of the random perturbations (one point for wind direction and one mile per hour for wind speed) were somewhat arbitrarily chosen.

2. The Effect of Variations in Wind Speed

To assess the response of the SAI airshed model predictions to systematic changes in wind speed, we conducted four simulations, uniformly varying the wind speed used in the base case by +50, +25, -25, and -50 percent. We then compared the predicted ground-level concentrations with those of the base case. These comparisons provided a rich information base that sheds light on certain characteristics of the SAI airshed model predictions.

Figures IV-6 through IV-21 present the average deviations and the local maximum deviations (both in absolute units and relative percentages) for the following species: CO, NO, O_3, and NO_2. As these figures show, the changes increase with time until they reach their peaks, which generally occur around early afternoon. This may be attributable to the large residue of pollutants present in the airshed at the beginning of the simulation and the consequent delay in the response of the model to changes in wind speed. Furthermore, since time is required for the reactions of substances to proceed, the rates of increase with time can be different for different species. This difference is evident in Figures IV-14 through IV-21.

Table IV-3

THE LARGEST DEVIATIONS IN THE GRID GENERATED BY RANDOMLY VARYING THE WIND SPEED

(a) $|D_{max}|$ in ppm

	Hour										
Type of Wind Field	6	7	8	9	10	11	12	13	14	15	16
Manually prepared	0.24	0.89	1.73	1.63	1.13	1.45	1.46	1.61	1.62	1.22	0.68
Automated	0.40	0.98	1.05	0.82	1.31	1.24	1.02	0.80	0.72	0.70	0.68

(b) $|d_{max}|$ in Percentages

	Hour										
Type of Wind Field	6	7	8	9	10	11	12	13	14	15	16
Manually prepared	4.3%	7.8%	12.0%	12.9%	15.6%	18.9%	18.2%	17.7%	20.2%	17.6%	20.7%
Automated	3.9	10.2	14.3	9.7	18.0	20.7	19.3	14.2	18.7	10.1	15.1

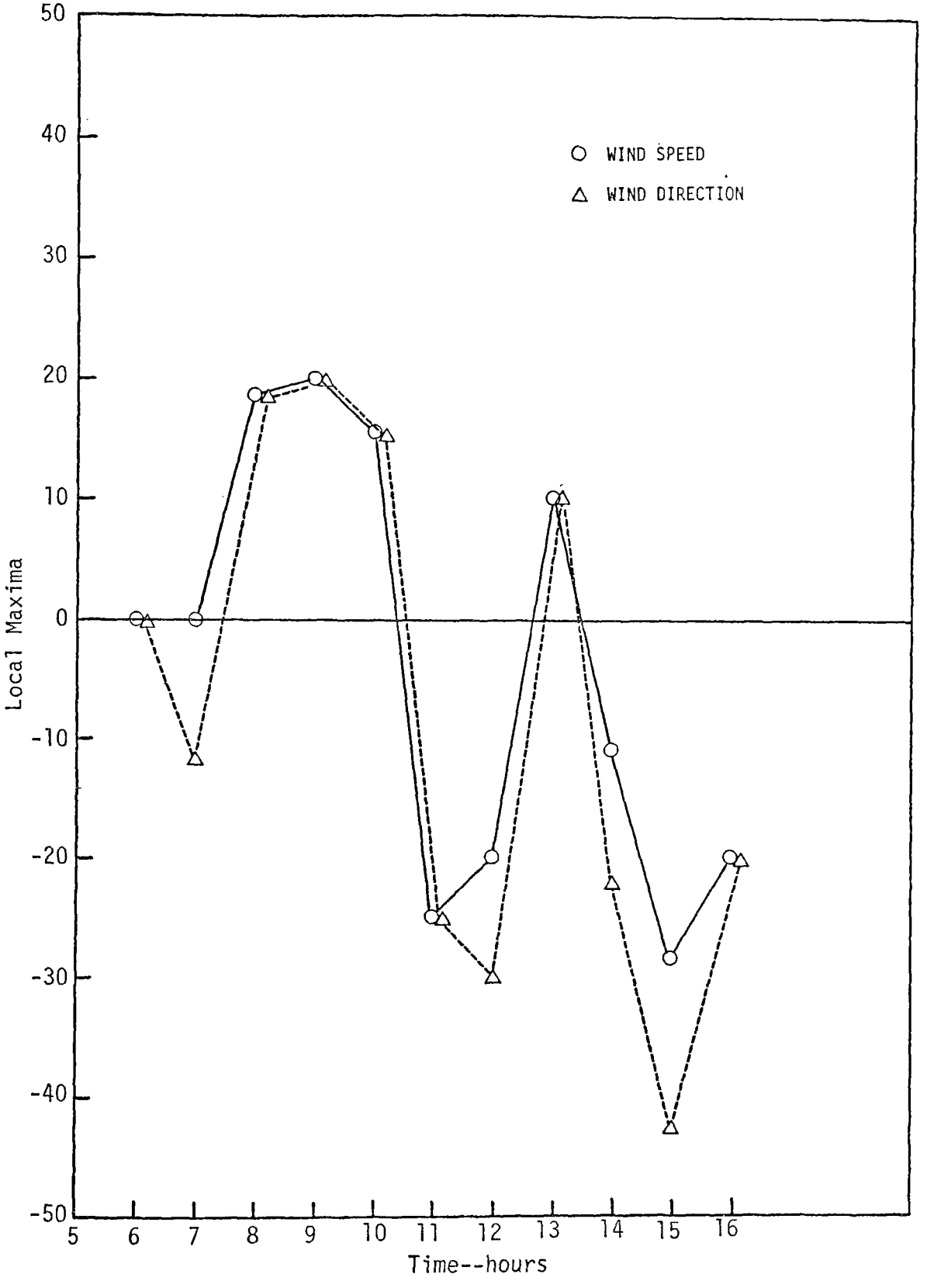

FIGURE IV-5. RELATIVE CHANGES IN WIND SPEED AND DIRECTION AT THE LOCATIONS OF MAXIMA FOR THE BASE CASE

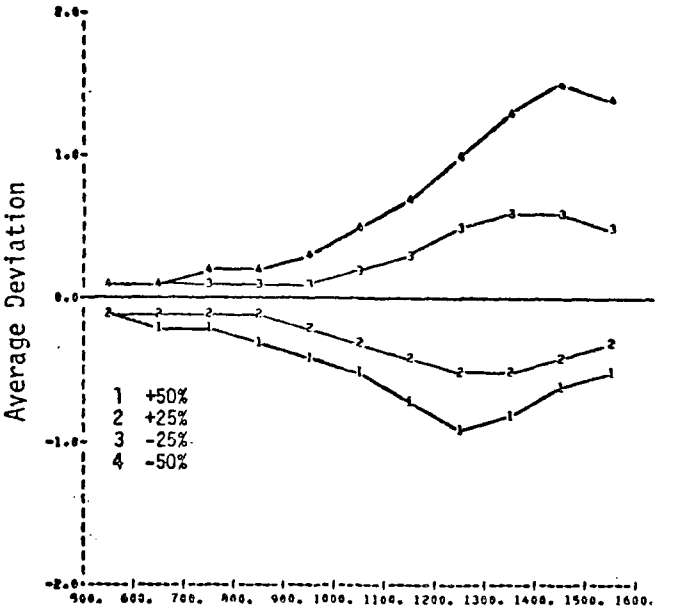

FIGURE IV-6. THE EFFECT--EXPRESSED AS AVERAGE DEVIATIONS--
OF VARIATIONS IN WIND SPEED FOR CO

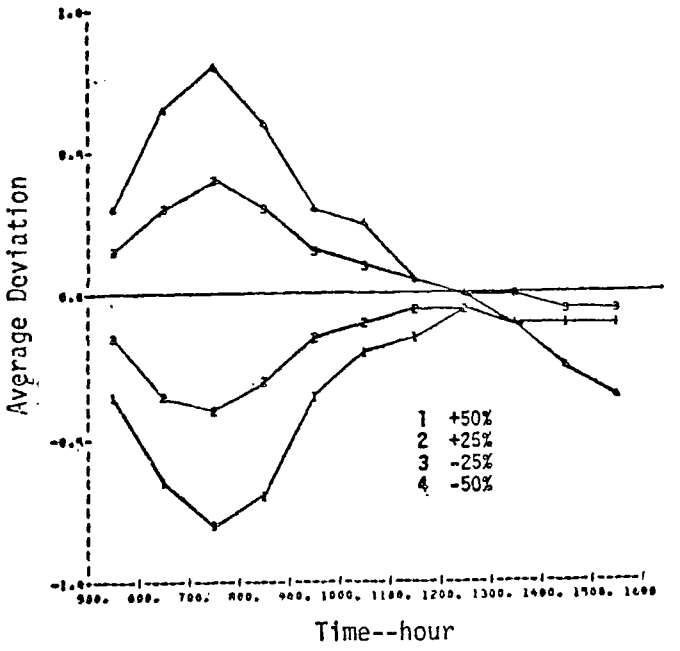

FIGURE IV-7. THE EFFECT--EXPRESSED AS AVERAGE DEVIATIONS--
OF VARIATIONS IN WIND SPEED FOR NO

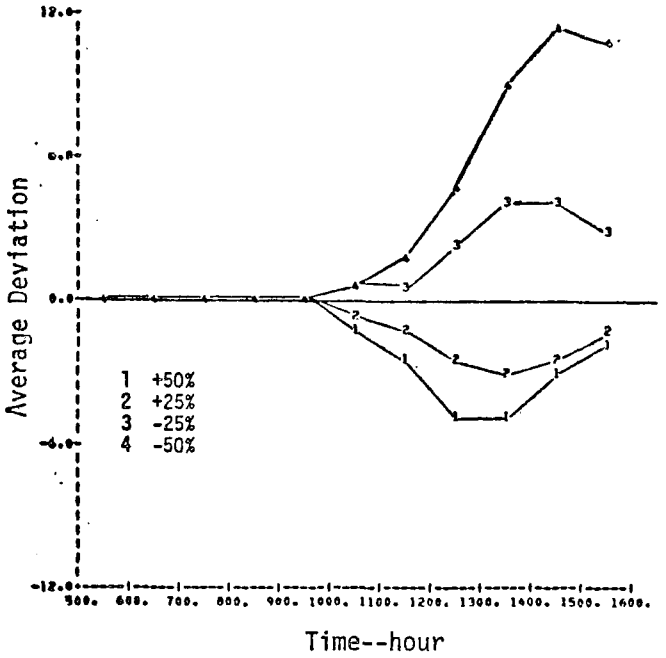

FIGURE IV-8. THE EFFECT--EXPRESSED AS AVERAGE DEVIATIONS--OF VARIATIONS IN WIND SPEED FOR O_3

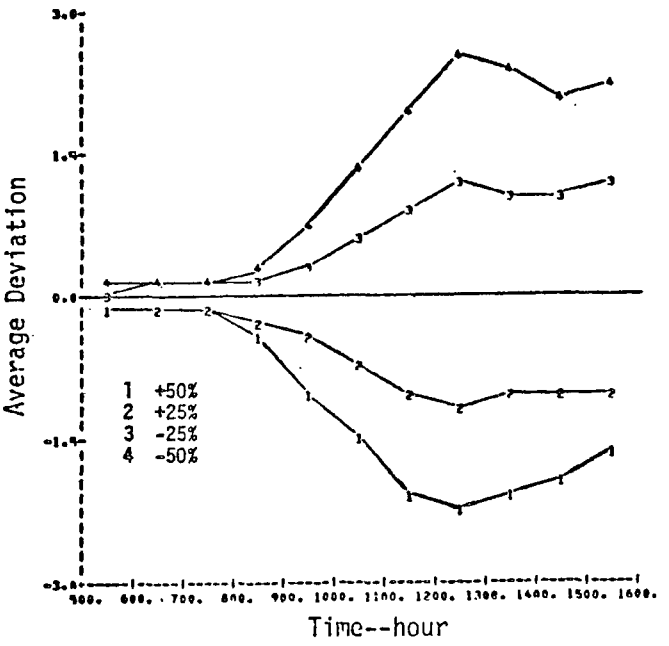

FIGURE IV-9. THE EFFECT--EXPRESSED AS AVERAGE DEVIATIONS--OF VARIATIONS IN WIND SPEED FOR NO_2

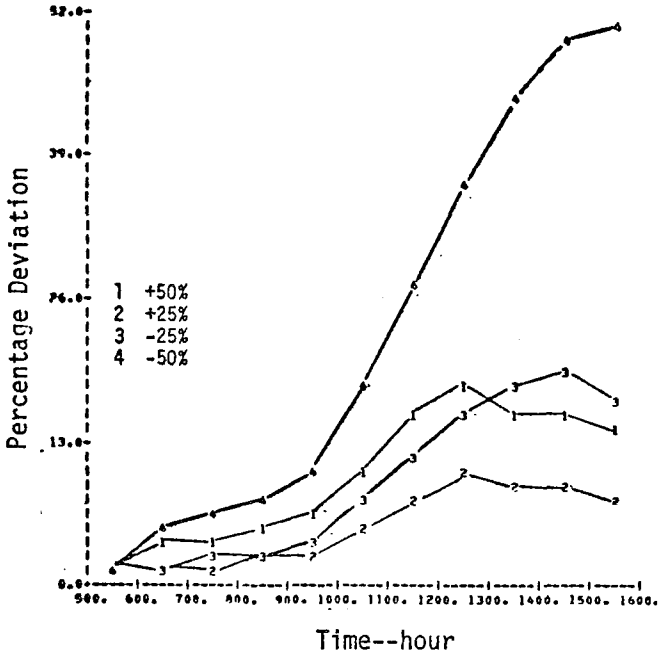

FIGURE IV-10. THE EFFECT--EXPRESSED AS PERCENTAGE DEVIATIONS--OF VARIATIONS IN WIND SPEED FOR CO

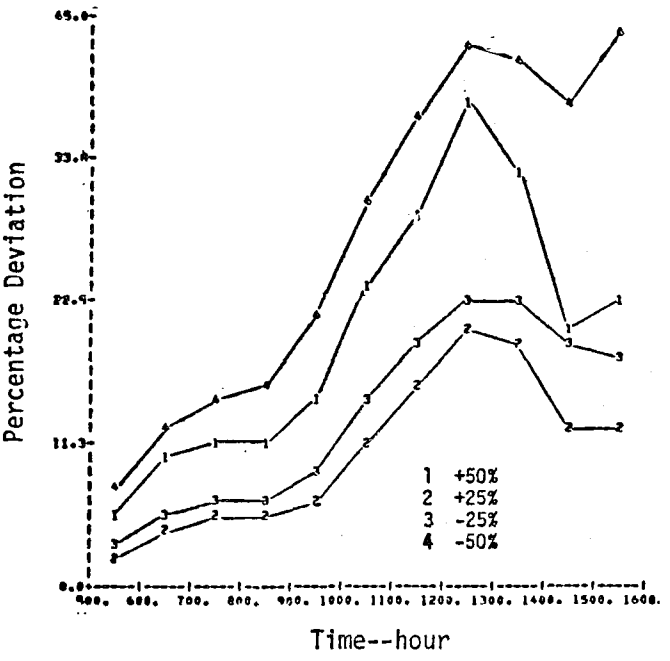

FIGURE IV-11. THE EFFECT--EXPRESSED AS PERCENTAGE DEVIATIONS--OF VARIATIONS IN WIND SPEED FOR NO

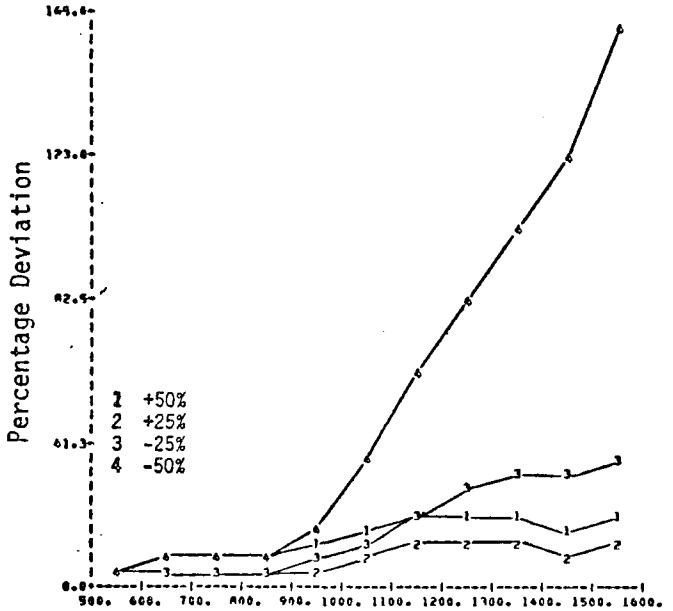

FIGURE IV-12. THE EFFECT--EXPRESSED AS PERCENTAGE DEVIATIONS--OF VARIATIONS IN WIND SPEED FOR O_3

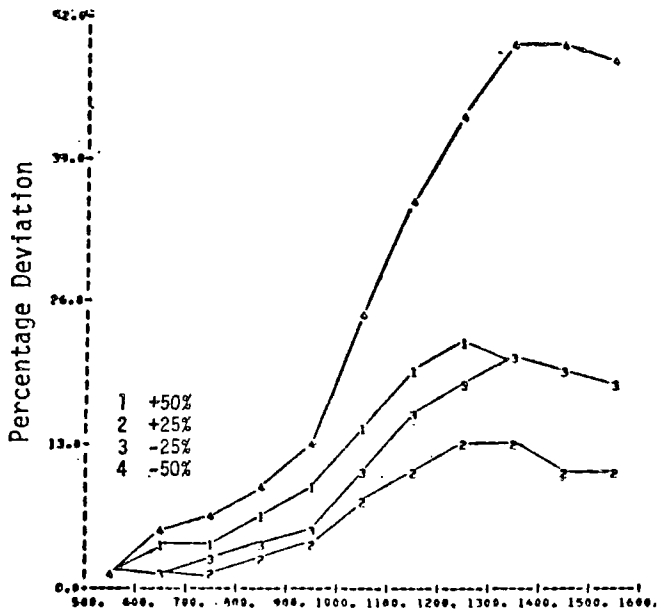

FIGURE IV-13. THE EFFECT--EXPRESSED AS PERCENTAGE DEVIATIONS--OF VARIATIONS IN WIND SPEED FOR NO_2

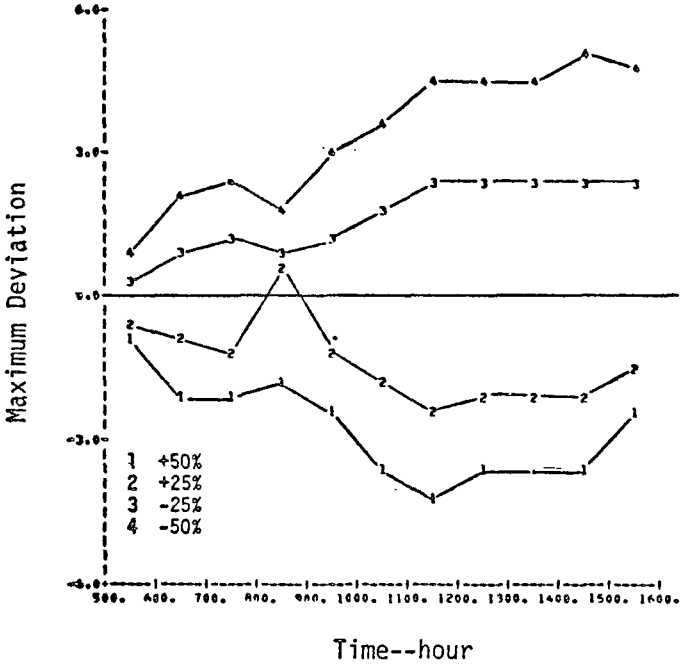

FIGURE IV-14. THE EFFECT--EXPRESSED AS MAXIMUM DEVIATIONS--OF VARIATIONS IN WIND SPEED FOR CO

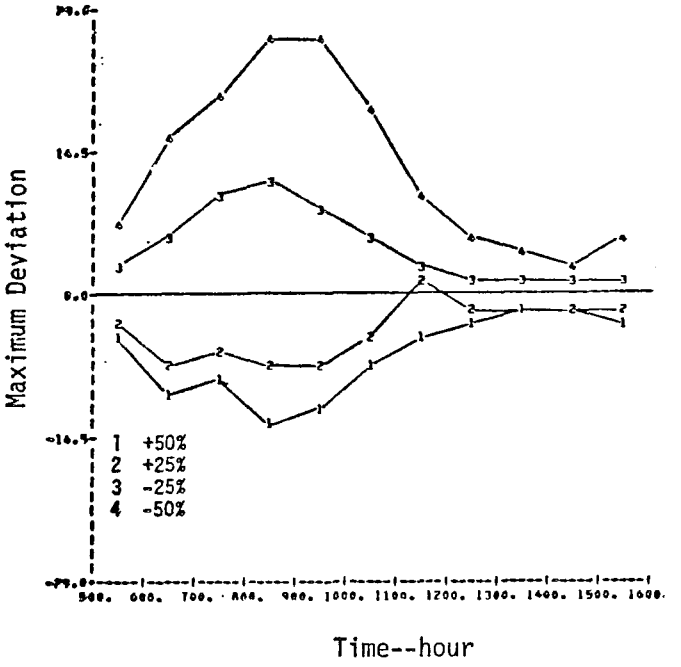

FIGURE IV-15. THE EFFECT--EXPRESSED AS MAXIMUM DEVIATIONS--OF VARIATIONS IN WIND SPEED FOR NO

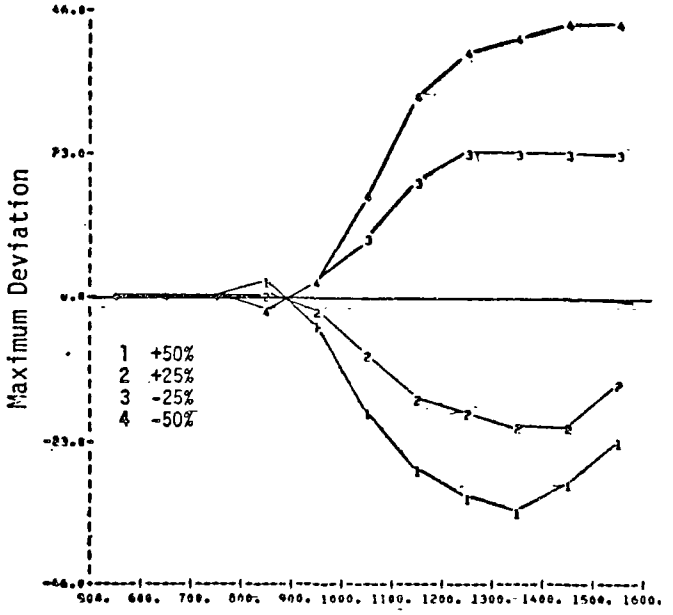

FIGURE IV-16. THE EFFECT--EXPRESSED AS MAXIMUM DEVIATIONS--OF VARIATIONS IN WIND SPEED FOR O_3

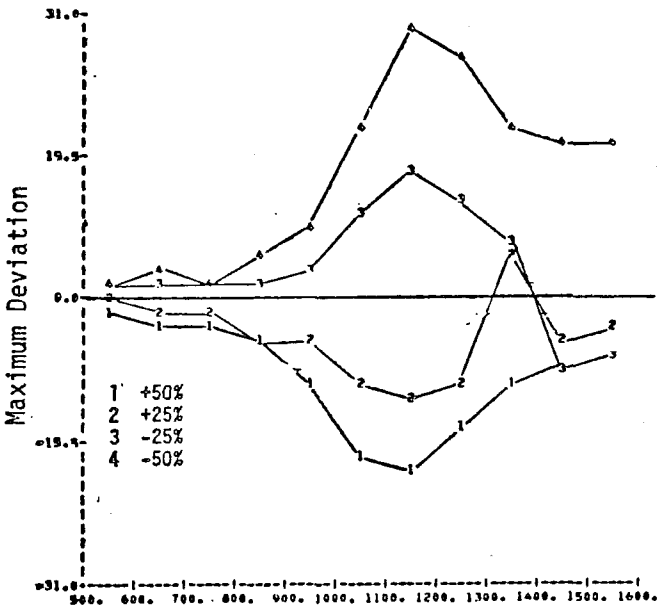

FIGURE IV-17. THE EFFECT--EXPRESSED AS MAXIMUM DEVIATIONS--OF VARIATIONS IN WIND SPEED FOR NO_2

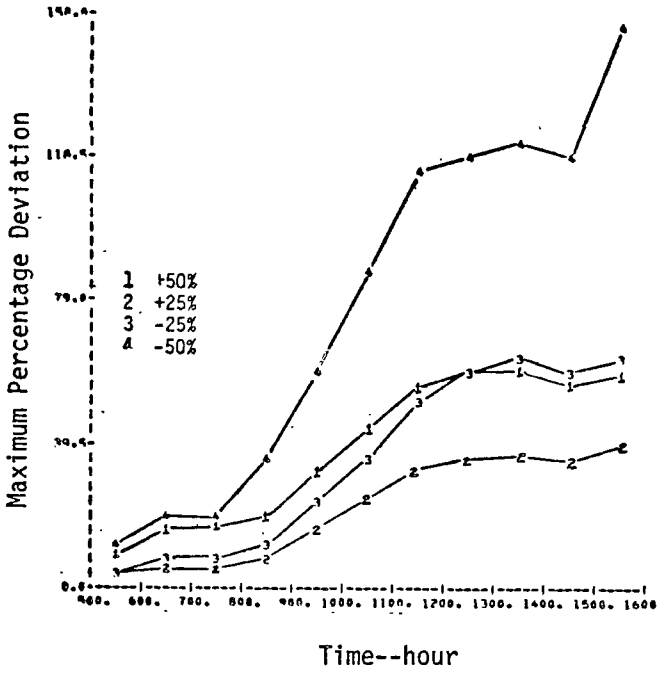

FIGURE IV-18. THE EFFECT--EXPRESSED AS MAXIMUM PERCENTAGE DEVIATIONS--OF VARIATIONS IN WIND SPEED FOR CO

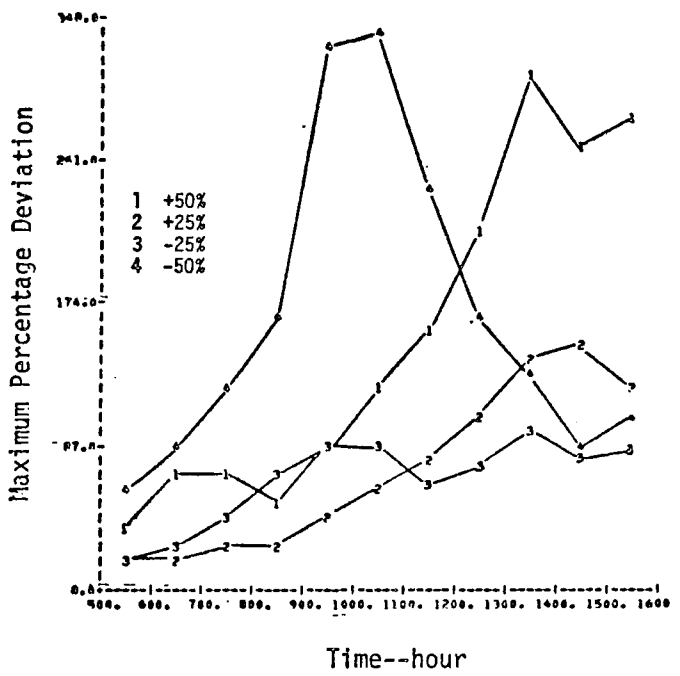

FIGURE IV-19. THE EFFECT--EXPRESSED AS MAXIMUM PERCENTAGE DEVIATIONS--OF VARIATIONS IN WIND SPEED FOR NO

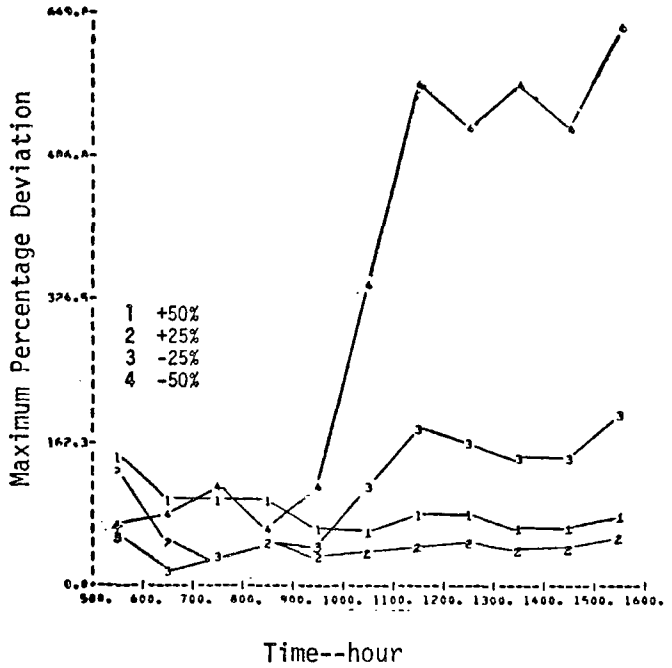

FIGURE IV-20. THE EFFECT--EXPRESSED AS MAXIMUM PERCENTAGE DEVIATIONS--OF VARIATIONS IN WIND SPEED FOR O_3

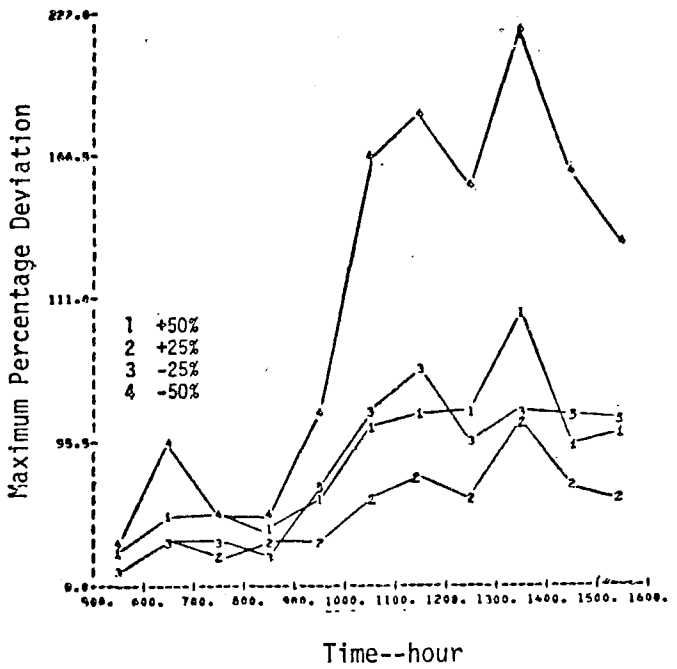

FIGURE IV-21. THE EFFECT--EXPRESSED AS MAXIMUM PERCENTAGE DEVIATIONS--OF VARIATIONS IN WIND SPEED FOR NO_2

The most interesting conclusion that can be drawn from Figures IV-6 through IV-21, however, is based on the fact that the changes do not follow the simple one-over-wind-speed law as predicted by a box model (Hanna, 1972). To illustrate this point, we consider a simple box model based on

$$c = k \frac{Q}{u} \quad , \tag{IV-9}$$

where

c = concentration,
Q = emissions strength,
u = wind speed,
k = proportional constant.

If the wind speed is changed by, say, x percent, then according to Eq. (IV-1), the box model would consequently predict

$$\tilde{c} = k \frac{Q}{\left(1 + \frac{x}{100}\right) u} \quad . \tag{IV-10}$$

Thus, the relative change in percentage obtained using the box model would be

$$d = \left| \frac{\tilde{c} - c}{c} \right| = \frac{x}{1 + \frac{x}{100}} \quad . \tag{IV-11}$$

For the four values of x used in our simulations, d has the following values (in percentages):

x	d
+50%	33.3%
+25	20.0
-25	33.3
-50	100.0

A comparison of the above tabulation with Figures IV-10 through IV-17 results in the observations listed below.

> The response of the SAI airshed model is time-dependent, whereas that of a simple box model is time-invariant. This difference is apparently due to the following deficiencies in the simple box model:
- The invocation of the steady-state assumption.
- The improper treatment of the initial conditions.

> The response of the SAI airshed model varies with each chemical species, whereas that of a simple box model does not. However, Hanna (1973) has extended the simple box model to chemically reactive substances. His results show that the concentrations of reactive species depend on the wind speed in a way that is more complicated than the simple one-over-wind-speed law.

> An anomaly was observed between 800 and 900 PDT in that an increase in the wind speed tended to induce an increase in the maximum deviation in CO concentrations. This effect may be attributable to the shift from a land breeze to a sea breeze regime during this period

> Measured in terms of the basin-wide average (see Figures IV-10 through IV-13), the responses of the SAI airshed model, even at the peaks, are considerably smaller in magnitude than those predicted using the box model. For example, the maximum responses for carbon monoxide, and inert species, are (in percentages):

x	d
+50%	19.6%
+25	11.8
-25	20.2
-50	51.7

These values are much smaller than the corresponding entries in the previous tabulation. However, Figure IV-10 shows that the +50 percent curve is very close to the -25 percent curve, as predicted by the simple box model.

> Measured in terms of the local maximum (see Figures IV-14 through IV-21), the response of the SAI airshed model can be significantly higher than that of the box model. Therefore, depending on the spatial average, the more elaborate SAI model provides a spectrum of responses, whereas the simple box model provides only one.

In view of these observations, we can conclude that, although a simple box model may retain some of the most important features of sophisticated airshed models, it also lacks many other ingredients that are more complex but are indispensable to a successful airshed model. The arguments for returning to the use of the simple box model have been under attack from a different direction by Hameed (1974). However, we believe that the evidence presented here, which is in line with the arguments expressed by Lamb and Seinfeld (1974), is more direct and fundamental.

As a final note, we would like to point out the potential application of the results of our sensitivity study to the development of repro-models (Horowitz et al., 1973). In particular, the cause-effect relationship between wind speeds and air quality that has been established in the sensitivity analysis could be very useful in generating the approximate functions needed in the repro-models.

3. The Effect of Variations in Turbulent Diffusivity

Eddy diffusion due to turbulent motions of the atmosphere is the principal mechanism for the dispersion of air pollutants. In the SAI airshed model, the treatment of turbulent diffusion is imbedded in the so-called K-theory, which involves the use of horizontal and vertical diffusion coefficients. In this section, we investigate the effect of varying these coefficients. Since we anticipated that interactions between diffusion and chemical reactions would not predominate under these conditions, we considered only the simplified case of an inert species.

a. Horizontal Diffusion

A simple order-of-magnitude analysis of the diffusion equation would show that horizontal diffusion, under typical conditions, is dwarfed by horizontal advection. However, to determine the importance of this term quantitatively, we chose carbon monoxide as the base case, using a constant (physical) horizontal diffusion coefficient of 50 m^2 sec^{-1}, which is a typical value for this situation. Next, we examined the effect of varying this

value by setting the coefficient first at zero and then at 500 m^2 sec^{-1}. These numbers undoubtedly represent the extreme values of the physical horizontal diffusivity.

Table IV-4 presents the results of these two sensitivity runs, which show that the effect of changes in (physical) horizontal diffusivity from 50 m^2 sec^{-1} to zero is minimal (less than 0.4 percent for basin-wide averages and less than 3 percent for maxima). Because of this result and because the horizontal diffusivity in the model is the sum of two components,

$$(K_H)_M = (K_H)_N + (K_H)_P \quad ,$$

where

$(K_H)_M$ = horizontal diffusivity in the model,
$(K_H)_N$ = horizontal diffusivity due to numerical diffusion,
$(K_H)_P$ = horizontal diffusivity due to physical diffusion,

either or both of the following two conditions must prevail:

> The advection term is much greater than the (numerical and physical) diffusion term.
> The magnitude of the numerical diffusion is much greater than 50 m^2 sec^{-1}.

In contrast, Table IV-4 shows that noticeable effects begin to emerge as the (physical) diffusivity is changed from 50 to 500 m^2 sec^{-1} (about 2 percent for basin-wide averages and 13 percent for maxima*). Logically, this implies that both of the following two considerations must apply:

---

* The effect on the average concentration of varying the magnitude of the diffusion coefficient is highly disproportionate. For instance, we showed in the next section that an order-of-magnitude change in the vertical diffusivity results in a change of only about 10 percent in average concentration.

Table IV-4

THE LARGEST DEVIATIONS IN THE GRID GENERATED BY RANDOMLY VARYING THE HORIZONTAL DIFFUSION

(a) $|\overline{d}|$ in Percentages

Case	Hour										
	6	7	8	9	10	11	12	13	14	15	16
$K_H \rightarrow 0$	0.07%	0.16%	0.23%	0.27%	0.30%	0.34%	0.34%	0.29%	0.22%	0.20%	0.17%
$K_H \rightarrow 500\ m^2/sec$	0.6	1.3	1.8	2.1	2.4	2.6	2.7	2.3	1.7	1.6	1.4

(b) $|d_{max}|$ in Percentages

Case	Hour										
	6	7	8	9	10	11	12	13	14	15	16
$K_H \rightarrow 0$	0.52%	0.88%	0.91%	1.39%	1.16%	1.38%	1.93%	2.02%	1.71%	1.48%	1.21%
$K_H \rightarrow 500\ m^2/sec$	4.4	5.9	7.6	11.4	9.2	10.4	12.6	12.9	11.3	9.6	8.2

> The advection term is not much greater than the diffusion term when the latter is 500 m^2 sec^{-1}.

> The magnitude of the numerical diffusion is on the order of 500 m^2 sec^{-1} or less.

Therefore, according to linear analysis, the estimated magnitude of numerical diffusion in the SAI airshed model is

$$\frac{1}{2} U\Delta x = \frac{1}{2} \cdot 4 \text{ m sec}^{-1} \cdot 3000 \text{ m} = 6 \cdot 10^3 \text{ m}^2 \text{ sec}^{-1} \quad .$$

The results of our analysis demonstrate that this estimate is at least an order of magnitude too high.

In summary, the sensitivity study reveals that the horizontal diffusion term becomes competitive with the advection term only when the magnitude of the former exceeds 500 m^2 sec^{-1}. Furthermore, this study implies that the magnitude of numerical diffusion is on the order of 500 m^2 sec^{-1} or less. Thus, these findings constitute evidence that numerical errors in the grid model are not as severe as one may think. Liu and Seinfeld (1974) have reached the same conclusion via a different approach.

b. Vertical Diffusion

Vertical diffusion is an important process in determining the distribution of air pollutants in the atmosphere. The magnitudes of vertical diffusivities depend strongly on atmospheric stability and on mixing depth and mildly depend on wind speed and other parameters. Because of the wide range of values for vertical diffusivity (typically from 10^{-1} to 10^2 m^2 sec^{-1}) and the lack of reliable means for measuring it directly, vertical diffusivity is the most difficult parameter to determine or estimate. Since the present state of the art allows only an order-of-magnitude determination, we varied vertical diffusivity by either increasing or decreasing the reference values in the base case (5 m^2 sec^{-1}) by a factor of 10.

The results of the calculated average deviations and maximum deviations, presented in Figures IV-22 through IV-33, show the following:

> As is true in all cases considered in the sensitivity study, the residue air pollutants are responsible for the gradual buildup of the effect of changing the vertical diffusivity.
> Roughly speaking, the effect on the ground-level concentrations of varying the wind speed by 25 to 50 percent is about the same as that of varying the vertical diffusivity by an order of magnitude.
> The effect of decreasing the vertical diffusivity is not linearly proportional to that of increasing the vertical diffusivity; the former is significantly larger. Furthermore, this discrepancy is more pronounced for secondary pollutants, such as ozone.
> The effect of varying the vertical diffusivity is not the same for local maxima and basin-wide averages; the effect for the latter is considerably smaller.

In addition to the usefulness of these observations in determining the response of the SAI urban airshed model to changes in atmospheric stability, these results also present additional evidence that a simple box model will not suffice. Succeeding sections present still further evidence in support of this conclusion.

4. The Effect of Variations in Mixing Depth

The height of the mixed layer is also an important meteorological parameter, since variations in it affect pollutant concentration levels. The mixing depth is usually determined from vertical temperature soundings. Since ±25 percent can be taken as an approximate measure of the uncertainty in determining the mixing depth, we varied the values used in the base case by these amounts. Figures IV-34 through IV-49 present the results of the sensitivity calculations, which show the following:

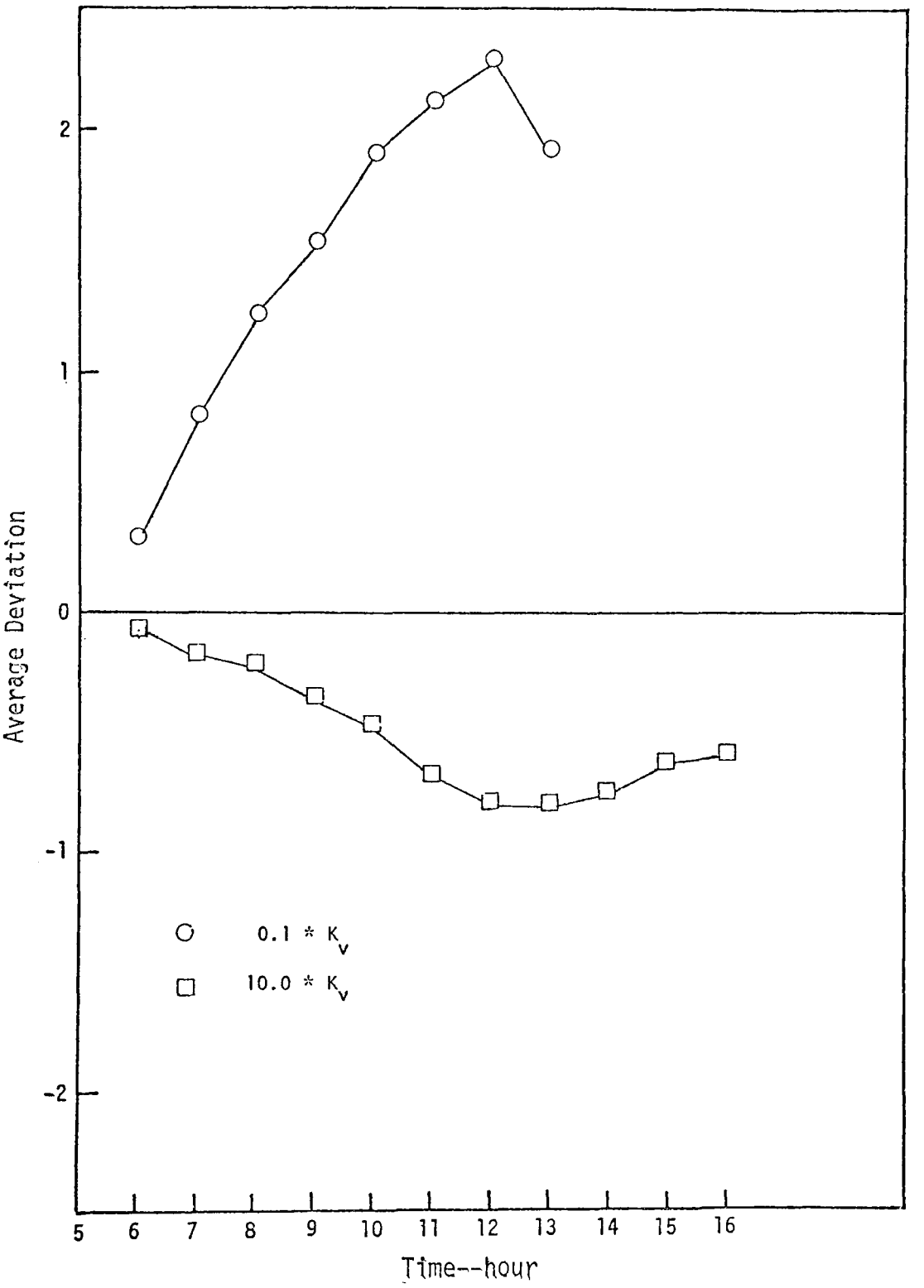

FIGURE IV-22. THE EFFECT--EXPRESSED AS AVERAGE DEVIATIONS--
OF VARIATIONS IN VERTICAL DIFFUSIVITY FOR CO

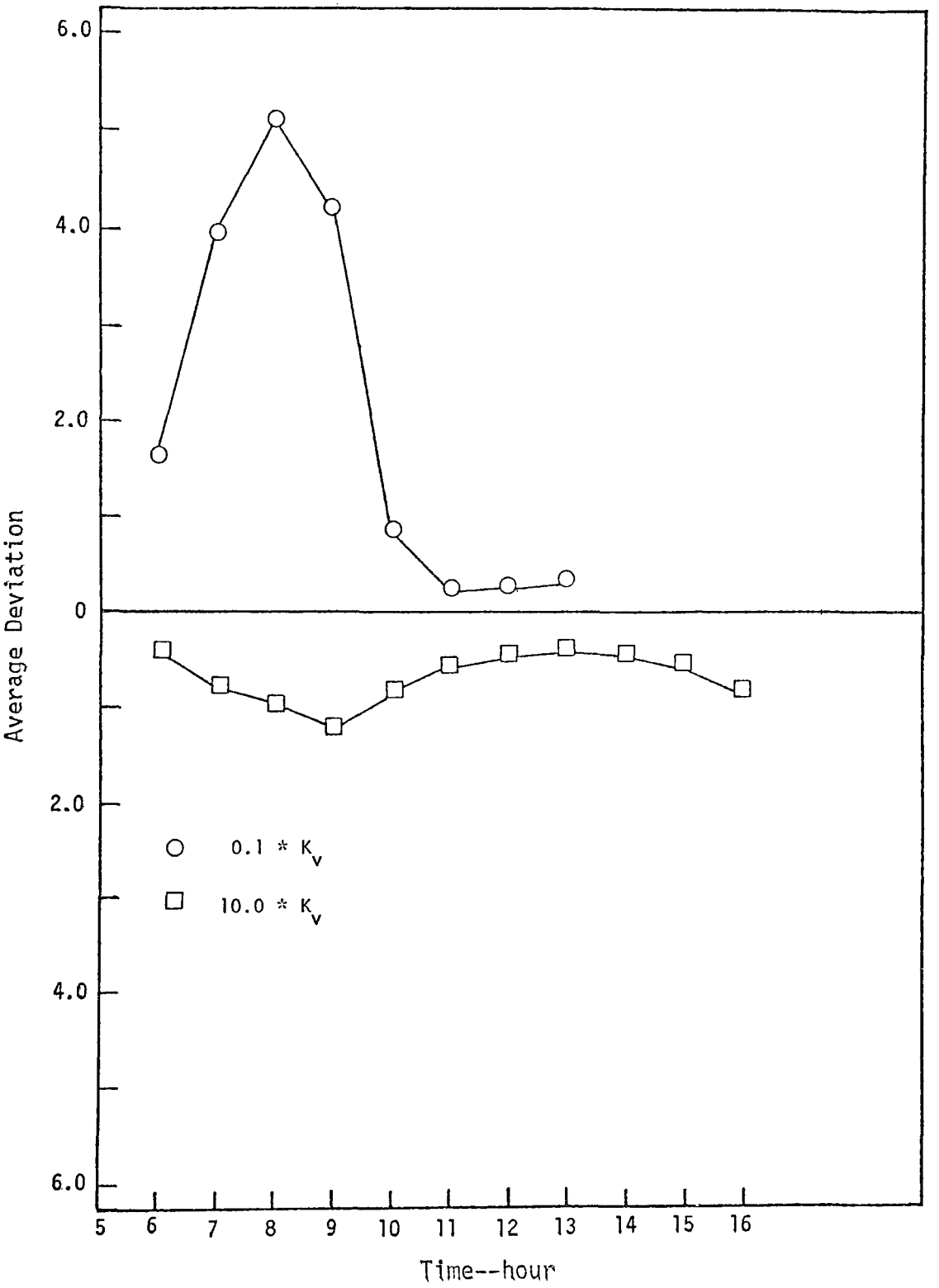

FIGURE IV-23. THE EFFECT--EXPRESSED AS AVERAGE DEVIATIONS--
OF VARIATIONS IN VERTICAL DIFFUSIVITY FOR NO

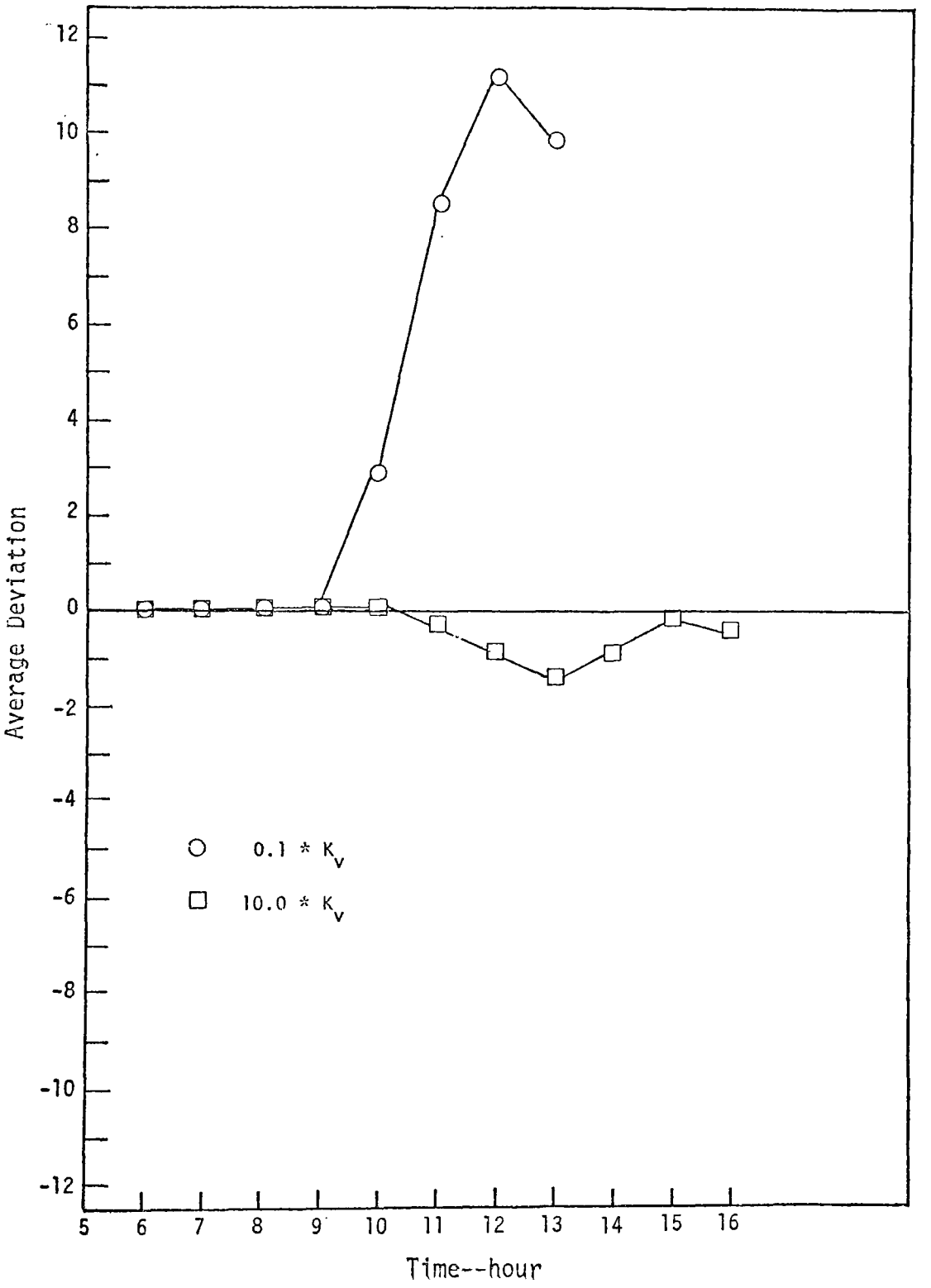

FIGURE IV-24. THE EFFECT--EXPRESSED AS AVERAGE DEVIATIONS--OF VARIATIONS IN VERTICAL DIFFUSIVITY FOR O_3

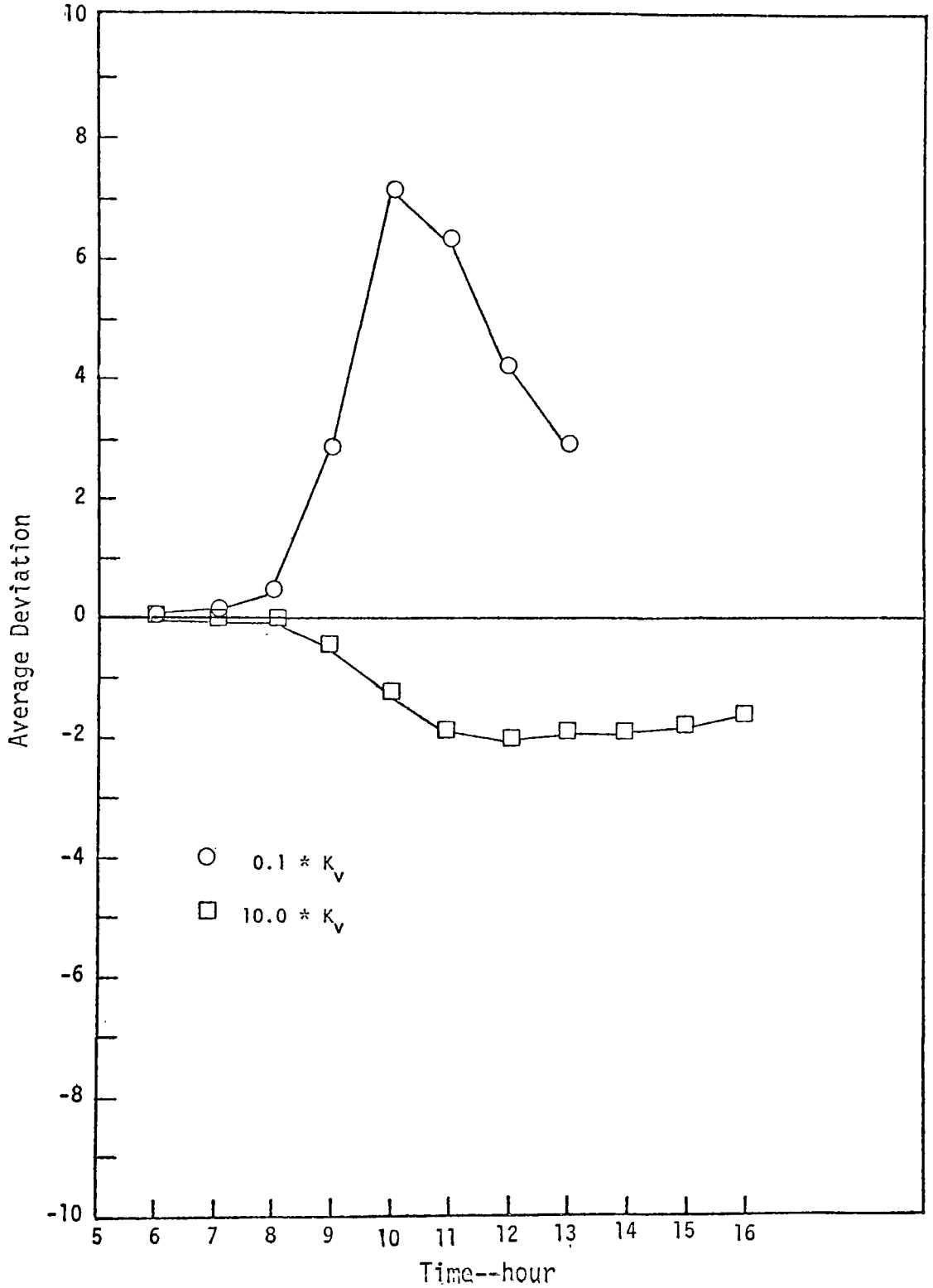

FIGURE IV-25. THE EFFECT--EXPRESSED AS AVERAGE DEVIATIONS--OF VARIATIONS IN VERTICAL DIFFUSIVITY FOR NO_2

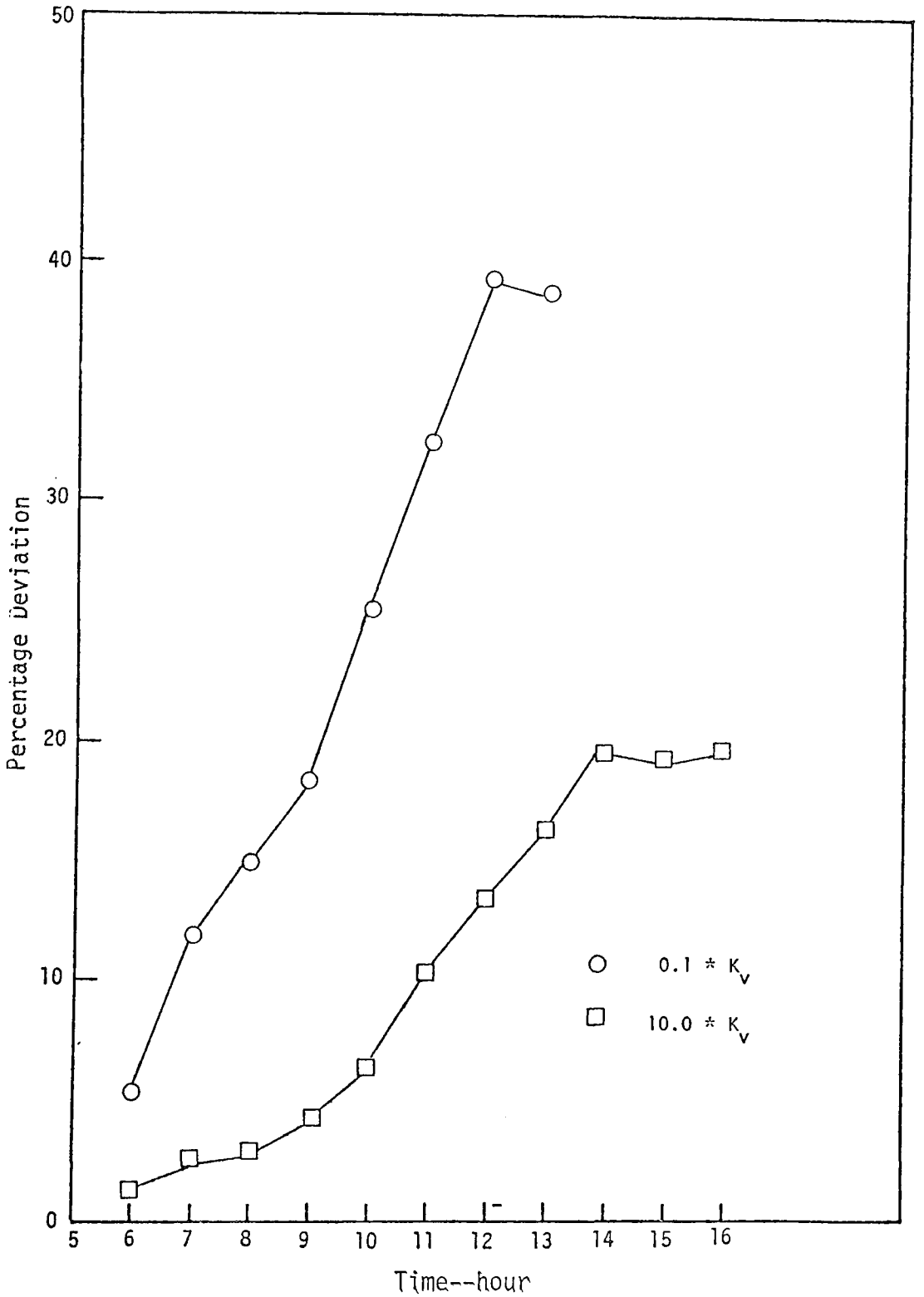

FIGURE IV-26. THE EFFECT--EXPRESSED AS PERCENTAGE DEVIATIONS--
OF VARIATIONS IN VERTICAL DIFFUSIVITY FOR CO

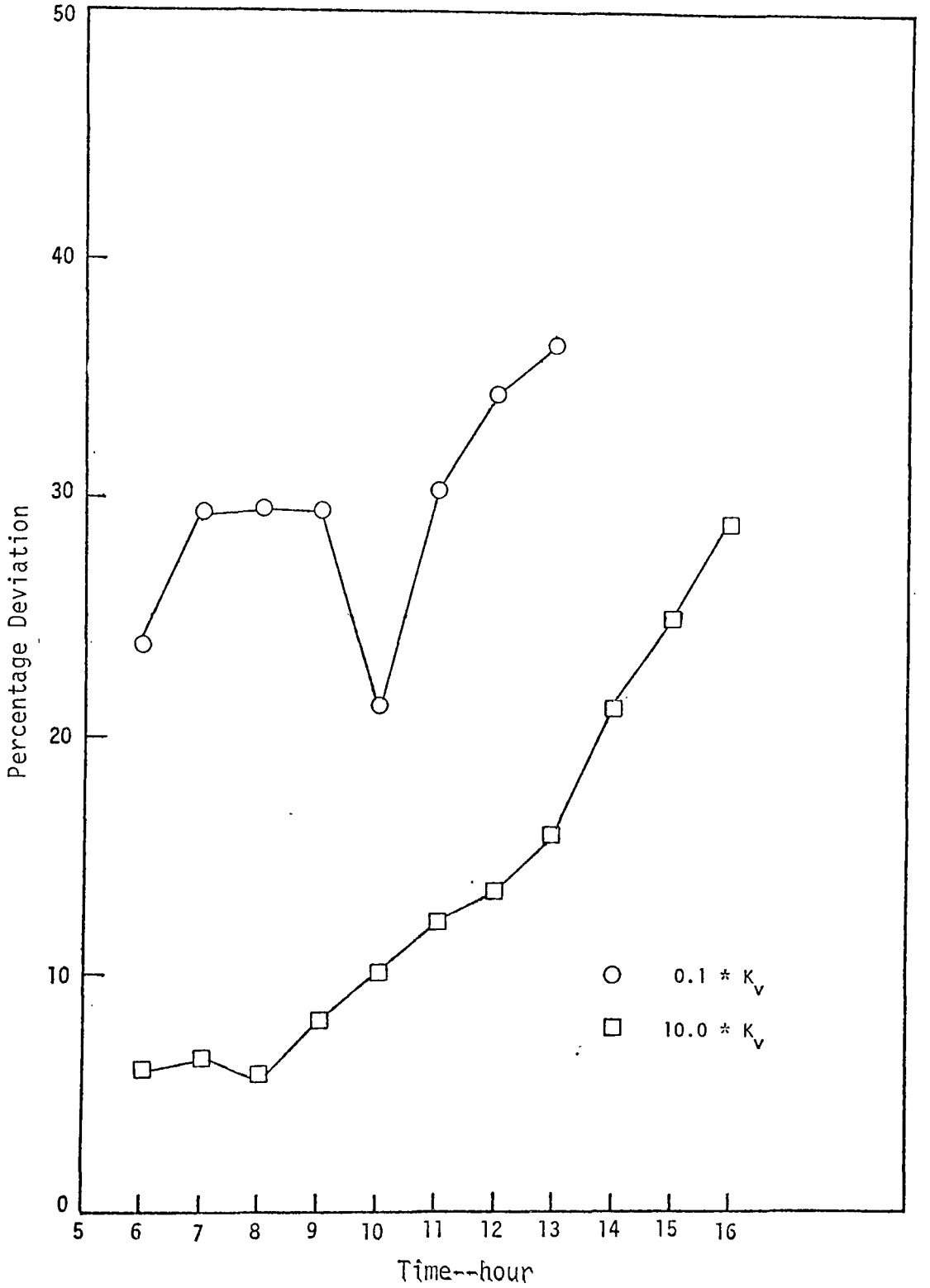

FIGURE IV-27. THE EFFECT--EXPRESSED AS PERCENTAGE DEVIATIONS--
OF VARIATIONS IN VERTICAL DIFFUSIVITY FOR NO

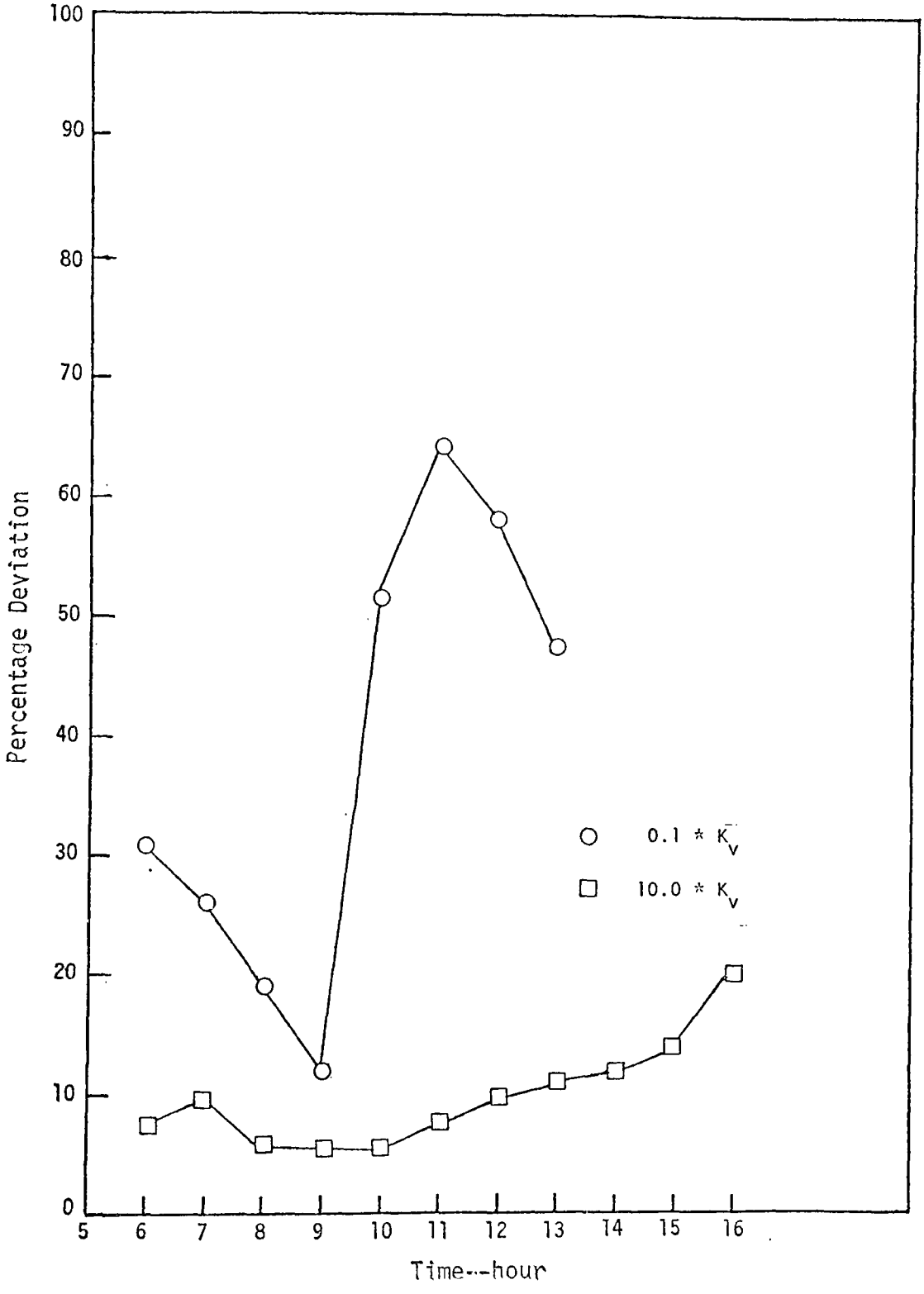

FIGURE IV-28. THE EFFECT--EXPRESSED AS PERCENTAGE DEVIATIONS OF VARIATIONS IN VERTICAL DIFFUSIVITY FOR O_3

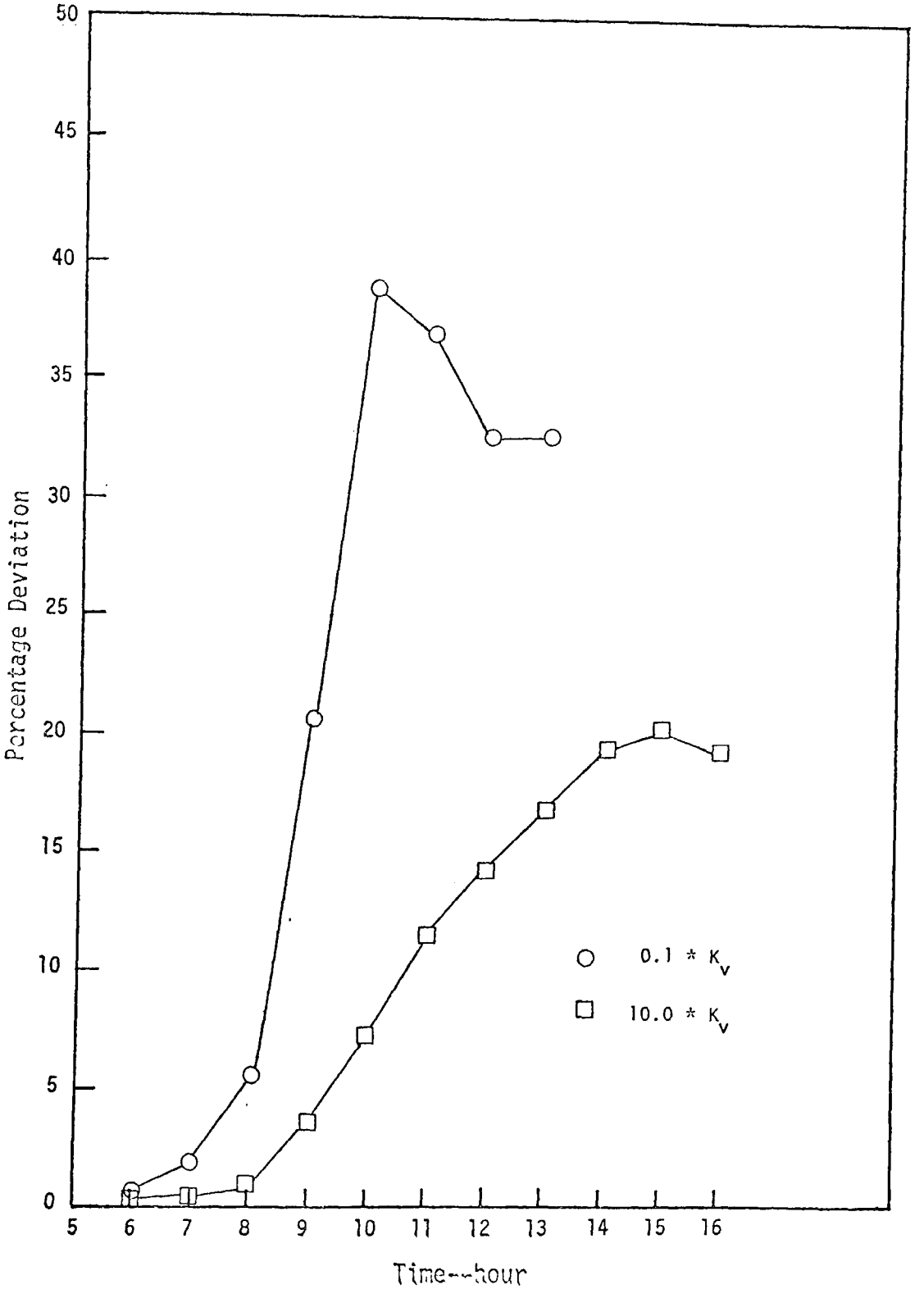

FIGURE IV-29. THE EFFECT--EXPRESSED AS PERCENTAGE DEVIATIONS--OF VARIATIONS IN VERTICAL DIFFUSIVITY FOR NO_2

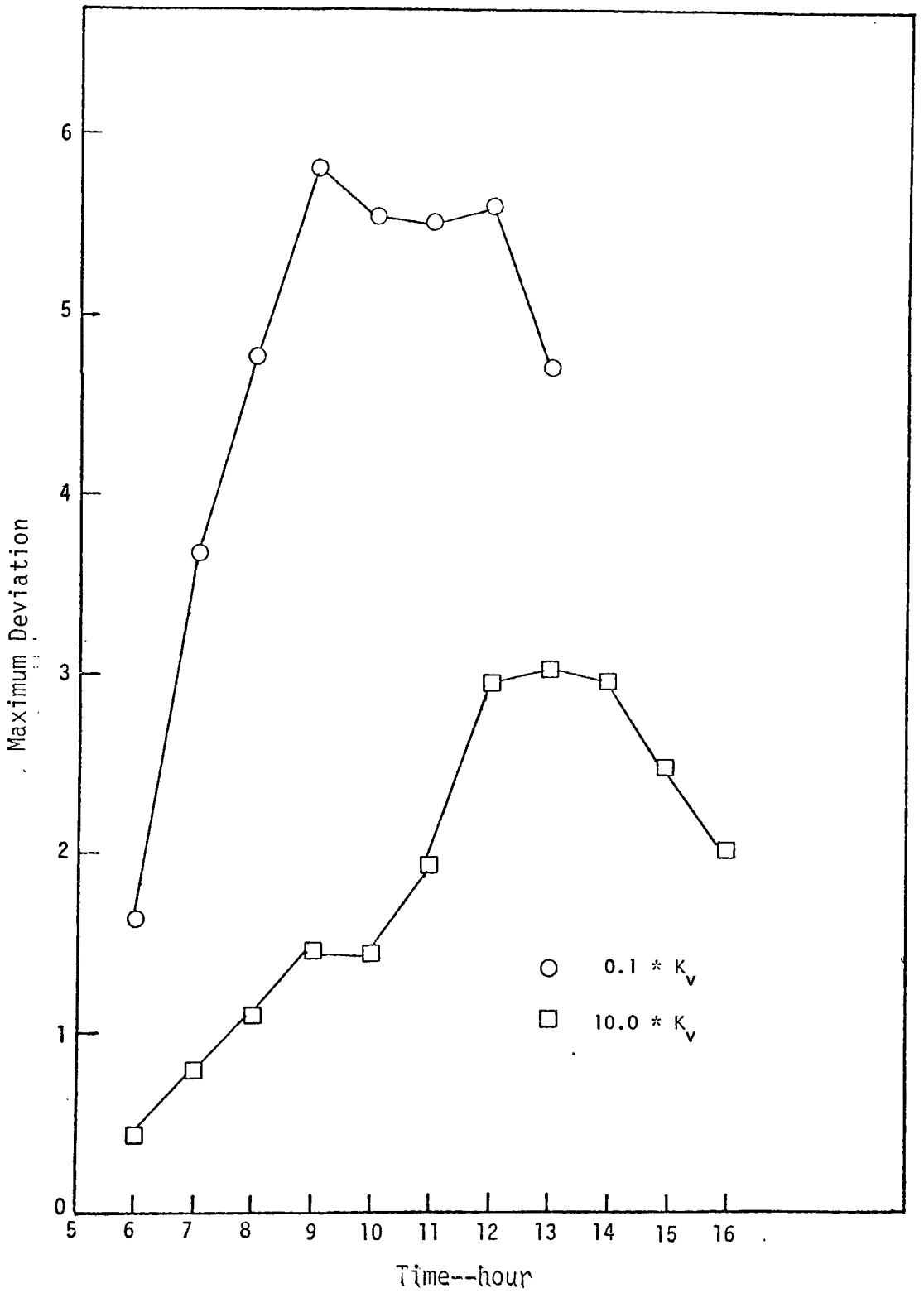

FIGURE IV-30. THE EFFECT--EXPRESSED AS MAXIMUM DEVIATIONS--
OF VARIATIONS IN VERTICAL DIFFUSIVITY FOR CO

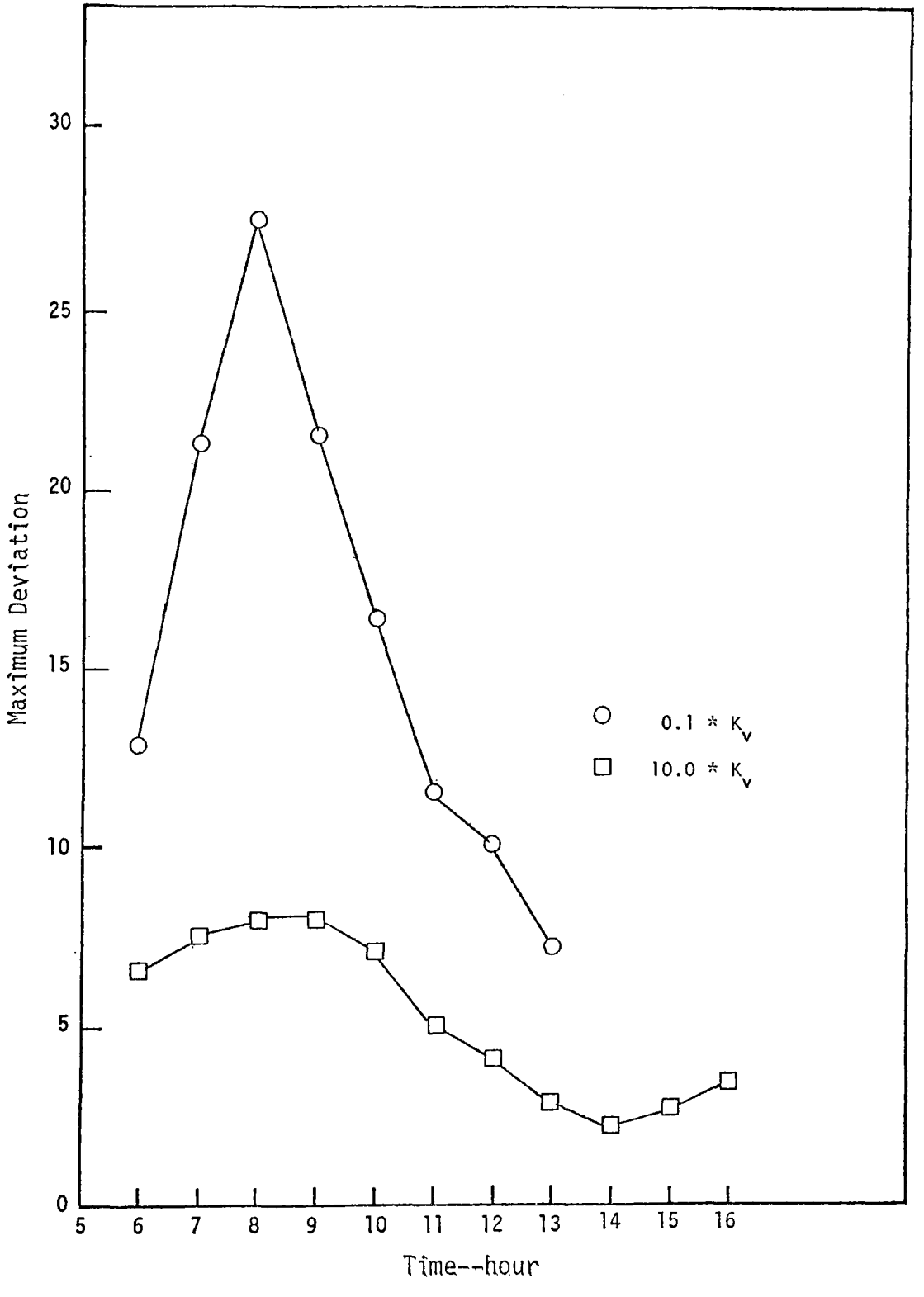

FIGURE IV-31. THE EFFECT--EXPRESSED AS MAXIMUM DEVIATIONS--
OF VARIATIONS IN VERTICAL DIFFUSIVITY FOR NO

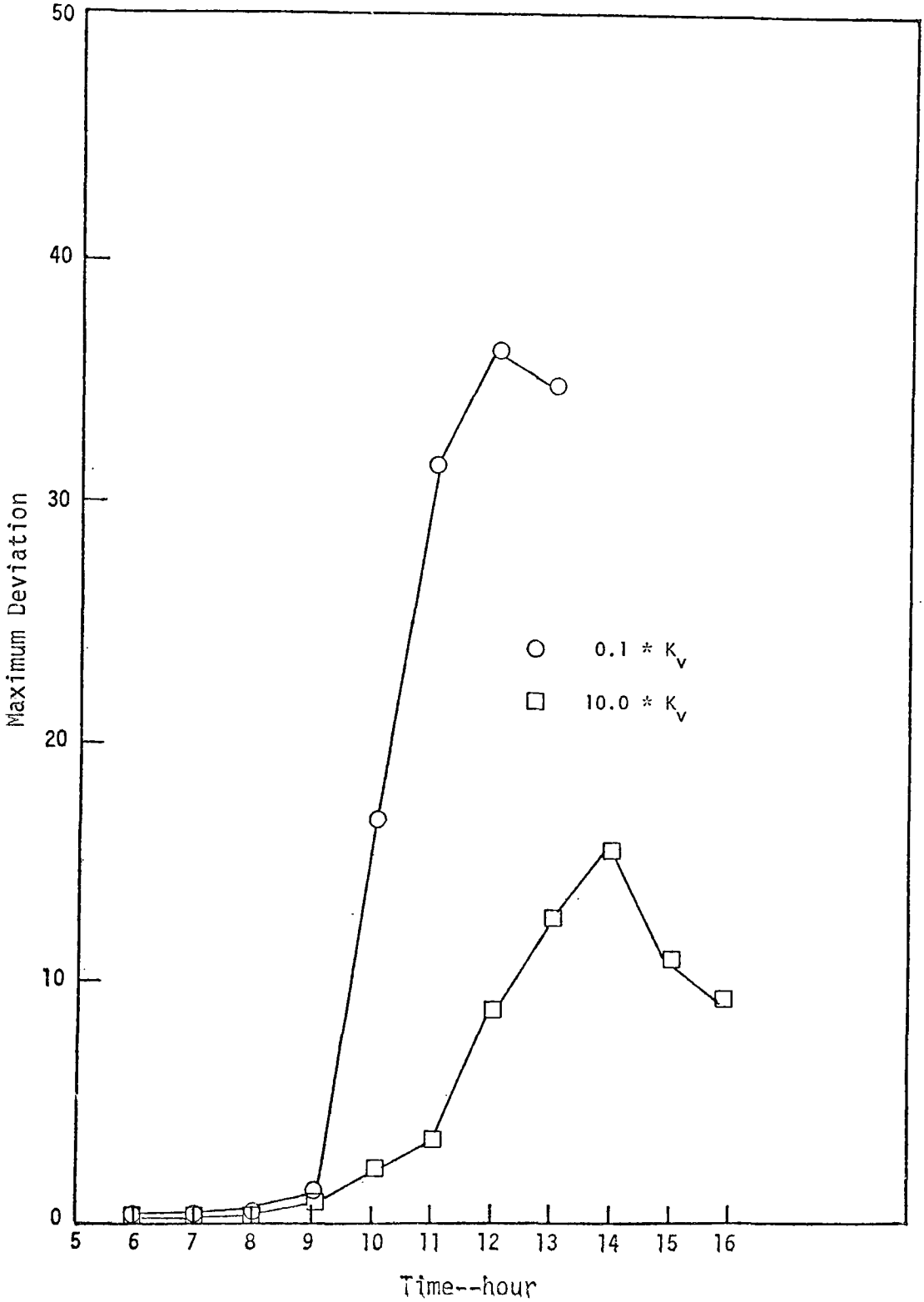

FIGURE IV-32. THE EFFECT--EXPRESSED AS MAXIMUM DEVIATIONS--OF VARIATIONS IN VERTICAL DIFFUSIVITY FOR O_3

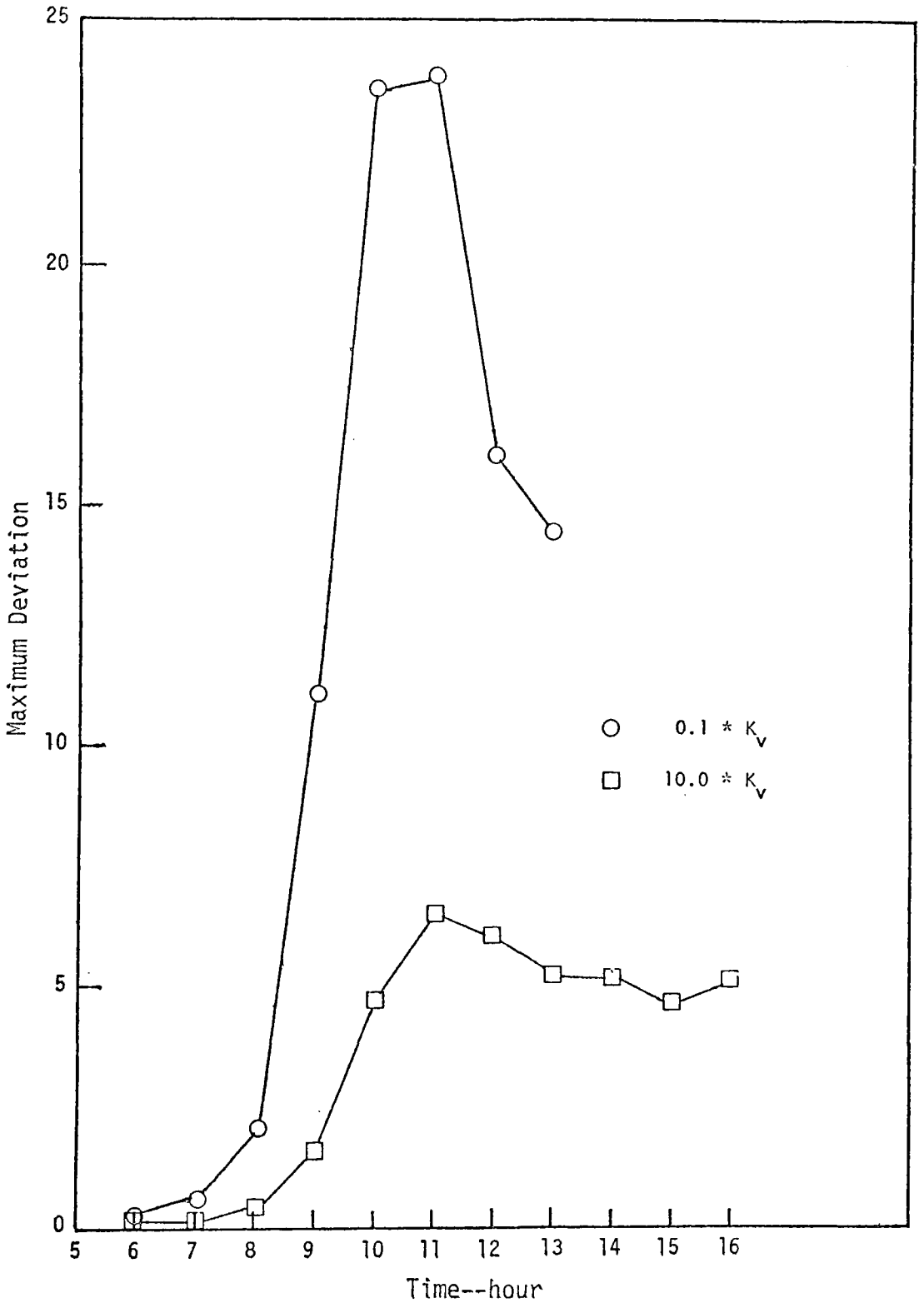

FIGURE IV-33. THE EFFECT--EXPRESSED AS MAXIMUM DEVIATIONS--
OF VARIATIONS IN VERTICAL DIFFUSIVITY FOR NO_2

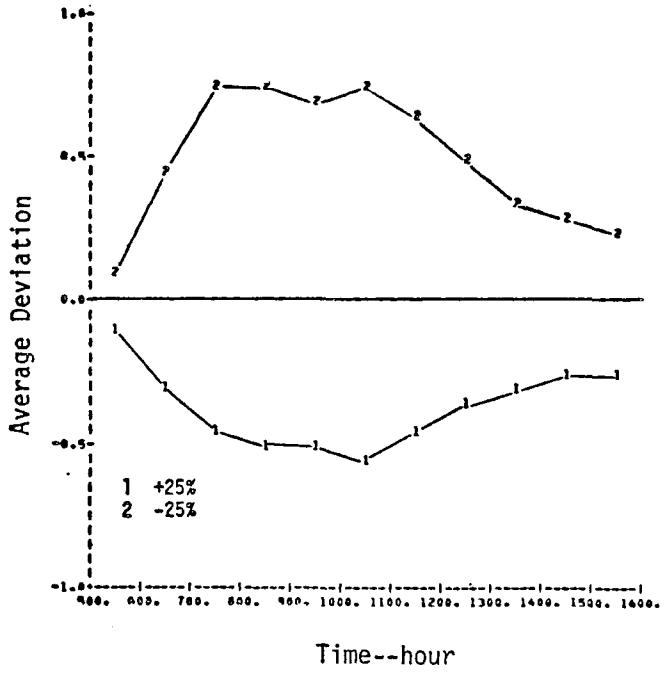

FIGURE IV-34. THE EFFECT--EXPRESSED AS AVERAGE DEVIATIONS--OF VARIATIONS IN MIXING DEPTH FOR CO

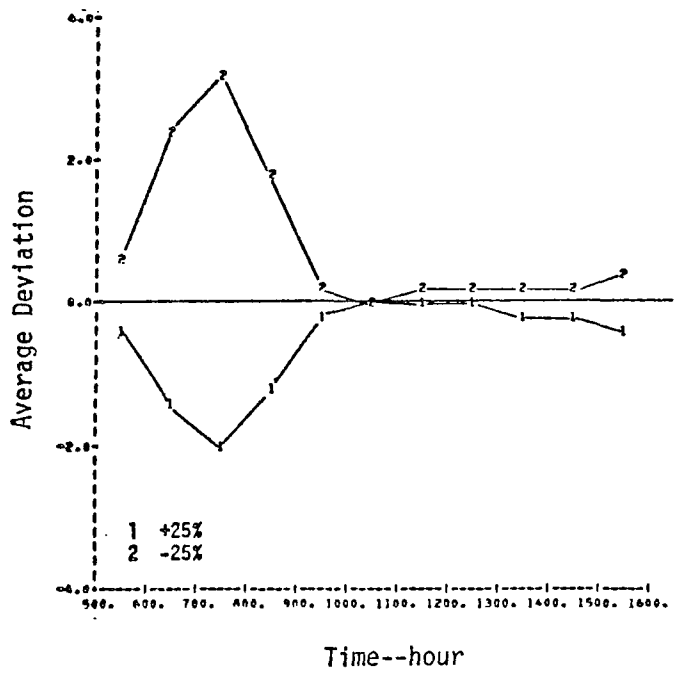

FIGURE IV-35. THE EFFECT--EXPRESSED AS AVERAGE DEVIATIONS--OF VARIATIONS IN MIXING DEPTH FOR NO

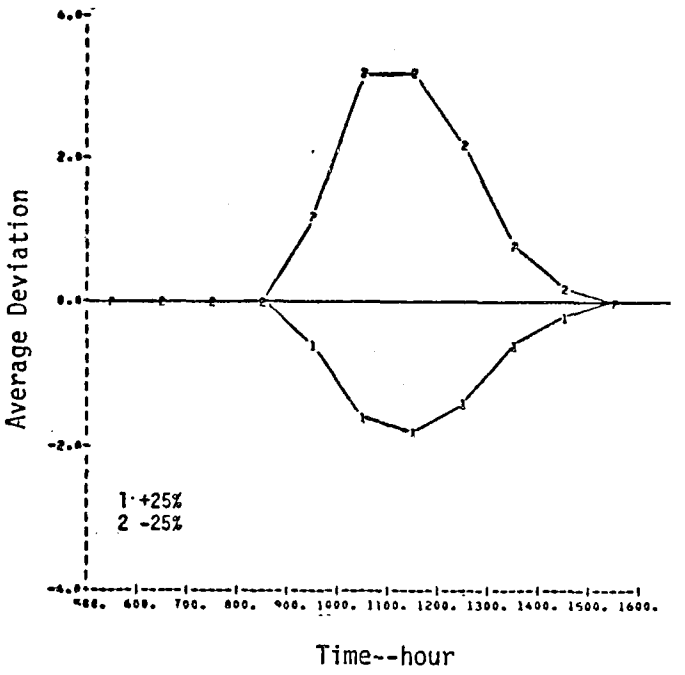

FIGURE IV-36. THE EFFECT--EXPRESSED AS AVERAGE DEVIATIONS--OF VARIATIONS IN MIXING DEPTH FOR O_3

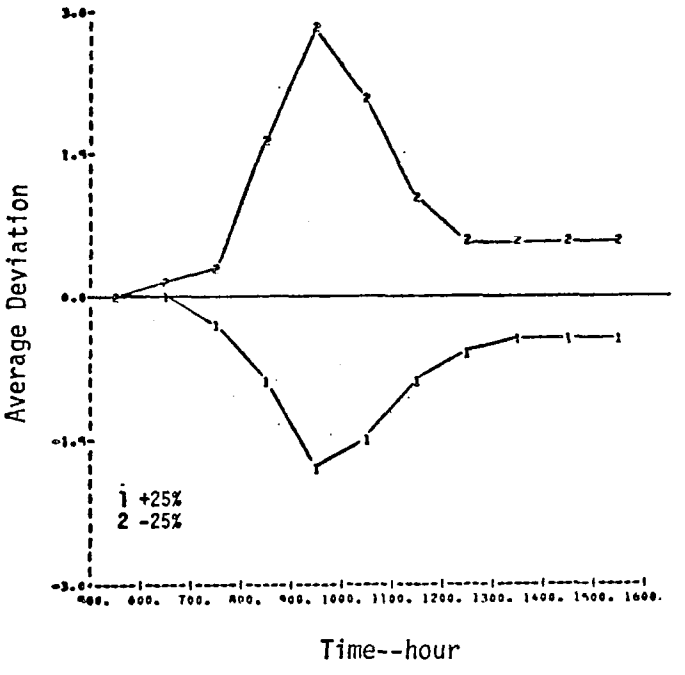

FIGURE IV-37. THE EFFECT--EXPRESSED AS AVERAGE DEVIATIONS--OF VARIATIONS IN MIXING DEPTH FOR NO_2

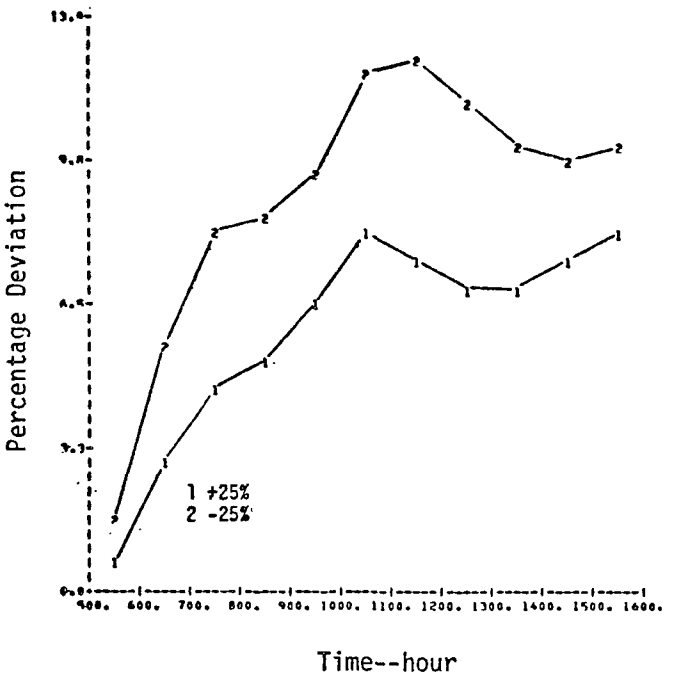

FIGURE IV-38. THE EFFECT--EXPRESSED AS PERCENTAGE DEVIATIONS--OF VARIATIONS IN MIXING DEPTH FOR CO

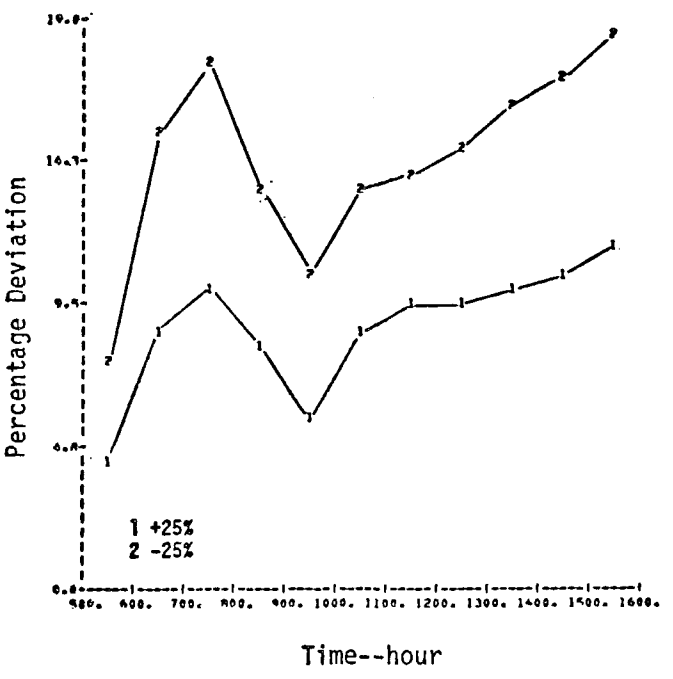

FIGURE IV-39. THE EFFECT--EXPRESSED AS PERCENTAGE DEVIATIONS--OF VARIATIONS IN MIXING DEPTH FOR NO

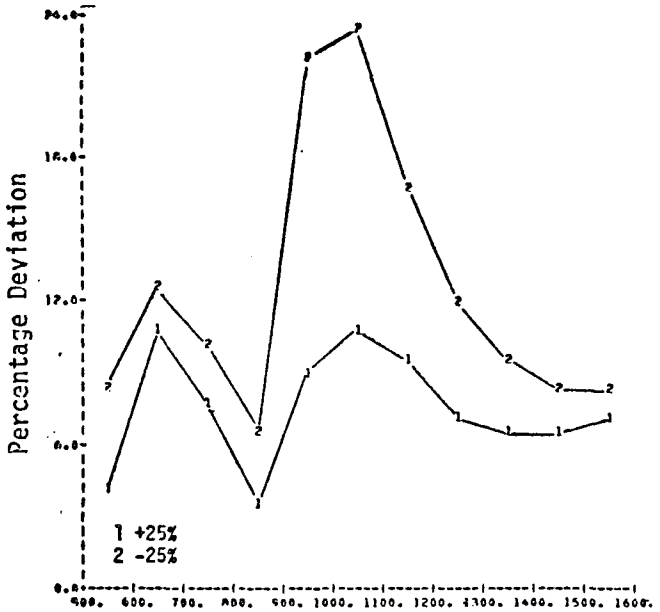

FIGURE IV-40. THE EFFECT--EXPRESSED AS PERCENTAGE DEVIATIONS--OF VARIATIONS IN MIXING DEPTH FOR O_3

FIGURE IV-41. THE EFFECT--EXPRESSED AS PERCENTAGE DEVIATIONS--OF VARIATIONS IN MIXING DEPTH FOR NO_2

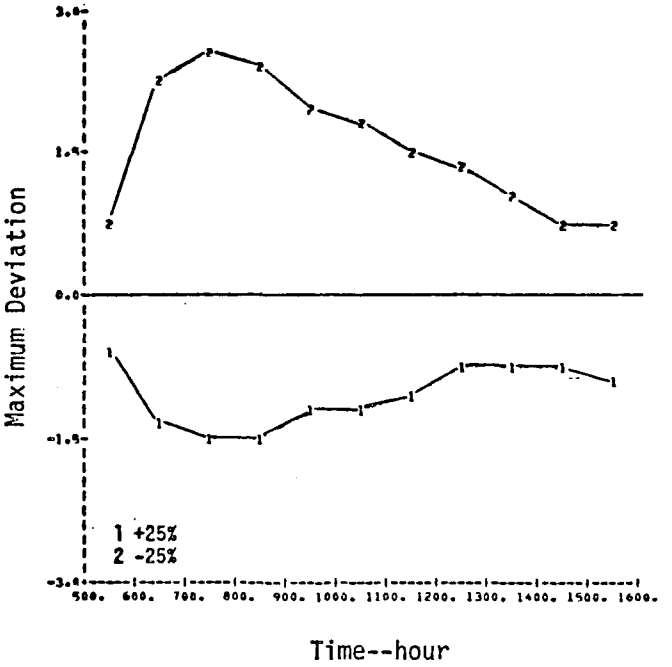

FIGURE IV-42. THE EFFECT--EXPRESSED AS MAXIMUM DEVIATIONS--OF VARIATIONS IN MIXING DEPTH FOR CO

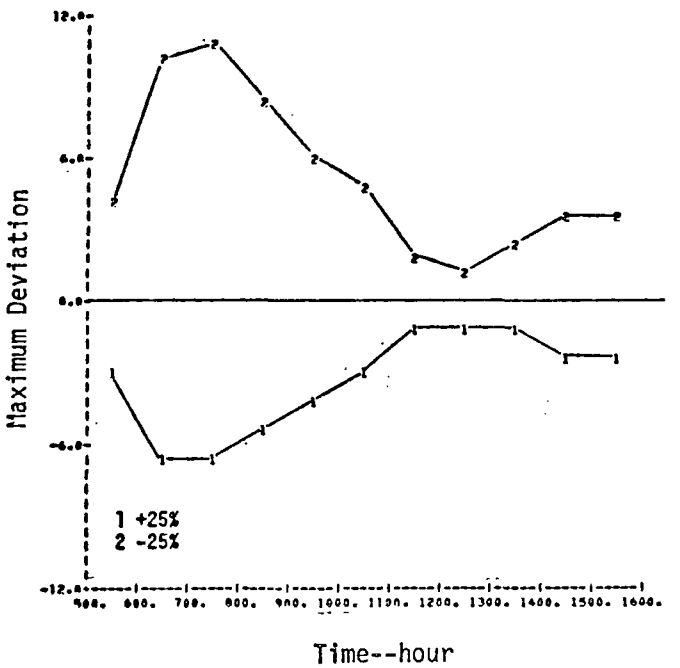

FIGURE IV-43. THE EFFECT--EXPRESSED AS MAXIMUM DEVIATIONS--OF VARIATIONS IN MIXING DEPTH FOR NO

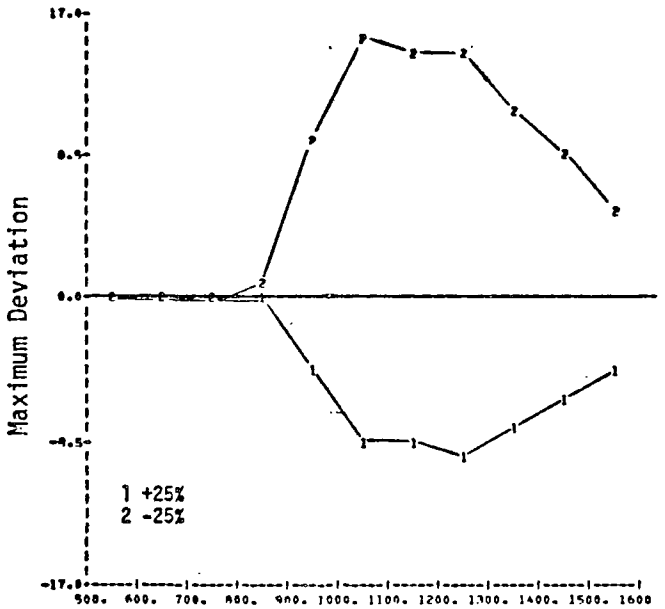

FIGURE IV-44. THE EFFECT--EXPRESSED AS MAXIMUM DEVIATIONS--OF VARIATIONS IN MIXING DEPTH FOR O_3

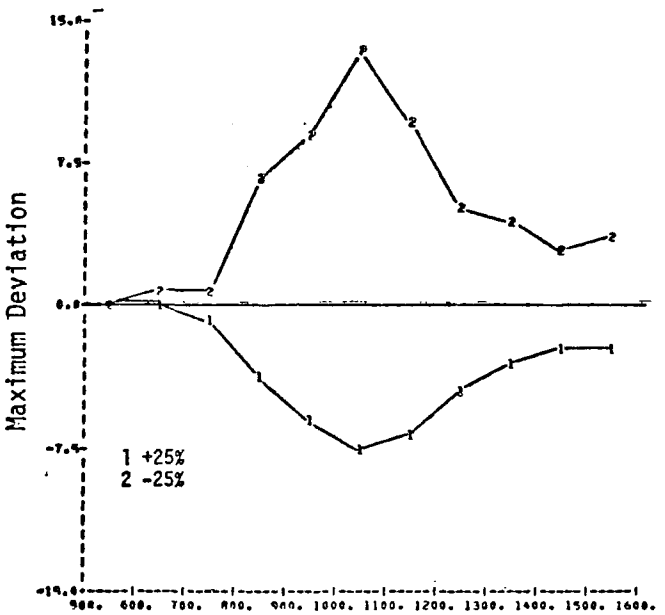

FIGURE IV-45. THE EFFECT--EXPRESSED AS MAXIMUM DEVIATIONS--OF VARIATIONS IN MIXING DEPTH FOR NO_2

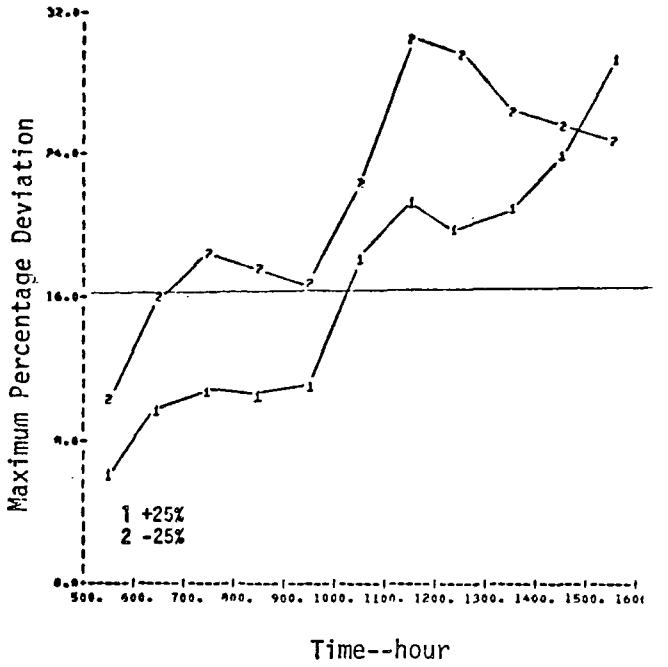

FIGURE IV-46. THE EFFECT EXPRESSED AS MAXIMUM PERCENTAGE DEVIATIONS--OF VARIATIONS IN MIXING DEPTH FOR CO

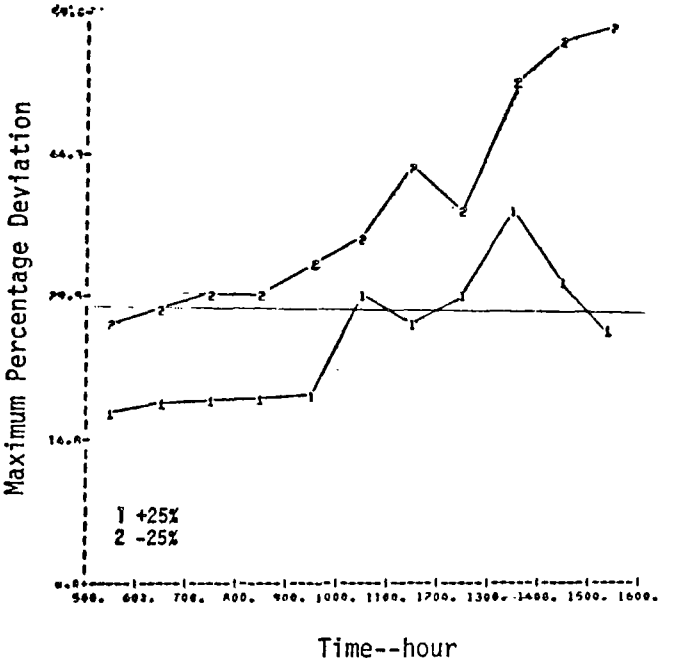

FIGURE IV-47. THE EFFECT--EXPRESSED AS MAXIMUM PERCENTAGE DEVIATIONS--OF VARIATIONS IN MIXING DEPTH FOR NO

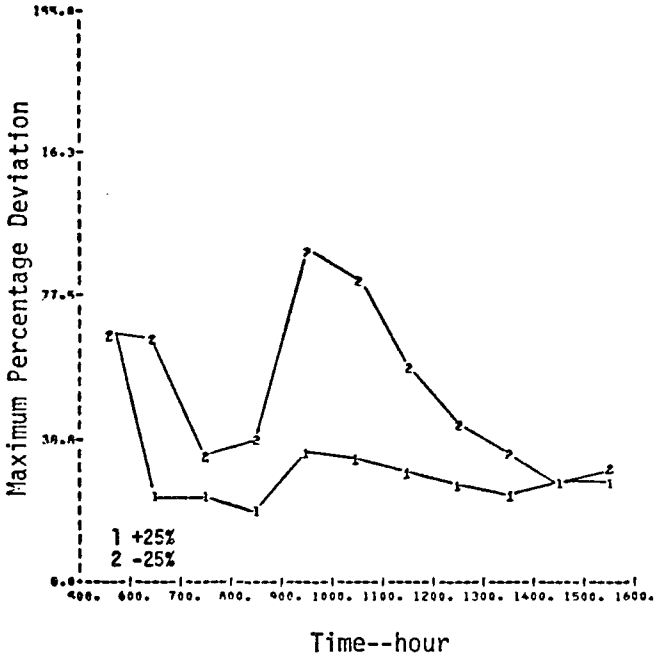

FIGURE IV-48. THE EFFECT--EXPRESSED AS MAXIMUM PERCENTAGE DEVIATIONS--OF VARIATIONS IN MIXING DEPTH FOR O_3

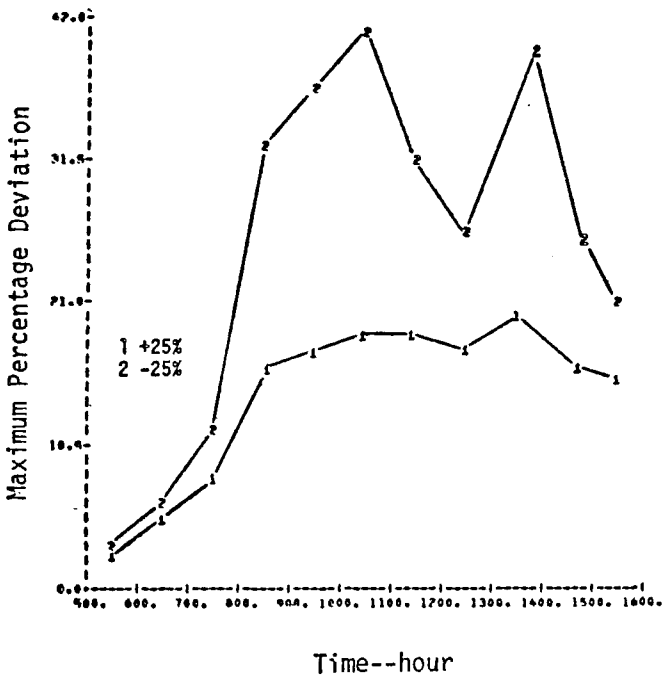

FIGURE IV-49. THE EFFECT--EXPRESSED AS MAXIMUM PERCENTAGE DEVIATIONS--OF VARIATIONS IN MIXING DEPTH FOR NO_2

- The buildup of the mixing depth variation effect is time-dependent.
- Decreasing the mixing depth has a greater effect on the ground concentration than increasing it. This result is more pronounced for reactive pollutants.
- The effect of changing the mixing depth is not uniform over the modeling region; it varies from place to place.
- The effect on ground-level concentrations of changing the mixing depth is roughly the same as that of changing the wind speed, as one would expect from a dimensional analysis.

5. The Effect of Variations in Radiation Intensity

Since the objective of airshed modeling is to simulate photochemical air pollution, concentration levels of both primary and secondary air pollutants that participate in the photochemical reactions are of particular interest. Hecht, Roth, and Seinfeld (1973) have analyzed the sensitivity of the kinetic mechanism used in the SAI airshed model. In particular, they estimated the sensitivities of predicted concentration histories in a smog chamber to variations in the magnitudes of the primitive and intermediate parameters in the kinetic model, such as the reaction rate constants and the stoichiometric coefficients. Hecht et al. concluded that the rate constant for the photolysis of NO_2, a function of UV light intensity, is one of the most sensitive parameters. Thus, in the present investigation, we varied the photolysis rate constant (or, equivalently, the radiation intensity) to determine the effect of photochemistry on the ground concentrations predicted by the SAI urban airshed model. In the base case, the radiation intensity varied with the hours of the day; for our two sensitivity runs, we increased and decreased the base-case values by 30 percent.

The results of these calculations, presented in Figures IV-50 through IV-65, show that, as expected, changes in the light intensity do not affect carbon monoxide. The following comments can be made about the three photochemically reactive species, NO, O_3, and NO_2:

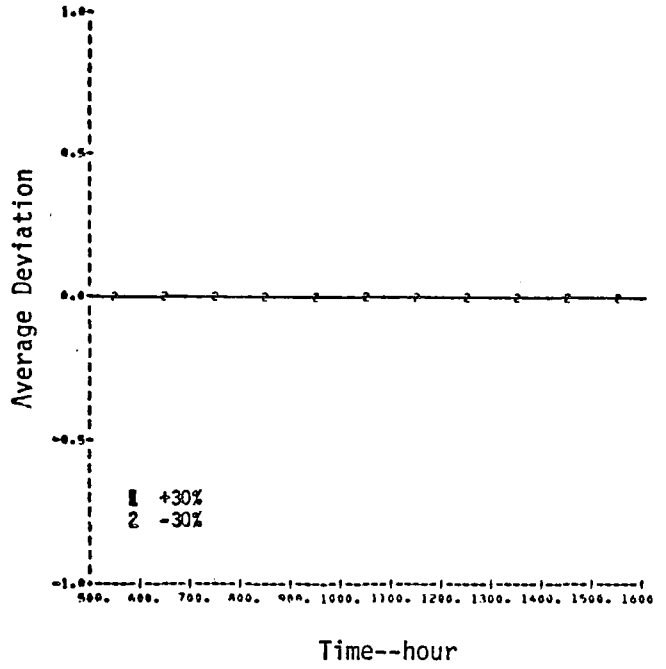

FIGURE IV-50. THE EFFECT--EXPRESSED AS AVERAGE DEVIATIONS--OF VARIATIONS IN RADIATION INTENSITY FOR CO

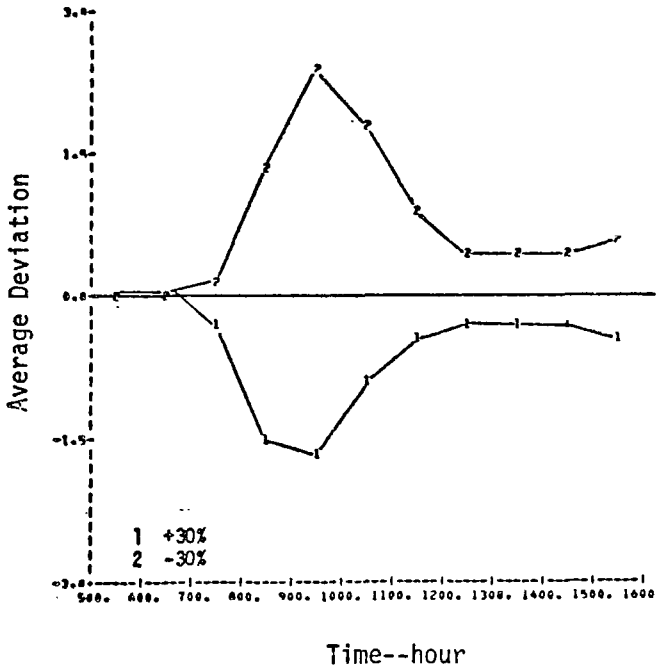

FIGURE IV-51. THE EFFECT--EXPRESSED AS AVERAGE DEVIATIONS--OF VARIATIONS IN RADIATION INTENSITY FOR NO

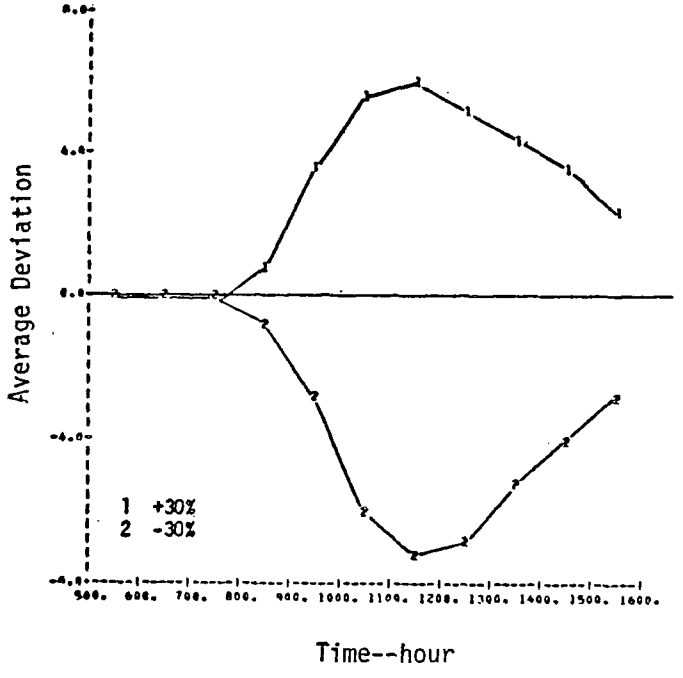

FIGURE IV-52. THE EFFECT--EXPRESSED AS AVERAGE DEVIATIONS--OF VARIATIONS IN RADIATION INTENSITY FOR O_3

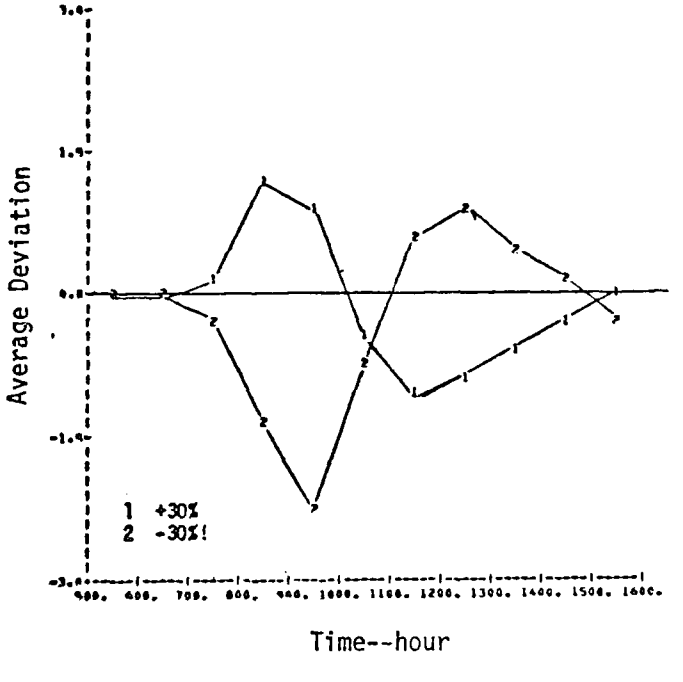

FIGURE IV-53. THE EFFECT--EXPRESSED AS AVERAGE DEVIATIONS--OF VARIATIONS IN RADIATION INTENSITY FOR NO_2

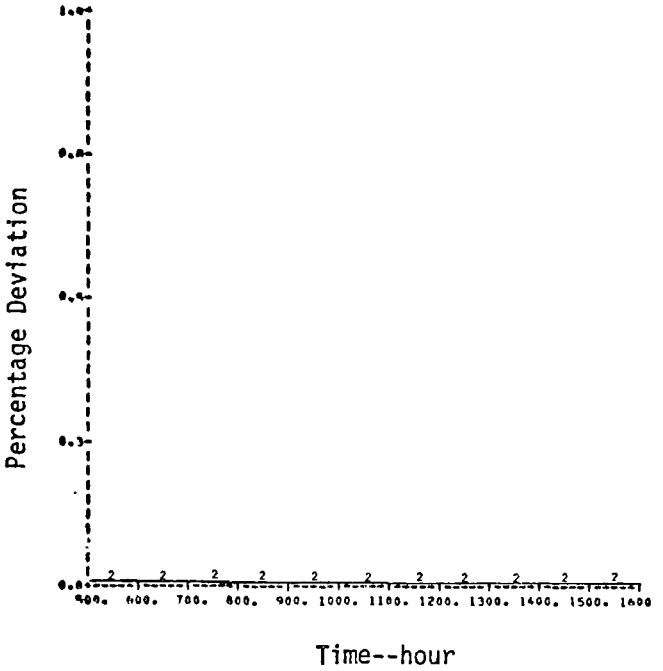

FIGURE IV-54. THE EFFECT EXPRESSED AS PERCENTAGE DEVIATIONS--OF VARIATIONS IN RADIATION INTENSITY FOR CO

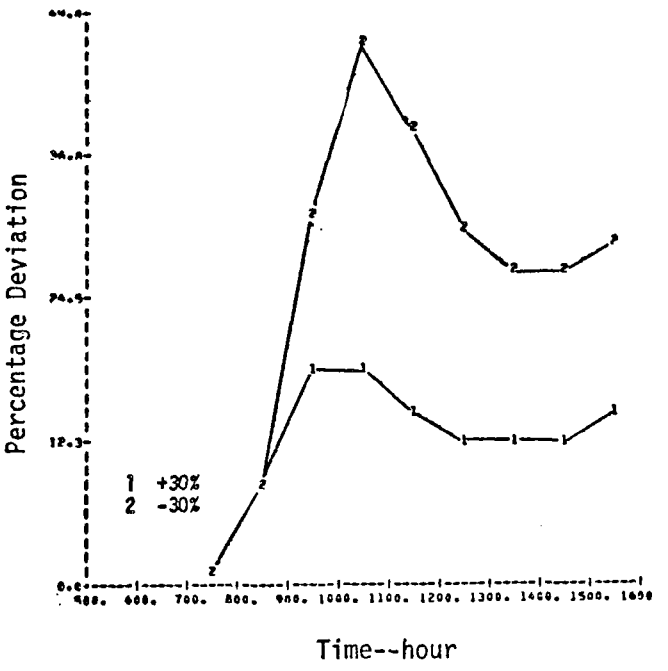

FIGURE IV-55. THE EFFECT--EXPRESSED AS PERCENTAGE DEVIATIONS--OF VARIATIONS IN RADIATION INTENSITY FOR NO

FIGURE IV-56. THE EFFECT--EXPRESSED AS PERCENTAGE DEVIATIONS--OF VARIATIONS IN RADIATION INTENSITY FOR O_3

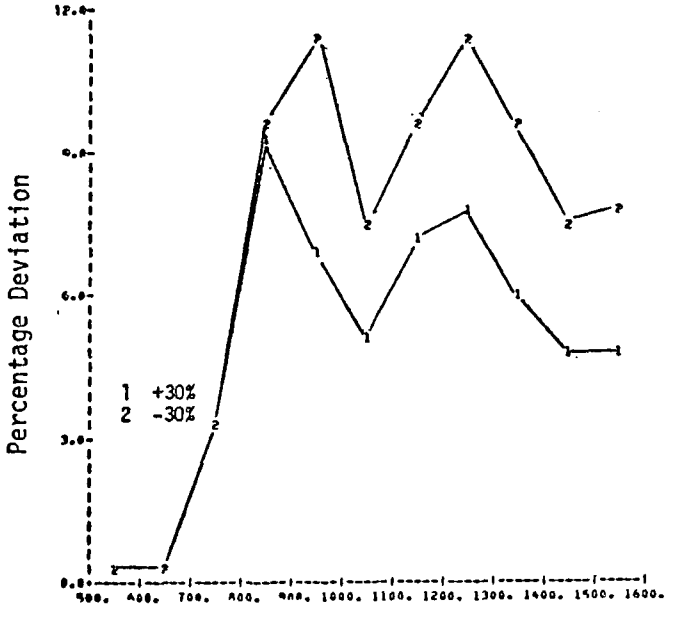

FIGURE IV-57. THE EFFECT--EXPRESSED AS PERCENTAGE DEVIATIONS--OF VARIATIONS IN RADIATION INTENSITY FOR NO_2

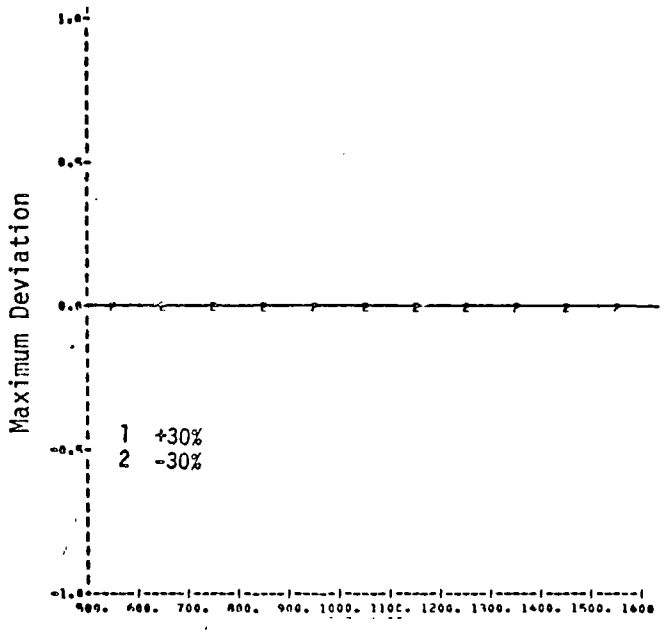

FIGURE IV-58. THE EFFECT--EXPRESSED AS MAXIMUM DEVIATIONS--OF VARIATIONS IN RADIATION INTENSITY FOR CO

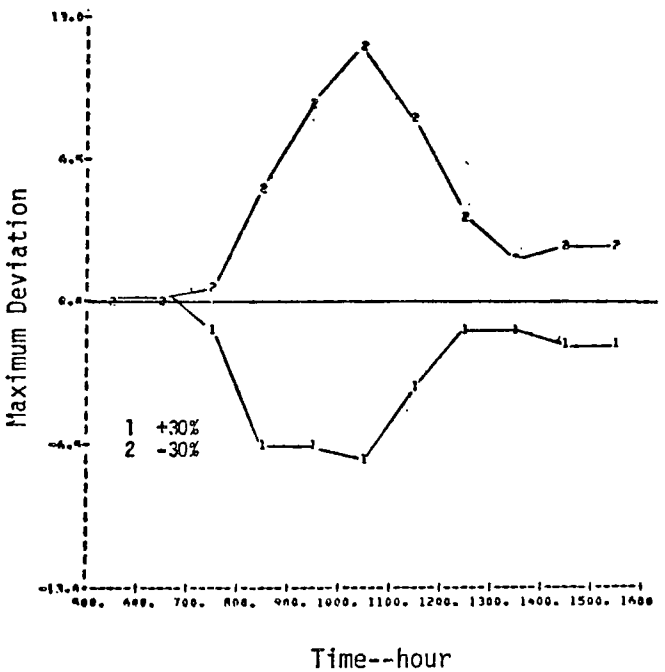

FIGURE IV-59. THE EFFECT--EXPRESSED AS MAXIMUM DEVIATIONS--OF VARIATIONS IN RADIATION INTENSITY FOR NO

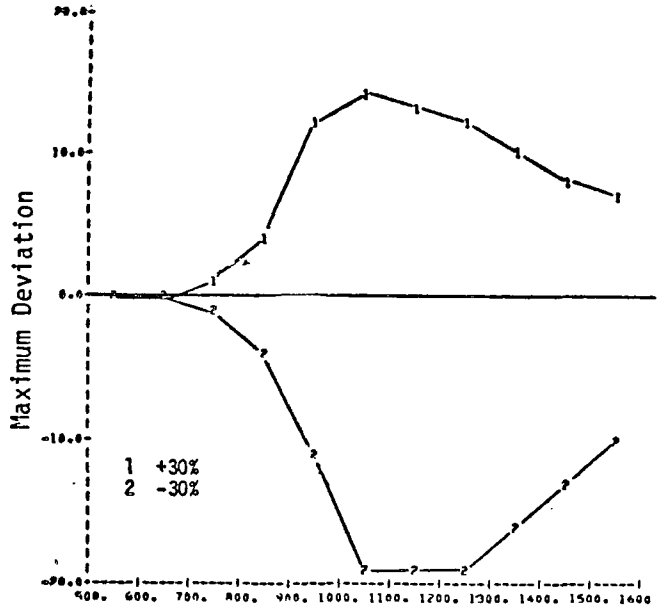

FIGURE IV-60. THE EFFECT--EXPRESSED AS MAXIMUM DEVIATIONS--OF VARIATIONS IN RADIATION INTENSITY FOR O_3

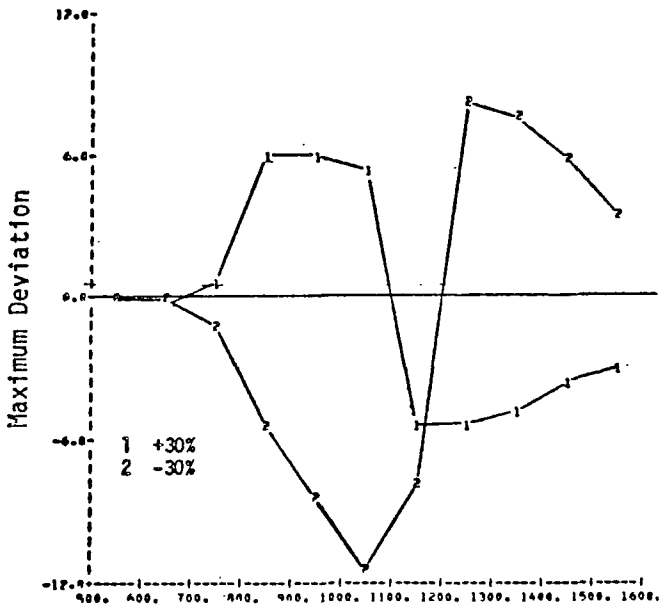

FIGURE IV-61. THE EFFECT--EXPRESSED AS MAXIMUM DEVIATIONS--OF VARIATIONS IN RADIATION INTENSITY FOR NO_2

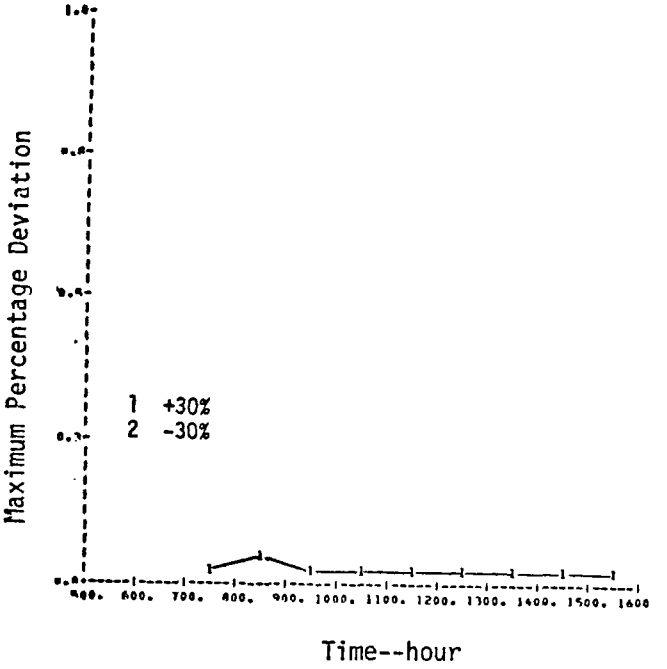

FIGURE IV-62. THE EFFECT--EXPRESSED AS MAXIMUM PERCENTAGE DEVIATIONS--OF VARIATIONS IN RADIATION INTENSITY FOR CO

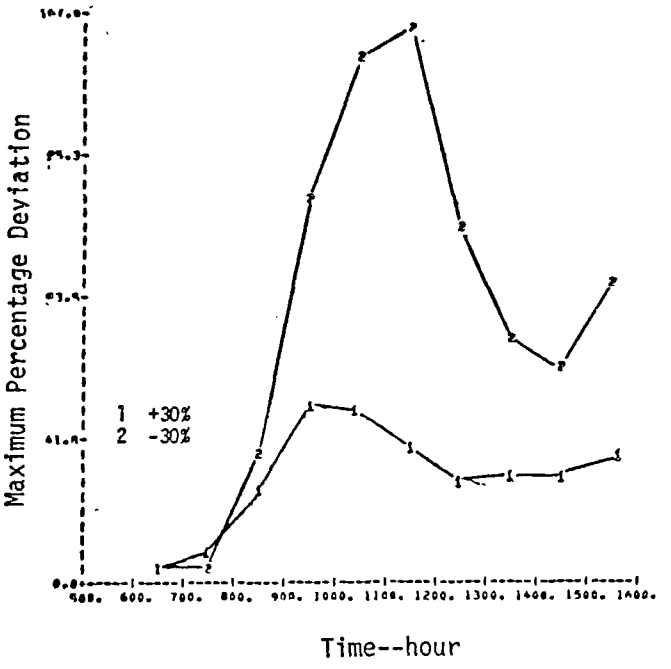

FIGURE IV-63. THE EFFECT--EXPRESSED AS MAXIMUM PERCENTAGE DEVIATIONS--OF VARIATIONS IN RADIATION INTENSITY FOR NO

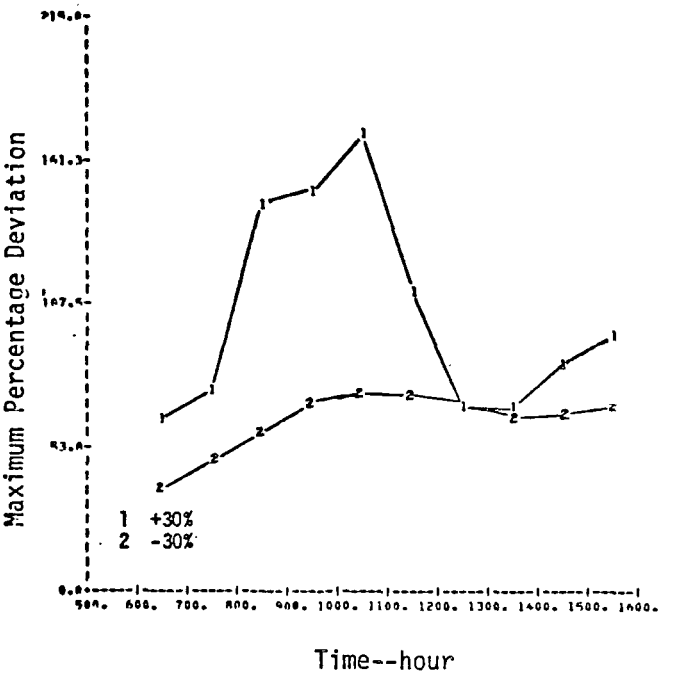

FIGURE IV-64. THE EFFECT--EXPRESSED AS MAXIMUM PERCENTAGE DEVIATIONS--OF VARIATIONS IN RADIATION INTENSITY FOR O_3

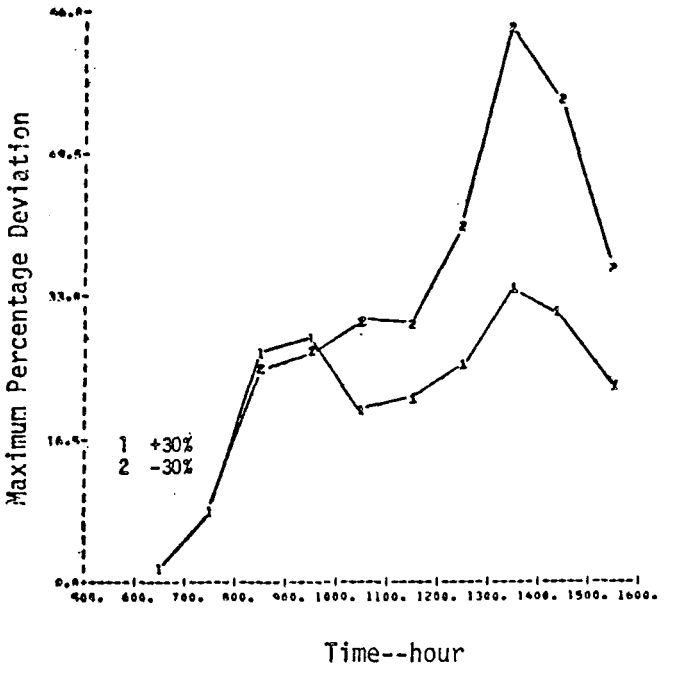

FIGURE IV-65. THE EFFECT--EXPRESSED AS MAXIMUM PERCENTAGE DEVIATIONS--OF VARIATIONS IN RADIATION INTENSITY FOR NO_2

- As in all of the other sensitivity experiments, the effects of varying the radiation intensity are time-dependent, reflecting the fact that the atmosphere plays the role of a reservoir.
- The effect of changing the light intensity is as significant as that of changing the wind speed. Both of these parameters are highly influential in determining ground-level concentrations.
- The effect of increasing the light intensity is to increase the NO_2 concentration levels in the morning and to decrease them in the afternoon. The reverse is true when the light intensity is decreased. These trends, clearly shown in Figures IV-53 and IV-61, can be explained simply as follows. According to the results of smog chamber experiments, the net effect of increasing the light intensity is to accelerate the conversion of NO to NO_2, thereby shifting the peak NO_2 concentration as illustrated in Figure IV-66(a). Consequently, the computed absolute difference shows a crossover at a certain point in time [Figure IV-66(b)]; this result appears both in the average deviation (Figure IV-53) and in the maximum deviation (Figure IV-61). Furthermore, as shown in Figure IV-66(c), a double peak variation occurs if the relative difference (in terms of percentage) is computed. Again, this effect can be observed in Figures IV-57 and IV-65.

6. The Effect of Variations in Emissions Rate

The last parameter we explored in the sensitivity study was the rate of emissions from the various pollutant sources. (Incidentally, this is also the only nonmeteorological parameter we investigated.) The emissions rate in the base case varies both temporally and spatially. Although many interesting sensitivity runs could have been made, we examined only the simplest possible case: We uniformly increased the emissions rate by 15 percent in one run and decreased it by 15 percent in another.*

* Although reactive hydrocarbons are not considered here, we also varied their emissions rate by the same percentages.

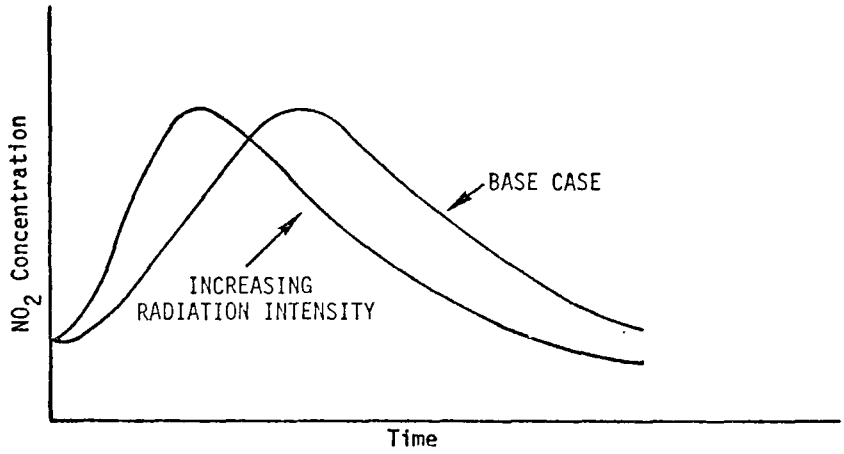

(a) Conversion of NO to NO_2

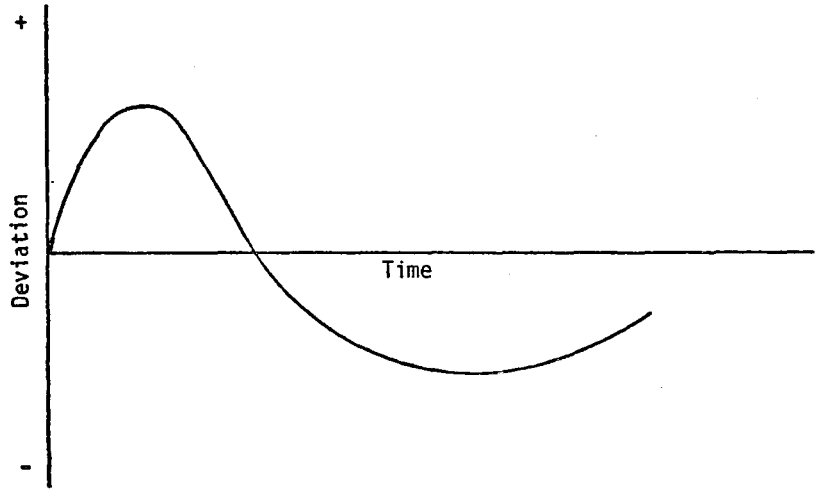

(b) Absolute Difference

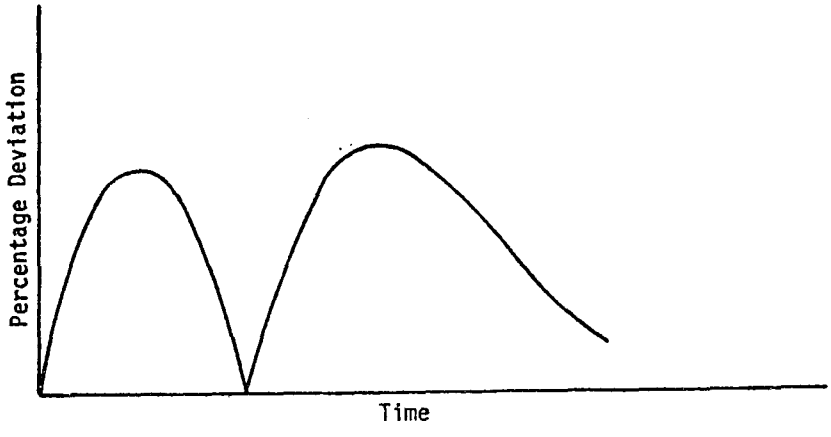

(c) Relative Difference

FIGURE IV-66. SKETCH ILLUSTRATING THE EFFECT OF CHANGES IN RADIATION INTENSITY

Figures IV-67 through IV-82 show the following interesting phenomena:

- The effects of increasing and decreasing the emissions rate are almost identical, particularly in the relative maximum deviations (Figures IV-79 through IV-82), which exhibit nearly perfect matches. This phenomenon is, of course, related to the fact that, as a first approximation, the concentration level is proportional to the emissions rate [see Eq. (IV-9)]. Therefore, among all of the parameters we considered, the emissions rate is probably the only one that may be amenable to a simple linear approach.
- The effect of changing the emissions rate varies not only with time, but also with chemical species. Even at their peaks, the basin-wide average percentage changes in the ground-level concentrations of CO and NO_2 (approximately 6 to 8 percent) are about the same. However, the corresponding maximum changes, with the exception of that for CO (approximately 10 percent), are all greater than the percentage change in the emissions rate (see Figures IV-79 through IV-82).

D. DISCUSSION AND CONCLUSIONS

In the work discussed in this chapter, we studied the sensitivity of the SAI urban airshed model to changes in the input parameters. The variables we explored were random perturbations in wind speed and wind direction, systematic variations in wind speed, horizontal and vertical diffusivities, mixing depth, radiation intensity, and emissions rate. Despite the arbitrary selection of the base case, a close scrutiny of the results of this study shows that they conform qualitatively to what one would expect physically. Thus, we believe that the conclusions drawn from these results have rather general validity.

As we attempted to demonstrate in Section C, many interesting findings or observations can be unearthed from the voluminous data set generated during this study. Two items, briefly discussed below, appear to be the most significant conclusions.

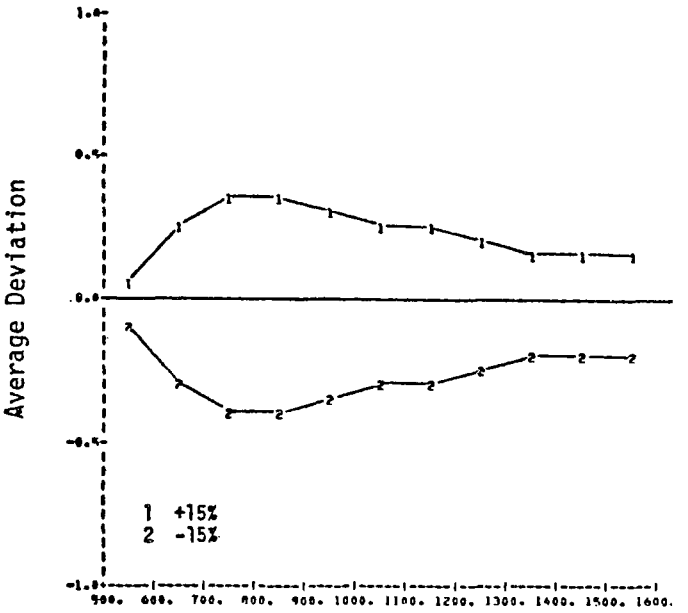

FIGURE IV-67. THE EFFECT--EXPRESSED AS AVERAGE DEVIATIONS--
OF VARIATIONS IN EMISSIONS RATE FOR CO

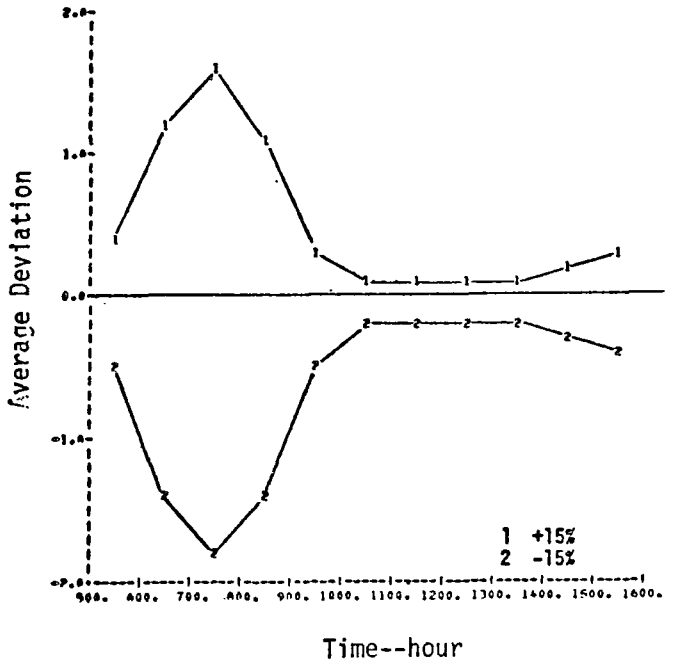

FIGURE IV-68. THE EFFECT--EXPRESSED AS AVERAGE DEVIATIONS--
OF VARIATIONS IN EMISSIONS RATE FOR NO

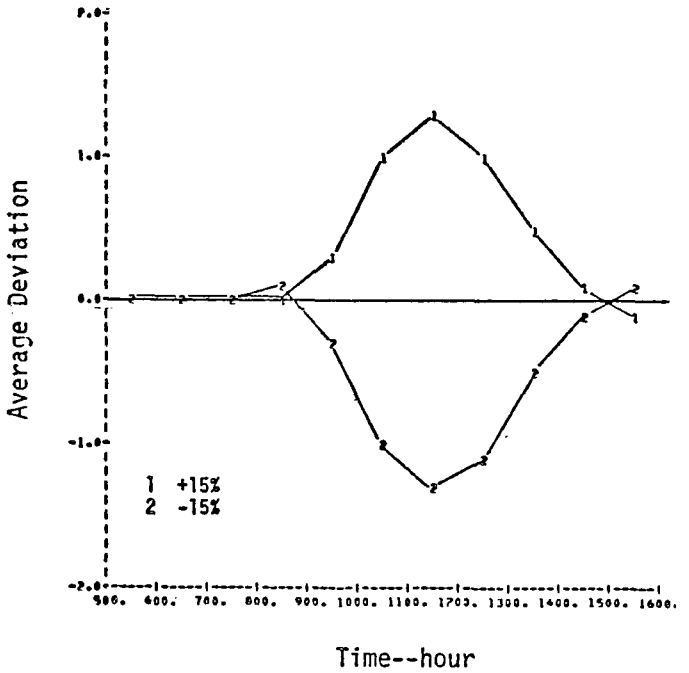

FIGURE IV-69. THE EFFECT--EXPRESSED IN AVERAGE DEVIATIONS-- OF VARIATIONS IN EMISSIONS RATE FOR O_3

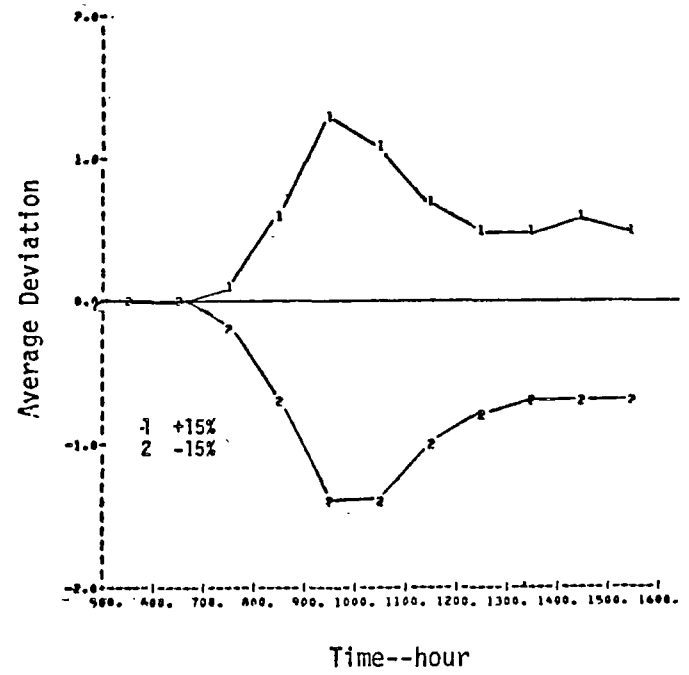

FIGURE IV-70. THE EFFECT--EXPRESSED IN AVERAGE DEVIATIONS-- OF VARIATIONS IN EMISSIONS RATE FOR NO_2

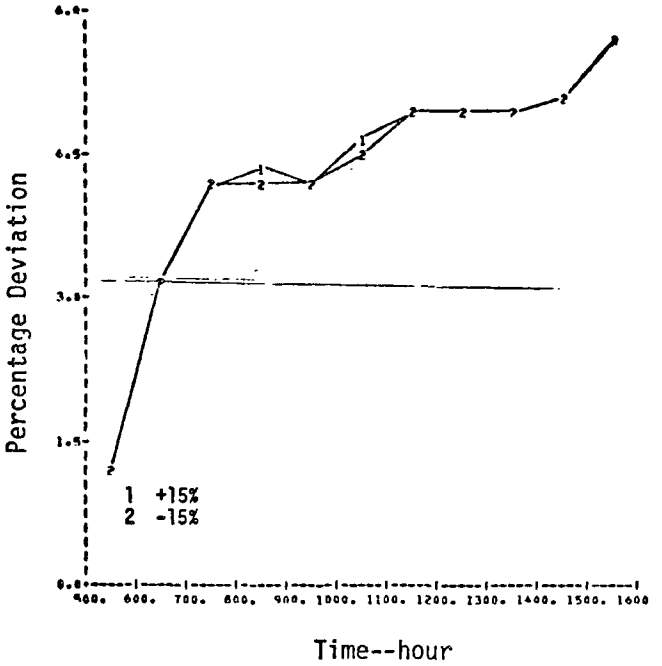

FIGURE IV-71. THE EFFECT--EXPRESSED AS PERCENTAGE DEVIATIONS--OF VARIATIONS IN EMISSIONS RATE FOR CO

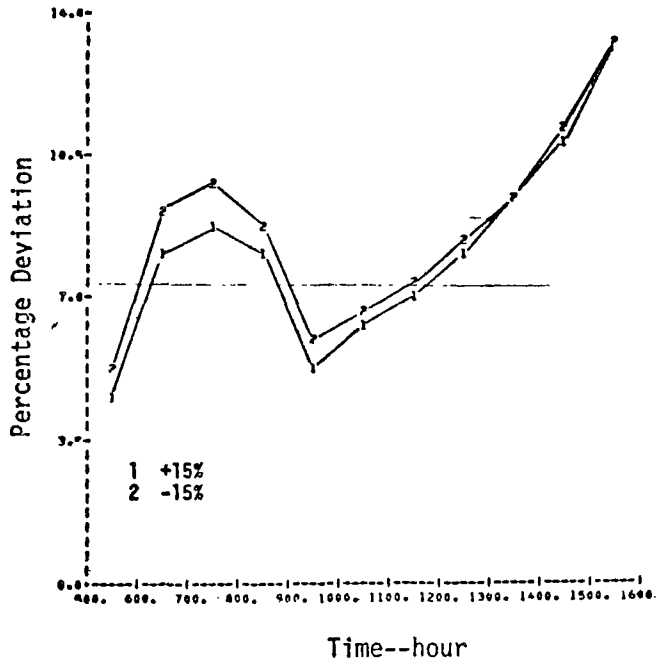

FIGURE IV-72. THE EFFECT--EXPRESSED AS PERCENTAGE DEVIATIONS--OF VARIATIONS IN EMISSIONS RATE FOR NO

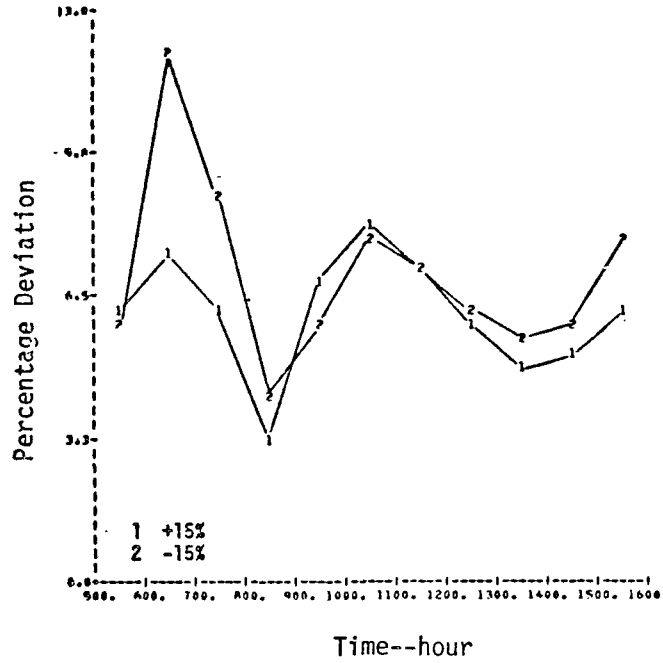

FIGURE IV-73. THE EFFECT--EXPRESSED AS PERCENTAGE DEVIATIONS--OF VARIATIONS IN EMISSIONS RATE FOR O_3

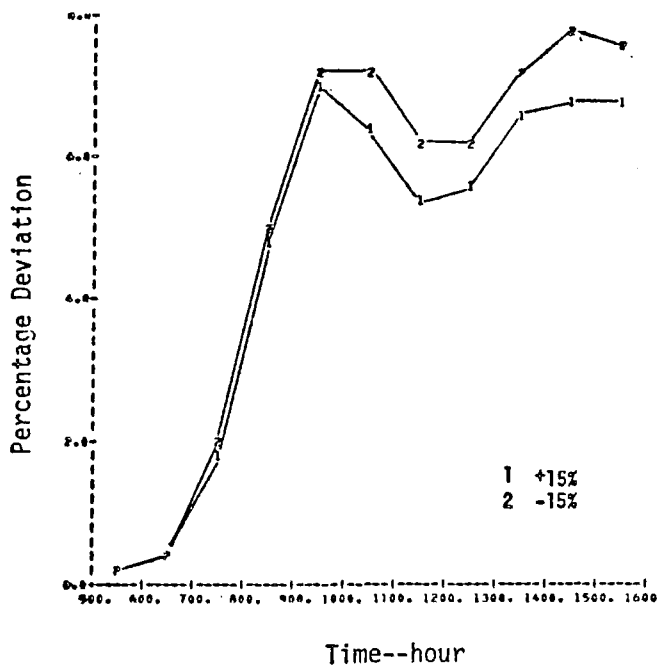

FIGURE IV-74. THE EFFECT--EXPRESSED AS PERCENTAGE DEVIATIONS--OF VARIATIONS IN EMISSIONS RATE FOR NO_2

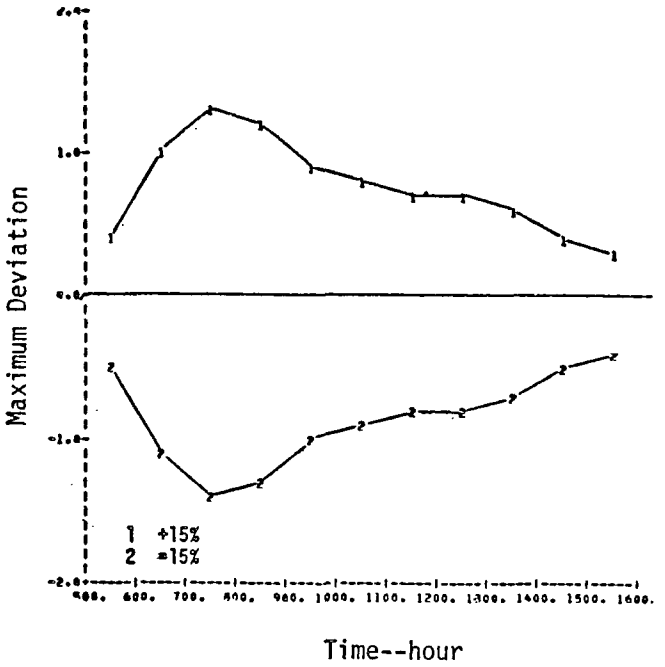

FIGURE IV-75. THE EFFECT--EXPRESSED AS MAXIMUM DEVIATIONS--OF VARIATIONS IN EMISSIONS RATE FOR CO

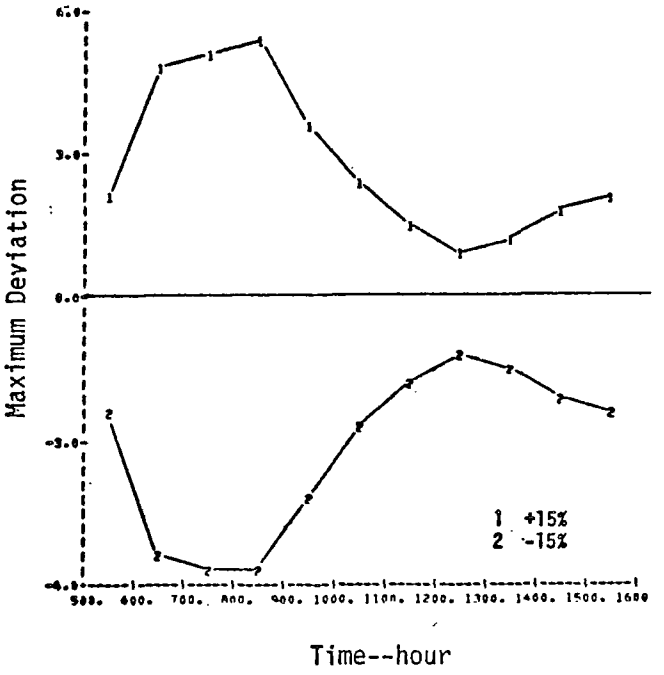

FIGURE IV-76. THE EFFECT--EXPRESSED AS MAXIMUM DEVIATIONS--OF VARIATIONS IN EMISSIONS RATE FOR NO

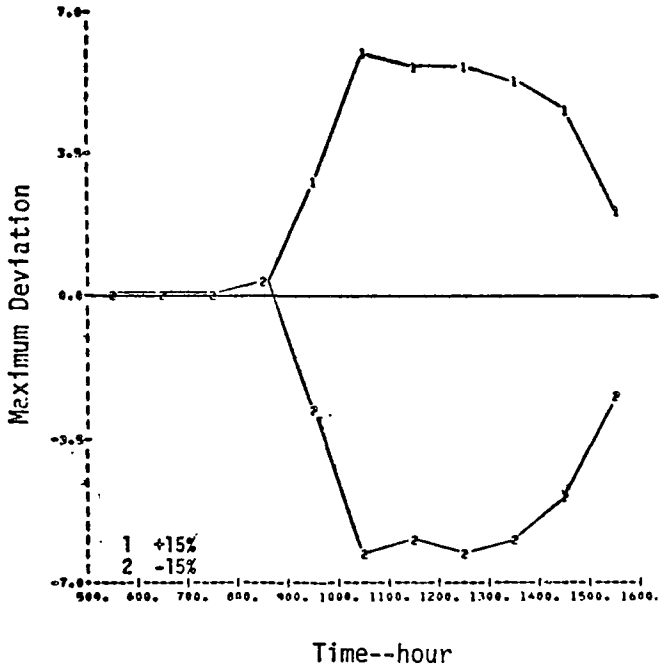

FIGURE IV-77. THE EFFECT--EXPRESSED AS MAXIMUM DEVIATIONS--OF VARIATIONS IN EMISSIONS RATE FOR O_3

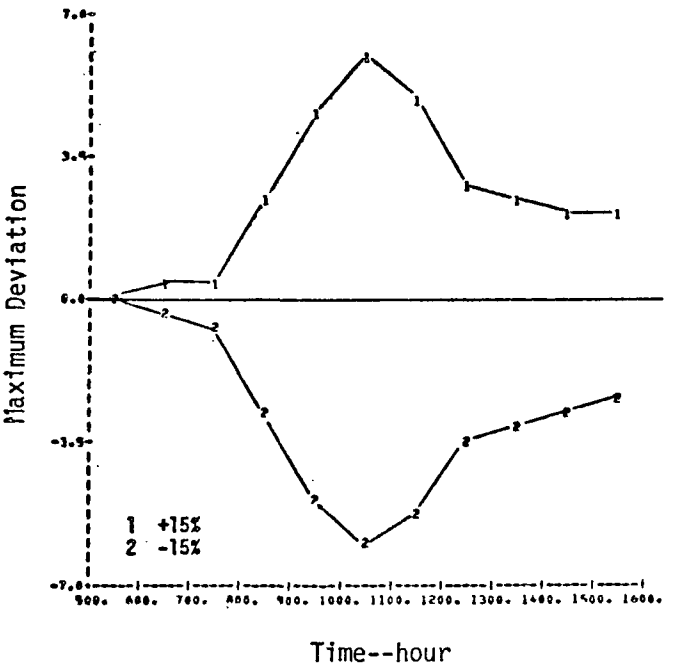

FIGURE IV-78. THE EFFECT--EXPRESSED AS MAXIMUM DEVIATIONS--OF VARIATIONS IN EMISSIONS RATE FOR NO_2

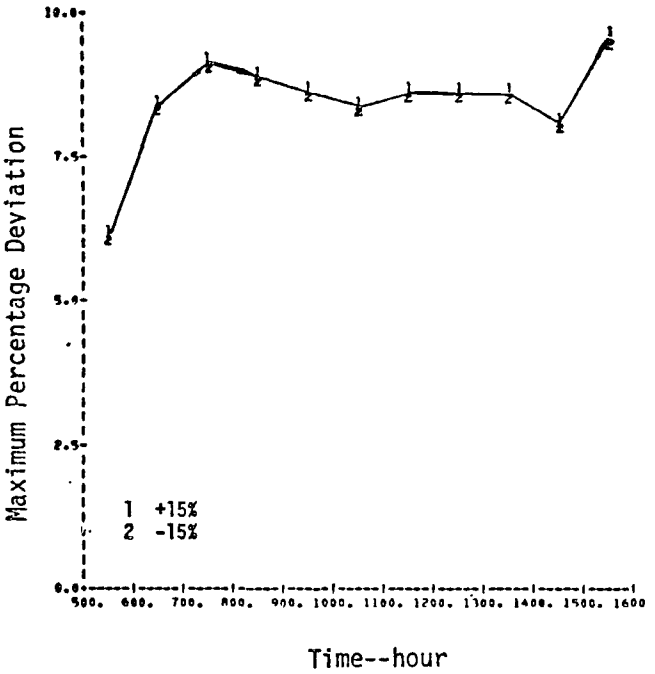

FIGURE IV-79. THE EFFECT--EXPRESSED AS MAXIMUM PERCENTAGE DEVIATIONS--OF VARIATIONS IN EMISSIONS RATE FOR CO

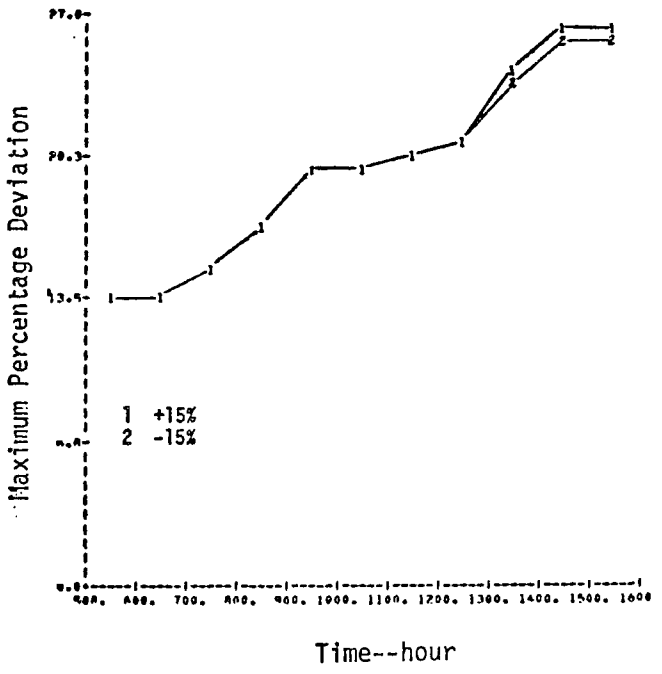

FIGURE IV-80. THE EFFECT--EXPRESSED AS MAXIMUM PERCENTAGE DEVIATIONS--OF VARIATIONS IN EMISSIONS RATE FOR NO

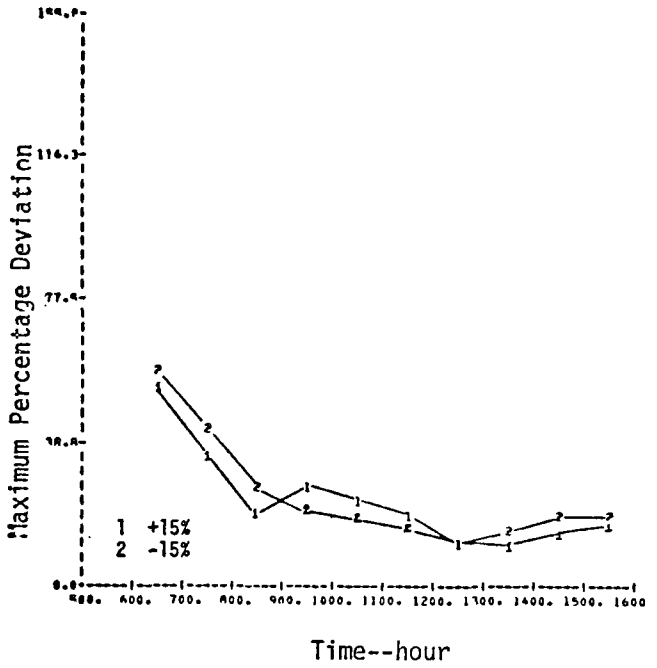

FIGURE IV-81. THE EFFECT--EXPRESSED AS MAXIMUM PERCENTAGE DEVIATIONS--OF VARIATIONS IN EMISSIONS RATE FOR O_3

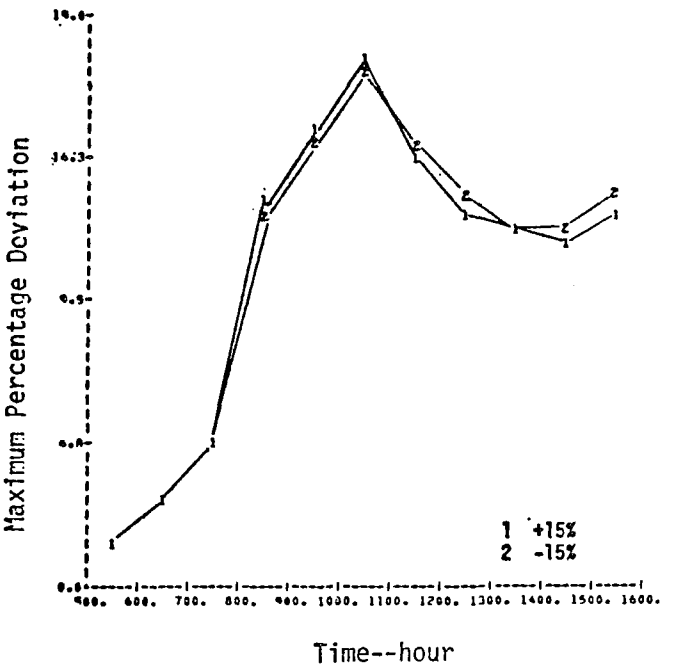

FIGURE IV-82. THE EFFECT--EXPRESSED AS MAXIMUM PERCENTAGE DEVIATIONS--OF VARIATIONS IN EMISSIONS RATE FOR NO_2

1. Justification for a Complex Model

Our study has demonstrated that the sensitivity of the SAI urban airshed model, a complex grid model, to variations in meteorological or emissions parameters is generally characterized by the following features:

- The effects are time-dependent.
- The effects vary spatially.
- The effects differ for different chemical species.
- The effects do not follow a simple rule, such as the inverse proportionality for wind speed.

With the possible exception of the effect due to variations in chemical species [as we stated earlier, Hanna (1973) has developed a box model to account for reactive species], none of the simple box models appear to be able to reproduce these essential features. The reasons for this failure are rather obvious. For example, inadequate or improper handling of the initial concentrations in the box model is responsible for its failure to produce the time-dependent behavior of the effects. Oversimplification in the simulation of advective and diffusive processes apparently makes the simple box model incapable of recreating the detailed spatial distribution of the pollutant concentrations or the correct dependence on the various meteorological and emissions input parameters. Thus, our sensitivity study provides direct evidence that a simple box model is not sufficient to simulate urban air pollution.

2. The Sensitivity of the SAI Model

The results of our assessment of the relative sensitivities of the SAI airshed model to various meteorological and emissions parameters can be used for several purposes:

- To give a rule-of-thumb estimate of the response of the model predictions to changes in the input parameters.
- To provide insights into the expected behavior of the SAI model in particular and into urban airshed models in general.
- To facilitate the development of a repro-model.

This section discusses the overall sensitivities of the SAI urban airshed model. As shown in Figures IV-83 through IV-86, we plotted the response (the peak values of the basin-wide averages) of the model predictions against changes in the input parameters for the four species considered in this study. The following observations emerge from an examination of these curves. First, with the exception of ozone, the slopes of the responses are less steep than those that are inversely proportional to the corresponding changes.* Second, the responses of CO and NO_2 tend to vary linearly in the log-log plot, whereas those of NO and O_3 tend to be nonlinear.

Using the slopes of the reponses as indices, we ranked the various input parameters according to their importance in affecting the model predictions. Table IV-5 presents this ranking.

*In the cases of radiation intensity and emissions rate, the slopes are directly proportional.

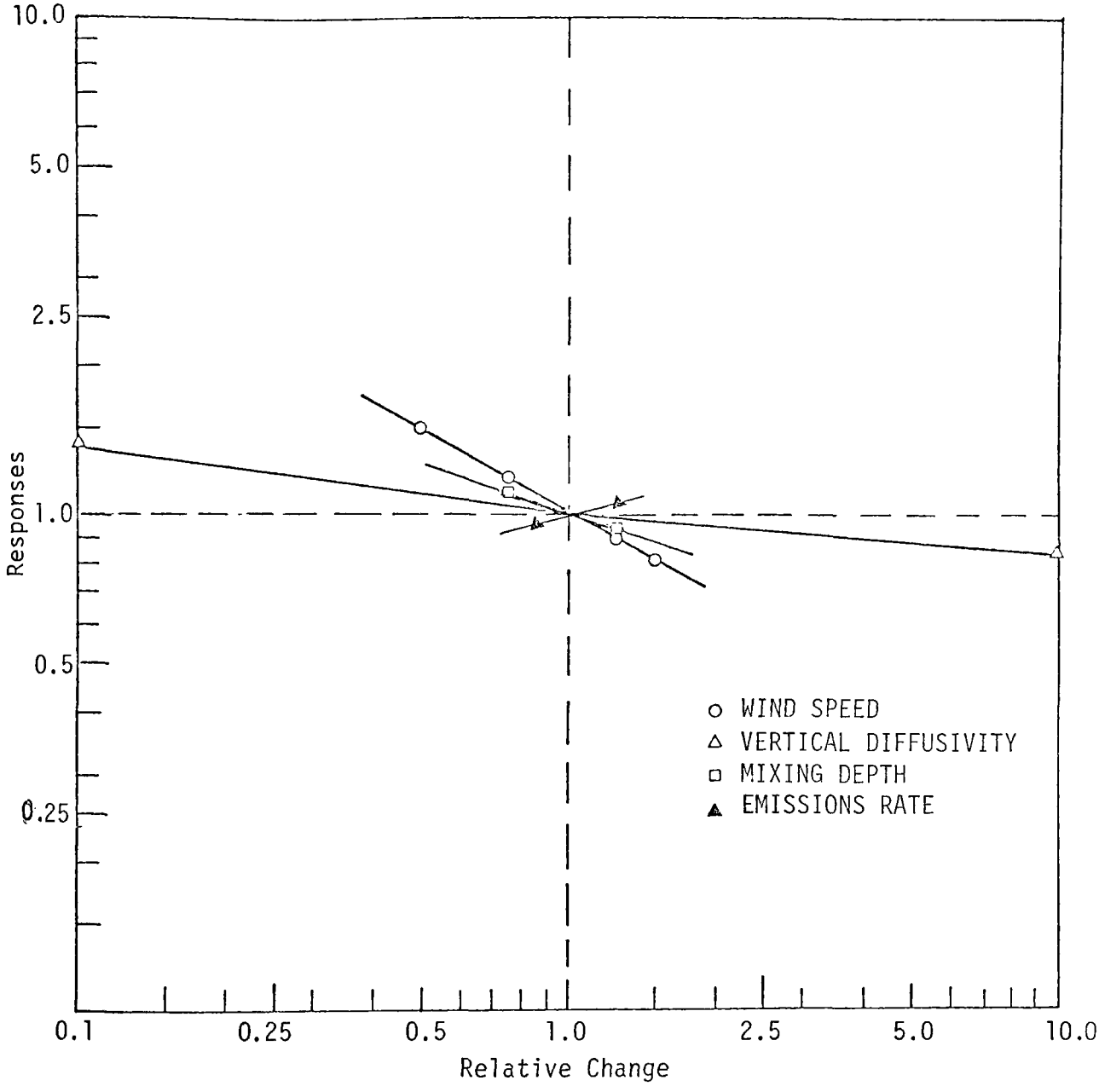

FIGURE IV-83. THE AVERAGE EFFECT OF CHANGES IN INPUT PARAMETERS ON CO CONCENTRATION

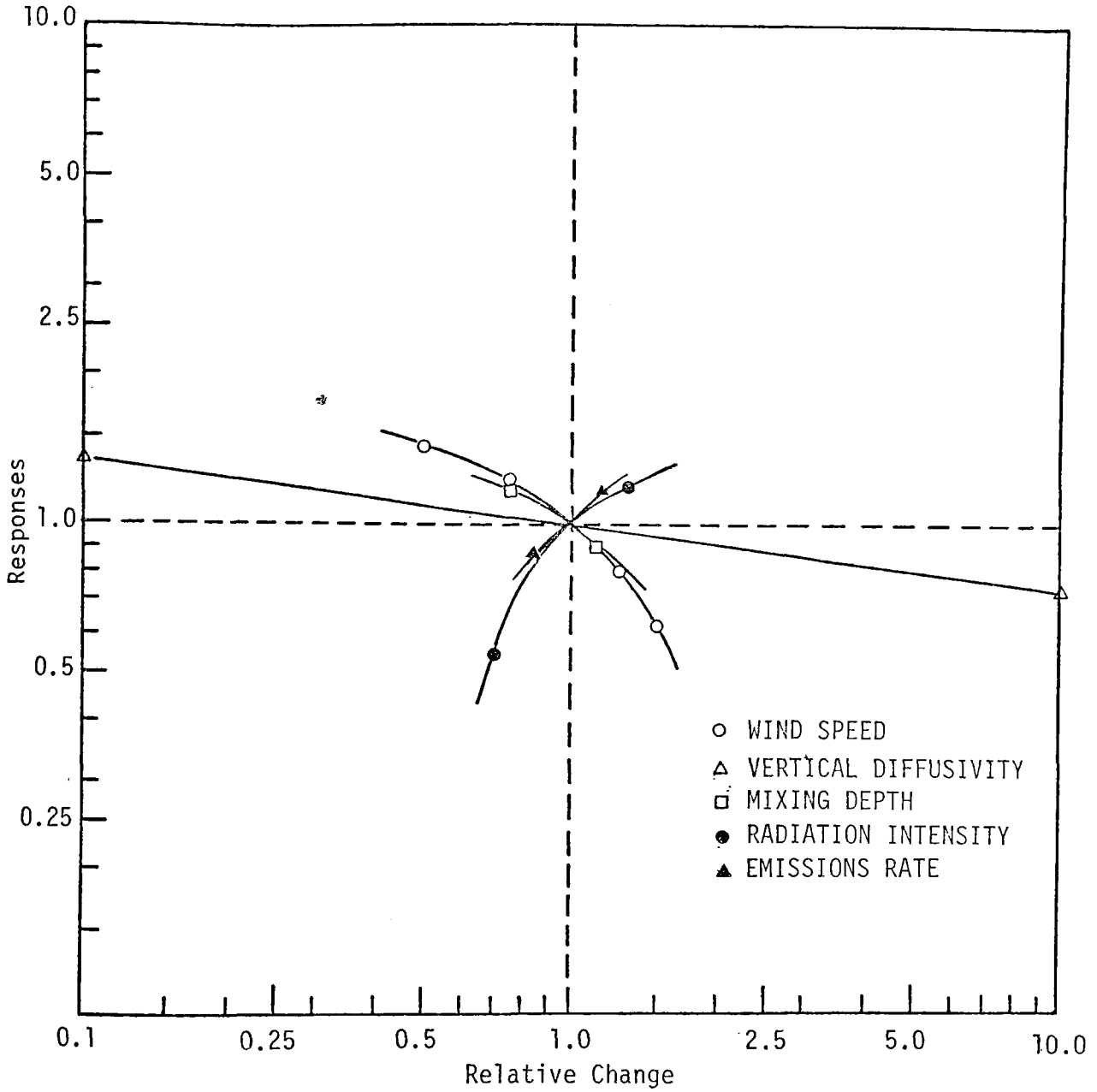

FIGURE IV-84. THE AVERAGE EFFECT OF CHANGES IN INPUT PARAMETERS ON NO CONCENTRATION

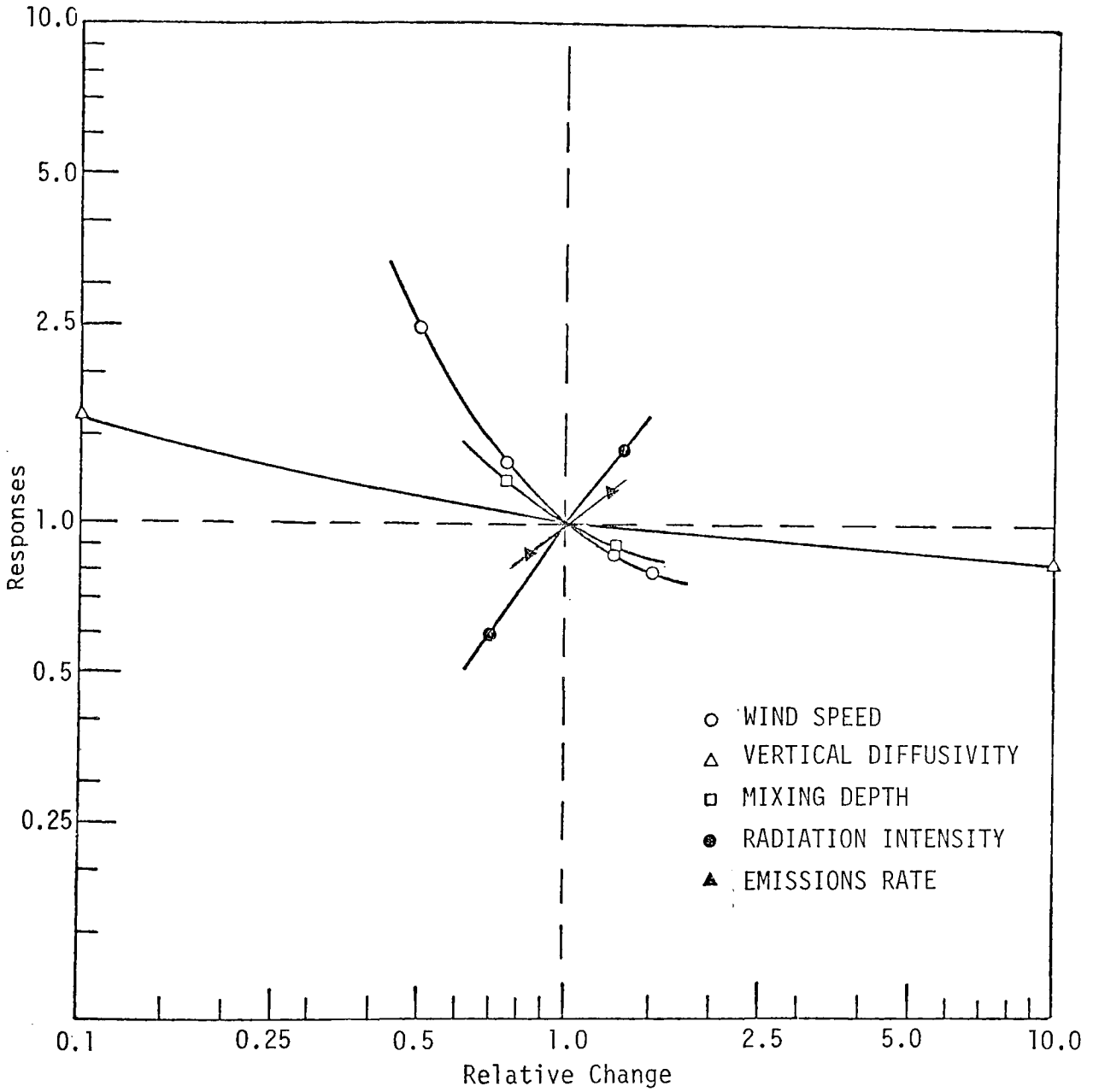

FIGURE IV-85. THE AVERAGE EFFECT OF CHANGES IN INPUT PARAMETERS ON O_3 CONCENTRATION

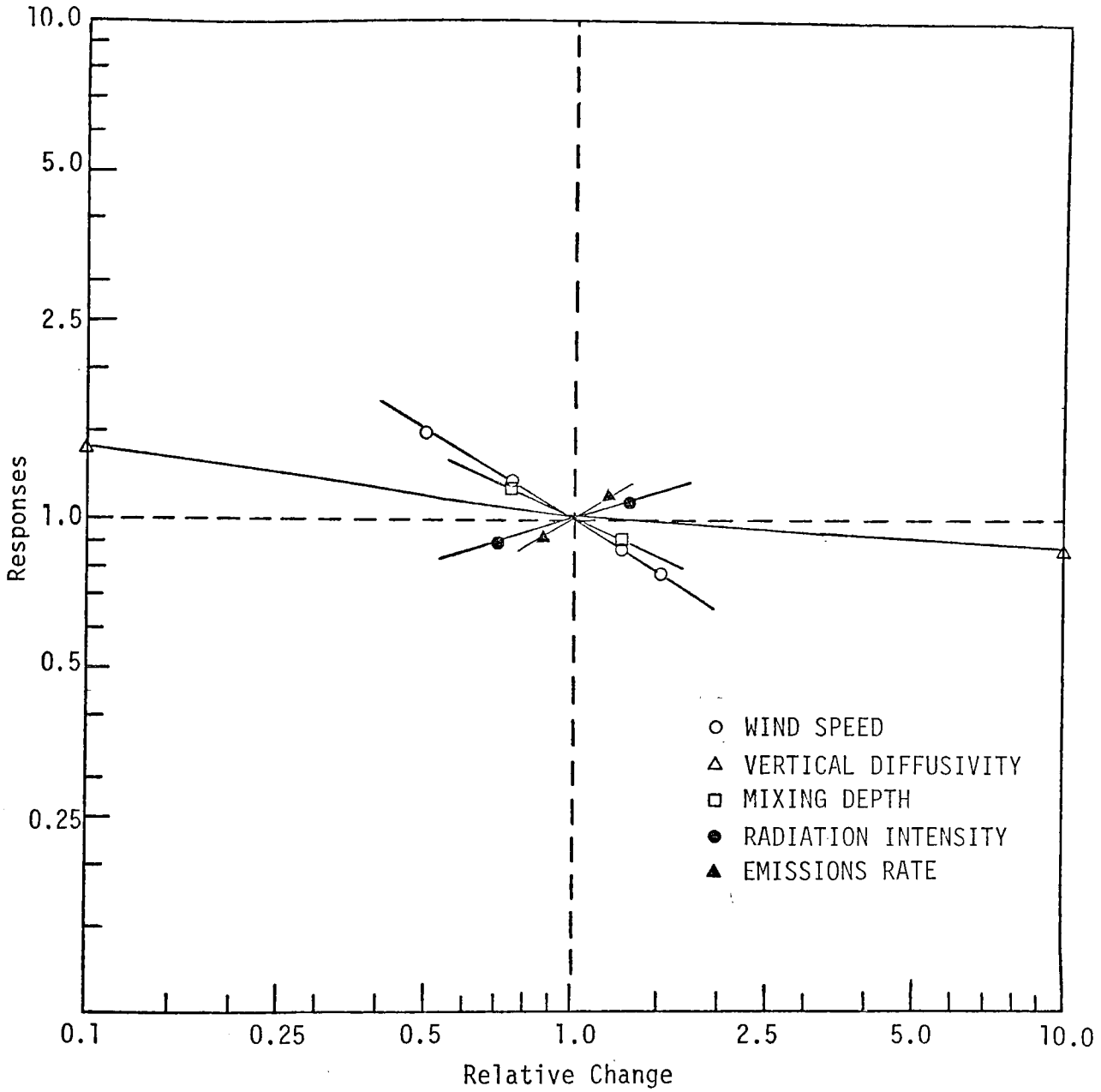

FIGURE IV-86. THE AVERAGE EFFECT OF CHANGES IN INPUT PARAMETERS ON NO_2 CONCENTRATION

Table IV-5

RANKING OF THE RELATIVE IMPORTANCE
OF THE INPUT PARAMETERS

Parameter or Variable	CO	NO	O_3	NO_2
Wind speed	A	A	A	A
Horizontal diffusivity	D	D	D	D
Vertical diffusivity	C	C	C	C
Mixing depth	B	B	B	B
Radiation intensity	D	A	A	B
Emissions rate	B	A	B	B

A = most important.

D = least important.

APPENDIX A
THE NONUNIQUENESS OF LAGRANGIAN VELOCITIES

APPENDIX A
THE NONUNIQUENESS OF LAGRANGIAN VELOCITIES

This appendix demonstrates that Lagrangian velocities, as conventionally defined, may not be unique in an atmospheric turbulent flow. We adapted the derivation we present here from a paper by Dyer (1973).

Consider an air column that is moving through a two-dimensional turbulent atmosphere, as illustrated below:

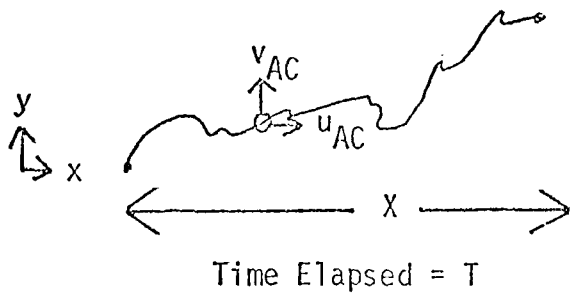

We can obtain the actual velocity of the air column, say, from tracer data, as a function of time (t) and location (x,y); we denote such velocities by $v_{AC}(x,y;t)$.

We can then obtain two types of Lagrangian averages:
a space average,

$$\langle v_{AC} \rangle = \frac{1}{X} \int_0^X v_{AC}(x,y;t)\, dx \quad ,$$

and a time average,

$$\overline{v}_{AC} = \frac{1}{T}\int_0^x v_{AC}(x,y;t)\, dt \quad .$$

Since $u_{AC} = dx/dt$, it follows that

$$\langle v_{AC} \rangle = \frac{1}{x}\int_0^T u_{AC} v_{AC}\, dt$$

$$= \frac{T}{x}\,\overline{u_{AC} v_{AC}}$$

$$= \frac{1}{\overline{u}_{AC}}\,\overline{u_{AC} v_{AC}} \quad .$$

In a turbulent atmosphere, if we assume that

$$u_{AC} = \overline{u}_{AC} + u'_{AC} \quad ,$$

$$v_{AC} = \overline{v}_{AC} + v'_{AC} \quad ,$$

then

$$\langle v_{AC} \rangle = \frac{1}{\overline{u}_{AC}}\left(\overline{u}_{AC}\overline{v}_{AC} + \overline{u'_{AC} v'_{AC}}\right) \quad ,$$

or

$$\langle v_{AC} \rangle - \overline{v}_{AC} = \frac{1}{\overline{u}_{AC}}\,\overline{u'_{AC} v'_{AC}} \quad .$$

Therefore, depending on the turbulence statistics, the two types of average Lagrangian velocities defined earlier can be different.*

* Phillips (1966) and Longuet-Higgins (1969) have pointed out the nonuniqueness of the Lagrangian and Eulerian velocities in studies of ocean currents.

Appendix B
WIND AND DIFFUSIVITY PROFILES IN THE LOWER ATMOSPHERE

APPENDIX B
WIND AND DIFFUSIVITY PROFILES IN THE LOWER ATMOSPHERE

In this appendix, we present a review of the literature dealing with the study of wind profiles and vertical diffusivity profiles in the lowest layer of the atmosphere. The purpose of this review was to estimate the magnitudes and exponents of the wind or vertical diffusivity profiles that commonly occur in an urban atmosphere.

1. Wind Profile

Micrometeorologists have intensively studied the variations of horizontal wind with height. In the 1940s, for example, Deacon (1949) in England and Laikhtman (1944) in the U.S.S.R. carried out comprehensive investigations of vertical profiles of mean wind velocity. They verified that in the surface layer (approximately a few meters above the ground), the logarithmic law for the mean velocity, under the condition that the atmosphere is neutrally stratified, is

$$\frac{u}{u_*} = \frac{1}{k} \ell n \left(\frac{z}{z_0}\right) \quad , \tag{B-1}$$

where u_* is the friction velocity, z_0 is the roughness parameter, and k is the von Karman constant. Departures from adiabatic conditions tend to increase the rate of change of wind speed with height under unstable conditions and to decrease the rate under stable conditions. Therefore, for these adiabatic cases, Laikhtman and Deacon proposed the following formula:

$$\frac{u}{u_*} = \frac{1}{k(1-\beta)} \left[\left(\frac{z}{z_0}\right)^{1-\beta} - 1 \right] \quad . \tag{B-2}$$

They found that the coefficient, a function of atmospheric stability, ranges as follows:

$\beta > 1$ for unstable conditions,
$\beta = 1$ for neutral conditions,
$\beta < 1$ for stable conditions.

Note that in the limiting case of $\beta \to 1$, the above formula reduces to the logarithmic law.

At greater heights within the planetary boundary layer (less than a few hundred meters above the ground), the vertical wind profiles are generally characterized by a power law. For example, the following general relationship has often been used.

$$\frac{u}{u_R} = \left(\frac{z}{z_R}\right)^m \quad , \tag{B-3}$$

where u_R is the wind speed at a reference height z_R. The exponent m depends on the stability of the atmosphere and the roughness of the ground surface. In a neutrally stable atmosphere in open country, the value of m is normally about 1/7, and it increases as the stability increases. DeMarrais (1959) obtained the following values for m:

Stability Class	m
1	0.1
2	0.15
3	0.20
4	0.25
5	0.25
6	0.30

In a recent study, Jones et al. (1971) also confirmed the dependence of m on the temperature lapse rate at urban sites. They found the following quantitative relationships between m and $\Delta\theta$, the potential temperature difference in °C between 530 and 30 feet:

$$m \simeq 0.2 \quad , \quad \Delta\theta < 0 \quad ,$$
$$m \simeq 0.21 \quad , \quad \Delta\theta = 0 \quad ,$$
$$m \simeq 0.33\ \Delta\theta + 0.21 \quad , \quad 0 < \Delta\theta < 0.75 \quad .$$

The surface roughness depends on the type of terrain. Typical values of m for different types of terrain, estimated from experimental data collected under fair weather conditions, are as follows:

Type of Terrain	Davenport (1965) Estimate	Shellard (1965) Estimate
Open country	0.16	0.16
Suburbs	0.28	--
Metropolitan	0.40	--

In summary, in an urban environment, the wind speed increases with height according to the power law. The exponent in the power law, being a function of atmospheric stability, is likely to be in the range $0.4 > m > 0.2$.

2. Vertical Diffusivity Profile

According to similarity analysis, the vertical diffusivity profile in the surface layer is intimately related to the wind profile we discussed above. In this layer, the inertia force is usually small compared with the viscous force. And, if we further assume that the horizontal pressure gradient is also negligible, the momentum equation finally reduces to

$$\frac{\partial}{\partial z}\left(K_M \frac{\partial u}{\partial z}\right) = 0 \quad . \qquad \text{(B-4)}$$

It then follows that, if the horizontal wind velocity is prescribed by a power law, such as that shown in Eq. (B-3), the vertical diffusion coefficient for momentum, K_M, can be described by a conjugate power law of the following form (with the subscript M suppressed):

$$K = K(z_R) \cdot \left(\frac{z}{z_R}\right)^n \quad , \tag{B-5}$$

where $n = 1 - m$. There is considerable evidence that the Reynolds analogy holds in the surface layer; i.e., the vertical diffusion coefficient, K_C, is proportional to the coefficient of vertical momentum transfer, K_M. Thus, the vertical diffusion coefficient for species can be described by the same expression, i.e., Eq. (B-5).

Many field experiments carried out recently (Ikebe and Shimo, 1972; Cohen et al., 1972) have verified the power law profile and have shown that vertical diffusivity varies with atmospheric stability in a manner similar to that of the horizontal wind, except that the effect of stability on vertical diffusivity appears to be stronger. This may result in the observed increases in mass diffusivity at sunrise and decreases at sunset that are much more pronounced than the observed diurnal variations in the momentum diffusivity (Israel and Horbert, 1970). Theoretically, the exponent in the power law, n, would be expected to be less than, equal to, or larger than one, depending on whether the atmosphere is stable, neutral, or unstable (Deacon, 1949). However, using field measurements of the vertical thoron profiles in the lowest meter of the atmosphere, Ikebe and Shimo (1972) estimated that $n = 1.2$ for neutral conditions, and $n = 1.3$ to 1.5 for unstable conditions. The above results agree with values derived from hourly average radon-gas concentration measurements made at greater heights (up to 271 meters) by Cohen et al. (1972). They found that $n = 1.4$ for stable conditions, $n = 1.2$ for neutral conditions, and $n = 1.5$ for unstable conditions. In summary, the range of variations in n, according to available experimental results, appears to fall within $1.5 > n > 1.2$.

Appendix C

A THEORETICAL ANALYSIS OF THE EFFECT OF RANDOM PERTURBATIONS OF THE MEASURED WIND

APPENDIX C
A THEORETICAL ANALYSIS OF THE EFFECT OF RANDOM PERTURBATIONS OF THE MEASURED WIND

In this appendix, we briefly examine the effect of random perturbations of the wind speed and wind direction measurements on the concentration field from a theoretical point of view. For the sake of simplicity, we use the following two-dimensional diffusion equation to illustrate this effect:

$$\frac{\partial c}{\partial t} + \frac{\partial}{\partial x}(uc) = \frac{\partial}{\partial z}\left(K_z \frac{\partial c}{\partial z}\right) \quad , \qquad \text{(C-1)}$$

where the last term represents the vertical diffusion.

Conceptually, we can see that the measured wind, u, used in Eq. (C-1) consists of a small and random part superimposed on the true wind. The random part can arise either as a result of instrumentation errors or data reduction procedures. Let

u_T = the true wind,

$\tilde{u}$ = the random error in the wind speed, wind direction, or both,

$\langle c \rangle$ = the resultant concentrations if the true wind is used,

$\tilde{c}$ = the deviation from the true concentration due to random error in wind speed, wind direction, or both.

Then,

$$u = u_T + \tilde{u} \quad , \qquad \text{(C-2)}$$

$$c = \langle c \rangle + \tilde{c} \quad . \qquad \text{(C-3)}$$

Substituting Eqs. (C-2) and (C-3) into Eq. (C-1) and taking the ensemble average, we obtain

$$\frac{\partial c}{\partial t} + \frac{\partial}{\partial x}\left(u_T \langle c \rangle\right) = \frac{\partial}{\partial x}\left(K_H \frac{\partial \langle c \rangle}{\partial x}\right) + \frac{\partial}{\partial z}\left(K_v \frac{\partial \langle c \rangle}{\partial z}\right) \quad , \tag{C-4}$$

where we have assumed that

$$\langle \tilde{u}\tilde{c} \rangle = -K_H \frac{\partial \langle c \rangle}{\partial x} \quad , \tag{C-5}$$

as we did in the treatment of eddy diffusion. Thus, the net effect of the random perturbations of the wind is to introduce a diffusion-like term in the atmospheric diffusion equation. This finding is, of course, not surprising because diffusion processes are characterized by their ability to promote randomness, as clearly demonstrated in our numerical experiments (Section C) by negative average deviations.

To estimate the magnitudes of the artificial diffusion coefficients created by the random perturbations, we interpret Prandtl's mixing length theory here as

$$K_H \sim (\Delta x)^2 \left(\frac{\tilde{u}}{L}\right) \quad , \tag{C-6}$$

where L is the separation between the two stations where the winds have been randomly perturbed For the case in which wind speed is randomly varied at every grid point,

$$\tilde{u} = 1 \text{ mph} \quad ,$$

$$L = \Delta x = 2 \text{ miles} \quad .$$

Thus, we obtain

$$K_H \sim 1.4 \times 10^3 \text{m}^2 \text{ sec}^{-1}$$

For random perturbations of the measured wind speed at every monitoring station, we have

$$\Delta x = 2 \text{ miles}$$

$$L \sim 10 \text{ miles}$$

Thus,

$$K_H \sim 0.28 \times 10^3 \text{ m}^2 \text{ sec}^{-1} \quad .$$

The effect of random perturbations of the measured wind angles can be similarly estimated if we assume an average wind speed. As shown in the following sketch,

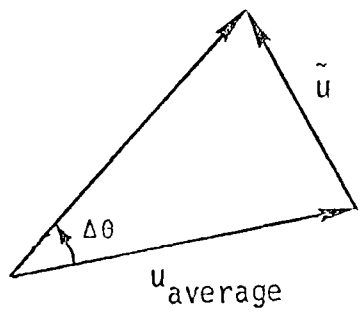

the equivalent random wind speed is approximately

$$\tilde{u} \sim u_{average} \sin \Delta\theta \quad .$$

Since $\Delta\theta = 22.5°$ in our numerical experiment, using an average wind speed of 5 mph yields

$$\tilde{u} \sim 2 \text{ mph} \quad .$$

Consequently, the artificial diffusivity should be twice as high as what we estimated before. This apparently explains the reason why, in our numerical experiments, the effect of random perturbations in wind direction is more pronounced than that of random perturbations in wind speed.

REFERENCES

Ackerman, B. (1974), "METROMEX: Wind Fields Over St. Louis in Undisturbed Weather," Bull. Am. Meteorol. Soc., Vol. 55, p. 93.

Calder, K. L. (1949), "Eddy Diffusion and Evaporation in Flow over Aerodynamically Smooth and Rough Surfaces: A Treatment Based on Laboratory Laws of Turbulent Flow with Special Reference to Conditions in the Lower Atmosphere," Quart. J. Mech. and Appl. Math., Vol. 12, pp. 153-176.

_____(1971), "Some Applications of Generalized Similarity Analysis to the Theory of Atmospheric Diffusion and Evaporation," Symp. on Air Pollution, Turbulence, and Diffusion, Las Cruces, New Mexico.

Cohen, L. D., S. Barr, R. Krablin, and H. Newstein (1972), "Steady-State Vertical Turbulent Diffusion of Radon," J. Geophys. Res., Vol. 77, No. 15, p. 2654.

Davenport, A. G. (1965), "The Relationship of Wind Structures to Wind Loading," Proc. Conf. on Wind Effects on Buildings and Structures, H.M.S.O., London.

Deacon, E. L. (1949), "Vertical Diffusion in the Lowest Layers of the Atmosphere," Quart. J. Roy. Meteorol. Soc., Vol. 75, p. 323.

DeMarrais, G. A. (1959), "Wind Speed Profiles at Brookhaven National Laboratory," J. Appl. Meteorol., Vol. 16, p. 181.

Dilley, J. F., and K. T. Yen (1971), "Effect of a Mesoscale Type Wind on the Pollutant Distribution from a Line Source," Atmos. Environ., Vol. 5, pp. 843-851.

Dyer, A. J. (1973), J. Atmos. Sci., Vol. 30, pp. 510-513.

Egan, B. A., and J. R. Mahoney (1972), "Numerical Modeling of Advection and Diffusion of Urban Area Source Pollutants," J. Appl. Meteorol., Vol. 11, pp. 312-322.

Eschenroeder, A. Q., and J. R. Martinez (1972), "Evaluation of a Photochemical Pollution Simulation Model," General Research Corporation, Santa Barbara, California.

General Research Corporation (1972), "Evaluation of a Diffusion Model of Photochemical Smog Simulation," EPA-R4-73-012, Volume A (CR-1-273), General Research Corporation, Santa Barbara, California.

Hameed, S. (1974), "Modelling Urban Air Pollution," Atmos. Environ., Vol. 8, pp. 555-561.

Hanna, S. R. (1973), "A Simple Dispersion Model for the Analysis of Chemically Reactive Pollutants," Atmos. Environ., Vol. 7, pp. 803-817.

_____ (1972), "A Simple Model for Calculating Dispersion from Urban Area Sources," J. Air Poll. Contr. Assoc., Vol. 21, pp. 774-777.

Hecht, T. A., P. M. Roth, and J. H. Seinfeld (1973), "Mathematical Simulation of Atmospheric Photochemical Reactions: Model Development, Validation, and Application," Report R73-28, Systems Applications, Incorporated, San Rafael, California.

Horowitz, A., W. S. Meisel, and D. C. Collins (1973), "The Application of Repro-Modeling to the Analysis of a Photochemical Air Pollution Model," EPA-650/4-74-001, U.S. Environmental Protection Agency, Durham, North Carolina.

Ikebe, Y., and M. Shimo (1972), "Estimation of the Vertical Turbulent Diffusivity from Thoron Profiles," Tellus, Vol. XXIV, No. 1, p. 29.

Israel, H., and M. Horbert (1970), "Tracing Atmospheric Eddy Mass Transfer by Means of Neutral Radioactivity," J. Geophys. Res., Vol. 75, No. 12, p. 2291.

Jones, P. M., M.A.B. de Larrinaga, and C. B. Wilson (1971), "The Urban Wind Velocity Profile," Atmos. Environ., Vol. 5, p. 89.

Laikhtman, D. L. (1944) "Profile of Wind and Interchange in the Layer of the Atmosphere near the Ground," Bull. Acad. Sci., U.S.S.R., Geog. and Geophys., Ser. 8, No. 1.

Lamb, R. G., and J. H. Seinfeld (1974), "Discussions on 'A Simple Dispersion Model for the Analysis of Chemical Reactive Pollutants'," Atmos. Environ., Vol. 8, pp. 527-529.

_____ (1973), "Mathematical Modeling of Urban Air Pollution--General Theory," Environ. Sci. Tech., Vol. 7, pp. 253-261.

Liu, M. K., D. C. Whitney, S. D. Reynolds, and P. M. Roth (1973), "Automation of Meteorological and Air Quality Data for the SAI Urban Airshed Model," Report R73-SAI-32, Systems Applications, Incorporated, San Rafael, California.

Liu, M. K., and J. H. Seinfeld (1974), "A Comparison of the Grid and Trajectory Models of Urban Air Pollution," American Meteorological Society/World Meteorology Organization, Symposium on Atmospheric Diffusion and Air Pollution, Santa Barbara, California.

Longuet-Higgins, M. S. (1969), Deep-Sea Res., Vol. 16, pp. 431-447.

Monin, A. S., (1959), "Turbulent Diffusion in the Surface Layer Under Stable Stratification," Advances in Geophysics, Vol. 6, pp. 429-436.

Monin, A. S., and A. M. Yaglom (1971), Statistical Fluid Mechanics, J. L. Lumley, ed., (M.I.T. Press, Cambridge, Massachusetts).

Orszag, S. A. (1970), "Transform Method for Calculation of Vector-Coupled Sums: Application to the Spectral Form of the Vorticity Equation," J. Atmos. Sci., Vol. 27, pp. 890-895.

_____ (1971), "Numerical Simulation of Incompressible Flows Within Simple Boundaries: Accuracy," J. Fluid Mech., Vol. 49, pp. 75-113.

Orszag, S. A., and M. Israeli (1974), "Numerical Simulation of Viscous Incompressible Flows," Annual Rev. of Fluid Mech., Vol. 6, p. 281.

Pacific Environmental Services (1973), "Controlled Evaluation of the Reactive Environmental Simulation Model (REM)," EPA R4-73-013a, Volume I, Pacific Environmental Services, Incorporated, Santa Monica, California.

Phillips, O. M. (1966), The Dynamics of Upper Ocean (Cambridge University Press, Cambridge, England).

Price, H. S., R. S. Varga, and J. E. Warren (1966), J. Math. Physics, Vol. 45, p. 301.

Reynolds, S. D., M. K. Liu, T. A. Hecht, P. M. Roth, and J. H. Seinfeld (1974), "Mathematical Modeling of Photochemical Air Pollution: III. Evaluation of the Model," Atmos. Environ., Vol. 8, pp. 563-596.

_____ (1973), "Further Development and Evaluation of a Simulation Model for Estimating Ground Level Concentrations of Photochemical Pollutants," Report R73-19, Systems Applications, Incorporated, Beverly Hills (now San Rafael), California.

Reynolds, S. D., P. M. Roth, and J. H. Seinfeld (1973), "Mathematical Modeling of Photochemical Air Pollution: I. Formulation of the Model," Atmos. Environ., Vol. 7, pp. 1033-1061.

Roberts, O.F.T. (1923), "The Theoretical Scattering of Smoke in a Turbulent Atmosphere," Proc. Roy. Soc. A., Vol. 104, pp. 640-654.

Roth, P. M., P.J.W. Roberts, M. K. Liu, S. D. Reynolds, and J. H. Seinfeld (1974). "Mathematical Modeling of Photochemical Air Pollution: II. A Model and Inventory of Pollutant Emissions," Atmos. Environ., Vol. 8, pp. 97-130.

Seinfeld, J. H. (1970), "Mathematical Models of Air Quality Control Regions," in Development of Air Quality Standards (Charles Merill Press, Columbus, Ohio).

Shellard, H. C. (1965), "The Estimation of Design Wind Speeds," Proc. Conf. on Wind Effects on Building and Structures, H.M.S.O., London.

Sklarew, R. C., A. J. Fabric, and J. E. Prager (1971), "A Particle-in-Cell Method for Numerical Solution of the Atmospheric Diffusion Equation, and Applications to Air Pollution Problems--Final Report," Systems, Science, and Software, La Jolla, California.

Smith, F. B. (1957), "The Diffusion of Smoke from a Continuous Elevated Point-Source into a Turbulent Atmosphere," J. Fluid Mech., Vol. 2, pp. 49-76.

Walters, T. S. (1969), "The Importance of Diffusion Along the Mean Wind Direction for a Ground-Level Crosswind Line Source," Atmos. Environ., Vol. 3, pp. 461-466.

Yordanov, D. (1965), "Diffusion from a Point Source in a Surface Air Layer with Unstable Stratification," Akad. Nauk Bolgar. Sofia; Doklady, Vol. 18, pp. 109-112.

_____ (1968), "On Some Asymptotic Formulae Describing Diffusion in the Surface Layer of the Atmosphere," Atmos. Environ., Vol. 2, pp. 167-180.

TECHNICAL REPORT DATA
(Please read Instructions on the reverse before completing)

1. REPORT NO.	2.	3. RECIPIENT'S ACCESSION NO.
EPA-600/4-76-016 a		

4. TITLE AND SUBTITLE	5. REPORT DATE
CONTINUED RESEARCH IN MESOSCALE AIR POLLUTION SIMUALTION MODELING. VOLUME I. Assessment of Prior Model Evaluation Studies and Analysis of Model Validity and Sensitivity	May 1976
	6. PERFORMING ORGANIZATION CODE
7. AUTHOR(S)	8. PERFORMING ORGANIZATION REPORT NO.
M.K. LIU, D.C. WHITNEY, J.H. SEINFELD, AND P.M. ROTH	EF75-23
9. PERFORMING ORGANIZATION NAME AND ADDRESS	10. PROGRAM ELEMENT NO.
SYSTEMS APPLICATIONS, INC. 950 NORTHGATE DRIVE SAN RAFAEL, CALIFORNIA 94903	1AA009
	11. CONTRACT/GRANT NO.
	68-02-1237
12. SPONSORING AGENCY NAME AND ADDRESS	13. TYPE OF REPORT AND PERIOD COVERED
ENVIRONMENTAL SCIENCES RESEARCH LABORATORY OFFICE OF RESEARCH AND DEVELOPMENT U.S. ENVIRONMENTAL PROTECTION AGENCY RESEARCH TRIANGLE PARK, N.C. 27711	FINAL REPORT 6/74-6/75
	14. SPONSORING AGENCY CODE
	EPA-ORD

15. SUPPLEMENTARY NOTES

16. ABSTRACT

This report summarizes three independent studies: an analysis of prior evaluative studies of three mesoscale air pollution prediction models (two trajectory models and one grid model), an examination of the extent of validity of each type of model, and an analysis of the sensitivity of grid model predictions to changes in the magnitudes of key input variables. The analysis of prior studies showed that the three models evaluated generally reproduced measured ground-level pollutant concentrations with less than acceptable accuracy. This outcome is the result partly of problems of inadequacies in the models themselves and partly of the nonrepresentativeness of the measurement data. In the validity study, the results indicate that numerical diffusion can introduce significant error in the grid model, whereas neglect of wind shear and vertical transport are most detrimental in the trajectory approach. The sensitivity analysis assessed the change in magnitude of predicted atmospheric pollutant concentrations due to variations in wind speed, diffusivity, mixing depth, radiation intensity, and emissions rate. The results of the sensitivity analysis showed that variations in these key input variables influence predictions according to the following order of decreasing influence: wind speed, emissions rate, radiation intensity, mixing depth, vertical diffusivity, and horizontal diffusivity. Moreover, the responses of CO and NO_2 tend to vary linearly with the meteorological and emissions parameters, whereas those of NO and O_3 tend to be nonlinear.

17. KEY WORDS AND DOCUMENT ANALYSIS

a. DESCRIPTORS	b. IDENTIFIERS/OPEN ENDED TERMS	c. COSATI Field/Group
*Air Pollution *Verifying *Photochemical Reactions *Reaction Kinetics *Numerical Analysis *Mathematical Models *Atmospheric Models *Sensitivity		13B 07E 07D 12A 14B 14G

18. DISTRIBUTION STATEMENT	19. SECURITY CLASS *(This Report)*	21. NO. OF PAGES
RELEASE TO PUBLIC	UNCLASSIFIED	246
	20. SECURITY CLASS *(This page)*	22. PRICE
	UNCLASSIFIED	